FACTORS AFFECTING THE MICROHARDNESS OF SOLIDS

by

Philip Michael Sargent B.A.

of

Wolfson College,

Cambridge

A dissertation submitted for the degree of Doctor of Philosophy in the University of Cambridge.

Preface

This dissertation, which is submitted for the degree of Doctor of Philosophy in the University of Cambridge, describes work performed in the Department of Metallurgy and Materials Science from October 1975 to July 1979 under the supervision of Dr.T.F.Page. Except where reference is made to the work of others, the results described and the interpretations ascribed to them are, to the best of my knowledge, original. This thesis is the result of my own work and includes nothing which is the outcome of work done in collaboration. No part of this thesis has been submitted for a degree at any other university; excluding the computer programs in appendix I, this thesis contains less than 60 000 words.

Dept. Metallurgy and Materials Science,
University of Cambridge

P.M.Sargent

July 1979

Acknowledgements

I am grateful to Dr.T.F.Page for his continual advice and encouragement, and to many of the research students and undergraduates in the department for stimulating discussions. I would like to thank Prof. Honeycombe for the provision of laboratory facilities and the assistant staff and the University Computing Service for technical assistance.

I would have found it impossible to have completed this thesis without the support of my friends and my parents (without whom I would have been impossible).

This study was supported by a studentship from the Science Research Council.

Preface

This dissertation, which is submitted for the degree of Doctor of Philosophy in the University of Cambridge, describes work performed in the Department of Metallurgy and Materials Science from October 1975 to July 1979 under the supervision of Dr.T.F.Page. Except where reference is made to the work of others, the results described and the interpretations ascribed to them are, to the best of my knowledge, original. This thesis is the result of my own work and includes nothing which is the outcome of work done in collaboration. No part of this thesis has been submitted for a degree at any other university; excluding the computer programs in appendix I, this thesis contains less than 60 000 words.

Dept. Metallurgy and Materials Science,
University of Cambridge

P.M.Sargent

July 1979

Acknowledgements

I am grateful to Dr.T.F.Page for his continual advice and encouragement, and to many of the research students and undergraduates in the department for stimulating discussions. I would like to thank Prof. Honeycombe for the provision of laboratory facilities and the assistant staff and the University Computing Service for technical assistance.

I would have found it impossible to have completed this thesis without the support of my friends and my parents (without whom I would have been impossible).

This study was supported by a studentship from the Science Research Council.

Summary

Microindentation hardness testing investigates the elastic and plastic behaviour of the surfaces and the bulk of solids. In this regime of small scale, high pressure deformation the/NORMAL bulk behaviour is modified and different mechanisms peculiar to different types of solid often assume a dominant role. This thesis classifies and examines these mechanisms, describes in which materials they can be expected to occur and why, estimates their effects on the deformation i.e. elasticity, yield stress, work hardening, displacement geometry, measured hardness and the uncertainties of measurement, shows under what circumstances measurements comparable with 'macro'-hardness can be made and indicates the wide range of other information that can be obtained using this simple test.

The inter-relationships between the fundamental factors which influence microindentation plasticity are explicitly described and the effects of varying external influences, such as temperature or dislocation density, on the microhardness are described in terms of these fundamental 'internal' factors. Investigations have been made in particular on the inter--relationships between indentation size and the density of grain boundaries (in MgO and stainless steel) and the relative contributions of elastic and plastic deformation (in MgO and metallic glasses).

A procedure for analysing data on the indentation size effect on micro--hardness has been devised and the problems of measuring hardness anisotropy have been investigated. A statistical method for comparing sets of hardness data from different materials has been developed.

Contents

"We cannot learn the cipher
Inscribed on our cell;
Stars taunt us with a mystery
Which we lack the lore to spell."

James Branch Cabell

"I am willing to taste any drink once."

James Branch Cabell

Chapter 1 - Why Microhardness ?

The principal practical use of diamond pyramid indentation hardness testing is to give an estimate of the typical bulk yield stress for one of a group of similar materials for quality control, identification, sample checking or checking uniformity across a single object.

Microhardness testing, which is generally the term used to describe hardness testing when the load on the indenter is less than a few kilograms, is used for the same purposes where the sample is very small or very thin, or when a brittle substance is tested and a large indentation would be rendered unmeasureable by cracking.

Microhardness measurements offer a unique method for investigating the plasticity and fracture of materials on the same scale as the mechanical interactions in the processes of friction, wear, abrasion, grinding, polishing and erosion by dust, wear debris, liquid drops or cavitation. Microindentation can be used to perform many tests, under different conditions, on the mechanical properties (including fracture toughness) of a small area on the surface of a single specimen.

This thesis is concerned principally with the microindentation process when indentations are formed entirely or largely by plastic flow. The science of indentation fracture mechanics is a recent and fast developing field whereas the study of indentation plasticity has progressed slowly over a period of decades. However, recent studies (Lawn 1979) indicate a critical rôle for plasticity in the nucleation of indentation fracture and therefore the two fields may become more interrelated than they are at present.

The main problem with using microhardness tests is the common lack of reproducibility and wide ranging results because of the strong influences of extraneous factors. These problems of materials characterisation, cleanliness, making and measuring indentations are so interrelated and varied as to produce apparently random differences

between the work of one laboratory and another. For example, the strong dependence of microhardness number on the size of the indentation is widely recognised and a standard load of 100 gf. is often used in mineralogical and glassy metals studies.

It is the purpose of this thesis to describe and investigate the influences of materials and experimental conditions on microhardness measurement and to indicate when, and by how much, such conditions affect hardness numbers and when additional information may be obtained from the test. It will be seen that the technique can be used to investigate these materials conditions which are often of interest in themselves.

The responses of materials to microindentation are extremely varied but there are always points of similarity. Different materials can be thought of as bringing out aspects of microindentation behaviour which are hidden in the responses of other materials. Therefore a very wide range of metals, intermetallics, glasses and ceramics have been studied here in order to assemble as complete a picture as possible of the responses of solids to microindentation.

A broad approach has been taken because of the wide range of physical, chemical and measurement effects which can influence the determination of microhardness. If any of these effects were omitted from the study, the value of the experimental work would be severely reduced because of the unknown effects of uncontrolled variables. This wide-ranging review means that a significant proportion of this thesis consists of critical examinations of other researchers' studies with a view to extracting from their work that which is relevant to microindentation behaviour.

Chapter two reviews the subject of microindentation hardness and it includes much from published work and personal communications from other researchers. However, all unacknowledged work in this chapter is the product of the current study. Those contributions which can most easily

be described in the context of a review of the literature (and which do not require a great deal of qualification with regard to experimental details) are included here. Thus the length of this chapter is deceptive; it is not merely a survey of published papers.

Whilst chapter two describes the mechanisms in the indented materials which determine the plastic response, chapter three is concerned with the experimental problems of making and measuring indentations and with the development of experimental and statistical techniques. These techniques have been designed to optimise the amount of useful information that can be obtained from measurements with respect to the effort and tedium associated with making and measuring large numbers of indentations.

The review in chapter two identifies several major obstacles to the interpretation of microhardness measurements, and in chapter four experiments are described which were made with the object of resolving these difficulties. The interpretation of the results is made with reference to the theories and hypotheses advanced in chapter two.

In chapter five the interpretation of the experimental results is used as a starting point to suggest more experiments designed to further elucidate the mechanisms of plastic flow beneath indenters in specific materials. New designs of microhardness testing machines are suggested to improve the accuracy and control of indentation testing and hence to render the interpretation of results more straightforward.

Chapter six concludes with a survey of the principal achievements of the study.

"If you give me six lines written by the most honest man, I will find something in them to hang him."

Cardinal Richelieu

Chapter 2 The Indentation Microhardness Test

The pyramid indentation hardness test is simple to perform but hard to interpret in terms of materials behaviour. This chapter reviews the field and, where appropriate, includes my own contributions which are either of a theoretical nature or are deductions from published data.

Firstly, simple and complex models of the stress and strain fields will be summarised, then descriptions of the mechanisms by which the indentations are formed, followed by the results of considering these two aspects together.

In the last three sections the problems of anisotropic and inhomogeneous materials and the effect of indentation size will be considered.

2.1 Indentation Models for Ideal Materials

None of the models considered in this section approach the problem of the relative sizes of the indentations' stress fields and the mechanisms, such as dislocations, of plasticity. Only fully ductile, perfectly homogeneous, isotropic materials will be considered here.

2.1.1 Simple Ideas

In this section, models applicable to rigid-plastic materials will be described, that is those materials for which the effects of elasticity can be considered to be neglible.

For both perfectly plastic (i) and work-hardenable (ii) materials a relation of the form:

$$H/Y = C \qquad 2.1.1a$$

has often been found to hold; where H is the hardness (the pressure over the projected area of the indentation), Y is the yield stress (flow stress for work-hardenable materials) and C is a constant. This relationship can be derived theoretically for the case of a perfectly plastic material indented by a rigid, flat die using slip-line field analysis (Tabor 1951). This analysis is only applicable to two dimensional sections. Finite element analysis has been used to show a similar relationship (Lee et al. 1972) but the cost of computations restricts this treatment to only two dimensions too.

Case (i)

A fine-grained, fully work-hardened metal is a fairly good approximation to a rigid-plastic material. For such materials, the constant C in equation 2.1.1a is calculated theoretically to be about 3 (Tabor 1951, Lee et al. 1972) for Vickers indenters and between 2.8 and 3.4 for ball indenters when the plastic region fully encompasses the contact area with the ball (Douthwaite 1970, Tabor 1971).

Case (ii)

Underneath an indenter, different parts of the plastically deformed material are strained by very different amounts (probably from zero to over 1000% for pyramidal indenters). By making the assumption that for all hardness indentations there is a single average representative strain (ε_r), the relationship of 2.1.1a can be applied to materials that work-harden (Tabor 1971), by taking Y to be the flow stress at a strain of ε_r rather than the yield stress. Empirically, a strain of 0.2 tan(β)* has been found to give fair correlations for many materials (Douthwaite 1970). For Vickers indenters (see appendix III), this strain is about 8% and C is empirically found to be about 2.9 for all pyramidal indenters (Tabor 1971). For ball indenters, C is found to be about 2.8.

The above correlations have been obtained using data from fine-grained, annealed metals for which the strain distributions beneath indenters can be expected to be fairly similar, but even so, there are many alloys for which C is greater than 3 , C = 4.4 has been observed (see figure 2/2). This clearly shows the inadequacy of the 'single representative plastic strain' hypothesis even for a class of broadly similar materials. However, if the idea of a constant C is retained, it may be considered that for different types of materials, different ε_r may be more appropriate, but this would reduce the model's usefulness in giving very quick, very rough estimates of the flow stress.

This simple model (equation 2.1.1a), which rests almost entirely upon empirical correlations, makes no statements about the relative sizes of indentations; but given a flow stress, it predicts a hardness value that should be measured whatever load is used to make the

---

*Footnote: β is the contact angle between the indenter and the surface.

indentation. Neither is the model concerned with the shape of the indentations, though there are marked differences between those of case (i) and those of case (ii) materials (which are dealt with further in section 2.3.2).

Generally, materials whose behaviour is described by the model deform on indentation by forming a 'pile-up'* or 'coronet' on the surface surrounding the indentation of displaced material. Therefore this model will be referred to as the 'surface-directed displacements model'.

2.1.2 Elastic-Plastic Models

For many materials, a significant proportion of the material displaced by the indenter is taken by elastic strain. This is particularly important for materials with a low ratio of Young's modulus to yield stress (E/Y).

Models have been developed which are similar to that of equation 2.1.1a, but which have a C factor which depends on the moduli, yield stress and Poisson's ratio of the material and the angle of contact of the indenter with the surface. Some of these will now be described.

When the material displaced by the indenter is accommodated by elastic compression (instead of flowing towards the surface to form a pile-up), the stress field is similar to that surrounding an expanding spherical cavity in the solid (Marsh 1964). This is true even for pyramidal indenters, as Samuels and Mulhearn (1957) have shown that the strain surrounding these rapidly assumes a spherical character (see figure 2/1).

Much work has been done using wedge-shaped indenters (Hirst and Howse 1969), comparing the results with theoretical analyses of

---

*Footnote: 'Pile-up' in this thesis will be used to mean a surface pile-up of displaced material and not, unless specifically indicated, a dislocation pile-up.

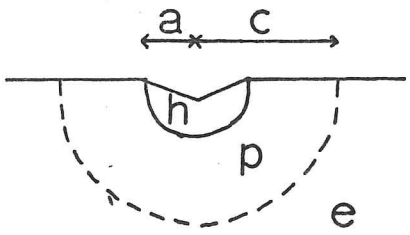

Figure 2/1

A diagram of the idealised deformation zones beneath an indenter in a material which deforms plastically.

h = the hydrostatic core

p = the volume of plastic deformation where there are large shear stresses as well as the hydrostatic component

e = the elastic 'hinterland' where there is still a large hydrostatic stress but where the shear stress is below the yield criterion

This view of deformation beneath indentations has been assumed to be reasonable for many years (see, for example, Tabor's review (1970)) and has been confirmed by the finite element analysis performed by Lee et al. (1972).

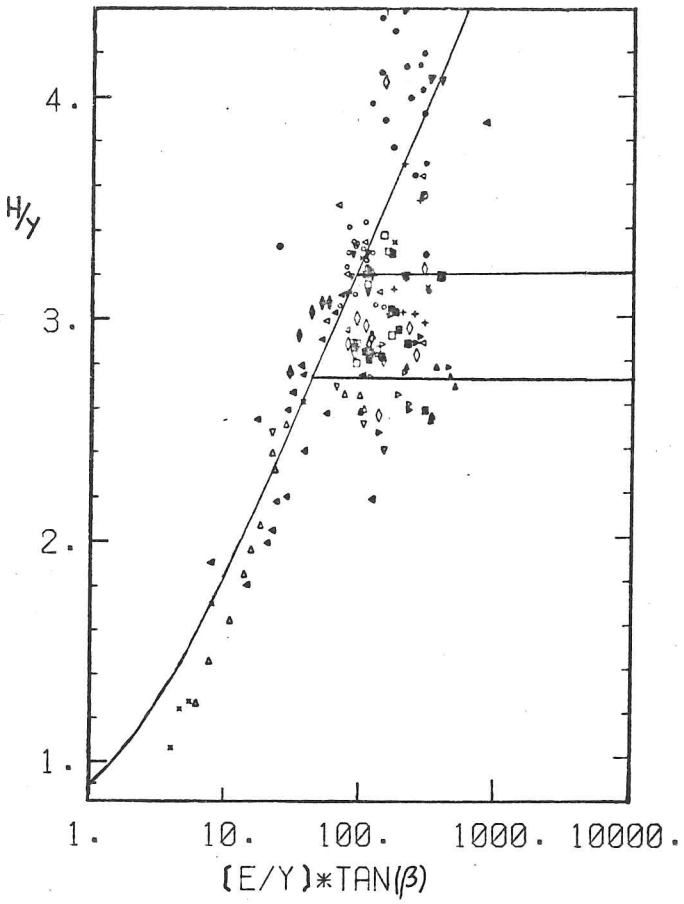

EXPERIMENTAL DATA

Symbol	Date	Source	Indenter	σ
■	1951	Tabor	Vickers	Flow stress after 6% strain
●	1958	Dugdale	Vickers	Flow stress after 6% strain
◀	1962/63	Nunes & Larson	Vickers	Flow stress after 6% strain
▩	1968	Speich & Warlimont	Vickers	Stress at 0.2% offset strain
×	1969	Hirst & Howse	Vickers	Flow stress
□	1969	Richardson	Vickers	Flow stress after 8% strain
+	1970	Doutmeyer	Vickers	Flow stress after 7.5% strain
⊠	1971	Farrell & Loh	Vickers	Flow stress after 8% strain
○	1971	Cahoon, Broughton & Kutzak	Vickers	Flow stress after 8% strain
◊	1972	Moore	Vickers	Flow stress after 7.42% strain
▼	1972	Greenhalgh	Vickers	Flow stress after 8-16% strain
▷	1955	Dugdale	Pyramids	Yield stress
▶	1954	Dugdale	Cones	Flow stress after 100-150% shear strain
▽	1965	Atkins & Tabor	Cones	Flow stress after 4-19% strain
◁	1949	Holm, Holm & Shobert	Spheres	Yield stress
▲	1951	Tabor	Spheres	Flow stress
△	1970	Johnson	Spheres	Flow stress
◆	1972	Lee, Masaki & Kobayashi	Spheres	Yield stress

Figure 2/2 (from Moore, 1974). This shows indentation hardness data from metals, collected from the period 1949 to 1972 using Vickers, Knoop, and spherical indenters and cones and pyramids of various shapes (i.e. various contact angles β). The lines at H/Y= 2.75 and 3.2 are the minimum and maximum values predicted by a variety of surface-directed displacement theories. The curve is calculated from equation 2.1.2b with a Poisson's ratio of 0.3 .

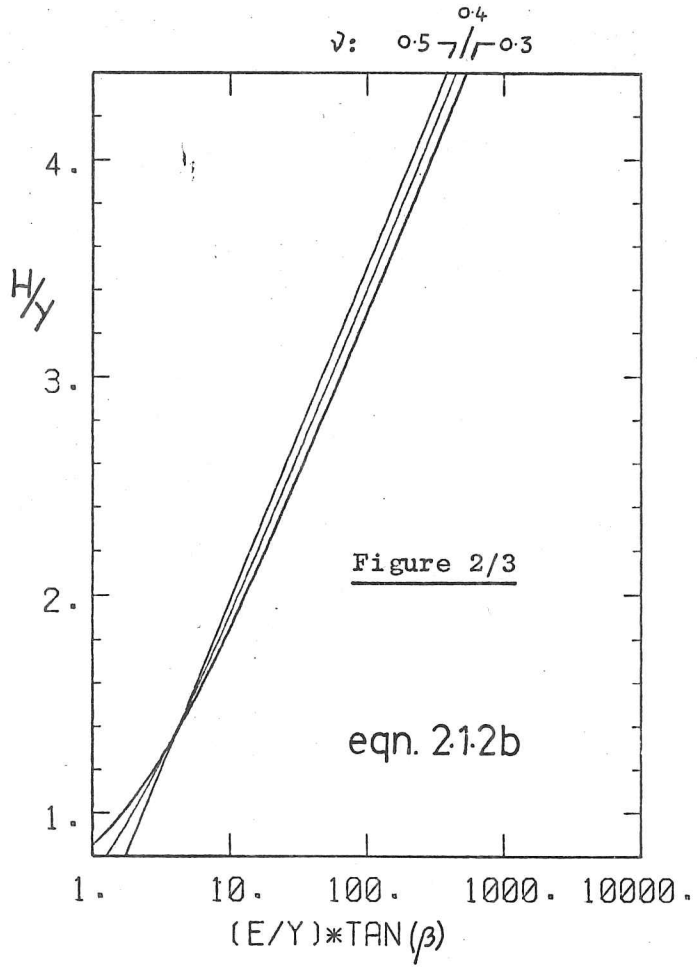

Figure 2/3

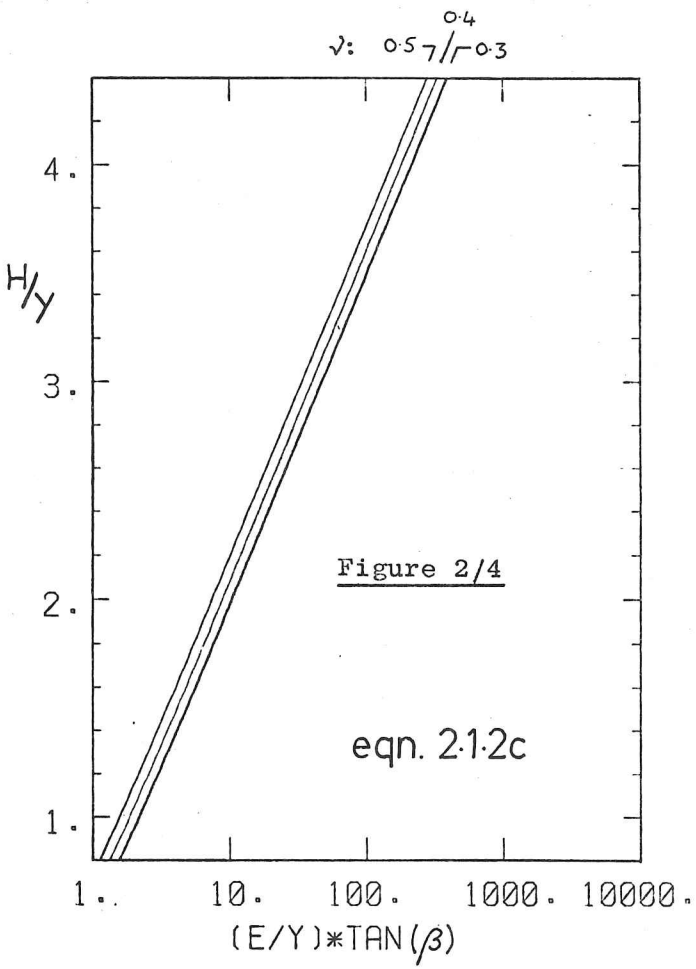

Figure 2/4

of expanding cylindrical cavities, as well as testing materials of different E/Y ratios with balls and pyramids (Marsh 1964, Johnson 1969, Moore 1974, Francis 1976, Studman and Field 1976). One consequence of this 'expanding spherical cavity' or 'radial displacement' model is the relation devised by Studman and Field using Johnson and Moore's work (equation 2.1.2a).

$$H/Y = 2/3\left[1 + \ln\left\{\frac{(E/Y)\tan\beta + 4(1-2\nu)}{6(1-\nu)}\right\}\right] \qquad 2.1.2a$$

Imaoka and Yasui (1976) found that finite element analysis produced a similar relationship. This model (equation 2.1.2a) has been extended to take account of the transition between the assumed hydrostatic core volume beneath the indenter (figure 2/1) and the plastically deforming zone (Studman, Moore and Jones 1977). An extra term was also introduced to take account of the changing contact angle for spherical indenters, which varies from zero to β during indentation.

$$H/Y = J + 1/2 + 2/3\left[1 + \ln\left\{\frac{(E/Y)\tan\beta + 4(1-2\nu)}{6(1-\nu)}\right\}\right] \qquad 2.1.2b$$

J is zero for cones and pyramids and -0.2 for spheres (see figure 2/3). This model of Studman, Moore, Jones and Field will henceforth be referred to as the 'SMJF' model.

Gerk (1976), by using a logarithmic 'true' strain approach, but without taking into account the hydrostatic/plastic transition, has derived the relationship shown in equation 2.1.2c(see figure 2/4):

$$H/Y = 2/3\left[1 + \ln\left\{\frac{1 - \exp(-(2/3)\tan\beta)}{1 - (1 - 2/3(1-\nu)Y/E)^3}\right\}\right] \qquad 2.1.2c$$

which gives a better fit to the data of Marsh and Hirst and Howse at low and high extremes of β.

These radial-displacement models are only applicable to elastic: perfectly-plastic materials, that is, those that do not work-harden or work-soften, and there are few materials for which this is completely true. However, the behaviour of nearly all materials which approach this condition is quite well described by the models, as can be seen from figures 2/2, 2/3 and 2/4.

When the ratio E/Y is greater than about 114, the H/Y value is about 2.75 and the pile-up mode of deformation begins to become significant, when E/Y is much ~~greater~~ less than 114, the deformation can be expected to be wholly by radial displacements.

2.1.3 Elastic-Plastic Work-Hardening Models

For a work hardening material one can define a representative flow stress which depends on the form of the compressive stress -strain curve and the form of the strain distribution beneath the indentation. This is a more sophisticated procedure than merely taking the representative stress to be that flow stress at 8% tensile strain, or 7.5% compressive strain (Douthwaite 1970). If the representative yield stress is y: where c and a

$$y = \frac{1}{\ln(c/a)} \int_a^c \frac{Y(r)}{r}.dr \qquad 2.1.3a$$

are from figure 2/1 and Y(r) is the flow stress as a function of the radius, r, from the contact point of the indenter.

From the representative stress one can derive:

$$H/y = J + 1/2 + \frac{2Y}{y} + 2/3 \cdot \ln\left(\frac{(E/Y)\tan\beta + 4(1-2\nu)}{6(1-\nu)}\right) \qquad 2.1.3b$$

where both the usual yield stress and the flow stress appear. This derivation is largely of academic interest as the determination of Y(r) for a real material is almost impossible (Studman, Moore and Field 1977).

Gerk (1976) extended his logarithmic strain, elastic-plastic model to deal with simple strain-dependent flow stress relationships and derived the result:

$$H/Y = 2/3\left[1 + \ln(\rho/\rho_0) + \frac{4(1+\nu)}{3}\frac{\Theta}{Y}\sum_{n=1}^{\infty}\left(\frac{\rho^n - \rho_0^n}{n^2}\right)\right] \qquad 2.1.3c$$

where Θ is the work hardening rate, and

$$\rho = 1 - \exp(-2/3\tan\beta)$$

$$\rho_0 = 1 - \left(1 - 2/3(1+\nu)Y/E\right)^3$$

Now, if an analytical expression for the stress-strain relationship of the material is assumed, it is possible to calculate explicitly the effect of work-hardening on the hardness. Gerk used the stress -strain relation:

$$\bar{s} = b((2/3)\bar{e} + 1.414e_0)^x \qquad 2.1.3d$$

where e_0 is the prestrain and

$$\bar{s} = \left[\sum_{i,j} (\sigma_i - \sigma_j)^2\right]^{1/2} \quad i,j = 1,3;\ i \neq j$$

$$\bar{e} = \left[\sum_{i,j} (\varepsilon_i - \varepsilon_j)^2\right]^{1/2} \quad i,j = 1,3;\ i \neq j$$

and σ_i and ε_i are the principal stresses and strains.

Gerk has numerically calculated solutions for a range of conical indenters indenting polycrystalline copper. He found some agreement with experiment for low values of prestrain and for blunt indenters; conditions in which the radial displacement mode of deformation is expected to dominate the surface-directed displacement mode.

2.2 Indentation Mechanisms in Real Materials

2.2.1 Plasticity Mechanisms

For the purpose of this section, a plasticity mechanism will be used to mean any mechanism leading to non-elastic, permanent deformation and not only slip and twinning.

There are a number of mechanisms which, because of the very high stresses, large hydrostatic component and high strain rate, occur on indentation which would not normally be activated at room temperature using a simple tensile test. The case of indentation of silicon carbide illustrates this very well. Silicon carbide is stiff, hard and brittle, yet, like other materials with these characteristics, it is known to deform plastically on indentation because the hydrostatic pressure surpresses the fracture mechanisms (Adewoye 1976, Sawyer 1979, Sawyer et al. 1979). The most important mechanism is likely to be dislocation slip; others which might be considered are twinning, densification, and block--shear (where the shear stress is greater than the theoretical strength of the solid - Kelly 1966).

Dislocations have been observed by transmission electron microscopy (TEM) beneath indentations even in diamond (Humble and Hannink 1978) and fine-scale twins and dislocations have been seen in silicon carbide. The twins (Sawyer 1979) are thought to be growth faults, whereas Hockey and Lawn (1975), Adewoye(1976) and Page et al.(1978) have observed glissile dislocations directly beneath indentations and friction tracks. Impact sites of particles have also been examined by TEM (Hockey et al. 1978) and the glissile dislocation structure produced is found to be similar to that beneath indentations.

One form of silicon carbide has the sphalerite (zinc blende) structure and below a threshold temperature (600°C, Trefilov et al. 1977),

Figure 2/5 - Hardness (H) and Phase Change Pressure (P_c)

Experimental hardness values are taken from Garbato and Rucci (1977) and experimental P_c values from Van Vechten (1973).

O indicates the most reliable values and

⊖ indicates the range of published values.

Experimental hardness values are known to have been measured in the low temperature, athermal range for Si, Ge and InSb, and in the higher temperature, thermal range for CaAs. The flow stress/temperature properties of the other compounds are unknown.

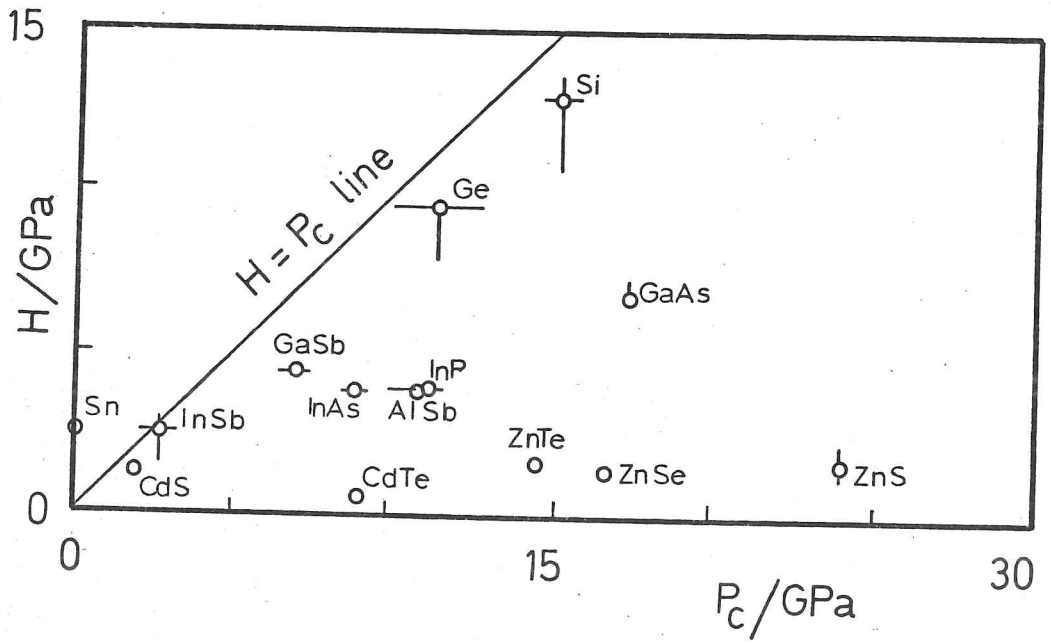

See pages 18 & 19.

Figure 2/6 - Predicted Low Temperature Hardness and Experimental Phase Change Pressure

The hardness is predicted for a compound QR by:

$$H^+ = \left[\frac{H_P}{(\beta/\alpha)P} + \frac{H_S}{(\beta/\alpha)S}\right] \cdot (\beta/\alpha)_{QR} \cdot 1/2 \qquad 2.2.1a$$

where H_P is the experimental hardness for element P and $(\beta/\alpha)_P$ is the force constant ratio for element P. P and S are the elements in Group IV which form a compound isoelectronic with the compound in question, QR. So, for the compound InSb the relevent elements are Sn and Sn and for the compound ZnS the elements are Ge and Si.

Since the hardnesses of the Group IV elements have been measured in the low temperature regime where slip is stress-activated, it is expected that H^+ predicts the hardnesses for the compounds in that low temperature regime. This procedure is necessary because there is insufficient experimental data on the low temperature hardnesses of the compounds available in the published literature.

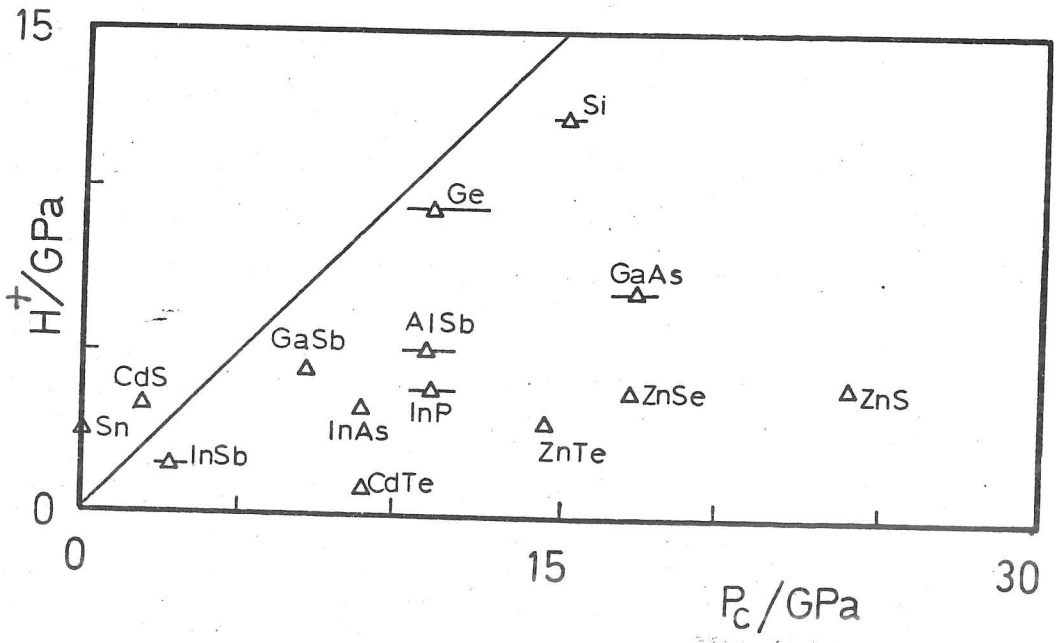

the hardness of crystals of this structure is controlled by stress-activated slip (Gilman 1975); above this temperature (which can be well below room temperature for some of these compounds), the indentation rate, i.e. the velocity of the indenter, probably has a critical effect on the measured hardness. This is because a high rate can lead to a higher stress being required to propagate the dislocations at the velocity necessary to accomodate the strain imposed by the indenter. This effect also occurs at higher temperatures but is expected to be less important. In addition, when the Peierls' stress becomes very low at high temperatures, there can be appreciable contribution to the hardness measured due to work-hardening (Gerk 1976). It should also be remembered that plastic deformation will also occur on unloading (Johnson 1963) and thus this rate should also be considered.

Sphalerites are capable of phase changes, similar to the tin alpha -beta transformation, in which there is a density increase of 20.9% (Van Vechten 1973). This has been directly observed in CdS by indenting with a spherical glass lens and observing the colour change under load (Gilman 1973). In silicon, a reversible increase in electrical conductivity has been observed in the material under a loaded indenter, which indicates a reversible phase change to a denser solid with a higher degree of atomic coordination. Generally, the transition pressures (P_c) are much higher than the indentation pressures (see figure 2/5).

The suggestion has been made that these phase changes may be the dominant factor determining the hardness of Ge, Si and diamond (Gerk and Tabor 1978) and SiC (Trefilov et al. 1977), but an analysis of published physical, thermodynamic and hardness data of IV, IV-IV, III-V, and II-VI elements and compounds shows that their hardnesses are very closely related to their bulk moduli, ionicity (Garbato and Rucci 1977), sublimation energy and central/non-central force ratio (β/α), whereas the phase change

pressure can be predicted from other, thermodynamic, data (Van Vechten 1973). Figure 2/6 shows a plot of predicted hardness pressures against experimental phase change pressures for some sphalerites. The predicted hardness (H^+) is calculated from the experimental hardnesses of the two elements which form a compound isoelectronic with the compound in question, and from the force ratio (β/α) of this compound. This is similar to Garbato and Rucci's work, except that this hardness H^+ should be similar to the experimental hardness of the compound in the athermal, stress-activated dislocation movement temperature range (i.e. below 600°C for SiC). This has been done because experimental hardness values in this temperature range are not available for most sphalerite compounds. The object of this comparison (figure 2/6) is to show that not only are the room temperature hardnesses different from the phase change pressure (P_c) but that the 'ideal', cold hardnesses are also unrelated to P_c. Therefore it is coincidental that the experimental points for Si, Ge, InSb, CdS and Sn lie close to the $H = P_c$ line and this relationship cannot be used to predict the phase change pressure from experimental hardness values (Gerk and Tabor 1978).

The experimental data for silicon carbide is not on figure 2/5 but the pressure P_c has been calculated from thermodynamic data to be 64 GPa (Van Vechten 1973), which is very similar to the hardness value of 69 GPa measured using a 50 gf. loaded Vickers indenter on the (0001) plane. It must be remembered that the final equilibrium pressure (the measured hardness) is the minimum pressure that the material is subjected to during the test. Thus, densification probably does occur in SiC on indentation, but may not be the dominant deformation mechanism (Sawyer et al. 1979).

The high hydrostatic pressure beneath indenters also affects the generation and movement of point defects. It is to be expected that vacancies will have higher nucleation energies and interstitials lower

nucleation energies. At high homologous temperatures this will affect the creep mechanisms but, even at relatively low temperatures, 'crowdions' may be active and may play an important part in accomodating the imposed strain (Velednitskaya et al.1975, Rozhanskii et al.1970) in MgO and alumina.

The magnitude of the shear stresses beneath the indenter can only be estimated, but a value of H/5 has been suggested by Tabor (1970). The shear stress beneath the indenter in silicon carbide is therefore about 13 GPa, which should be compared with the expected theoretical shear strength of E/30 - equivalent to about 15 GPa (Eddington et al.1975) for a typical sample of SiC.

Thus, the 'mussed-up' zone, the small volume of material beneath indentations in SiC which has been seen to have suffered large rotational strains and to contain unresolvably dense dislocation tangles (using TEM, Page et al.1978), may have been caused by densification and/or block shear. On unloading, the crystal is thought to have relaxed back from the densified/sheared state to something near the original structure (Adewoye 1976, Page et al.1978, Hockey and Lawn 1975).

In glasses, the plastic deformation may be due to viscous flow, which strongly depends on the temperature and loading rate. In metallic glasses, 'shear bands', of unknown structure, appear to be the plasticity mechanisms (see section 4.3). In inorganic, non-metallic glasses, some kind of non-viscous, 'cold-flow' mechanism may operate (Bartenev et al. 1969) in addition to both reversible and non-reversible densification (Neely and Mackenzie 1968). Densification is easily observed in silicate glasses and perspex by the change in refractive index (Peter 1970, Bassett 1977), and Imaoka and Yasui (1976) have shown that densification probably accounts for about half the plasticity in silicate glass by comparing experimental data with finite element analysis of indentation mechanics.

2.2.2 Fracture

The role of fracture in producing permanent indentations is two -fold: firstly, directly, by crushing in porous materials and spalling, and secondly, by influencing the stress state beneath the indenter so as to affect the plasticity mechanisms. Cracks can also be initiated by dislocation mechanisms, and this has been observed in MgO (e.g.Keh 1960), and SiC (Sawyer 1979, Naylor and Page 1979, Trefilov et al.1977).

The quantitative understanding and application of indentation fracture mechanics (Lawn and Wilshaw 1975) is a recent and important development . However, this thesis is concerned with the formation of the indentation, and cracking will only be considered where it influences this.

Fracture cannot displace material except by chipping or spalling, and indentations where these are the dominant modes of deformation have not been used in the current study. A fine network of micro-cracks may be able to relieve shear stresses, such that the number of independent slip systems required to form an (apparently wholly plastic) indentation may be reduced from the five necessary for arbitrary deformation (Groves and Kelly 1964), and such fine cracks have been observed in SiC and Al_2O_3 (Hockey and Lawn 1975).

The interactions betweem cracks and plasticity mechanisms are not well understood and will not be dealt with further, except to say that, for any material, there appears to exist a size (or load) limit below which all indentation, whether by diamond indenters or dynamic particle impact, is plastic with no cracking occurring at all (Lawn and Evans 1977).

2.3 Yielding and Microhardness

In this section, the major classes of discrepancies between the behaviour of real materials and that of model materials (section 2.1) will be described. Figure 2/7 summarises some of the causal relationships between the concepts covered in this and preceding sections.

2.3.1 Flow Mechanisms and Strain Distribution

The Tabor relationship uses the flow stress at 8% strain ($Y_{8\%}$):

$$H = 2.8\, Y_{8\%} \qquad 2.3.1a$$

and is applicable, within limts, to most work-hardening metals for two reasons: firstly, the flow mechanisms of dislocation glide are essentially the same in the hardness test as in the tensile or compression test used to measure $Y_{8\%}$, and secondly, the strain field is more or less the same in these metals and therefore a single representative strain (8%) can be chosen representing that field. Circumstances and materials where these conditions do not hold will now be discussed.

Different Flow Mechanisms

An example of this type of deviation can be found in the work of Westbrook (1958), who found that the relationship for single crystals of the halite structure could be represented by

$$H = 35\, Y \qquad 2.3.1b$$

(see figure 2/8) where Y is the yield stress on the primary slip system. The applicability of this is further discussed in 4.5.3. Hopkins et al. (1973) found that the constant lay between 4 and 17 (instead of being around 2.8) for mixed KCl:KBr crystals. This type of deviation from the

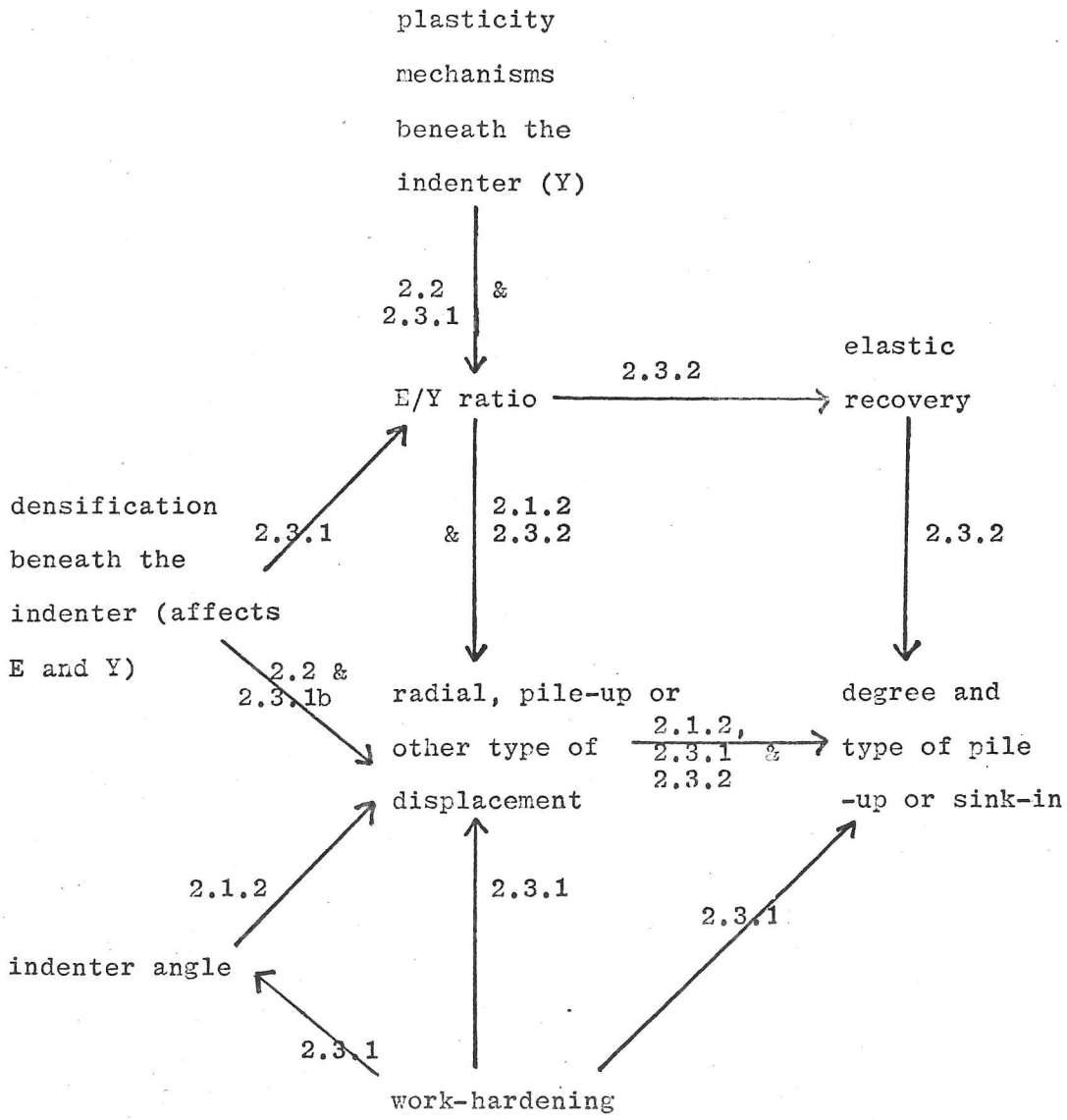

Figure 2/7 Mechanical Effects on Indentation Shape

Arrows are labeled with the section numbers where the connection appears in the text.

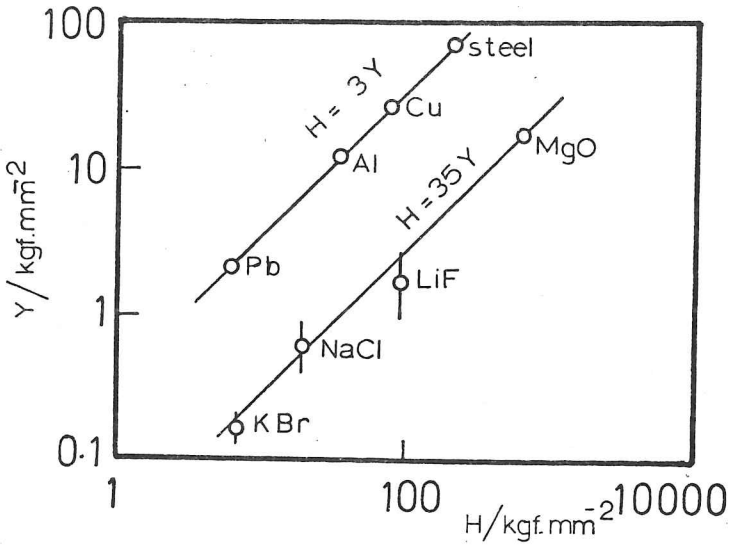

Figure 2/8 (from Gilman (1973))

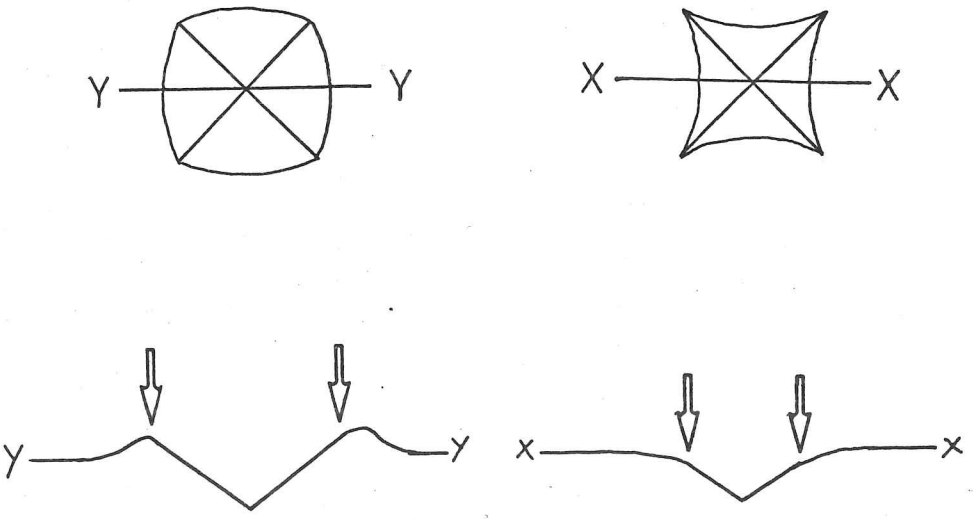

Figure 2/9

Demonstration of how 'starred' and 'barreled' indentations can be due to sink-in and pile-up respectively.

relationship of equation 2.3.1a occurs because a different flow stress is measured by the hardness test from that measured by the compression test. The primary slip system in halite structure crystals is usually $\{110\}\langle 1\bar{1}0\rangle$, whereas on indentation the $\{100\}\langle 1\bar{1}0\rangle$ slip system must also be activated too. The strain imposed by a compression along $\langle 100\rangle$ is uniaxial, and, as such, can be accommodated by only the three independent shears which are characteristic of the $\{110\}\langle 1\bar{1}0\rangle$ system. The strain around an indentation requires five independent shears (Groves and Kelly 1963) and thus the secondary slip system (or some other deformation mechanism, see 4.5.3) must also be activated. The critical resolved shear stress for yield on the secondary slip system can be a hundred times that of the primary in the halite structure (Gilman 1959, Swain and Lawn 1969).

This difference, due to strain type, between the hardness and the compression tests is fairly subtle, in that dislocation slip is the dominant mechanism in both. The hydrostatic pressure in the hardness test can also influence slip because of the slight dilation around dislocation cores (Spitzig et al. 1976) and this is especially important in ionic solids where charge effects are important (Haason 1974).

A more obvious difference between the hardness and compression tests is where the hydrostatic pressure beneath an indenter causes densification of the material, in which case the 'flow' stress measured by the hardness test will be affected by the critical pressure for densification .

Different Strain Distributions

Gerk (1976) has tentatively shown that for many materials (alkali halides and pure f.c.c. metals) their hardnesses may become dominated at high temperatures by their work hardening characteristics rather than their yield or flow stresses. This deviation from Tabor's relation (equation 2.3.1a) is because of a change in the strain distribution. As the temperature increases, the hardness drops and levels off to a constant

value (then drops again as the melting point is approached). Gerk interprets this as showing that the hardness is limited by the dislocation mobility at low temperatures, and,as the mobility increases with temperature, dislocation reactions (work-hardening) become more important in hindering deformation. One might expect the Tabor constant to remain at about 2.8 to 3.0 over the temperature range because the flow stress would be subject to the same mobility effects, as long as the strain rate was the same. However, the representative strain (8% for low temperatures) might be expected to change,as the strain distribution will be different in the high temperature regime. Unfortunately,the relevant yield and flow stresses for the different temperatures are not readily available for comparison with Gerk's hardness values,and thus the effect of this change on the Tabor constant is unknown.

When single crystals or other anisotropic solids are indented,there is a radically different strain distribution (which is covered in section 4.2).

If densification occurs in the hydrostatic zone then the strain distribution will not resemble any of the models of indentation behaviour.

Work-Hardening

It has been shown (2.1.3) how work-hardening can influence the behaviour of both the radial displacement and pile-up types of deformation. Now, the influence of work hardening on which of these types of displacement occurs will be described.

As the indenter penetrates the material,work hardening increases the flow stress,which means that the indenter is surrounded by a hardened cap of material which is carried with it. Thus,the load is spread over a wider area in the softer material by the harder cap,and a depression, or 'sink-in', is produced surrounding the indentation proper. The effect of the cap is also to change the effective angle of contact of the indenter,

making it appear blunter, which will also slightly affect the type of displacement (see equations 2.1.2a to 2.1.2c).

Vickers indentations in 'pile-up' and 'sink-in' materials show the characteristic 'star' (pincushion) and 'barrel' shapes when viewed normally (see figure 2/9); this is due to the contrast mechanism whereby the indentations are observed in an optical microscope (discussed in section 3.1). The edge of the indentation is usually taken to be where the contrast changes abruptly, which occurs at the point where the gradient of the surface changes (indicated by arrows on figure 2/9).
When scanning electron microscopy is used,the depth of field is sufficient to enable the whole of the pile-up to be seen (see figures in 2.4.1 and 4.4).

Since work-hardening leaves the modulus of the material unchanged, it may be conjectured that,in some cases,the E/Y ratio may be decreased to below 114 so that there may be radial displacement close to the indenter (in the cap) and surface directed displacement at a distance. However, such a complex problem of stress analysis is probably not amenable to analytic solution and would require 3D finite element computation.

2.3.2 Elasticity and Microhardness

In stiff materials and in materials with plasticity mechanisms only for less than five independent shears, the elasticity of the material supports a significant fraction of the load on the indenter.

Elastic Recovery of the Indentation

On unloading the indenter, the material will tend to expand elastically and will be prevented from doing so completely, that is from entirely refilling the indentation, by the plastically deformed material. Johnson (1968) has shown that plastic deformation will also occur on unloading, driven by the elastic recovery.

Microhardness measurements are usually made by optically measuring the size of the indentation after the indenter has been removed, thus elastic recovery of the indentation can lead to serious overestimation of the hardness if the measured indentation is smaller than it was under load. The Rockwell hardness testing machines avoid this by measuring the depth of the indentation under load, but the minimum load available on these machines is 15 kgf.

In isotropic materials, spherical indentations recover equally in all directions, whereas Vickers and Knoop indentations recover in the depth and over the faces, but hardly at all along the diagonals (Beeukes et al. 1973). This is because at the corners there is a sharp edge which maximises the plastic deformation yet, because it is far from the centre of the indentation, the elastic recovery appears to be small. Thus a sharp groove is left cut into the surface along the indenter's edges even if the indentation recovers completely over the facets when the load is removed. (This is especially obvious with indentations in polymers.) Therefore it is possible to measure a remnant of the loaded indentation even when the

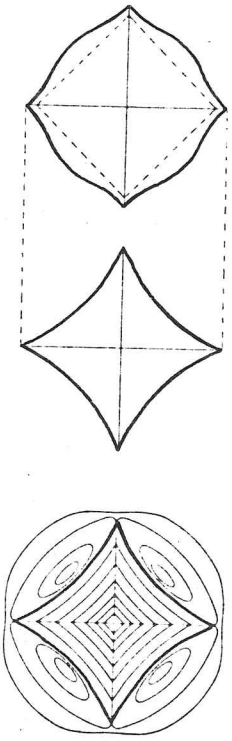

Figure 2/10 (from Buckle 1960)

(a) This is a diagram of the shape of an indentation in an elastic, ductile solid (such as perspex) whilst the indenter is still under load. The heavy line shows the line of contact between the indenter and the surface of the material.

(b) This is a diagram of the shape of the indentation after the indenter has been removed.

(c) This is a diagram of an interference micrograph of the indentation in (b). The pile-up is visible next to the edges of the indentation and the contours inside are curved because the indentation has contracted elastically across the faces but not along the diagonals.

indenter has been removed.

The effectiveness of this technique can be tested by measuring the size of the indentation under load using special apparatus, either by observing from the other side of a transparent specimen, or with a combined objective/indenter where one observes through the transparent diamond indenter (Muller 1973). Alternatively, if the indenter is coated with a thin layer of fine powder (evaporated carbon, sublimed NH_4Cl, or even lipstick (Dunegan 1961)) then the size of the indentation under load can be ascertained by examining the area wiped clean on the indenter. To make measurements of unrecovered hardness rapidly and easily it would be necessary to use apparatus which measured the depth the indenter penetrates, this is discussed in chapter five.

Pyramidal indenters are favoured for practical use partly because elastic recovery can generally be ignored when measuring the diagonals. Interference microscopy can be used (Buckle 1960) for measuring the depth of indentations and hence, since the shape of the indenter is known, the amount of recovery in the depth. In aluminium, not a particularly stiff material, the elastic recovery in the depth amounts to 1½%, whereas the recovery along the diagonals is undetectable (Buckle 1960, 1973).

Elastic recovery, in addition to pile-up and sink-in, can cause star-shaped Vickers indentations when the depth and facets recover and the diagonals do not. As can be seen from figure 2/10, pile-ups can also be present but, for very elastic solids, the recovery has a greater effect and thus the indentation is star- rather than barrel-shaped. Presumably, if the two effects are matched there will be no apparent distortion and the indentation will be square. However, in such a case, the contours inside the indentation will still be curved.

In anisotropic materials, whether mostly elastic or plastic, the elastic recovery is generally masked by the much greater influence of the anisotropy on the plastic deformation and the pile-ups (but not always, see section 4.2).

Measurements of Elastic Recovery

Berdikov and Babanin (1977) have measured the elastic recovery in the depth of Vickers indentations made in several types of silicon carbide and alumina ceramics and single crystals, and found it to be between 41% and 66%. They did this by measuring the indentation depth under load by measuring the displacement of the indenter as it penetrated, and by measuring the indentation depth after unloading by interference microscopy. However, their measurements of indentation diagonals (after recovery) are inconsistent with their measurements of indentation depths, the diagonals were all too large by at least 3 microns, and no confidence limits were placed on any of the data. Thus, it is unfortunately not possible to use their data to examine the depth and diagonal relaxations in these stiff materials, and no other data on this subject has been published.

Degtyarev and Lagveshkin (1977) measured recovered and unrecovered ball indentations in steels and found that the pile-up on the softer samples made the recovered indentations appear larger than the unrecovered ones in spite of the shrinkage due to elastic contraction.

Thus, the field of elastic recovery measurement is largely unexplored but there are experimental difficulties and specialised equipment is required to make reliable measurements.

Elasticity and Strain Compatibility

The strain around an indentation is probably a fair approximation to an 'arbitrary strain' which requires five independent shears (from the five independent elements of the strain tensor) to be satisfied. These five shears are usually interpreted in terms of slip, twin, or kink vectors, thus in cubic materials the $\{1\,1\,1\}\langle 1\bar{1}0\rangle$ slip system has five independent shears, whereas $\{1\,1\,0\}\langle 1\bar{1}0\rangle$ and $\{1\,0\,0\}\langle 1\,\bar{1}0\rangle$ have only three each. If the volume of material under strain does not remain constant, that is if plastic densification or elastic compression is important, then the five-shears criterion is relaxed and fewer than five can be available and yet fully-plastic indentations can still be formed.

The problem remains of 'how much' elasticity is required to enable fully-plastic indentations to be formed just using, for example, $\{1\,1\,0\}\langle 1\bar{1}0\rangle$ slip in MgO, or just $\{1\,1\,0\,0\}\langle 1\,1\bar{2}0\rangle$ and $(0\,0\,0\,1)\langle 1\,1\bar{2}0\rangle$ in SiC. This is important because fully-plastic indentations are observed in <u>all</u> materials (however limited their plasticity) if they are made small enough. In fact, in MgO and SiC it is believed that elasticity is not sufficient and that secondary plasticity mechanisms operate (see section 4.5.1 and Sawyer et al.(1979)).

Hutchinson (1977) has considered the situation where a semi-brittle polycrystalline solid is uniformly strained and it is necessary to consider the elasticity in order to ensure strain compatibility across the grain boundaries. His model shows that this is feasible but that even a little strain on a very stiff fifth shearing system is a great help, alternatively, if the strain rate varies between grains then an arbitrary strain can be accommodated if some creep mechanisms are active. However, the question of 'how much' elasticity is required for arbitrary strain on a single crystal remains unanswered.

2.3.3 Indentation Creep and Time-Dependent Effects

Both the indentation rate (the velocity of the indenter) and the dwell time at full load can affect the measured microhardness, especially in materials which are also susceptible to chemomechanical effects (see section 2.5.2). However, these two parameters of indentation rate and dwell time cannot usually both be easily varied on the same microhardness instrument: dwell time is easily controlled on the Leitz 'Miniload', or on any machine where the indenter is dead loaded, but is controlled with difficulty on the Reichardt machine where the force is changed by varying the displacement of a spring by hand. Conversely, indentation rate in dead loaded machines is often controlled by an oil-filled dash -pot, and whilst a valve usually permits adjustment of the damping characteristics of the arm holding the indenter, this is not easy to do in a repeatable manner as the number of air bubbles and the temperature of the oil affect the viscosity. Indentation rate in the Reichardt machine is controllable in theory, if one has a steady hand.

Various laboratories have used screw-driven mechanical testing machines to make indentations (Gregorev et al. 1977, Fröhlich et al. 1977, and see section 3.1.3 and chapter 5) but the vibration problem is severe and microhardness indentation rate experiments have not been attempted with this type of apparatus. This kind of experiment would be feasible, though perhaps only for 'macro'hardness, using a new type of machine which has been built by Barbato et al.(1978), where the indenter is driven by elastically strained metal bellows (see section 5.3).

Particle and liquid drop impact situations are dominated by strain rate effects (Evans and Wilshaw 1977, Ruff and Wiederhorn 1979), but for microhardness indentation (sometimes described as 'quasi-static indentation') only dwell time experiments, and no indentation rate experiments, appear to have been performed to investigate time-dependent

effects. These approaches are well suited to the study of creep mechanisms and of some aspects of the chemomechanical effect (see 2.5.2), but they are not well suited to the study of dislocation velocity : instantaneous stress level relationships, though this has been attempted (Gerk 1975, 1976). Therefore,the remaining part of this section describes results from dwell time experiments only.

In metals, indentation creep is generally simply related to conventional creep at the same temperature (Mulhearn and Tabor 1960), though Latanision et al.(1978) have shown that Zn displays a chemo--mechanical effect (see 2.5.2) which indicates that indentation creep in Zn might involve some unusual mechanisms.

In semiconducting and insulating ceramics, the melting points are generally much higher than for metals, and indentation creep predicted from conventional mechanisms would be much smaller than that which is observed. In part, this could be due to creep in the bulk, below the indenter, due to some of the exotic mechanisms described in 2.2.1: crowdionic diffusion, block shear, or densification. However, for many ceramics, the creep rate has been shown to be environment-sensitive which indicates that surface, as well as bulk, plasticity is important. This low temperature creep is termed Anomalous Indentation Creep (AIC), as the creep rate decreases with temperature and is only detectable using low loads such that the indentation depth remains less than about 3 microns (Walker 1973). In MgO, LiF, KBr, Al_2O_3, TiC and Ge, the AIC is thought to be due to the chemisorption of water; in LiF the AIC rate drops to zero above 70°C (but the static hardness is still reduced by chemisorbed water until the crystal has been heated to 200°C, Macmillan 1973).

Orientation Dependence of Creep in Alkali Halides

AIC in single crystals is affected by the orientation of the crystal. Brookes et al.(1975) have shown that MgO, LiF and NaCl, which

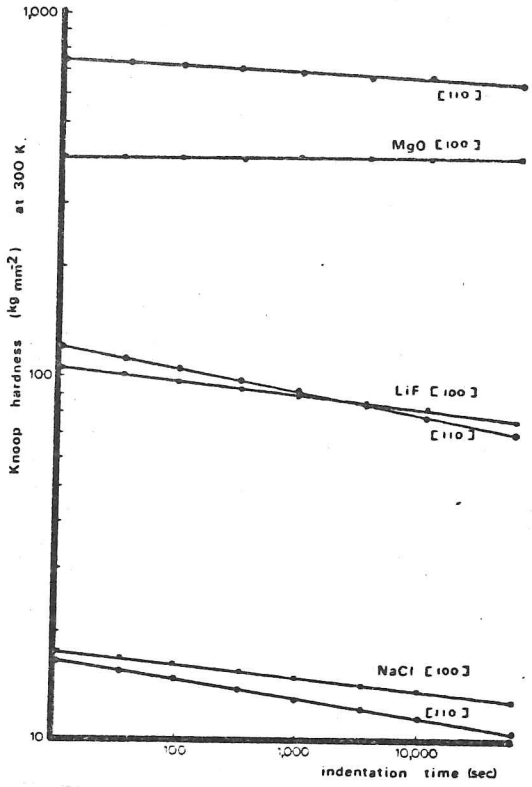

Figure 2/11

(from Brookes et al.1975)

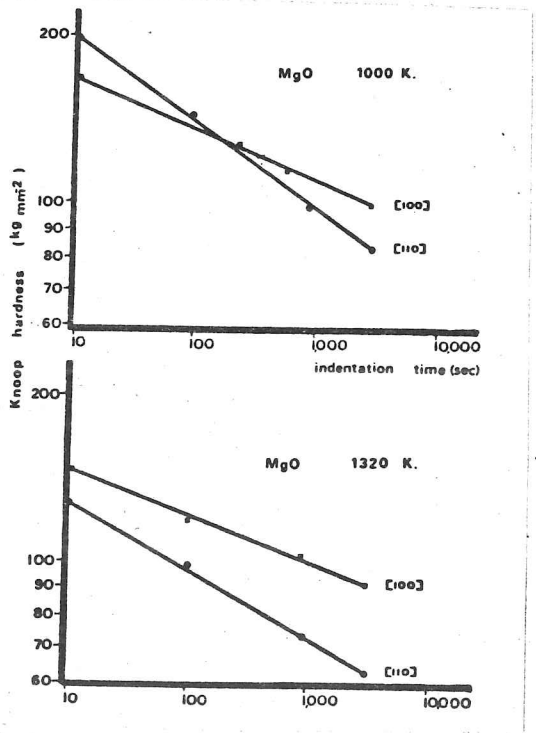

Figure 2/12

(from Brookes et al.1975)

have the same crystal structure, have the same AIC rate dependence on dwell time at full load, on temperature, and on crystal orientation (figures 2/11 and 2/12). The creep rate is always higher when the Knoop indenter has the long diagonal along $\langle 110 \rangle$ rather than along $\langle 100 \rangle$. Hence, for high homologous temperatures, and long indentation times, all three crystals display a hardness anisotropy which is the exact opposite of that predicted by the effective resolved shear stress model (see section 4.2.2) using the observed primary slip system $\{110\}\langle 1\bar{1}0 \rangle$, but at lower temperatures and shorter indentation times the model and the observations are in agreement. The high temperature/long time hardness anisotropy is consistent with slip occurring on the $\{100\}\langle 1\bar{1}0 \rangle$ slip system (Brookes et al.1975, and see section 4.2.3) and this is discussed further in section 4.5.2.

Boyaskaya et al.(1979) have also observed the inversion of the Knoop hardness anisotropy by comparing KCl and NaCl with LiF and MgO at room temperature. However, they found the Vickers hardness anisotropy to be the same for all four crystals, which indicates that the geometry of slip around Knoop indentations is more sensitive to secondary plasticity mechanisms than is the geometry around Vickers indentations.

2.4 Hardness of Single Crystals

Any type of faceted, pyramidal hardness indenter can be used to measure hardness anisotropy, but the most commonly used is the Knoop indenter. This indenter has 2mm plane symmetry which, when measuring hardness, is superimposed on the plane group symmetry of the test surface. Thus, on a $\{111\}$ cubic surface, a Knoop indenter will show a six-fold hardness anisotropy. This superimposition means that a Knoop indenter introduces a centre of symmetry and therefore cannot be used to detect any hardness anisotropy due to crystal polarity on, for example, the $\{10\bar{1}0\}$ surface of an α-SiC crystal. (This would require the use of a triangular (Berkovich) indenter or a pentagonal indenter (Brookes and Moxley 1975)).

The following sections briefly review what is known about dislocation geometry around indentations in single crystals, especially for crystals of the halite structure which have been extensively studied. However, very little of this knowledge has been used in the development of models designed to predict the form of the hardness anisotropy of single crystals. Some of these models are reviewed and the most successful (the effective resolved shear stress model) has been revised and extended in this current study. Some predictions for the hardness anisotropy of silicon carbide are compared here with experimental hardness anisotropies. Finally, the problem of comparing Vickers and Knoop hardness anisotropies is mentioned prior to its experimental investigation in section 4.2.2.

2.4.1 Indentation Geometry in Single Crystals

Buckle (1973) has reviewed the indentation of ductile single crystals in terms of the shapes of the indentations and their pile-ups, and Chen and Hendrickson (1973) have made an examination of the dislocation movement around microindentations in pure silver. The small scarcity of work in this field of metallic crystals compared with that

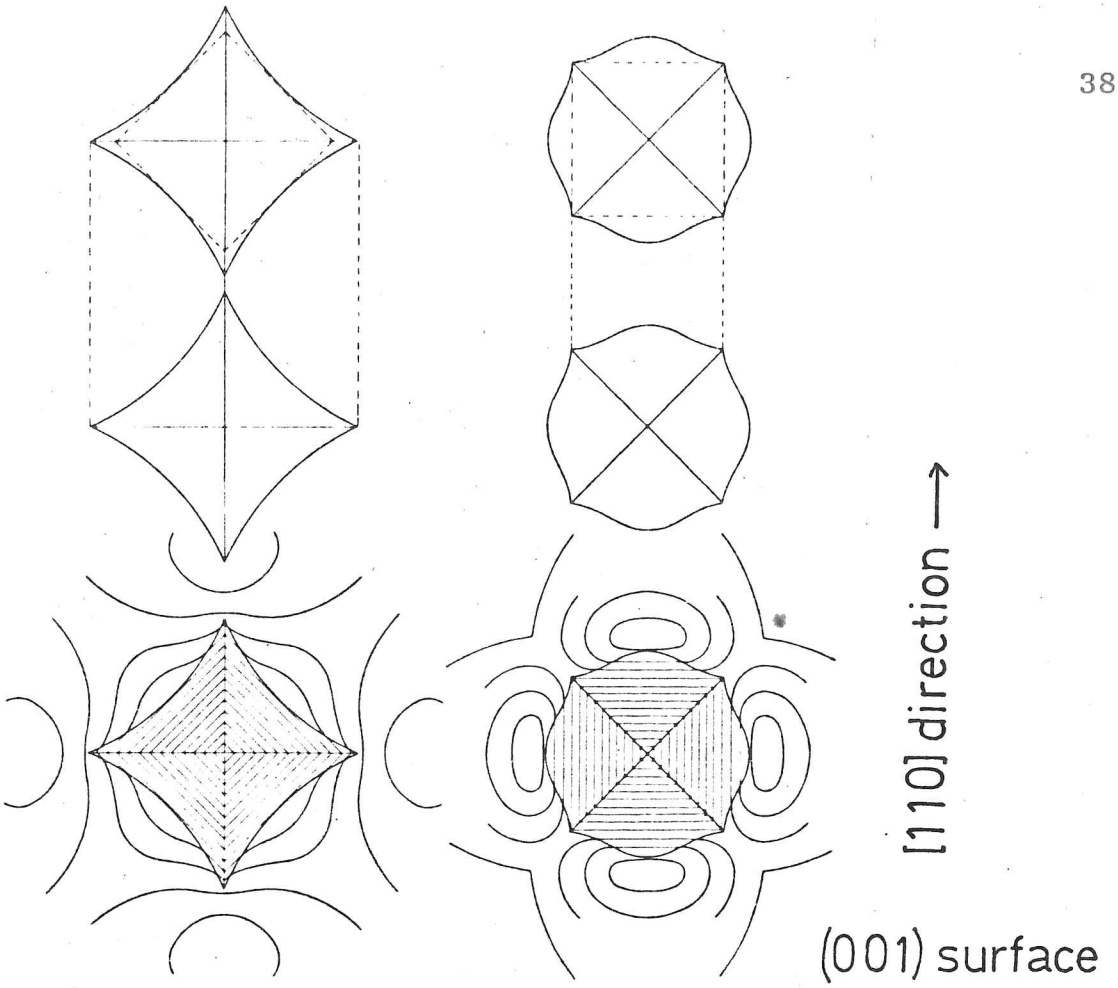

Figure 2/13 (from Buckle (1960))

Diagrams of Vickers indentations on a single crystal of aluminium, orientated at 45° to one another, showing the effects of crystallographic pile-ups. The contours shown in the bottom figure correspond to expected fringes (see 2/14).

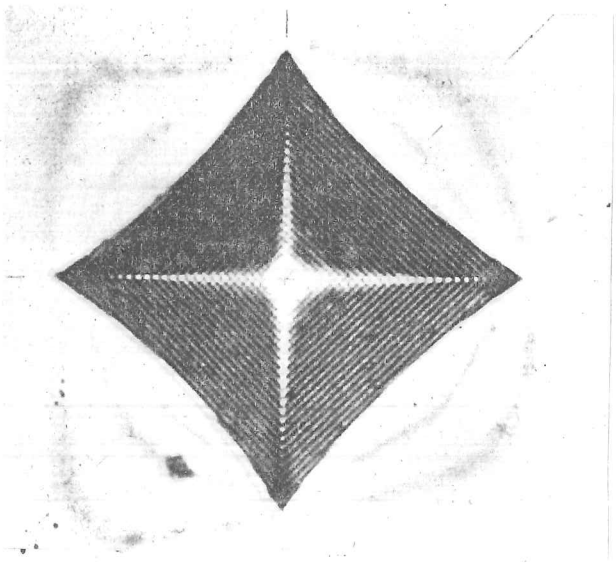

Figure 2/14 (from Buckle (1960))

Interference micrograph of an indentation in a single crystal of Al.

performed on alkali halides is probably due to the difficulty of preparing non-workhardened surfaces from materials which cannot be cleaved. Some of the conclusions of the work of the authors mentioned above will now be summarised.

Indentation Plasticity in Ductile Crystals

In section 2.1.3, pile-up and sink-in adjacent to the faces of indentations in isotropic materials were shown to cause 'barrelling' and 'starring' of the indentations. This was due to the work-hardening characteristics of such materials. In a single crystal, 'barrelling' and 'starring' occur according to the orientation of the indentation: the pile-ups are produced only in certain directions because material displacement occurs via the mechanism of slip, which can only occur in certain directions in the crystal. Figures 2/13 and 2/14 show the effect for indentations on the (001) surface of aluminium single crystals.

There is a third mechanism for barrelling/starring of indentations which can also only occur in anisotropic materials, but which does not depend, as do the work-hardening and crystallographic slip mechanisms, on the formation of surface pile-ups or sink-ins. This is anisotropic elastic recovery. This is discussed in detail in section 4.2.2 but it can be seen to have had no effect on the aluminium in figure 2/14, as the interference fringes on the sides of the indentation are straight. If elastic recovery had occurred, they would be curved because the indentation would have recovered more across its faces than along the diagonals (see section 2.3.2).

Indentations made in almost any ductile or semi-brittle single crystal exhibit rays of dislocations which radiate from the contact point in specific crystallographic directions. These can be revealed by etching, whereby the etch pits form a 'rosette' surrounding the indentation. This has been performed for silver crystals by Chen and Hendrickson (1973). Alternatively, the dislocation rays can be observed by transmission electron

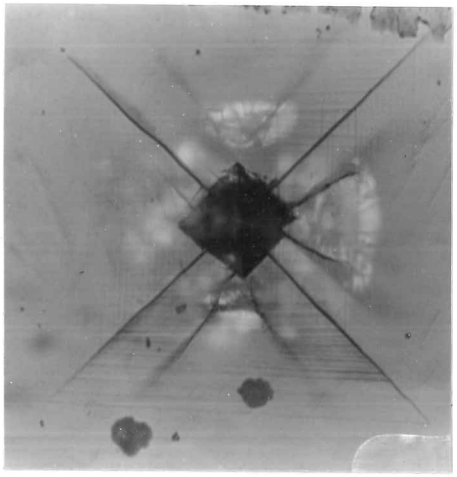

Figure 2/15

Optical micrograph of a 1000 gf. Vickers indentation on the (001) surface of an MgO single crystal.
325x
Note the slip steps along ⟨010⟩ directions and the cracks along ⟨110⟩ directions.

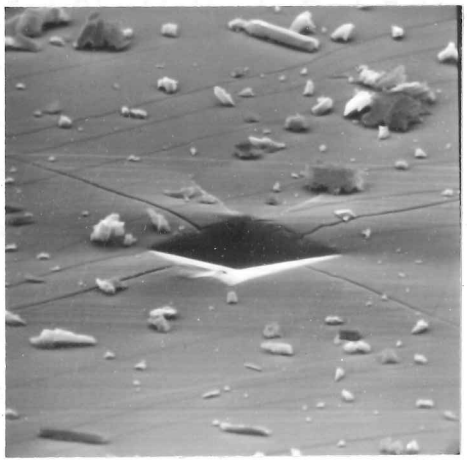

Figure 2/16

SEM micrograph of a 300 gf. Vickers indentation on the (001) surface of a freshly cleaved MgO single crystal.
1000× 75° tilt, 30kV
Note the pile-ups in addition to the slip steps and cracks.

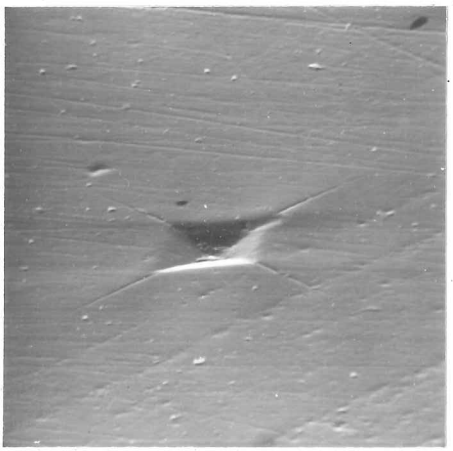

Figure 2/17

SEM micrograph of a 100 gf. Vickers indentation in a single crystal of LiF on the (001) surface.
220× 75° tilt, 30kV
Note the ⟨110⟩ cracks and the slight pile-up.

microscopy (TEM) (e.g. Leiko et al.1977). These investigations show that both dislocation slip towards the surface (in silver and molybdenum) and prismatic punching of dislocation loops (in molybdenum) can accommodate material displaced by the indenter.

The study on silver shows that there is a pronounced indentation size effect on both the hardness and the relative rosette size in this material. Smaller indentations cause lower hardnesses to be measured and have proportionally longer dislocation rays associated with them, but no explanation was advanced for this behaviour.

Indentation Plasticity in Semi-Brittle Crystals

Plastically formed indentations and dislocation etch pit rosettes are easily observed in semi-brittle materials because of the simplicity of preparing clean, non-workhardened surfaces by cleaving or mechanical polishing (e.g. Keh 1960, Burnand 1972). TEM observations have also been made of the dislocations in many brittle and semi-brittle solids, e.g. MgO (Velednitskaya et al.1975), Al_2O_3 (e.g. Hockey 1973), Si (e.g. Hu 1975) and SiC (e.g. Hockey et al.1978). These materials form plastic indentations by the operation of primary dislocation slip and secondary plasticity mechanisms, which may be slip on secondary slip systems or a variety of more unusual mechanisms (see section 2.2.1). The secondary mechanisms are presumed to operate because, in semi-brittle materials, primary slip cannot accommodate the arbitrary strain imposed by the indenter (see section 2.3.2).

Primary Slip in Halite Structure Crystals

The dominant and most obvious deformation mechanism in halite structure crystals is primary slip on the $\{110\}\langle 1\bar{1}0\rangle$ slip system. The geometry of dislocation loops on the slip planes has been studied in detail by many researchers for NaCl, LiF and MgO. It has been observed that, depending on the orientation of the particular $\{110\}$ slip plane with respect to the surface of the crystal, the loops sometimes surround the indentation

and sometimes do not (Nadgornii and Stepanov 1963, Patel and Sutaria 1971). The lengths of the dislocation rays on the slip planes at 90° to the surface are usually shorter than those rays on slip planes at 45° to the surface, but not always, and the relative lengths of the rays depends on the homologous temperature, the load, and the indentation rate (Boyarskaya and Grabko 1973, Pande and Murty 1974).

The diversity of dislocation geometry on just the six {110} slip planes is further complicated by the presence of cracks on the {110} planes perpendicular to the indented surface (see figures 2/15 and 2/16) which occur in the harder crystals (e.g. MgO and x-irradiated LiF). These cracks are nucleated* by dislocation reactions (Keh 1960) and they can be seen in figures 2/15 and 2/16 to extend to the exact limit of the area covered by the slip steps parallel to {010} directions. These slip steps are caused by slip on the {110} planes at 45° to the surface. Figure 2/15 shows four other small cracks, also roughly parallel to {110}, and two more of the same type can be seen in figure 2/16. These appear to be related to the subsurface lateral cracks (white areas in figure 2/15). However, it should be noticed that no cracks are observed on {100} planes, the normal cleavage planes for halite structure crystals.

Figure 2/16 shows the surface topography effects which cause orientation-dependent 'barrelling' and 'starring' of indentations in halite structure crystals in the same way that they are caused in ductile metal crystals. This has been observed in LiF as well as in MgO (see figure 2/17 in which the indentation is orientated to produce a starred indentation). The cracking and pile-up are less pronounced than in MgO, and no slip steps are visible, but the deformation clearly has the same geometry as that shown in figure 2/18, which is from Armstrong and Wu's paper (1978) in which the detailed dislocation movements causing the pile-ups and surface grooves are described. (Figure 4/40 in section 4.5.3 shows the effect of temperature on the surface topography in MgO.)

---

*Footnote: The cracks are presumed to grow according to the theories of indentation fracture mechanics (Lawn and Swain 1975).

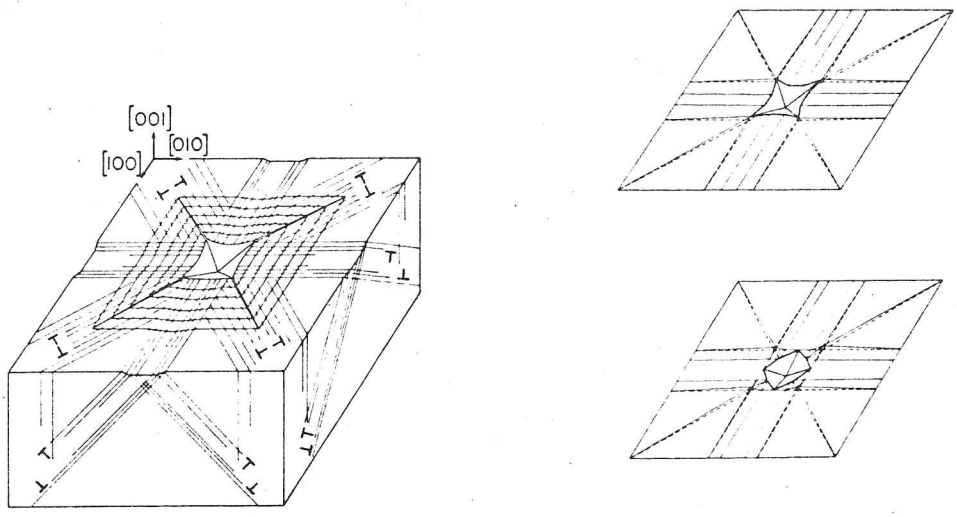

Figure 2/18 (from Armstrong and Wu (1978))

Diagrams of indentations in MgO showing the dislocation rays, slip steps, cracks and the process whereby surface topography affects the shapes of the indentations.

Secondary Slip in Halite Structure Crystals

In halite structure crystals, high ionic polarisibility and high homologous temperatures encourage slip on the $\{100\}\langle 1\bar{1}0\rangle$ slip system (Gilman 1959, Hulse et al. 1964). In MgO, the critical resolved shear stress (CRSS) for yield on the secondary slip system is about 100 times that on the primary slip system at room temperature, i.e. 0.09 T_m (Hulse et al. 1964) and $\{100\}\langle 1\bar{1}0\rangle$ dislocations are not observed around indentations either by etch pitting (Burnand 1972) or by TEM (Velednitskaya et al. 1975*). However, at 1600°C (0.59 T_m), the CRSS is only twice as great as that of the primary slip system (Hulse et al. 1964) and, in fact, general ductility is observed in MgO single crystals above 0.43 T_m (Day and Stokes 1964) since

---

*Footnote: Velednitskaya et al. claim to have observed $\{100\}\langle 1\bar{1}0\rangle$ dislocations beneath indentations, but close examination of the structure of the edge dislocations in their critical micrograph reveals that it has been misorientated by 45° with respect to the other TEM micrographs.

at these temperatures, diffusion-controlled creep mechanisms become important. Below 800 C°(0.34 T_m), there are no creep mechanisms active in bulk MgO, and it is even impossible for slip bands on two {110} planes at 90° to one another to interpenetrate (Day and Stokes 1964). However, slip on {100} planes may be facilitated beneath indenters by the high hydro--static pressure. Pressures in excess of 0.6 GPa have been observed to make general plasticity possible in polycrystalline MgO at room temperatures (Auten and Radcliffe 1976). The mechanism of this effect is thought to be easier slip on {100} planes caused by compression of the dislocation cores (Haason 1974). However, slip nucleated cracking (as around indentations) limits the ductility of polycrystals even at 1.0 GPa. The hydrostatic pressures beneath indentations are probably of the same order as the hardness, which for MgO at room temperature is about 8 GPa, and such a high pressure may make non-slip plasticity mechanisms possible (see below). Nevertheless, there is indirect evidence for the occurrence of $\{100\}\langle 1\bar{1}0\rangle$ slip in MgO at room temperature from the study of hardness anisotropy and anomalous indentation creep (see below).

Zaitsev et al.(1977) have measured a higher flow stress in hydrostatically compressed NaCl, and cross slip on {100} and {111} slip planes has been observed in NaCl at room temperature by TEM (Strunk 1975, 1977), presumably because, although pressurisation increases the flow stress, the increase is less for secondary slip systems than for the primary slip systems.

Hardness Anisotropy and Indentation Creep Evidence for Secondary Slip

The results of Brookes et al.(1975) on the inversion of the hardness anisotropy in alkali halides at high homologous temperatures and long indentation times were summarised in section 2.3.3. The high temperature/ long dwell time anisotropies are typical of those observed in materials in which $\{100\}\langle 1\bar{1}0\rangle$ is the primary slip system (e.g. PbTe - Gilman (1959)).

Although etch pitting showed no trace of $\{100\}\langle 1\bar{1}0\rangle$ slip for the

high temperature/long dwell time indentations, it is thought that secondary slip may occur only in a localised zone directly beneath the indenter. This can be compared with the situation for α-SiC, where $\{1\bar{1}00\}\ \langle 11\bar{2}0\rangle$ slip is known to control the hardness anisotropy on $\{0001\}$ surfaces (Adewoye 1976, Sawyer 1979, Sawyer et al.1979), but etching reveals no rosette at all (Adewoye and Page 1976). Therefore, the tendency towards the inversion of the anisotropy for long indentation times indicates that secondary slip on $\{100\}\langle 1\bar{1}0\rangle$ occurs in MgO at room temperature, despite the lack of direct observational evidence.

Crowdionic Diffusion

The very high hydrostatic pressures and shear stresses beneath indenters can approach phase transformation pressures and the theoretical strength of of solids (see section 2.2.1). These unusual plasticity mechanisms are likely to affect the magnitude, but not the anisotropy, of the hardness if no significant crystallographic channelling of point defect diffusion occurs. Such a mechanism has been proposed for MgO by Velednitskaya et al.(1975) who observed cathodoluminescence surrounding indentations which they claimed was not due to dislocations. A similar 'crowdionic diffusion' mechanism has also been proposed to explain the formation of plastic indentations in Al_2O_3 (Rozhanskii et al.1970).

Indentation and Rosette Size Effects

Since the identity of the primary active slip system and the geometry of the dislocation loops around indentations are well known for halite structure crystals, it is surprising that the relationships between the dimensions of the dislocation rays, the sizes of the indentations, the measured hardnesses and the critical resolved shear stresses (for primary slip) are still unclear.

Firstly, the relationship between the diameter of the etch pit rosette extending in $\langle 110\rangle$ directions on (001) planes and the size of the indentation will be considered. A micrograph of such a rosette is shown in figure 2/19.

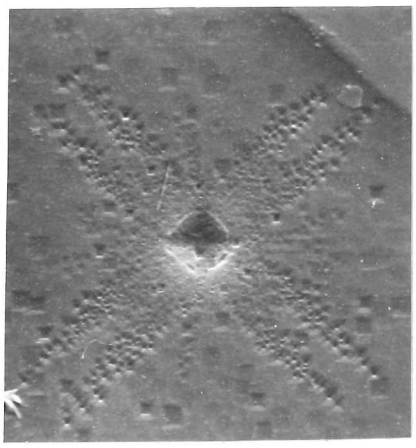

Figure 2/19

SEM micrograph of a 5 gf. Vickers indentation in LiF etched to display the etch pit rosette.
3000× 30kV, 30° tilt

It is not known whether the dislocations in the rays exert a significant back stress on the indenter when it is loaded, and hence whether the dislocation mobility along the rays determines the hardness, or whether the size of the indentation is almost entirely controlled by mechanisms directly beneath the indenter (which would involve secondary mechanisms in addition to primary slip). If secondary mechanisms are important, then the rosette size and the measured hardness should be fairly independent and the ratio of the rosette diameter (D) to the indenter diameter (d) can be expected to vary over a wide range for different crystals. Naturally, since the dislocations in the rays accommodate material displaced by the indenter, the sizes of the rosette and the indentation will never be completely independent.

In any one type of crystal, the size of the indentation can be varied by changing (a) the load on the indenter, (b) the orientation of the indenter on the crystal, or (c) the 'intrinsic' hardness of the crystal. This latter quantity may be varied by changing the proportions of solute elements, by irradiation hardening (either by electronic damage, or by electronic and displacement damage), or by changing the dislocation density. Any of the above treatments can be used to investigate the relationship between the rosette size and the indentation size, and hence to investigate the relative importance of the dislocation rays and the mechanisms operating only beneath the indenter.

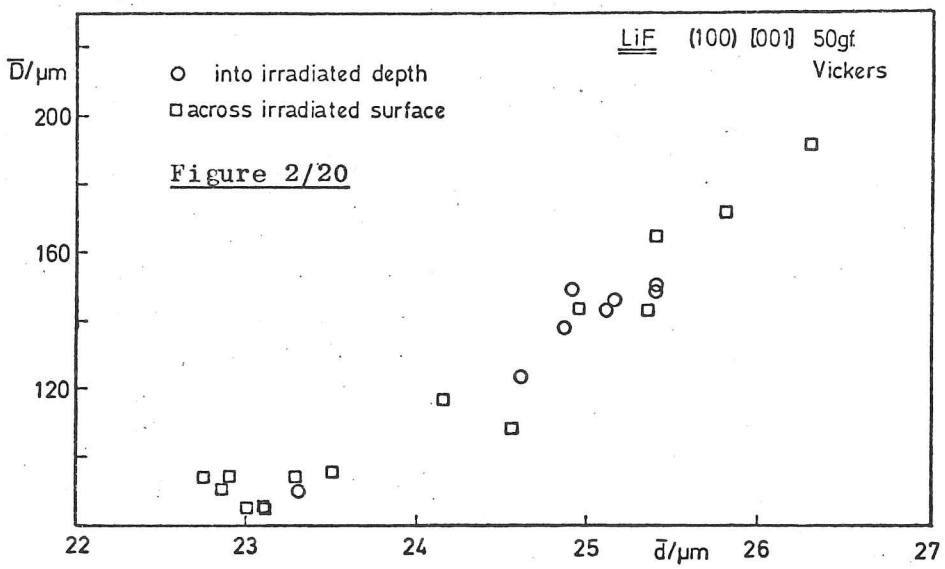

Figure 2/20

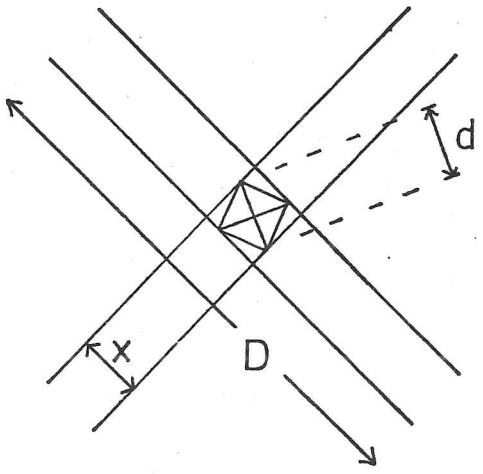

Figure 2/21

Diagram of an indentation and rosette showing the lengths mentioned in the text.

Burke and Auckland (1978) have examined the effects of orientation, load and irradiation hardening on the ratio $\bar{D}/\bar{d}$ ($\bar{d}$ is the arithmetic mean of the two diagonal measurements of an indentation, $\bar{D}$ is similarly defined). The results of the irradiation hardening experiment (Cr Kα x-rays were used) are shown in figure 2/20. It appears that there is no simple relationship between '$\bar{d}$' and '$\bar{D}$' for the effects of orientation and load (10 gf. to 100 gf.), but there appears to be a linear relationship for different degrees of irradiation hardening.

Savenko and Shchukin (1976) also found a lack of proportionality between '$\bar{d}$' and '$\bar{D}$', but found a constant ratio between the indentation

size and the width (x) of the dislocation rays for indentations made over a range of loads in both NaCl and LiF. This is not surprising, as the width is closely related to the caliper diameter of the indentation in the direction of the ray (see figure 2/21). Conversely, Varchenya et al. (1970) found that the d/D ratio remained constant in LiF for indenter loads between 1 gf. and 20 gf.

Clearly, there is scope for a systematic investigation to be made of the relative sizes of indentations and rosettes in alkali halides by means of the methods suggested above. The estimates of the relative significance of the primary and secondary plasticity mechanisms, which could be derived from such an investigation, are not readily obtainable by any other method. This is further discussed in section 4.5.3.

Rosette Size and CRSS for Primary Slip

Whatever the relationships between deformation under the indenter and the propagation of dislocations along the rays, it is clear that the length of the ray will depend on the mobility of dislocations on the primary slip system.

Hopkins et al.(1973), using doped KCl, found an inverse proportionality between the ray length and the CRSS for primary slip. However, this held only for the harder, more heavily doped, crystals, and the more complex relationship for the softer crystals was interpreted as being due to subgrain boundaries, or other macroscopic defects, on a larger scale than that of the doping ions. This could, perhaps, be further investigated by measuring the indentation size effect on the rosette size.

Davidge (1967) found that there was a direct proportionality between CRSS and ferric ion content in iron doped MgO and that the relationship between CRSS and ray length was monotonic, though not linear, and that even the ℓg(CRSS)/ℓg(ray length) relationship was not linear over the whole range.

Thus, measurements of the rosette size can be used to measure the CRSS, but only if the effect has been calibrated first.

2.4.2 Microhardness Anisotropy Models

Any model which can predict hardness anisotropy must examine the effect of the orientation of the indenter on the shear stress resolved onto all the possible active slip systems in the material. If all the slip systems have a low resolved shear stress then that indenter orientation is predicted to be hard. Unfortunately there are no exact descriptions of the stress fields beneath real pyramidal indenters and so a simplified approximation for the stress field has to be used. Wonsiewwicz and Chin (1973) calculated the stress for a simplified indenter (a wedge) whereas Brookes, O'Neill, and Redfern (1971) assumed a simplified stress state next to the indenter and included an extra constraint factor to allow for some of the imperfections of this simplification.

In order to resolve stresses onto the slip systems the material next to the indenter is assumed not to rotate during indentation (Gerk also assumed this in his derivation of equation 2.1.3c) even though the model of Brookes et al (the effective resolved shear stress, or ERSS model) then goes on to use the degree to which the material is left free to rotate as a parameter.

The two types of model will be described and conclusions drawn from the comparison.

The Cylindrically Symmetric Model

Wonsiewicz and Chin's analysis likens a Knoop indenter to a wedge with the same included angle (25°) and assumes that the stress field is the same as that surrounding and expanding cylindrical cavity (Hirst and Howse, 1969). No allowance is made for the fact that there is a free surface bisecting the cylinder and therefore it is implicit

that the expected hardness anisotropy will be only direction dependent, that is the same hardness will be predicted if the long axis of the indenter is along [uvw], whichever of the planes in that zone is the surface being indented. This corroborates with the experimental data for Al single crystals (Garfinkle and Garlick, 1968) and for SrF_2, BaF_2, NaCl, and AgCl (Chin et al, 1972, 1973) and, perhaps, for Cr and V (Alexander and Carlson, 1969) but not with the data for the basal plane of hexagonal metals (Brookes et al, 1971).

The model calculates the work required for the deformation of each volume element to a strain which is related to the average shear strain on a slip system by the Taylor factor (M); this is in turn calculated using the minimum work analysis of Bishop and Hill (1951). To do this a function representing the work hardening ~~of the~~ is required and the Hollomon relation:

$$\sigma = K' \cdot \varepsilon^n \qquad 2.4.2a$$

is used. The expected Knoop hardness number is then proportional to the average work integrated over all the volume elements:

$$KHN = K \cdot 1/\pi \int_{-\pi/2}^{\pi/2} M^{1+n}(\theta) \cdot d\theta \qquad 2.4.2b$$

Using the two parameters 'K' and 'n', very good fits to the data from Al single crystals can be achieved with this method, however, the value of the work hardening exponent (n) thus obtained is found to be too high when compared with the stress-strain curve for Al. This is not surprising as the Hollomon relation is well known (Reed-Hill, 1973; Sargent, 1976) to be extremely unstable in 'n' with respect to very small prestrains in the test material. However, by taking work-hardening into account, this model supplies a parameter (n) which can be used to give a measure of the model's reliability by comparing it with an independently derived value.

The Effective Resolved Shear Stress Models

These models are derived by considering a loaded indenter, stationary with respect to the crystal, for which the effects of its edges and tip on the plasticity are negligible with respect to the effects of its facets . Thus the model situation is a vertically-loaded stationary inclined plane in a perfect crystal, considering each facet individually. To this loaded plane there are two reaction forces in the crystal: a frictional tensile force parallel to the facet plane, and a compressive force normal to it. Either, or both, (Garfinkle and Garlick 1968, Calder and Armstrong 1973), of these forces are then resolved onto the slip systems in the crystal and then the calculation is repeated for the other facet planes and for all indenter orientations. Those orientations where there is a high resolved shear stress on one of the slip systems are predicted to be softer than those where the resolved shear stresses are all low. However, there are various methods which can be used to combine the effects of the indenter facets together and this has been reviewed by Arnell (1974).

The model is modified if the resolved shear stress on each slip system is multiplied by a constraint factor, whose magnitude depends on the relative orientations of the indenter facet and the slip system, and this effective resolved shear stress (ERSS) is then used, as above, to predict the hardness anisotropy. The reason for introducing this constraint factor is to allow for the constraints on the plastic deformation produced by the presence of the indenter (Daniels and Dunn, 1949) and also to introduce a bias in favour of those slip systems which transport material towards the surface (Brookes et al, 1971).

For metals which form pile-ups such a bias is reasonable but for elastic/plastic solids one would expect the Radial Displacement Model to be more appropriate (see 2.1.2), and one would also expect a compressive-force based model to be more accurate than one based on

tensile forces. Nevertheless, although the model of Brookes et al. is based on tensile forces, it is very successful in predicting the hardness anisotropy on MgO, Al_2O_3, SiC (to a degree, see below) and LiF as well as MnS, NaCl, Al, Cu, W, Nb, V, Cr, Ti, Zr, Mg, Zn and Co. Thus the same theory, based on tensile stresses and on the premise that displacements will be surface-directed and not radial, predicts the hardness anisotropies of both elastic/plastic and fully-plastic materials. Hence the conclusion can be drawn that the radial displacement model is not applicable to even the stiffest elastic/plastic solids if they are single crystals.

The stresses in the modelled zone beneath indenters are possibly compressive, despite the success of the model of Brooks et al., Arnell (1974) has obtained a better fit for the anisotropy in Co with a model based on compressive stresses and claims that experiments on twinning in Zn show that the stresses are compressive in reality. This indicates that the success of the ERSS model based on tensile forces alone may be fortuitous and that if the phenomena of yield, flow, work-hardening and a different type of constraint factor were taken into account, a compressive stress based model may prove to be more accurate. However, at present there is no obvious method either for measuring the stresses directly or for extending the model to include yield and flow effects. The constraint factor and the effect of work-hardening will be discussed below.

ERSS Models: Constraint Factors

The constraint function of the ERSS model has a single value which is dependent on the relative orientation of two cartesian coordinate systems: that of the indenter (C_1) and that of the crystal (C_2). The relationship between two such systems is conventionally described by the transformation (M) of one system into the other by successive rotations about three axes by three angles (the Euler angles). These rotations must be done in sequence otherwise the orientation is

ambiguous (Matthews and Walker 1973). Thus:

$$C_2 = M_{SN}(\alpha_3).M_{SD}(\alpha_2).M_F(\alpha_1)\,C_1 \qquad 2.4.2c$$

and M_{SN}, M_{SD} and M_F are defined below.

Consider the cylinder of material parallel to the steepest line (F) in the facet of the indenter (see figure 2/22), H is in the facet and parallel to the surface of the material, G is perpendicular to F and H. If initially AR is parallel to H, SD parallel to G and SN is parallel to F, then first rotate the slip system axes about F by α_1, then rotate about the SD axis (which has moved from G) by α_2, and finally rotate about SN by α_3. α_1, α_2 and α_3 now unambiguously describe the orientation relationship and are suitable parameters to be used in the formulation of the constraint function. However, in the general case these angles are difficult to calculate, since none of the angles marked on figure 2/22 are Euler angles.

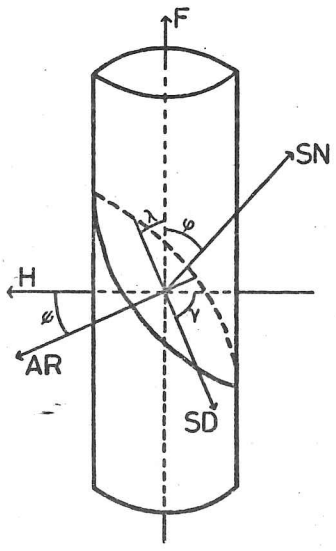

Figure 2/22

There are several conditions which apply to any constraint factor (even before such things as pile-up and radial displacements are considered): firstly, is the slip centrosymmetric ? That is, is (hkl) [uvw] slip exactly the same crystallographically as (hkl) $[\bar{u}\bar{v}\bar{w}]$ slip ? Clearly, if the crystal has no centre of symmetry then the slip direction may be (but not necessarily) polar (Gay, 1972). However, there is no evidence that the critical resolved shear stress for yield of any slip system in any material is affected by the crystal's polarity in this manner; neither is there evidence to the contrary, as no experiments to test this hypothesis appear to have been performed. If one assumes that plasticity is centrosymmetric, even in acentric crystals, then the constraint factor will also be symmetrical with respect to the intervals 0 to 90 degrees and 180 to 90 degrees, nevertheless, the full range 0 to 180 degrees must be used when calculating the constraint factor to prevent ambiguity in the orientation relationship. The centrosymmetric assumption has been implicit in the constraint factors of Daniels and Dunn and of Brookes et al. and this may be why the ERSS model has never been extended to twinning and kinking mechanisms; because these mechanisms are always acentric, and the effect of this on the constraint factor has not been recognised.

The second general condition is that the gradient of the constraint function (CF) would not be reasonably expected to be discontinuous anywhere, for any of its parametrical angles. Thus a boundary condition on the constraint function (CF) would be:

$$\left.\frac{\partial CF}{\partial \alpha}\right|_{\alpha-\delta} = \left.\frac{\partial CF}{\partial \alpha}\right|_{\alpha+\delta} \qquad 2.4.2d$$

where δ is arbitrarily small and α represents any and all of the parametrical angles. Therefore any function which can be expressed as a Fourier series in 3 dimensions over the range 0°to 90° (or, for acentric mechanisms, 0°to 180°) for the three Euler angles, would be a suitable contraint function.

Now, it will be shown below that the exact form of the CF on the

predicted hardness anisotropy is relatively unimportant compared with its boundary conditions. This is fortunate as these boundary conditions are more easily visualised than the CF itself. Neither of the two sets of conditions that will now be described is unambiguous, in that quite different orientations of the indenter to the crystal have the same CF value, therefore they will be described in the same terms as used by their authors, rather than by using the Euler angles. Figure 2/22 shows the coordinate system of the slip system: SN is the slip plane normal, SD is the slip direction and AR is the axis of rotation of the slip system, at right angles to SN and SD. Vector G, which is the direction of the compressive stress, is not shown, but is is perpendicular to F and H, pointing out from the indenter. The angles used by Daniels and Dunn, and Brookes et al., are marked on the diagram.

It must be remembered that the constraint factor merely modifies the resolved shear stress (RSS) and that when this is zero, the value of the CF does not affect the predicted hardness anisotropy. The RSS is zero when ϕ or λ equals 90°.

$$RSS = (L/A).\cos\phi.\cos\lambda \qquad 2.4.2e$$

where L is the load on the cylindrical element and A is its cross-sectional area (see figure 2/22).

Daniels and Dunn used a CF with boundary conditions:
CF = 0 (maximum constraint, ERSS=0) when $\psi = 90^\circ$ and
CF = 1 (minimum constraint, ERSS=RSS) when $\psi = 0^\circ$.
They argued that then $\psi = 0^\circ$ there was no constraint on the rotation of the slip system, as deformation proceeded, about its axis AR, whereas when $\psi = 90^\circ$, the axis AR was perpendicular to the facet of the indenter and the slip system could not rotate.

This may be visualised more easily if two more elements are considered: parallel cylinders, exactly like that shown in figure 2/22, placed either side, with the same H and parallel F vectors. There will be high constraint on material being displaced sideways, into one of the

adjacent cylinders, and less constraint on material being displaced outwards and upwards, towards the surface (assuming the formation of surface pile-ups). When ψ is near 90°, material is being rotated into neighbouring elements, when ψ is 0°, material is displaced upwards. This constraint factor is shown explicitely in equation 2.4.2f.

$$CF = \cos\psi \qquad 2.4.2f$$

Brookes et al. found that the Daniels and Dunn model was incomplete because dislocations were observed on slip planes in MgO for orientations of the indenter where the Daniels and Dunn model predicted a zero ERSS. Therefore Brookes et al. modified the CF such that a finite ERSS was predicted for the relevant slip planes.
Brookes et al. used the boundary conditions:
CF = 0 (maximum constraint, ERSS=0) when $\gamma = 0^\circ$ (which makes $\psi = 90^\circ$) and
CF = 1 (minimum constraint, ERSS=RSS) when $\psi = 0^\circ$ (which makes $\gamma = 0^\circ$)
Thus Daniels and Dunn's criteria are retained, but the degree of freedom for the condition of maximum constraint is reduced such that it is only attained when the slip direction is parallel to the horizontal in the facet of the indenter (H). This is because if γ exceeds 0 then the slip plane can rotate even when ψ is close to 90 . However, if the situation where both γ and ψ are close to 90 is visualised, the CF takes a value close to 0.5 but the material can still only rotate into neighbouring cylindrical elements. This apparent defect of the constraint factor of Brookes et al. has little impact on the predicted hardness anisotropy because, in such a position, the RSS is close to zero (Sawyer 1979, Brookes 1979). However, Burnand (1972) found slip on planes in MgO for which the predicted ERSS (using Brookes' CF) was zero, therefore this CF is no better than that of Daniels and Dunn, apart from its empirical success for a wide range of materials. The analytic description of the CF used by Brookes et al. is given in equation 2.4.2g.

$$CF = \tfrac{1}{2}(\cos\psi + \sin\gamma) \qquad 2.4.2g$$

Here I will suggest boundary conditions which are appropriate for a model based on centrosymmetric slip. If they were to be incorporated into a program to make hardness anisotropy predictions they should be expressed

in terms of Euler angles, and the analytic formulation, from the boundary conditions given, would not be as simple as that of the Daniels and Dunn, and of Brookes et al..

1. For the constraint due to the static presence of the indenter:-

a) low constraint when the slip direction is parallel with the indenter facet,

b) high constraint when the slip direction is directed towards, or away from, the indenter facet, i.e. parallel to G.

2. For constraint due to adjacent elements:-

a) low constraint when the axis of rotation is parallel to the facet horizontal H,

b) high constraint when the axis of rotation is perpendicular to the facet horizontal H (these are Daniels and Dunn's criteria).

3. For constraint due to preference for the formation of pile-ups rather than for the displacement of material radially:-

a) low constraint when the axis of rotation is parallel to H,

b) high constraint when the axis of rotation is parallel to F.

These constraints are appropriate for both tensile- and compressive-stress based models, or for models which use a mixture of compressive and tensile stresses (e.g. Armstrong and Raghuram 1973).

It can be seen that once the boundary conditions have been decided upon, the exact formulation of the CF itself is somewhat arbitrary; generally there are an infinite number of Fourier series which will fit the boundary conditions. Daniels and Dunn, and Brookes et al. used the simplest formulation. However, if several functions are used, it is possible to examine the stability of the whole model with respect to small changes in the CF. I suggest that if wildly different hardness anisotropies are predicted using slightly different CFs for a particular slip system - indentation section geometry, then the model's predictions should be treated with great suspicion as, after all, the "real" form of the CF is unknown. Conversely, if several different CFs produce predictions which are closely in agreement, then they can be used with a corresponding degree of confidence.

Different constraint functions have been used to predict the hardness

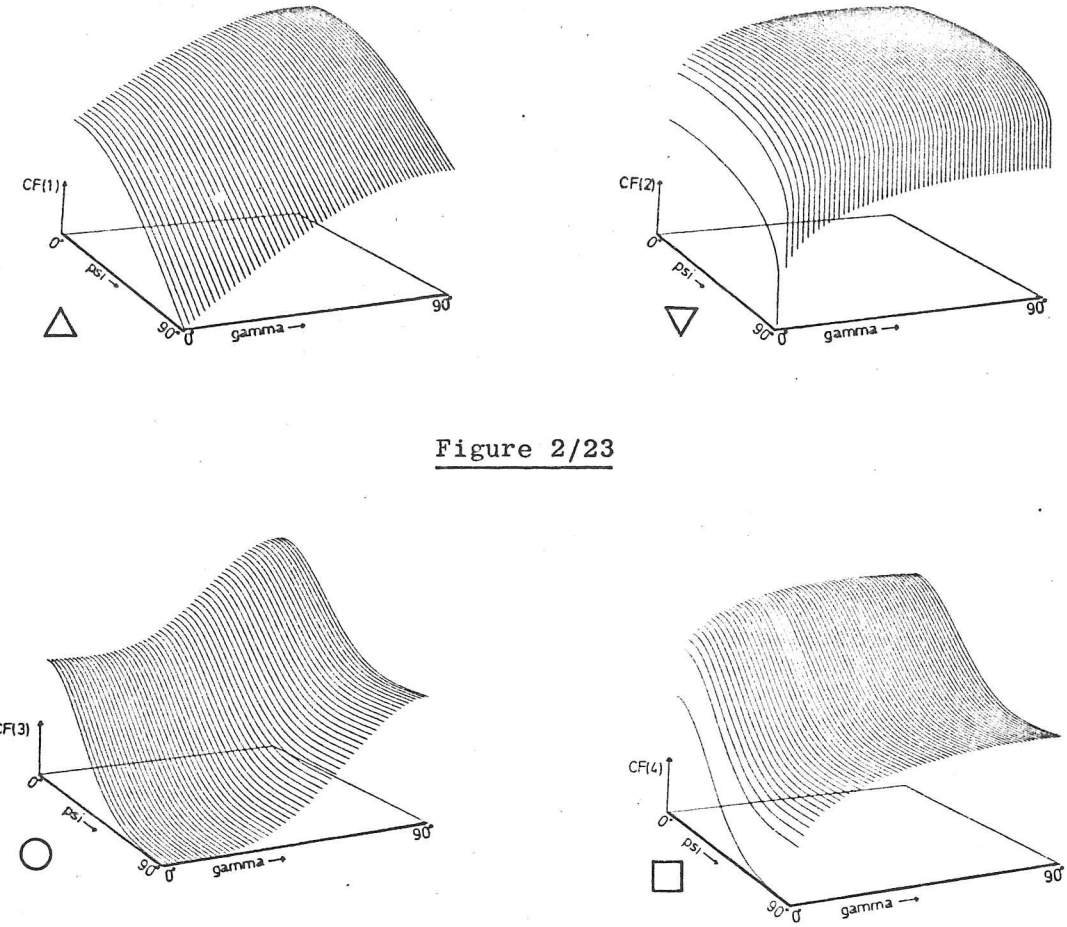

Figure 2/23

anisotropy on the basal plane of α SiC single crystals, all the CFs satisfy the boundary conditions of Brookes et al.

CF(1)	=	$\frac{1}{2}(\cos\psi + \sin\gamma)$	△	2.4.2h
CF(2)	=	$\frac{1}{2}(\cos^{1/4}\psi + \sin^{1/4}\gamma)$	▽	2.4.2i
CF(3)	=	$\frac{1}{2}(\cos^{4}\psi + \sin^{4}\gamma)$	○	2.4.2j
CF(4)	=	$\frac{1}{2}(\cos^{4}\psi + \sin^{1/4}\gamma)$	□	2.4.2k

These four functions are plotted against ψ and γ in figure 2/23, the symbols next to the equations and the figures serve to identify the predicted hardness anisotropies in figure 2/24.

The ERSS model has been revised using the ideas of Arnell (1974) concerning the method by which the calculated constraints on the slip systems due to each of the four facets of the indenter are merged to produce a predicted hardness anisotropy. This revised model (the program is listed in appendix I) produces a value 'f' for each orientation of the indenter on the surface of the crystal.

From equations 2.4.2e and 2.4.2h to k, 'F_i' is defined for the i'th facet of the indenter, for a particular constraint factor, by:

$$ERSS = (L_i/A).F_i(\phi, \lambda, \gamma, \psi) \qquad 2.4.2\ell$$

An ERSS value is calculated for each facet of the indenter using this equation then, assuming equal strains under each facet of the indenter and no work hardening, the pressure acting over the indenter (the hardness) is proportional to the sum of the stresses over the four facets:

$$H \propto \sum_{i=1}^{4}(L_i/A) \qquad 2.4.2m$$

But, for yield beneath the indenter facets to occur, the ERSS must equal the CRSS on the relevant slip system(s). Thus, from equation 2.4.2ℓ :

$$\frac{L_i}{A} = \frac{CRSS}{F_i} \qquad 2.4.2n$$

Therefore:

$$H \propto CRSS. \sum_{i=1}^{4} (1/F_i) \qquad 2.4.2o$$

and defining 'f' by:

$$f = \sum_{i=1}^{4} (1/F_i) \qquad 2.4.2p$$

gives a proportionality between the hardness and the geometrical factor 'f':

$$H \propto CRSS.f \qquad 2.4.2q$$

and 'f' is calculated for each slip system, for each crystal section and for every orientation of the indenter on that section.

If yield and flow on indentation occurs only on the primary slip system (the one assumed by the model), with no work-hardening, then the measured hardness for any orientation would be expected to be directly proportional to 'f' for that orientation. Predicted Knoop 'f' anisotropies for the {0001} surface of 6H αSiC (see Ramsdell (1947) for the notation system for SiC polytypes) are shown in figure 2/24 for four possible slip systems using all the four constraint factors described above (figure 2/23).

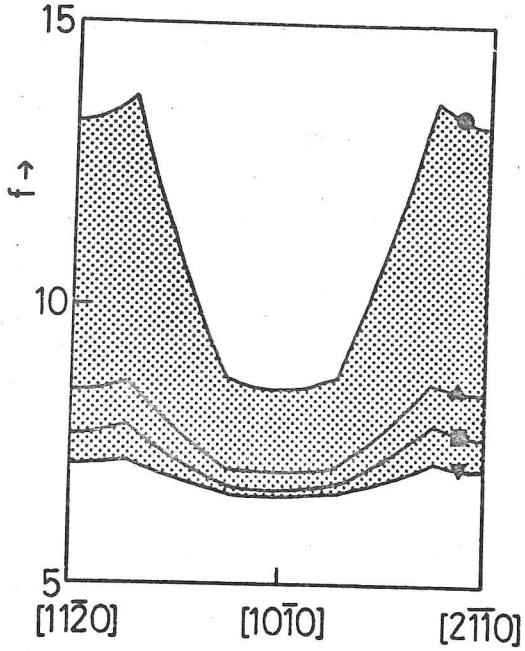

slip system $\{0001\}\langle 11\bar{2}0\rangle$

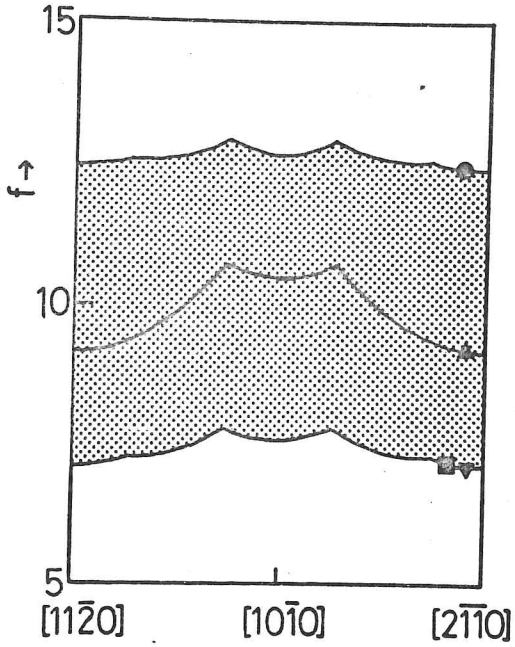

slip system $\{1\bar{1}00\}\langle 11\bar{2}0\rangle$

Figure 2/24 - 'f' plots on {0001} 6H SiC

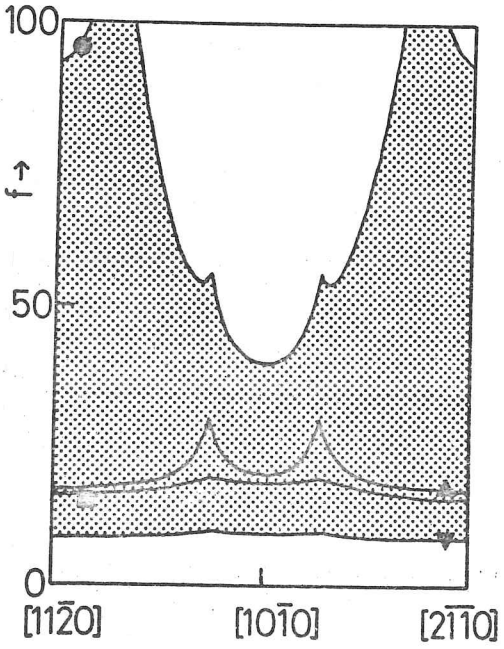

slip system $\{3\bar{3}01\}\langle 11\bar{2}0\rangle$

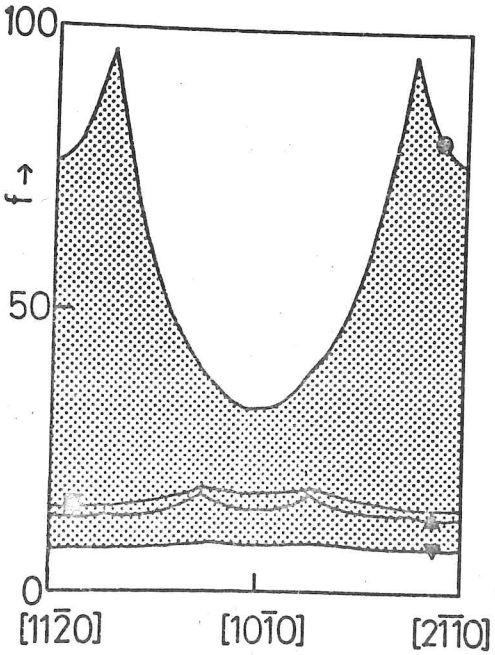

slip system $\{1\bar{1}01\}\langle 11\bar{2}0\rangle$

Figure 2/25

A plot of Sawyer's results (Sawyer 1979) for the Knoop hardness anisotropy on the basal plane of 6H SiC.

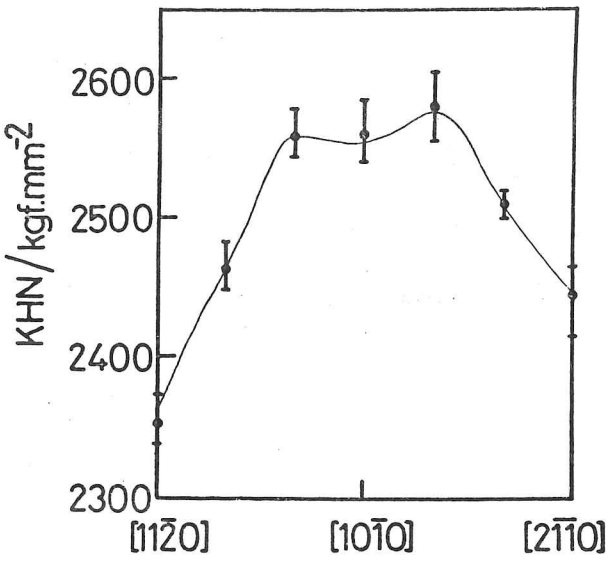

Sawyer's results for the experimental hardness anisotropy are shown in figure 2/25 and will be compared with the predicted hardness anisotropies. The predictions using the pyramidal slip systems (slip on the $\{3\bar{3}01\}$ and $\{1\bar{1}01\}$ planes) can be seen to be much more unreliable than those on the basal and prismatic planes as a much greater range in 'f' values for different CFs is predicted for the pyramidal slip systems. Comparing the prismatic slip and basal slip predictions with the experimental results it can be seen that prismatic slip probably dominates the anisotropic deformation mechanisms when αSiC is indented on the basal plane. Without using the different CFs, one might have been able to conclude that any slip of the type $\{h\bar{h}0\ell\}\langle 11\bar{2}0\rangle$ was responsible; in fact, this is still the correct interpretation as the unreliability of the model for pyramidal slip does not mean that those slip systems do not operate in reality.

The operative slip systems for indentation on the prismatic planes of 6H SiC are thought to be both $\{0001\}\langle 11\bar{2}0\rangle$ and $\{1\bar{1}00\}\langle 1\bar{1}20\rangle$, but they operate for different orientations of the indenter. This has enabled an estimate to be made (Sawyer, Sargent and Page 1979) of the relative critical resolved shear stresses on these two systems. Basal slip is thought to have a CRSS between 1.2 and 2.1 times that for prismatic slip (Sawyer, Sargent and Page 1979).

ERSS Models: Work-Hardening

The ERSS model was originally devised without any consideration of the work hardening which usually accompanies indentation. Calder and Armstrong (1973) put forward the suggestion that a degree of work hardening was equivalent to an increase in the critical resolved shear stress and was, itself, dependent on the relative orientations of the indenter and the slip system:

$$KHN \propto \frac{(CRSS + wht)}{\text{orientation dependent factor}} \qquad 2.4.2r$$

whereas Arnell used:

$$KHN \propto (CRSS \cdot \text{orientation dependent factor}) + wht \qquad 2.4.2s$$

and considered that the work hardening term (wht) was probably only weakly dependent on orientation as the work hardening of single crystals (assuming stage III slip) is very similar for different orientations. He considered that work hardening would increase the hardness in all indenter orientations and thus would decrease the magnitude of the anisotropy. Conversely, equation 2.4.2r indicates that even if wht itself is independent of orientation, it will nevertheless increase the magnitude of the hardness anisotropy.

The reason why these alternative formulations were put forward is easy to see, Arnell found that the theory (without work hardening) predicted a larger anisotropy than he observed in Co, whereas Calder and Armstrong found that the theory predicted a smaller anisotropy (by 50 or 60%) than they observed in Ni, Al, Cu, and Fe-Si3%. However, there is a real difference between 2.4.2r and s, in that in the former the CRSS for each slip system is replaced by (CRSS + wht), whereas in the latter the amount of hardening under each facet of the indenter is assumed to be independent of both the yield stress (CRSS) under that facet and the yielding and work hardening under the remaining facets. Thus Calder and Armstrong's theory (eqn.2.4.2r) makes more sense, with the proviso that Arnell is probably correct (eqn.2.4.2s) when he suggests that

the wht is not itself dependent on the relative orientations of the indenter and the slip system.

Conclusions

This review of geometrical models of hardness anisotropy has, so far, omitted an important problem; the difficulty of knowing when a model does adequately describe the data and when it does not. For example, Brookes et al. considered their efforts successful when they were able to predict that the hardness on the basal plane of SiC was higher in the $\langle 1\bar{1}00 \rangle$ direction than in the $\langle 11\bar{2}0 \rangle$ direction, and similarly with two other pairs of directions on the two prism planes. Later work (Sawyer 1979, Sawyer et al. 1979) has shown that between these specific orientations the anisotropy is complex and cannot be explained by assuming deformation only by a single slip system.

By using different boundary conditions for the constraint function, different hardness anisotropies can be predicted for the same slip system, and by "fine-tuning" the constraint function, within the same boundary conditions, it may be possible to produce any "required" prediction from any slip system. Then, if the magnitude of the anisotropy is either too large or too small, a "suitable" work hardening term could be used to make the final fit.

Thus the models as they stand now have too many degrees of freedom when compared with the sparse experimental data, often of dubious reiability, available. An authoritative model may emerge broadly on the lines of those described here, but only when researchers who appreciate the problems of making reliable microhardness measurements have accumulated a very much larger volume of experimental data.

2.4.3 Vickers and Knoop Hardness Anisotropy

From the arguments presented in the preceeding sections it can be seen that although most studies on hardness anisotropy have been done using Knoop indenters, the bulk of the work on stress analysis, indentation shape and rosette formation have been done for Vickers indenters. Therefore it is fairly important to know whether the two indenters measure the same anisotropy. One would expect the Vickers indenter to show a smaller magnitude of anisotropy, that is, a smaller fractional difference between the hardest and softest directions, because the stresses beneath Vickers indenters are known to approximate to a hemispherical symmetry quite close to the indenter (at least in isotropic materials such as steel (Samuels and Mulhearn (1957)). The Knoop indenter is closer to a wedge shape, and the behaviour beneath the two indenters can be expected to be quite different despite the similar angles the indenters' facets make with the material's surface: 22° for Vicker's and 25° for Knoop's (perpendicular to the long axis)..

One way of comparing anisotropies measured by the two indenters is to take the arithmetic mean of the KHN with the KHN for the orient--ation at 90 degrees (figure 2/26):

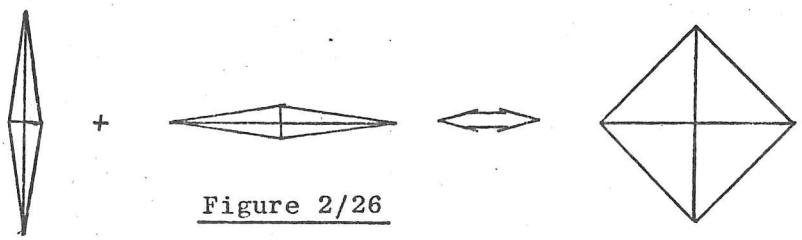

Figure 2/26

Armstrong and Raghuram (1973) have shown that this method produces identical Vickers and 'pseudo-Vickers' hardness anisotropies for Niobium single crystals, but does not fit the data for MgO as the VPN and KHN anisotropies are 45 degrees out of phase. They explain this as being

due to the $\{110\}_{90}$ cracks surrounding the Vickers indentations changing the stress field to one with significant stresses normal to $\{110\}_{90}$. However, these cracks are nucleated and grow by dislocation reactions (Keh 1959, 1960) and the reason they do not form around Knoop indentations is that, for the same load, a Knoop indentation is much shallower and displaces less material than a Vickers indentation (Burnand 1972).

It will be shown in section 4.2.3 that the different hardness anisotropies measured by the two indenters in MgO are due to the crystal's restricted capacity for slip and the different shapes of the two indenters.*

In some materials the Young's modulus to yield stress ratio (E/Y) will affect the measured hardness anisotropy if either the modulus or the yield stress is anisotropic. This is the case for orientated polymeric materials Balta-Calleja and Bassett 1977) in which the Vickers and Knoop hardness anisotropies are 90° out of phase. The question of the 'correct' hardness anisotropy of materials with orientated microstructures and the problems of elastic recovery which affect the measurement will be discussed in section 4.2.2 in the light of experimental evidence.

While different methods of measuring hardness anisotropy are being discussed, it is relevent to mention scratch hardness testing. Hardness anisotropies measured by this method are generally not centrosymmetric, as they have to be when measured by Vickers or Knoop indentation (these indenters have 4mm and 2mm plane symmetry respectively) and often the magnitude of scratch anisotropy is greater than that measured by indentation. A brief review of the subject and a description of a model similar to the ERSS model for indentation hardness anisotropy is given by O'Neill et al.(1973).

---

*Footnote: The same argument as that presented in section 4.2.3 has, very recently, been published by Rickerby (1979).

2.5 The Indentation Size Effect

If a continuum model of plasticity is assumed, ie. that the activation volumes of the plasticity are small compared with the size of the smallest indentation, then the equilibrium pressure on indentation (the hardness) would be expected to be the same for all sizes of indentations and pyramidal indenters would be expected to produce identically shaped indentations at all loads (the Kirpichev--Kik law of similitude, Shoroshov et al 1977).

At present all the quantitative models of plasticity on indentation (see section 2.1) assume continuum plasticity and are therefore incapable of describing the indentation size effect (ISE) except in the case where it is due to macroscopic superficial layers of different hardness from the bulk material (see 2.5.2 and 2.5.3).

Spherical indenters do not preserve geometrical similarity unless smaller indentations are made with carefully chosen smaller radii indenters. Even when this is done an indentation size effect has been shown to exist on a very fine scale (Gane 1970) and was explained as being due to the lack of mobile dislocations or easily activated sources in the very much smaller stressed volumes used in their work. The softening which might be expected for higher dislocation densities from this theory was not observed (Gane and Cox, 1970) and it is now thought that a thin 'dirt' layer caused the effect, now that the work has been repeated in ultra-clean apparatus using Auger spectroscopy to check for the presence of surface layers (Pethica, 1979).

Sharp pyramidal indenters are generally assumed to induce a sufficiently high stress at the tip to nucleate dislocations in unfaulted material when loaded to a few grams force (to overcome the initial elastic contact caused by the finite radius at the tip). Thus in the usual microhardness regime the effect of the density of

dislocation sources has no measureable effect, and the effect of increasing the dislocation density is to increase the hardness because of the higher yield stress.

There are many mechanisms which can be visualised as causing an indentation size effect (ISE). Smaller indentations require dislocation loops to be more sharply curved, which would increase the stress required to propagate them, and the effect of the surface on both elastic and plastic influences on dislocations is proportionately smaller for larger indentations. These, and other mechanisms, will be discussed below, but first the various ways in which the ISE can be quantified will be described so that later discussion be placed on a firmer basis.

2.5.1 Analytic and Empirical Functions

There are two approaches that can be taken when considering the change in the measured hardness with decreasing loads. Firstly, that the change is real, in that it represents the intrinsic behaviour of the material, or secondly, that if some distorting factors are removed, then a 'load independent hardness number' can be obtained. In the first case, where the effect is assumed to be real, a theory can be devised to explain the effect (e.g. that it is due to grain size effects) or the best fit empirical function can be found. A physical theory can then be looked for in terms of that function. In practice, only the second option is possible because complete quantitative theories for the indentation size effect have too many adjustable parameters to be useful.

The second approach, where the effect is assumed to be due to measurement problems, is to devise a function in which the measurement offset appears as a constant and that function then fitted to the data.

Therefore the two approaches both lead to the same action: fitting analytic functions to indentation load/indentation size data. The empirical function which fits most of the data well (Burnand 1972) and which makes no assumptions about the cause of the ISE is given by equation 2.5.1a.

The best general purpose empirical function describing the ISE for pyramidal indenters is:

$$L = a.d^n \qquad 2.5.1a$$

a, n are constants, L is the load, and d is the indentation diagonal. This is the 'log-index' relation, sometimes called the "Meyer Law" after a similar relationship applicable only to spherical indenters where the ISE is caused by work hardening effects (Tabor, 1951). If there is no ISE then the parameter 'n' will be exactly equal to 2.0 . Note that this is an empirical function and thus must never be used for extrapolation beyond the range of the data.

Now, if one can introduce extra factors into the function such as to retain the fit to the data, but to make 'n' become equal to 2.0, then one can look for an explanation to the ISE in these extra factors rather than in the rather unmanageable index 'n'. The two equations:

$$L = a_2.(d - c)^2 = a_2.d_2^2 \qquad 2.5.1b$$

$$L - L_0 = a_3.d^2 \qquad 2.5.1c$$

both achieve this. Equation 2.5.1b (Tarazov and Thibault, 1947) assumes that the 'real' indentation diagonal length is d_2 and that the factor 'c' is introduced to account for the error in measuring 'd' because of the finite resolving power of the microscope and to allow for calibration errors between different microhardness testers. Alternatively, one can consider d_2 to be the 'original' diagonal length under load, and 'c' to be the amount of elastic recovery on unloading in addition to the calibration errors. For 2.5.1b to describe the data adequately 'c' must be the same length over the entire indentation size range and material dependent. Tarazov and Thibault had an ingenious argument, with which I completely disagree, to explain why the elastic recovery should be the same over the indentation size range. They say that since the shape of the indentation is the same, the stresses at the ends of the diagonals will always be the same, and thus the elastic contraction at the ends of the diagonals will always be the same. This idea ignores the elastic contraction of the rest of the indentation; I believe that

whilst the contraction may not be exactly in proportion to the size of the indentation, because of other ISE mechanisms, it will nevertheless be roughly in proportion.

Equation 2.5.1c introduces the factor L_0 and again there are two arguments to justify its inclusion. Firstly, the microhardness tester may be badly calibrated with a discrepancy between the indicated and the actual load. Secondly, it has been postulated that the imperfection at the tip of the indenter means that there is an initial load that must be applied before the stress will be high enough to produce a plastic indentation. This may be true for very small indentations but in most situations, once plastic flow has begun, surely it is unreasonable to expect the exact shape of the tip to continue to affect larger indentations. Therefore it does not make sense to identify L_0 with this minimum indenting load as L_0 is applied to correct the entire range of indentation sizes.

These two equations have been tested on results from a range of steels and ceramics, using both Vickers and Knoop indenters, by Young and Rhee (1978). (They did not use a statistical technique for comparing the accuracy of the fit for the different functions, as has been suggested by Sargent and Page (1978), but instead made estimates by eye.) When function 2.5.1c was fitted, L_0 was found to be unreasonably large and different for different specimens, but 'c' was found to be a reasonable length for elastic recovery. However, Sawyer (1979) found that if the 'elastic contraction' theory were correct, his indentations made using a 100 gf. load would have had to have contracted by a third of their total length. This is unreasonable.

In this thesis I have used function 2.5.1a to analyse the data from experiments on the ISE for the following reasons:

(a) I do not believe the theories which have been applied to the other two functions, and if the three functions are judged merely as empirical equations then 2.5.1a is superior because:

(b) the ISE index 'n' is directly related to the gradient of the

load/indentation size relation:

$$n = \frac{d}{L} \cdot \frac{\partial L}{\partial d} \qquad 2.5.1d$$

and 'n' is commonly between 1.8 and 2.0, though for pure annealed copper I found it to be 1.5, and Crocker and Wilson (1978) measured it to be about 4 for PbTe alloys

(c) the parameter 'a' in 2.5.1a can be used to derive a hardness number which is that measured for an indentation of standard size (which must be in the experimental range of the data, see 3.2) e.g. with a diagonal of 10 microns, whereas all other 'standard' microhardness values are defined for a particular load eg. 100gf., which means that in materials of very different hardness the 'standard' hardness values are not comparable because they refer to entirely different size ranges.

Admittedly the use of an empirical function does not greatly improve the understanding of the ISE (and even this method is not as straightforward as it might appear, see 3.2) but it is necessary to have a consistent method of measuring the magnitude of the ISE so that the effects of experimental parameters can be evaluated, and perhaps, better theories can be developed in the future.

2.5.2 Surface Hardening Effects

It is clear that the more the hardness of a surface layer differs from that of the bulk, the greater the indentation size effect (measured by the amount by which the ISE index differs from 2.0, assuming that there are no other causes of the effect) will be. The immediate effect of a solid layer is the sampling effect, small indentations merely measure the hardness of the layer, whereas larger indentations also sample the bulk hardness. However, there are secondary effects too, as the presence of the surface or a surface layer affects the plasticity of the top layer of the bulk material. Thus, even when a macroscopic surface layer is absent, there are three components present: the environment (air, some other fluid, or vacuum), the surface-affected zone, and the bulk. These secondary, or

environmental, effects on the surface plasticity are present in all materials and are complex and poorly understood (see figure 2/27).

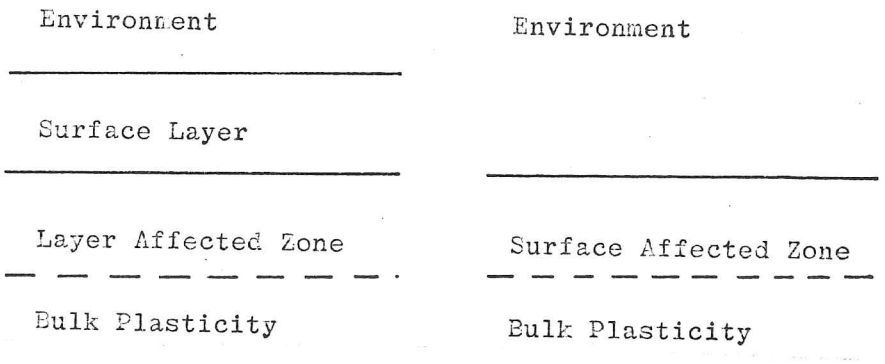

Figure 2/27

Solid Layers

Surface layers will be present after carburising, decarburising, nitriding, ion-implantation or a wide variety of treatments; oxides are always present on metals unless cleaned in ultra-high vacuum and checked with Auger electron spectroscopy (Pethica, 1978). Work hardened layers are produced by grinding, wear, or polishing of nearly all materials and this can be illustrated by selected area channelling patterns of the surface. This was performed on mechanically polished MgO to check that no such layer was present (Sargent and Page 1978). In glasses, stressed surface layers of different density from the bulk can be produced by ion-exchange or leaching (Marshall and Lawn 1977) or by differential cooling from the melt. However, internal stresses in a surface layer make the indentation microhardness test unreliable, but if the indentation behaviour of the unstressed surface is known, the technique can be used to measure these surface stresses (Hagan et al, 1977).

The direct effect of a "thick" (8 micron) surface layer of a harder material is shown in figure 2/28 Here the ISE becomes more severe when the loads are increased beyond 50 gf. when the depth of the

indentation becomes more than a tenth of the thickness of the layer (even the 200 gf. indentation has only a depth of 2.2 μm - Buckle 1973). The data for figure 2/28 is given by Buckle, but he fitted two straight lines to the plot, intersecting at the 50 gf. load measurements; here it is shown that a smooth curve fits the data just as well, in agreement with the results of the model described in section 2.5.3.

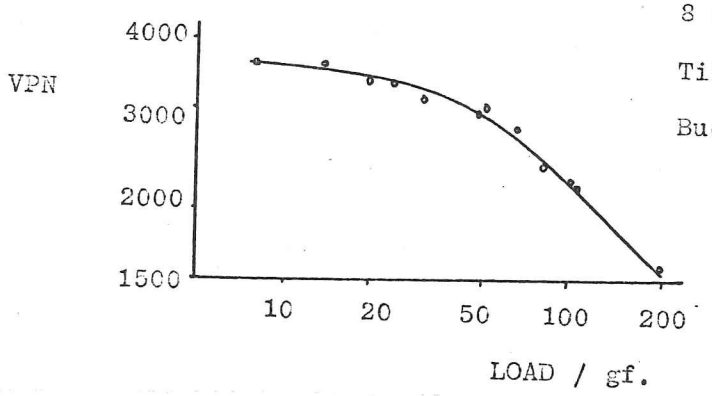

Figure 2/28

In this case, the secondary effect of the coating on the plasticity of the steel is probably insignificant compared with the primary effect. However, when the layer is very thin, as with oxides on "clean" metal surfaces, or when there is no solid surface layer, the secondary effects clearly must dominate and this is dealt with in the following section.

Surface Plasticity

Surfaces are structurally, chemically and electronically different from the bulk; the top atomic layer has a lattice parameter normal to the surface which is typically 5% less than that of the bulk, there may be dangling bonds or different chemical binding, and there is a finite chance that electrons from the solid spend part of their existence beyond the surface (Latanision 1977). The rest of this section has been well covered by the 1975 NATO advanced study institute on "Surface Effects in Crystal Plasticity" but, whilst some of the mechanisms can now be described and understood in physical terms, quantitative estimates of their effects are, as yet, not possible.

The surface influences plasticity by affecting the operation of dislocation sources and the propagation of dislocations in the surface affected zone. Such dislocations may intersect the surface or remain

wholly within the crystal, in the former case they can be statically pinned or be subject to velocity dependent drag.

When the environment contains no chemically active species it still influences the behaviour of dislocations, even for a perfect surface in vacuum there will be image forces attracting dislocations towards the surface and reducing the critical stress for dislocation multiplication near the surface. However, in nearly all real situations there is a thin oxide layer which, since it usually has a higher modulus than the metal, attracts distant dislocations and repels close ones, and will also impede dislocation egress because of the different Burger's vector in the oxide and the possible presence of a network of mismatch dislocations at the boundary. If the surface energy of the layer is different from that of the bulk, then its presence can either help or hinder dislocation escape when the geometry of the dislocations is such that slip steps are formed. Elastic straining of the material can cause a brittle surface layer to crack, and the stress pulse can then produce a tangle of new dislocations below the layer in the bulk, thus work-hardening the surface. Even when there is no oxide or hydroxide surface layer, adsorbed gases can change the surface energy when present only as a monolayer.

When dislocations are prevented from leaving the crystal, they exert back stresses which, if their sources are close by, inhibit further dislocation multiplication, thus increasing the yield stress and, in later stages of deformation, the work-hardening rate.

Thus, because of the presence of defects, surface ledges and image forces, the surface is generally both an easy source and an obstacle for dislocations, and its influence on the operation of sources has been shown to extend to 60 to 100 microns below the surface in Al, Au, Fe and Cu. The surface is also a good vacancy sink and thus the vacancy concentration, and probably the concentration of impurities, both substitutional and interstitial, will be different near the surface. Grain boundaries, which are also vacancy sinks, have been shown to affect the yield stress (measured by microhardness) up to 100 microns into the bulk because of the effects of impurity segregation (Braunovic and Haworth, 1974).

All the above effects probably occur to a greater or lesser extent in all crystalline materials in a clean, dry environment. However, when the environment is corrosive, contains solvents, is an electrolyte, or polar, then electronic properties become important.

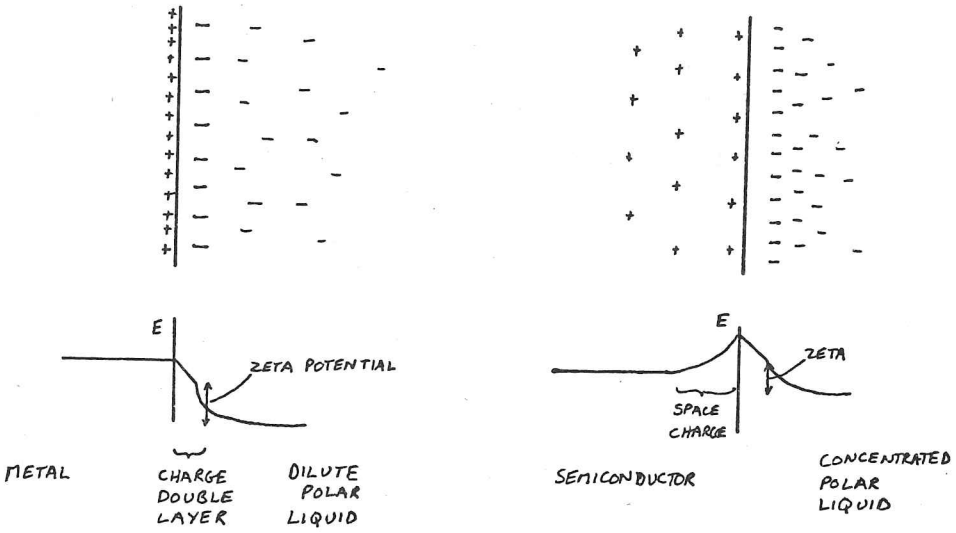

Figure 2/29

The zeta potential is a measure of the surface charge in the near-surface of the solid (Westwood and Macmillan 1973).

Experimentally it is found that the hardness of semiconductors, insulators, and pure metals is a maximum when the zeta potential (see figure 2/9) is zero, i.e. when there is no double charge layer at the surface. The zeta potential can be varied by changing the concentration or type of electrolyte or, for a conductor, by changing the applied potential. In pure metals this effect is thought to be due to the effect on the surface energy, which is thought to be a maximum when there is no charge double layer. Thus, slip systems which cause slip steps on the surface are inhibited, and thus the hardness is a maximum, when the zeta potential is zero. However, this mechanism only works when the yield stress is relatively low and there are very few internal obstacles to slip, and when the dominant slip system causes slip steps. Thus, in zinc the zeta potential influences microhardness on the basal plane, but not the prism planes, because on the prism planes no slip steps are produced.

The plasticity in non-metallic solids is relatively insensitive to surface energy effects because the Peierls' stress is so high, but in these materials, unlike metals, the concentration of charge carriers is low enough for the space charge to penetrate to a depth of about a micron . This space charge changes the energy levels of the valence and conduction bands and the isolated defects in the band gap: vacancies, interstitials, dislocation jogs and kinks. The electrostatic interactions of surface dislocations (which carry strings of alternate charges in ionic crystals even when there are no jogs) and defects will also depend on the electrical conduction in this zone, either by optically or thermally activated electronic conduction, or by pipe diffusion of ions along dislocations. The precise mechanisms which cause the space charge to increase the mobility of dislocations at the surface, and thus decrease the hardness, are unknown and at present can only be guessed at. One known factor, from environmentally affected drilling rates, is that the time constant for at least some of the mechanisms must be as low as 10^{-5} s.

In corrosive or solvating media, dislocations can be pinned where they intersect the surface because an etch pit is formed; if the medium is only weakly corrosive, the dislocation can drag along the surface causing an etch groove. This is distinct from a postulated 'dislocation drag effect' caused by electrostatic and elastic interactions because the retarding force on the dislocation caused by pitting will decrease as the dislocation velocity increases.

A further hardening effect for small indentations does not depend on the properties of the surface as such, but on the absolute scale of the deformation. Small indentations require nearby dislocation loops to be of greater curvature than for large indentations, and this will increase the stress required to propagate such loops. Mott (1956) postulated that smaller indentations would require slip to occur on more closely spaced slip bands than those around larger indentations and that this close spacing would increase the flow stress.

2.5.3 Surface Hardening Models

It has been shown that there are a great many mechanisms which can cause an indentation size effect (ISE) on microhardness by changing the hardness (yield stress) of thin surface layers from that of the bulk. Different mechanisms, for example, the operation of image forces and the effect of charge double layers, will affect the plasticity of the bulk material to different depths and thus there will be a multi-layer effect, with a yield stress gradient within each layer. However, these descriptions of possible mechanisms governing the ISE are not sufficient for a quantitative investigation.

A very simplified model has been considered and its properties have been investigated numerically, the results being expressed in terms of the "log-index" measure of ISE which has also been used to analyse experimental data . The model bulk material has a hardness H_2 and is covered with a surface layer of thickness L and hardness H_1. This single layer situation is a major simplification, no gradual change in hardness between the layers is assumed and neither are any criteria of strain compatibility across the interface taken into consideration.

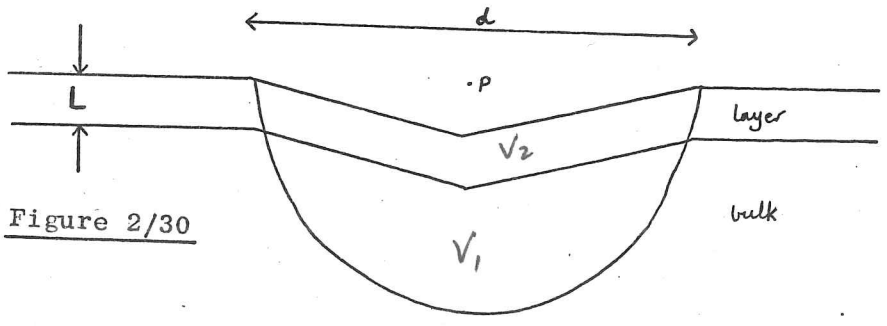

Figure 2/30

A Vickers indentation (diagonal d) is assumed to measure only the hardness of the hemispherical volume centred on the point P (figure 2/30)

with radius d/2 (Samuels and Mulhearn 1957). Within this hemisphere is the pyramidal space where the indenter penetrates and two volumes: V_1 of bulk material and V_2 of surface material(the effects of elastic compression and surface pile-up are ignored and the layer is assumed to have the same thickness everywhere). The hardness of the composite structure, H, is calculated by a simple law of mixtures:

$$H = (H_1V_1 + H_2V_2)/(V_1+V_2) \qquad 2.5.3a$$

These simplifications have been made in order to reduce the number of parameters in the model: as has been shown in section 2.5.2, the form of the load/indentation size relation and the quality of the data available are such that almost any function with two or more parameters can be made to fit. This model has only two parameters, H_1 and H_2. The ratio 'd/L' is varied over a range such that, at one extreme, the hemisphere is entirely contained within the surface layer and, at the other, the influence of the layer is neglible.

This model can be used for two distinct physical situations: (a) the ISE case where there is a surface layer of fixed thickness and a number of indentations of varying size are made in it, and (b) where indentations of a fixed size are made in a layer which changes in thickness (This second case has not been further considered here.) Thus, for the first situation, the model enables one to make a crude prediction of the dependence of the hardness on the indentation size H(d) from the layer thickness and hardness. The empirical function of equation 2.5.2a, the log-index relation, can be used to obtain a H(d) function in the following way: hardness measured with a Vickers indenter is defined by:

$$H = 1854.4 \cdot F/d^2 \qquad 2.5.3b$$

where F is in gf., d is in μm and H is in $kgf.nm^{-2}$. Thus, an alternative expression for the log-index relation is given in equation2.5.3c.

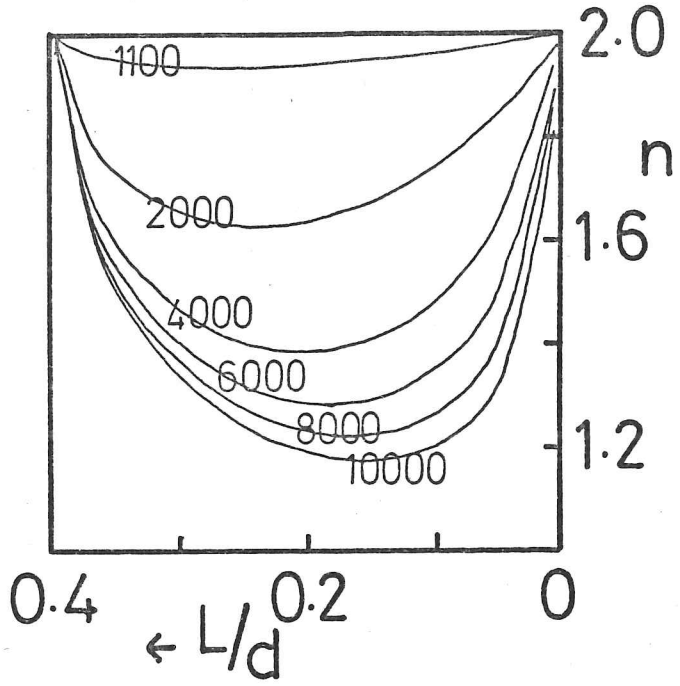

Figure 2/31

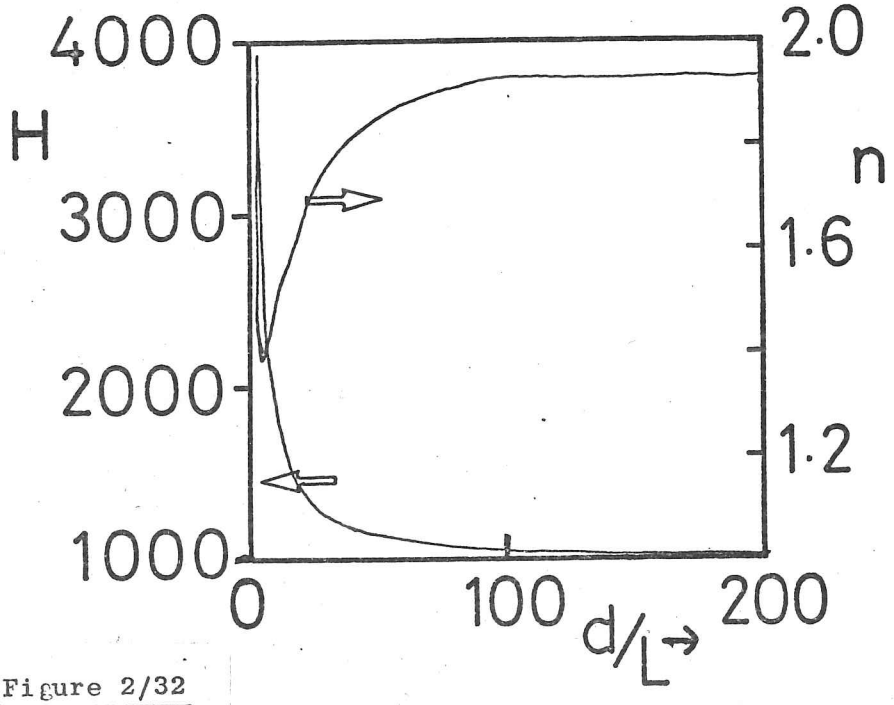

Figure 2/32

$$H = 1854.4 \cdot a \cdot d^{n-2} \qquad 2.5.3c$$

differentiating:

$$\frac{\partial H}{H} = (n-2)\frac{\partial d}{d} \qquad 2.5.3d$$

Both $\partial H/H$ and $\partial d/d$ can be calculated for any value of d (taking F to be constant) and thus the model can be used to predict the log-index 'n' for any indentation size. If the log-index relation holds for the model situation, then the value of 'n' would be predicted to be the same over the whole range of indentation sizes. The results calculated using the model are shown in figures 2/31 & 2/32 : in 2/31 the bulk hardness was set to 1000 $kgf.mm^{-2}$ and the layer-hardness to the value marked on each of the curves. Figure 2/32 plots both the 'n' prediction and the 'H' prediction for the case where the superficial hardness is 4000 $kgf.mm^{-2}$ the 'n' curve is the same as that in the previous figure but the horizontal axis is inverted.

If experimental data for MgO single crystals (data set MSXA11, see section 4.5.2) is compared with predictions from the model, a rough fit can be obtained if a layer 0.05 to 1.2 μm thick, with a hardness of 1500 $kgf.mm^{-2}$, is assumed to exist. With such a crude model, the values cannot be more than an estimate, but it should be remembered that the induced charge effects described in section 2.5.2 are thought to affect the top 1 μm of the solid (Westwood and Macmillan 1973).

The model shows that the ISE is more severe when the hardness of the of the layer and the bulk diverge and that as indentation size becomes markedly different from the layer thickness, the log-index does approach 2.0, as expected. It is interesting that figure 2/32 shows that only a very thin layer has a strong effect on hardness and the ISE index, and that as the indentations become very much larger than the thickness of the layer, there is still an effect on the hardness and 'n' only approaches 2.0 asymptotically. This asymptotic region, where 'n' is roughly constant

(about 1.96 for this model) over a wide range of indentation sizes, means that the log-index relation fits here. The value of 'n' here is roughly similar to that found for a very large number of inorganic single crystals by Burnand (1972): 1.86. Burnand made an extensive review of published log-index values and found that they clustered about 1.8 to 1.9, which he interpreted to be a fundamental property of the microhardness test, i.e. he gave no further explanation. It is proposed, on the basis of the above, that this effect is due to measurements being made in the asymptotic regime for crystals whose surface layers are affected by surface plasticity mechanisms.

2.5.4 The Defect Density Theory

The presence of defects, e.g. dislocations, precipitates and grain boundaries, in a crystal affects the yield stress and the hardness, and if the spacing of these defects is significant compared with the size of the stress field beneath an indentation , the stress fields from differently sized indentations will interact with different numbers of defects and there will be an ISE on hardness. In this section the effects of point and line-defects will be considered, grain boundaries being dealt with in section 2.7.

Three different types of defect must be distinguished: (a)mobile defects, ie. glissile dislocations, (b) sessile defects, such as vacancies, interstitials, precipitates and sessile dislocation structures, and (c) dislocation sources, which will almost invariably be associated with dislocation networks. A distinction must also be made between indentation by spheres or by pyramids. Spherical indenters will produce an elastic (Hertzian) stress field in the test material before the stress becomes high enough to produce plastic yielding. A pyramidal indenter will induce such a high stress at its first point of contact that it will activate nearby sources immediately, and may nucleate dislocations homogeneously.

Since a perfectly sharp point cannot be achieved in practice, and the tip of a pyramidal indenter approximates to a spherical cap, spherical indenters of known radius are always used for making very small indentations (down to 0.2 micron diameter)(Cane and Cox 1970).

Glissile dislocations alone will have only a very slight effect on hardness as, even in a heavily cold-worked material, there are only about 10^4 per square micron (ie. spaced every 20nm), and this is not sufficient to enable a plastic indentation to be formed merely by their rearrange--ment. To form an indentation plastically requires the operation of dislocation sources, which will be numerous in such a dense network. Sessile defects, such as vacancies and precipitates, will raise the hardness if they are small enough, and spaced closely enough, for several of them to be included in the stress field beneath the indenter, but if the indenter penetrates between defects, then as the size of the indentation increases, the measured hardness will change from that of the matrix only to that of the composite material. In the changeover there will be an ISE. This is analogous to the layer/bulk situation described previously but with a significant difference: as there is a random distribution of point defects there will be a great deal of scatter in the hardness measured around the transition range:

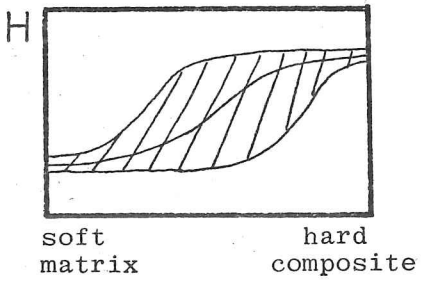

Figure 2/33

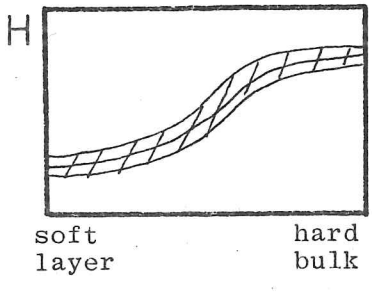

Figure 2/34

where the indentation size increases from left to right and the shaded areas represent the experimental scatter.

When the indentation is small compared with the separation of dislocation sources, assuming that a spherically tipped indenter is used, significant distortion of the strain field will occur as slip will begin at the first source to exceed its nucleation stress, and not at the

point of highest stress beneath the indenter. Thus, as the indentations are made at lower loads, higher pressures at the point of indentation are required to activate the nearest sources and the material appears to get harder. As the indentations are made smaller, a point is reached where the stress is high enough to homogeneously nucleate dislocations in the perfect crystal, and this is the maximum hardness.

Shorshorov et al. (1977) attempted to derive a quantitative model which would describe how the hardness was governed by the distance between dislocation sources . They considered a layer, thickness L, whose "outer limit....coincides with the surface of the indenter, and the inner depends on the nearest mean distance from the surface of the indentation to the most mobile defect."

If the projected (square) area of the indentation (produced by a Vickers indenter) is F, then the projected area of the layer is F_a:

$$F_a = (\sqrt{F} + 2L)^2 \simeq F(1 + 2L\sqrt{F^{-1}})^2 \qquad 2.5.4a$$

therefore:

$$H \simeq H_a(1 + 2L\sqrt{F^{-1}})^2 \qquad 2.5.4b$$

where H_a is the "mean contact pressure over F_a" and H is the hardness. Shorshorov et al. then deduced:

$$\frac{\partial H}{H} \simeq -\frac{4L}{\sqrt{F}+2L} \cdot \frac{\partial d}{d} \qquad 2.5.4c$$

(where d is the diagonal of the indentation) by assuming H_a to remain constant whilst differentiating with respect to d, as: "It is well known that the hardness becomes practically a constant value for large pyramidal or conical indenters." I consider this to be incorrect as it is not in the 'large indentation regime' that they are applying the model, in fact, the whole point of modelling the ISE is that the hardness does change. However, equation 2.5.4c may be combined with 2.5.3c:

$$n = 2 - \frac{(16(L/d)^2 + 5.687(L/d))}{(1 + 8(L/d)^2 + 5.687(L/d))} \qquad 2.5.4d$$

The expected relationship between log-index and the layer thickness was plotted - see figure 2/35, which also contains the 4000 $kgf.mm^{-2}$ line from figure 2/32 (dotted) for comparison. Both curves approach 2.0 for large indentations but, whereas the model described in 2.5.3 also

Figure 2/35

This figure shows relationships between 'n' and layer thickness/ indentation size ratio for Shorshorov's and Sargent's (see 2.5.3) models.

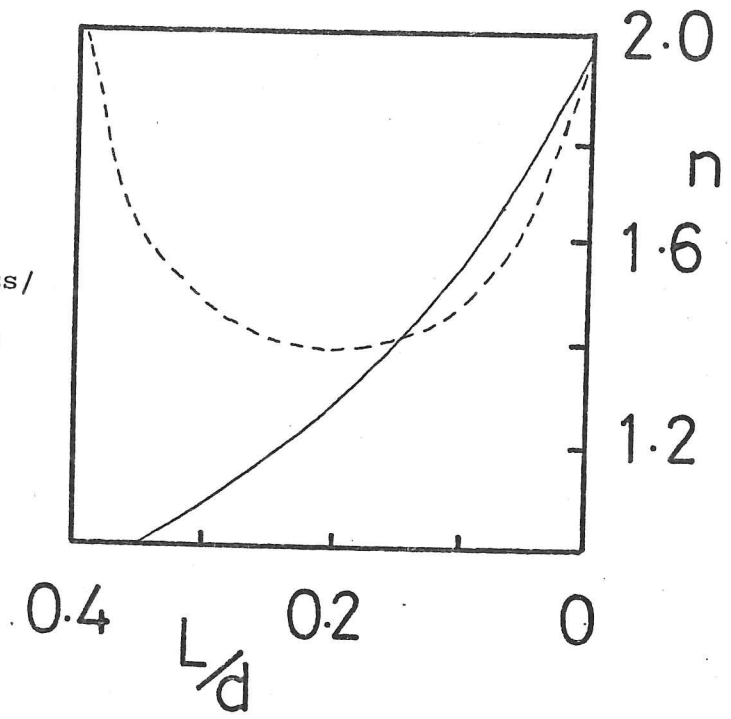

assumes that there will be no ISE (i.e. n=2) when indentations are contained within the layer, the model of Shorshorov et al. does not take the eventual homogeneous nucleation into account, and the predicted ISE becomes more and more severe as the indentations become smaller. The two models can be compared in this way because the Shorshorov model is really a bulk/layer model, and is applied to the defect density situations by stating that the layer thickness is related to the mean spacing between sources. This will only hold when there are enough sources nearby to make this 'continuum' view valid. Thus layer/bulk models can only be used to examine the defect density theory when there is a high density of defects and the effective layer thickness is small. A more realistic model would examine the ways in which one source can relieve an arbitrary stress, and then simulate different distributions of sources with different nucleation stresses in the stress field beneath an indentation. However, in view of the current lack of knowledge concerning this stress field even in homogeneous materials, such an undertaking cannot be attempted.

Gane and Cox (1970) found that increased dislocation density added to the hardness at small indentation sizes but did not shift the indentation size at which the hardness began to increase (figure 4 of their paper) as would be expected if the defect density theory were governing the ISE and and if, as is fairly certain, the source density were directly related to the dislocation density. This means that the ISE is not due to the finite spacing of sources in their material (gold) and, in fact, there is no experimental evidence that this mechanism occurs in any material. Later work by Pethica (1979) indicates that the measurements of Gane and Cox may have been affected by a contaminant film, but the experiment has not yet been repeated.

For very small volumes, work hardening during indentation ceases to occur, even though a higher dislocation density increases the hardness. This is thought to happen because the dislocations glide out of the stressed volume before they can interact with each other.

2.5.5 Pile-Up Effects

In isotropic materials, surface pile-ups of displaced material are produced along the edges of indentations but not at the corners, if material is not too stiff (see sections 2.1.2 and 2.3.1), and so do not affect the measurement of the diagonal.

In anisotropic materials, the pileup is positioned crystallographic--ally with respect to the indentation, and, depending on the orientation of the indenter, can interact with the corners of the indentation (see 2.4.1). In this case, the magnitude of the pileup can affect the magnitude of the measured hardness. Buckle has measured the heights of pileups relative to the indentation depths for a large number of randomly-orientated copper and aluminium crystals (grains). He found that the smaller the indentation, the smaller the relative size of the pileup (see figure

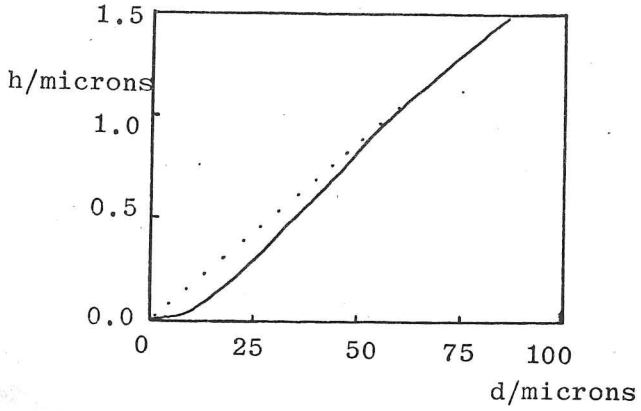

Figure 2/36

(From Buckle (1960))

2/36, the dotted line is the expected linear relationship). The reasons for this are not immediately obvious. For very small indentations (less than 0.01 microns in diameter), the surface energy becomes comparable with the plasticity energy, and this might reduce the size of the pileup, but the steady relative decrease in the pileup height below d=50 μm (figure 2/36)requires another explanation.

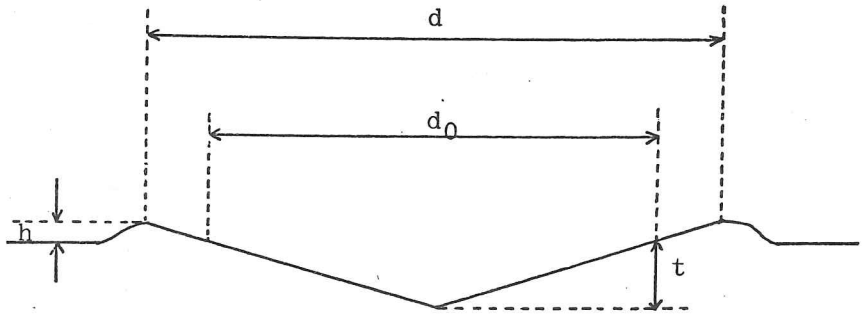

Figure 2/37

It is known that a decrease in the size of the indentation often produces an increase in hardness which is a real, and not a measurement error, effect. Thus, for smaller indentations, the yield pressure will be a higher proportion of the Young's modulus and there will be a tendency towards radial, rather than pile-up, displacement as E/Y drops below 114, thus decreasing the height of the pile-up. This hypothesis could be investigated if the effect of the hydrostatic pressure beneath the indenter on the modulus were known, and if careful measurements of pile-up height

and indentation size were made on a close-packed crystalline material (which would not be subject to plastic densification).

It would be interesting to know the h/t (= $(d-d_0)/d_0$) ratio (see figure 2/37) for large indentations, where there is no ISE, in a range of rigid-plastic materials with no work-hardening. This would give a base line from which one could distinguish between fully plastic and partially elastic-plastic indentations solely on the basis of a pileup measurement.

Therefore pileups may serve to amplify, by introducing a measurement effect, the ISE due to other mechanisms, and then only in materials where the pileup can occur at the corners of the indentation because they are anisotropic.

2.5.6 Critical Fracture Size

This thesis is concerned with the formation of indentations by plastic deformation. The critical fracture size is relevant because below this size, all indentations are plastic, whereas larger indentations may be cracked. However, unless the material completely fragments on impact, plasticity mechanisms still dominate the behaviour (see 2.2.2).

The mechanisms of crack initiation on indentation have been the subject of much study recently because of the need to develop materials that are highly resistant to erosion by fast moving particles supported in fluids, eg. coal combustion in fluidised beds, coal liquifaction, etc. Lawn and Evans (1977) have shown that for indentation by sharp particles, there is a minimum load (P*), below which no cracking occurs at all, whatever the flaw size distribution and however brittle the material; also that there is a minimum flaw size (c_0) below which no cracking occurs, whatever load is applied. These are related to the hardness (H) and fracture toughness (K_c) of the material by :

$$c_0 \propto (K_c/H)^2 \qquad 2.5.6a$$

$$P^* \propto K_c^2/H^3 \qquad 2.5.6b$$

The coefficients of proportionality depend on the geometry of the indenter. These relationships show that NaCl is expected to require a load to initiate cracking which is 50 times that required for SiC and 667 times that required for MgO . Lawn et al.(1975) used a slightly different argument to derive a 'brittleness index':

$$a^* \propto \Gamma E/H^2 \qquad 2.5.6c$$

where a^* is the indentation size at which the median crack is equal in size to the indentation, Γ is the fracture surface energy, and E is the Young's modulus. This is equivalent to equation 2.5.6a but making the Griffith approximation of ΓE being proportional to K_c.

2.6 Microstructure and Microhardness

In determining which microstructures are likely to affect microhardness, one should first look at the influences of microstructure on those quantities which have already been found to influence micro--hardness. Thus, increasing the dislocation, grain boundary, or point defect density of a pure annealed crystal will increase the yield stress, which will raise the hardness. A fine, equiaxed, untextured grain structure will be mechanically isotropic, whereas if the grains are (a) elongated or (b) textured, then (a) plastic anisotropy or (b) elastic and plastic anisotropy respectively will influence indentation. The addition of second phase particles can affect the overall modulus as well as increasing the yield stress, but this will not be significant for most metals reinforced with intermetallic precipitates. However, carbon, glass and ceramic particles and fibres have quite different moduli from the metals and polymers they are used to reinforce, and even single-phase polymers can have large variations in modulus across injection mouldings.

All the microstructures mentioned above have straightforward effects on hardness when they are on a much finer scale than the indentation itself. The microstructure can have more direct, and much more poorly understood, influences when it is on the same scale as the indentation as, for example, when the stress field is smaller than the spacing between precipitates or, as described in 2.5.4, between dislocation sources. When an indentation covers two or three grains of a semi-brittle solid, e.g. MgO, catastrophic cracking usually occurs because of strain mismatch across the grain boundaries, but, nevertheless, most of the deformation is plastic. In a fully plastic material, such an indentation is distorted because of the different orientations of easy slip in the different grains.

When the grain size is substantially less than the indentation size, a Hall-Petch type relationship is often found to hold in ductile metals. This is expected from the equations :

$$H = CY \qquad 2.1.1a$$

and the Hall-Petch relationship:

$$Y = Y_0 + k_y.g^{-\frac{1}{2}} \qquad 2.6a$$

where 'g' is usually the grain size, but can also be the subgrain size (Thompson 1975) or domain size (Hannink and Murray 1972). Thus:

$$H = H_0 + k_h.g^{-\frac{1}{2}} \qquad 2.6b$$

where the quantity H_0 must always be found by extrapolation from the fine grained regime because coarser grains change the type of yielding, causing deviation from this relation. Therefore H_0 is not the hardness of the material at 'infinite' grain size, at $g^{-\frac{1}{2}} = 0$.

There has been a great deal of confusion in the past concerning the methods whereby these grain sizes are measured, and several different grain size parameters have been correlated with hardness, sometimes in a mutually contradictory manner (Rhines, 1977). The grain size measured by the mean linear intercept (N_1 in the nomenclature of Rhines) is, in fact, half the mean grain boundary area per unit volume: it is an areal property of the whole structure and is not connected in any way with the average grain diameter. Thus, the mechanism usually postulated to explain the grain size dependence of yield stress, that of dislocation pile-up across the grain (either in the grain (Honeycombe 1968), or along and edge of the grain boundary (Hirth 1974, Sargent 1976)) activating slip in the next grain, is not supported by the experimental data. In a "well-behaved" equiaxed material with a gaussian grain size distribution, there may well be a rough proportionality between the grain diameters and N_1, and this may explain the success of the equation 2.6b in describing the data empirically. The situation is confused by the fact that all

the grain size parameters (see Rhines,1970,1977) do vary with N_1 when the microstructure is "well-behaved" and that experimental results over a considerable size range (1 to 7) are imprecise enough to fail to distinguish between first, second and third powers of N_1. Thus, the data can usually be fitted equally well to a number of 'g' parameters, and the reason that $g^{-\frac{1}{2}}$ has been used, rather than some other power, is that researchers in the past thought that it had some theoretical basis, ie. the pileup model. This theory has been shown to be totally inadequate and there is no reason why the yield stress (and thus the hardness) should be related to the grain size by a simple analytical function (Ashby 1970, Thompson et al. 1973, Sargent 1976). However, because of the difficulties in making precise measurements of both hardness and grain size, and because of the insensitivity of the plasticity mechanisms to the parameter used to measure the grain size, the Hall-Petch hardness relationship (2.6b) is almost always good enough to describe data empirically, even when 'g' is the distance between precipitates or fibres and not grain size (Jindal and Gurland 1974).

It can be seen from 2.1.1a and 2.6b that:

$$\frac{H_0}{Y_0} = \frac{k_h}{k_y} = C \qquad 2.6c$$

but in fact it is almost always found that:

$$\frac{H_0}{Y_0} > \frac{k_h}{k_y} \qquad 2.6d$$

(Farrell and Loh 1971, Armstrong and Jindal 1968, Douthwaite 1970, Raghuram and Armstrong 1970, Jindal and Gurland 1974, Schulson and Roy 1977), though Nouet and Deschanvres (1973) found the opposite inequality. That these two ratios are not identical should not be surprising as the first, H_0/Y_0, compares the hardness and uniaxial strain measures of the yield stress, whereas k_h/k_y compares these two measures of the grain size sensitivity to yield, which is related to the work hardening behaviour (Ashby 1970). This inequality may well be

due to the extra strain which occurs on indentation. Tabor estimated the strain to be 8% and found that 2.1.1a fitted the data much better when Y was set equal to the flow stress after the material had been strained a further 8%, in which case one should use the flow stress Hall-Petch equation:

$$Y_f = Y_0' + k_e.g^{-\frac{1}{2}} \qquad 2.6e$$

(Thompson 1975) where the dependence of k_e on strain is far from simple as it depends on the dislocation-density/strain relationship and also on the grain size, thus:

$$Y_f = Y_0' + k_e(g,e,\rho) \qquad 2.6f$$

and k_e has even been known to decrease with strain (Marcinkowski and Fisher 1965). Theoretically:

$$k_e = k_y + \text{constant.(Taylor factor)}^{3/2} \qquad 2.6g$$

(Johnson and Feltner 1970, Sargent 1976), therefore it is unsurprising that the equality of 2.6c does not hold. Unfortunately there is no published data on the equality:

$$\frac{H}{Y_{f_{+8\%}}} = \frac{k_h}{k_{e_{+8\%}}} = C \qquad 2.6h$$

which could only be an approximation, but may be closer to the data than 2.6c.

2.7 Indentation Size and Microstructure Size Relationships

If one particular type of microstructural feature dominates the hardness and other influences, e.g. surface layers, are insignificant then the hardness may remain constant if both the indentation size and microstructure size are increased in direct proportion. The hardness is not expected to remain precisely constant, there is still the Hall-Petch relationship influencing yield stress and hence hardness, but there should not be any ISE caused by changing 'regime', i.e. from pseudo-single crystal hardness (when the indentation is entirely within one grain) to fully polycrystalline behaviour. This conjecture remains untested as systematic experiments varying both scales at once are lacking in precision (see chapter 4) and published data compares a fixed point on one scale with a range on the other, i.e. hardness values using a fixed load (or indentation size) on materials with different grain sizes (Jindal and Armstrong 1969), or a range of indentation sizes on one particular material (Buckle 1973), (Sargent and Page 1978). If the conjecture were shown to be true over a certain size range, it would be a convincing argument that plasticity mechanisms acted on a scale much smaller than the sizes of the indentations in that size range.

The available data and theories will now be considered for ductile and brittle materials. All the points for ductile materials are relevant to brittle materials but not vice versa.

2.7.1 Ductile Materials

Buckle (1960, 1973) has considered the situation where indentations of different sizes are made on a material with a microstructure of a particular characteristic grain size, but he has not extended his ideas to the situation where the scale of the microstructure also varies between specimens. This has been investigated and reported by Sargent and Page (1978) for MgO, but the approach is valid for metals.

If the secondary influences do not cause any significant ISE, the hardness for three materials of increasing grain size (1 to 3) would be expected to follow the pattern shown in figure 2/38 . as indentations are made at different sizes by using different loads.

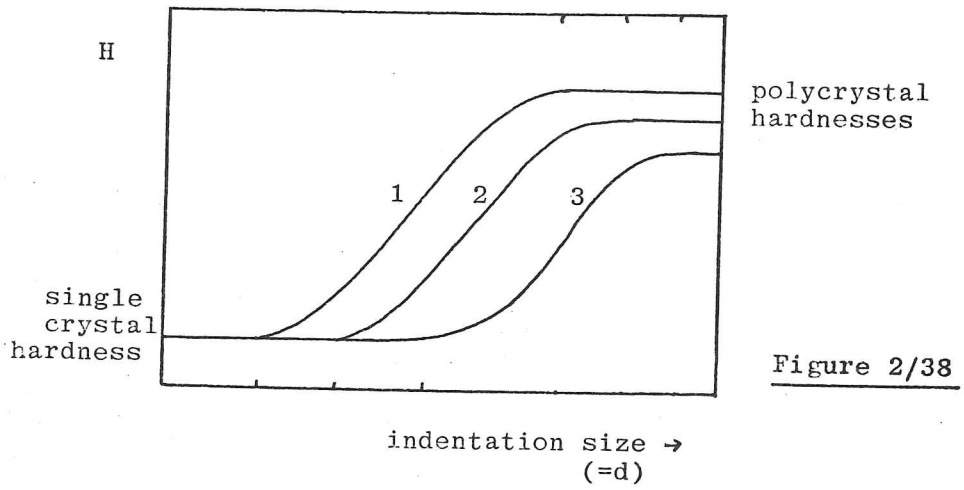

Figure 2/38

Each of these curves will be subject to a great deal of experimental scatter (as shown for one curve in 2/33), which is a consequence of the interactions of indentations with one or two grains, as mentioned in section 2.6. At each of the end points, when the indentations are either much smaller than, or much larger than, the grains there will

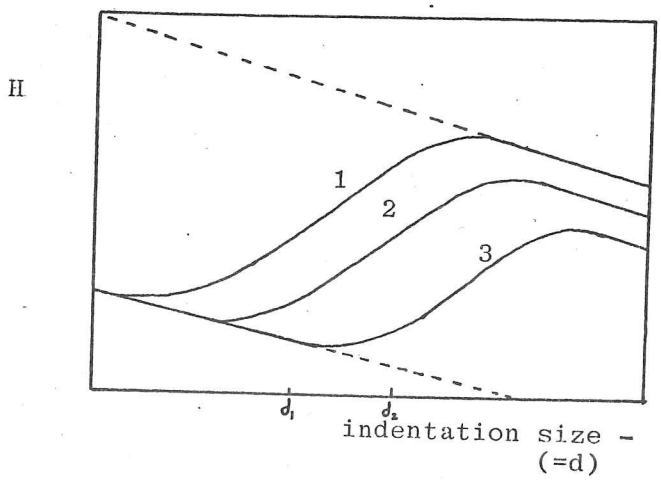

Figure 2/39

be no ISE and thus the curves are horizontal. The three materials will have different macroscopic yield stresses because of their different grain sizes, but the hardness of a single grain should be the same if the material is annealed and has not undergone any strain (which can lead to grain-size dependent dislocation densities).

If an ISE due to causes other than changing microstructure size is present, the anticipated situation will be as shown in figure 2/39. Here it is assumed that the 'macro'hardness values on the right of the diagram are for indentations larger than the grains, but small enough to be still affected by the ISE due to, for example, a surface layer.

Precisely the same effect on microhardness will be expected for precipitate size, or spacing, as for grain size (or 'grain boundary spacing'). Thus the experimental hardness/indentation-load relationship for a Cu-Ti alloy (figure 2/40) should be compared with the range where curve 3, in 2/39 reaches the 'macro'regime.

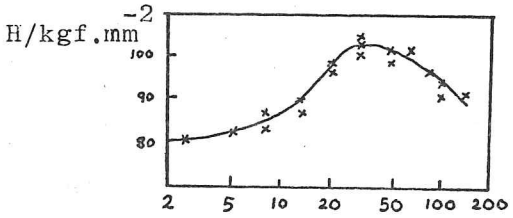

Figure 2/40 . (from Bückle, 1973)

The abscissa is the load, not the indentation size, but the same trend is expected. Here the transition to 'macro'hardness values is confirmed by metallographic examination. The 50 gf. indentations are significantly larger than the precipitates and the smallest indentations are not contained within either the matrix grains or the needle-like precipitates.

2.7.2 Brittle and Semi-Brittle Materials

Brittle materials are generally stiffer and harder than ductile materials, but plastic indentations can always be formed if they are made small enough (see 2.5.6). However, there is a lower limit on the size at which useful indentations can be made, because of the finite resolving power of the optical microscope. Scanning electron microscopy can be used to extend this range, but a point is reached where indentations become indistinct, not because of a visibility effect, but because the edges and corners are rounded and the uncertainty in the diagonal length due to this becomes comparable with the indentation size. The cause of the rounding is not clear, but it must be a direct consequence of the pattern of plastic flow because it is too large-scale for surface tension to have a significant effect.

With hard materials such as MgO, the visibility and the cracking set lower and upper limits to the indentation sizes that can be measured, but for soft metals, indentations can be made and measured over the full range of the microhardness testing machine. This full range on the Leitz Miniload is 5 to 1000 gf., which means that, for a metal of VPN=100 $kgf.mm^{-2}$ the size range is still only 9 to 134 microns. When data is only available from a restricted indentation size range, such as between d_1 and d_2 in figure 2/39, the ISE index relation fits very well, but the ISE index measured will change if either the indentation size range, or the microstructure scale (grain size), is changed.

In ductile materials, grain boundaries strengthen the solid by impeding slip, but in brittle and semi-brittle materials, the grain boundaries can be weaker than the bulk because they are more susceptible to fracture. This may be because dislocation pileups cause stresses which cannot be relieved in the next grain (Keh et al 1959), and this effect can be aggravated in materials which have 'dirty' grain boundaries. Such materials, eg. MgO or BeO, have low melting-point substitutional

impurities to improve mass transfer by diffusion during hot pressing, but these impurities segregate at grain boundaries and decrease the intergranular fracture energy (Johnson, 1976). Data for BeO is shown in 2/41 and a similar plot for MgO is in chapter 4. S_v is the grain boundary surface area per unit volume.

BeO – Hardness / G.B. Surface Area

Figure 2/41 Data taken from Armstrong et al. (1963).

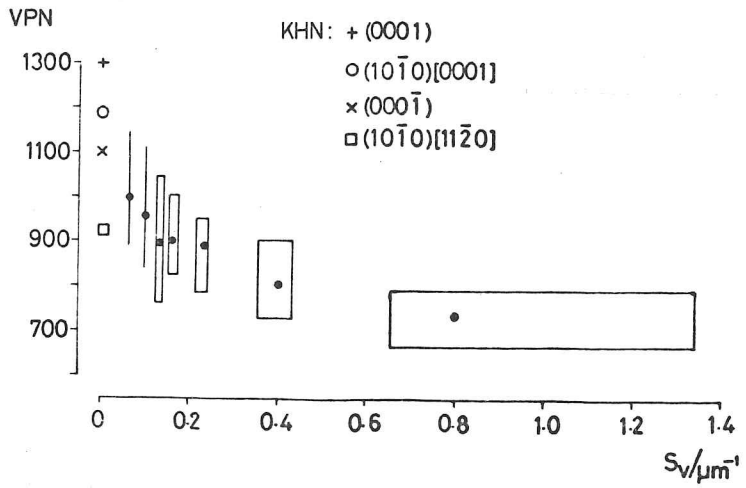

Where a material gets softer as the grains get smaller, k_h from equation 2.6b is negative, and the grain boundaries are weaker than the bulk. Kessler et al.(1974) have shown that the fracture energy of polycrystalline MgO is independent of grain size, when it is fully dense, and thus the decrease in hardness is not caused by a grain size dependent grain boundary weakening.

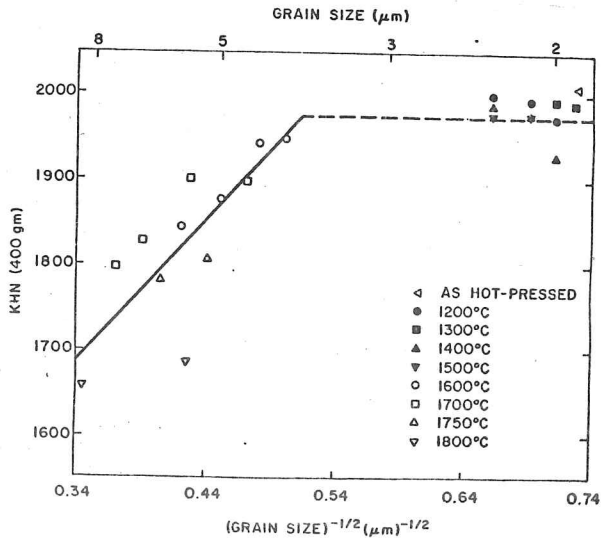

Figure 2/42
Data supplied by Bradt (1978).

Alumina, however, shows the opposite behaviour, k_h is positive, though it does decrease towards zero for fine grain sizes (Skrovanek and Bradt 1979). This alumina (see figure 2/42) was made by hot pressing without additives and thus shows the same kind of grain size dependence of hardness as a metal, even though cracking does occur at the load used.

"It is quite a three-pipe problem"

Sir Arthur Conan Doyle

3 Measurement and Analysis of Indentation Hardness

This chapter reviews the experimental problems of hardness measurement, of controlling indentation loads and of measuring the dimensions of the indentations. The correct statistical treatment of these measurements depends on the type of experimental error and an appropriate treatment for the quantitative investigation of the ISE has been devised taking this into account. This treatment leads both to a reproducible method for measuring the ISE index and a method of determining whether two sets of measurements on different specimens are significantly different from one another.

3.1 Errors and Uncertainties in Indentation Hardness Measurement

This section reviews the experimental difficulties in applying a constant and calibrated load to make an indentation and in measuring that indentation: its diameter, depth, pile-up height, the lengths of its associated cracks and dislocation rosettes, and the observations of the slip steps.

The influence of the response of the material on the ease with which these quantities are measured is discussed, the effects of the response on the magnitude of these quantities having been already discussed in chapter 2.

The special measurement problems associated with using standard laboratory equipment to make displacement controlled indentations are discussed.

3.1.1 Control and Calibration of the Load Used

(a) Effective Load and Loading Rate

Generally errors involved in making indentations become more significant as the loads used are reduced and the indentations become smaller; absolute loading errors due to unbalanced lever mechanisms or unzeroed springs are clearly only important when the load offset becomes a significant fraction of the total used. However, even if the dead load is accurately calibrated, vibration and inertial effects can increase the effective load. The indenter is deccelerated and cones to rest as the indentation is made and if the velocity of the indenter is high enough the kinetic energy of the indenter and lever system will significantly affect the formation of the indentation, similarly, vibration will increase the velocity and hence the kinetic energy. If the indenter system has a mass of 10g and excerts a dead load of 10gf, then an indenter velocity of 500 microns s^{-1} would increase the effective load by 1% if the indentation is 1 micron deep (i.e. H = 370 kgf/mm^2). This indenter velocity is not likely to have a significant effect because of the kinetic energy, but the effect on the strain rate will be significant and the yield stress/of all materials are strain rate sensitive to some extent. This is likely to be more severe for semi--conductors and semi-brittle materials which generally have large stress exponents (N) arising from dislocation velocity control:

$$\dot{\varepsilon} \propto \sigma_y^N \qquad 3.1.1a$$

The strain rate sensitivity of surface-plasticity mechanisms (as described in 2.5.2) is almost completely unknown, but the occurance of anomalous indentation creep under dead load indicates that it may exist.

Therefore the static load exerted by the mechanism must be zeroed and calibrated, and the indenter velocity must be kept constant if comparable measurements are to be made.

The time at full load must also be standardised because of indentation creep (both conventional and anomalous) . This must be long enough for all significant cracking and dislocation movement to cease but it must not be long enough for indentation creep mechanisms to have an influence where these are not the same as those controlling the "instant" response. Generally 5 to 60s are the periods that have been used as standard by other researchers and in this work a 15s period has been used for the room temperature work.

If there are random vibrations with periods of more than a few seconds then they may cause a'creep-mimic' effect (Moore, 1974) as the longer the dwell time the greater the probability that an impulse will occur and hence the longer the dwell time, the lower the measured hard--ness will be.

(b) Axial Loading

Thibault and Nyquist (1947) originally found that the hardness was reduced when measured using asymmetrical indentations made when the surface of the material was not perpendicular to the indenter axis. This is to be expected as half the square of the mean diagonal measurement is an overestimate of the area of the indentation when it is not square. However, Mulhearn and Samuels have shown that even taking this geometrical effect into account the equilibrium hardness pressure is less for asymmetrical indentations (using the Vickers indenter) in steels. Moore (1974) has shown that the geometrical mean, rather than the arithmetic mean, of the indentation diagonals gives a better estimate of the area and thus small asymmetries (up to 20%, or 7° inclination from the vertical) can be tolerated when making measurements. This can be compared with the earlier 'safe' limits of 2° (Vickers) and ½° (Knoop) suggested by Thibault and Nyquist. The lower hardness measured from skew indentations is more likely to be due to sideways movement of the indenter than to the different stress state.

(c) Indenter Shape

Vickers indenters used for macrohardness measurements often have a chisel tip about 0.5 μm long (see figure 3/1): whereas microhardness indenters should appear to be perfectly sharp in an optical microscope although, in fact, they will have a slightly rounded tip. These imperfections lead to inaccurate measurements from small indentations and hence an indentation size effect on macrohardness can exist though the effect for microhardness, when the tip radius is estimated to be 0.1 to 0.01 μm, is probably insignificant as the smallest indentations used in this study are about 3 μm in diameter.

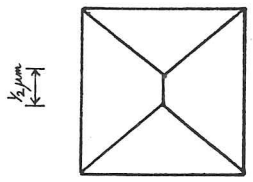

Figure 3/1

3.1.2 Indentation Size Measurement

(a) Instrumental Effects

The most critical measurement for determining hardness numbers is that of the indentation diagonal. This is the measurement likely to be subject to the greatest random error, and probably, the greatest systematic error. In addition, since $H \propto d^{-2}$ an error of x% in d produces an error of 2x% in H.

The problems of resolving indentations in the optical microscope have been reviewed by Moore (1974) and, briefly, by Burnand (1972); the error is twice the Resolution Limit (RL):

$$RL = \frac{0.61 \cdot \lambda}{\text{numerical aperture}} \qquad 3.1,2a$$

which is 0.5 μm for a numerical aperture of 0.65, i.e. for the 40× objective on the Leitz Miniload. However, diffraction effects cause the points where the contrast changes most rapidly (i.e. the points where the corners of the indentation appear to be) to be further apart than they should be. Thus a systematic shift of 0.25 RL is expected, which

should be compared with the expected standard deviation of the measurements, due to diffraction effects, of 0.25 RL. These predictions have been contradicted by comparison of optical and scanning electron microscopy of indentations (Burnand, 1972 and Haglund, 1970) which has shown that the systematic error in optical measurements makes the indentations appear smaller.

While optical microscopy obscures the edges and corners of the indentations, scanning electron microscopy causes problems because of the depth of field of the image. The edges of all real indentations are rounded (see figure 3/2): and optical imaging produces a sharp differentiation (because of the limited numerical aperture, shown in the figure as a stop) from a smooth curve, whereas an SEM resolves the whole indentation and a decision must be made by the operator as to which point should be taken as the edge of the indentation. This introduces a subjective and systematic variation.

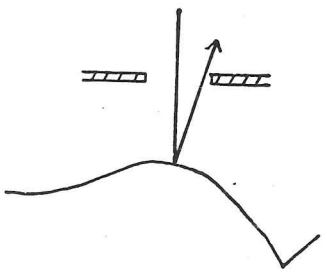

Figure 3/2

It has been suggested (Varchenya et al. 1970) that dislocation etch pit rosette diameters could be used instead of indentation diagonals as they are larger and more accurately measureable. However, it has been shown (section 2.4.1) that a simple proportionality between the two lengths does not always exist.

3.1.2(b) Effect of Test Material on Indentation Visibility

As mentioned above, an accurate measurement of an indentation depends upon acheiving a sharp contrast between the 'inside' and the 'outside' of the indentation, where these have to be defined in terms of the viewing system's effective numerical aperture.

This good contrast is difficult to achieve if the material is transparent e.g. glass, LiF, MgO, or if also suffers from lateral and intergranular cracking on indentation. In the first case, a black background gives better contrast than white, but often the image is then too dark to make measurements. When cracking occurs the scattered light can obscure even the shape of the indentation. The solution in both cases is to sputter-coat the surface with a few hundred Ångstroms of gold to increase the surface reflectivity. This renders the surface topography much more visible (the indentation, the median vents and the intersection of the lateral cracks with the surface). To specifically study sub-surface cracks, polarised light microscopy of uncoated specimens is recommended , which should be followed by coating the surface and using the techniques for opaque specimens: Nomarski interference microscopy and Tolansky interferom-etry to give qualitative and quantitative, respectively, information about the topography.

3.1.3 Displacement Controlled Indentation

Some pilot experiments were made with a Vickers indenter fixed to the cross-head of a screw-driven mechanical testing machine (Instron 1195) driven at its slowest speed (0.83 μms^{-1}) with a continuous force readout from a load cell in series with the specimen. There was no independent displacement measurement, the distance travelled by the indenter was inferred from the crosshead velocity and the duration shown on the chart-recorder trace (which was driven at 83 mms^{-1}).

The time of first contact was determined to an accuracy of $\pm$ 0.2s and hence displacements were theoretically absolutely measurable to $\pm$ 0.16 μm.

In order to make useful comparisons between hardnesses measured using this method and those measured using the Leitz Miniload it was necessary to extract from the recorder trace the information about the residual plastic indentation. The force measured on unloading was subtracted from the force measured on loading at positions of equal displacement (i.e. depth of indentation).

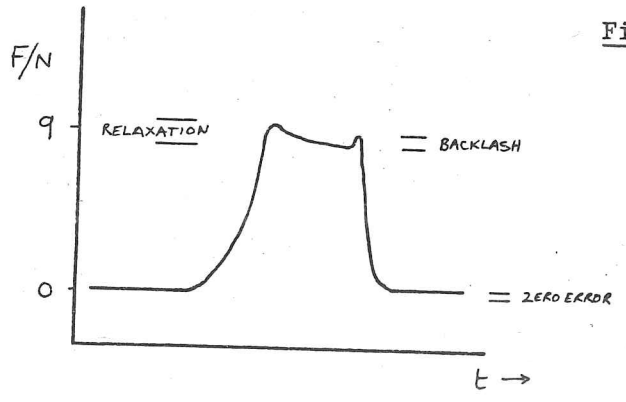

Figure 3/3

The unloading curve contains the information about the elasticity of the specimen, jig, load cell and machine, and the plasticity that occurs on unloading (Johnson, 1968). Unfortunately the apparatus was subject to stress-relaxation and backlash in the screws and thus the uncertainty in

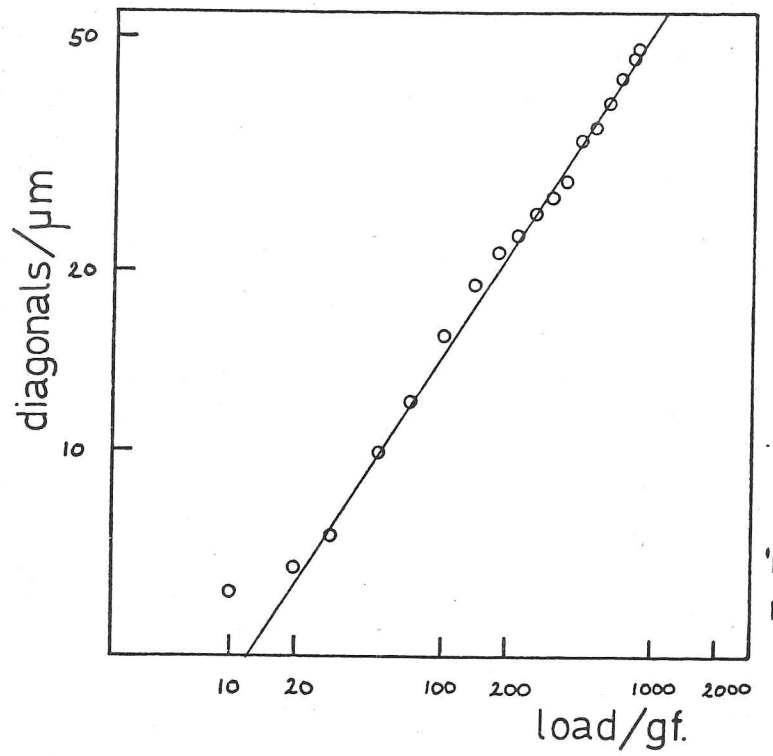

ISE INDEX
= 1.804 ± 0.129

3/4

M9D2P2

'PURE PLASTIC'
DATA

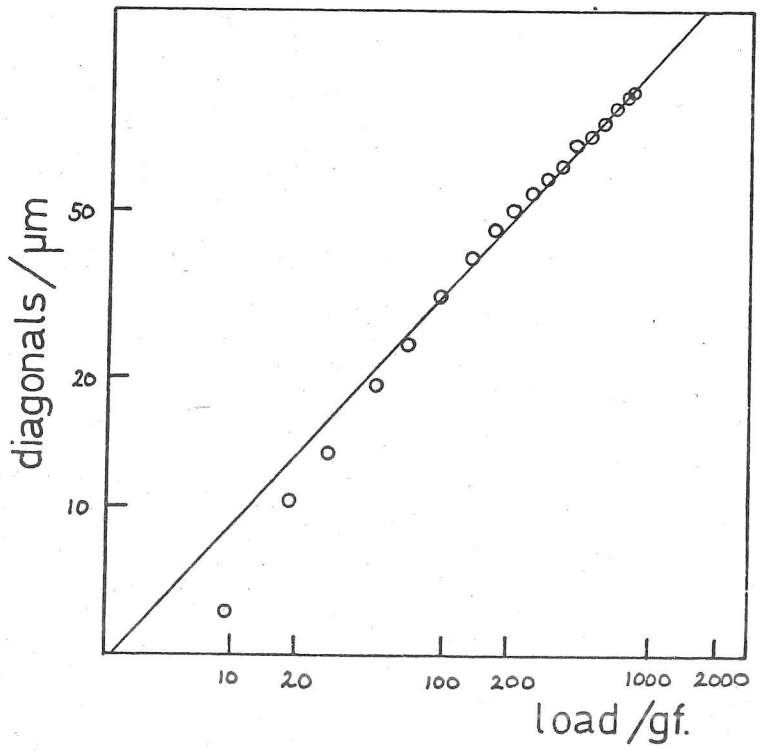

ISE INDEX
= 1.814 ± 0.133

3/5

M9D2EP2

LOADING CURVE

the displacements on unloading was of the order of microns, which was not good enough, being roughly the same as the depth of the indentation. Figure 3/3 shows a diagram of the loading, holding, and unloading curves from the chart recorder trace for a polycrystalline MgO specimen (MGO9). Figures 3/5 and 3/6 are ln/ln plots of the loading curve and the 'loading minus unloading' curves respectively.

While the stress relaxation and the machine elasticity could be calibrated and allowed for it is doubtful that the same could be done for the backlash. This requires the use of an independent method for measuring the penetration of the indenter; a capacitive displacement transducer would probably be the simplest with the required accuracy. The problems of vibration were not investigated systematically but were obviously severe.

Fröhlich et al. (1977) and Degtyarev et al. (1977) have made macro-hardness measurements using mechanical testing machines and in this regime the problems mentioned above are less critical, however they made no allowance for the elasticity of the jig and machine in their work which would still have been important.

At first sight the use of a servo-hydralic machine, rather than a screw-driven machine, would circumvent most of the difficulties, but such machines have very strong load-fluctuations at the resonant period of the servomechanism. It has been suggested (Paetke, 1979) that a stack of piezoelectric crystals in series with the specimen and linked electrically to an independent displacement measuring device could be used to eliminate these vibrations and to simulate an 'infinitely hard' machine, but for making displacement controlled microhardness indentations it is simpler to design a machine for the purpose, and this is discussed in chapter 5.

3.2 Measuring the Indentation Size Effect

Only when hardness indentations can be made and measured reproducibly under controlled conditions can the effect of a range of conditions be investigated. Measuring the indentation size effect (ISE) on microhardness entails measurement of hardness using a range of loads but keeping the other variables described in chapter 2 constant. However, it is necessary to define what is meant by 'indentation size effect' with due regard for the experimental problems.

3.2.1 ISE Definition and Experimental Procedure

The indentation size effect, that is, the change in hardness for a change in indentation size, is essentially unmeasurable:

$$\text{ISE index} = \text{Function}\left[\left.\frac{\partial H}{\partial d}\right|_{d=d_i}\right] \qquad 3.2.1a$$

The ideal ISE value is defined at a specific indentation size whereas the experimental scatter means that in practice it can only be measured over a range of indentation sizes. This means that the measurement of ISE is subject to two variance contributions, from the experimental scatter and from the change in the ideal ISE over the range of indentation sizes used for its determination.

The method of data analysis was developed according to several guidelines: it had to produce ISE values comparable with those produced by the methods of other workers and it had to be capable of being used on data published from which an ISE value had not been calculated. The method had to give estimates of the errors in the quantities it measured so that differences between results from different specimens could be interpreted sensibly. If possible, the analysis also had to be easily usable by other researchers so that truely comparable measurements of ISE could be made in the future using a standard method.

Bearing these points in mind, the problem was attacked from two directions. Firstly, a statistical treatment was developed using the log-index relationship, described in 2.5.1, and expressing the ISE as a value in the same range as published log-index values. The treatment is applicable to measurements made using any kind of hardness indenter over any load or indentation size range. Secondly, certain practical constraints were adhered to for all the experimental measurements made in the present study to reduce the variability introduced by poorly understood variables; in addition to taking the precautions described in 3.1 to reduce errors in individual measurements. Thus all measurements of ISE were made using a standard load range. This meant that wide variations in indentation size occured between hard and soft materials but this was done, rather than using a fixed indentation size range, because the latter was felt to be too time consuming and was unlikely to be used by other workers in their own experiments.

The same number of measurements were made at each load in the standard range (10, 20, 50 and 100 gf.) to prevent the interpolated hardness value (see 3.2.3) being weighted towards the hardness at any one load and to reduce the number of indentations required to obtain a usable estimate of the ISE index. The particular loads in the standard range were chosen so that measurements made using the Leitz Miniload would be absolutely comparable with those made using the high temperature, controlled atmosphere/vacuum microhardness testing machine ('Bessie') designed by Wilberforce Scientific Developments. For full details of this apparatus see Naylor (1978).

When measuring the ISE for large grain-size polycrystalline materials Vickers indenters are preferable because the variance introduced by the hardness anisotropy of the grains is less for Vickers than for Knoop indenters. Therefore, for compatibility, all measurements of ISE were made, unless otherwise indicated, with the same Vickers indenter (V-04).

3.2.2 Random Errors and Error Ellipsoids

The analytic function that comes closest to describing the ISE in the same terms as the 'ideal' ISE is the log-index empirical function (described in 2.5.1 and 2.5.3) where:

$$n - 2 = \frac{d}{H} \cdot \frac{\partial H}{\partial d} \qquad 2.5.3d$$

and the log-index (n) is commonly used as a measure of the ISE by those researchers who do not try to explain away the effect as being due to measurement, or elasticity, difficulties alone. Fortunately the log-index relationship is one of the better empirical functions and thus the measure-ment of an ISE value can be accomplished by fitting the function to the data by a least squares method (see 3.2.3) and using 'n' as the quantitative ISE index. However, there are several ways of fitting an analytic function to experimental data, and the type of experimental scatter determines the best method. When making indentations using a dead-loaded machine and measuring them with an optical microscope nearly all the scatter is in the diagonals' measurements at fixed loads. Therefore the procedure developed fits the function by minimising the squares of the deviations in these measurements (see 3.2.3). Most researchers do not state which deviations they use to make the fit, and those that do, use the deviations in load, which is incorrect.(Adewoye, 1976).

The fitting procedure calculates the variance in the log-index which is a consequence of the experimental scatter and calculates confidence limits for both the ISE index and the interpolated hardness value (the hardness which would be measured from a well behaved indentation exactly 10 microns in diameter). The ten micron hardness ($H_{10\mu m}$) was chosen because it has obvious physical meaning, which 'a' (equation 2.3.2a) does not. If the range of indentation diagonals in the data includes ten microns then there is only a small covarience between 'n' and '$H_{10\mu m}$' which means that the ellipsoid axes (see 3/6) are roughly parallel to the plot axes.

Confidence limits on a single variable can be displayed graphically using error bars, but when two non-statistically independent variables are involved an error ellipsoid can be plotted (see 3/6 and the next section). (A brief description of this procedure also appears in Sargent and Page, 1978.)

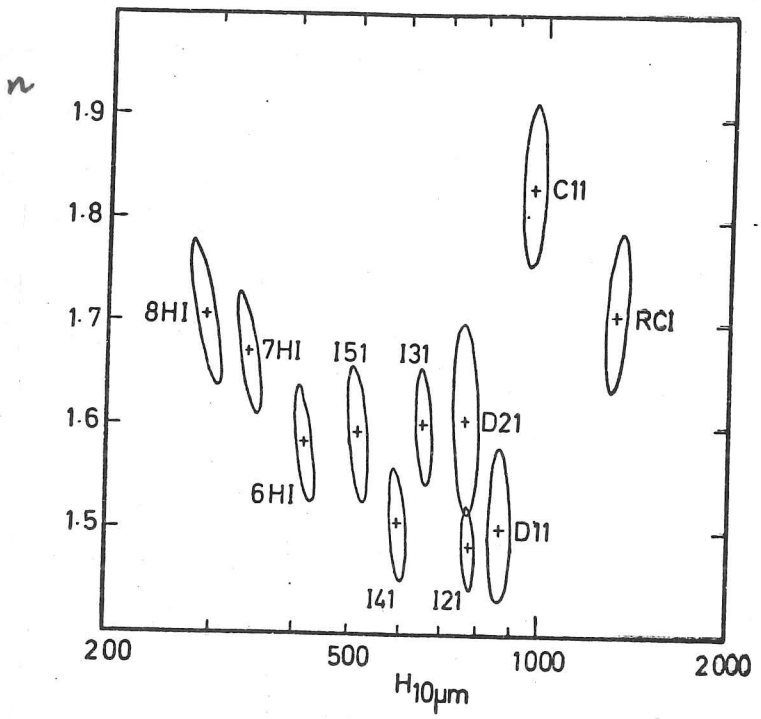

Figure 3/6

For each ellipsoid there is a 95% probability that if a very large number of measurements are made on the specimen then this 'very accurate' pair of values (n and $H_{10\mu m}$) would lie somewhere inside the ellipsoid calculated from the current results. However, it is important to realise that the area of the ellipsoid represents only the random scatter within each set of data (and any change in 'ideal' ISE over the load range) and does <u>not</u> allow for variations between sets of data due to inadequately controlled variables such as visual acuity, relative humidity, or indenter velocity.

Confidence limits on a single variable can be displayed graphically using error bars, but when two non-statistically independent variables are involved an error ellipsoid can be plotted (see 3/6 and the next section). (A brief description of this procedure also appears in Sargent and Page, 1978.)

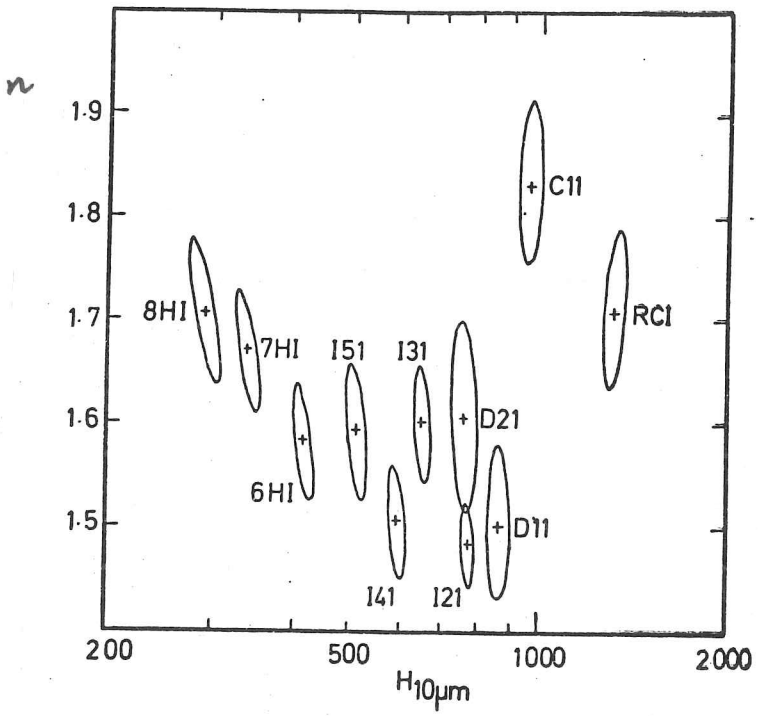

Figure 3/6

For each ellipsoid there is a 95% probability that if a very large number of measurements are made on the specimen then this 'very accurate' pair of values (n and $H_{10\mu m}$) would lie somewhere inside the ellipsoid calculated from the current results. However, it is important to realise that the area of the ellipsoid represents only the random scatter within each set of data (and any change in 'ideal' ISE over the load range) and does not allow for variations between sets of data due to inadequately controlled variables such as visual acuity, relative humidity, or indenter velocity.

3.2.3 Calculating the ISE Index and Confidence Ellipsoids

The ISE index and confidence ellipsoids are calculated from a set of data consisting of the loads put on the indenter L_i and the diagonal measurements of the indentations d_i (where i = 1,N). The ISE index 'n' is calculated by fitting the data to the function:

$$L = a.d^n \qquad 3.2.3a^*$$

where 'a' is another fitted parameter. The problem is to find values of 'a' and 'n' which describe a curve which goes as close as possible to the experimental points (see figure 3/7). An experimental point is defined by a pair of values L_i and d_i. The method used is to take a log/log transformation of the data and to fit it to a log/log transformed function (equation (b)) which is a straight line (see figure 3/8). Natural logs are used throughout.

$$\ln(L) = \ln(a) + n.\ln(d) \qquad (b)^*$$

For experimental data a least squares fit is the best to use; the parameters 'a' and 'n' are calculated to minimise the sum over the experimental points of the squares of the distance of the experimental point from the line. Now there are two different methods for doing this involving two different residual distances r(L) and r(d). For a particular point (d_i and L_i) and a given line (i.e. given values of 'a' and 'n') the two residual distances are parallel to the two axes of the graph and are given by equations (e) and (f) using the definitions of d and L in equations (c) and (d), see figure 3/9.

---

*Footnote: In this section, the 50 equations will be identified only by the relevent letter, i.e. (b), the prefix 3.2.3 should be assumed to be present.

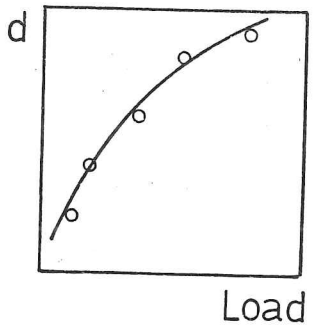

Figure 3/7

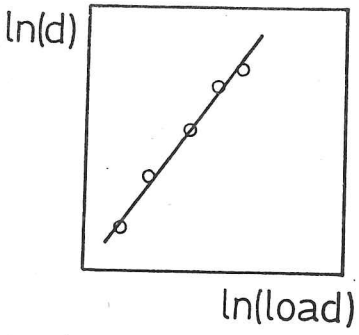

Figure 3/8

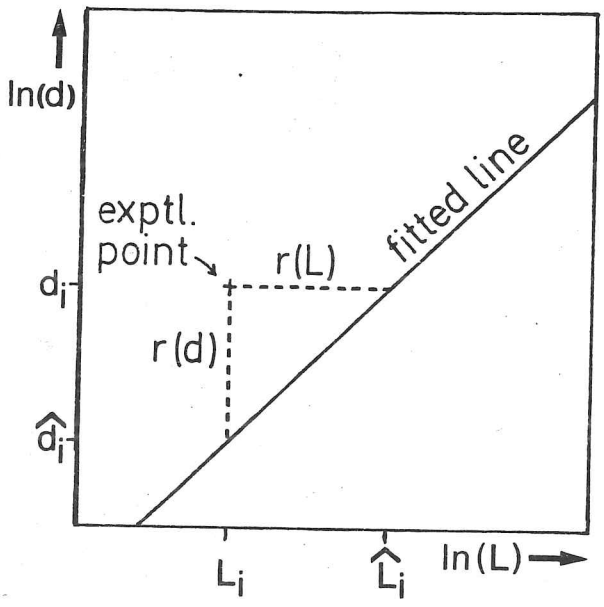

Figure 3/9

$\hat{d}_i$ is the expected size of the indentation given the the load used (L_i) and the relationship between d and L given by the line. $\hat{L}_i$ is, similarly, the expected load given d_i.

$$\ln(\hat{L}_i) = \ln(a) + n.\ln(d_i) \qquad (c)$$

$$\ln(\hat{d}_i) = \frac{-\ln(a)}{n} + \ln(L_i) \qquad (d)$$

The residual distances r(L) and r(d) are defined by:

$$r(L) = \ln(L_i) - \ln(\hat{L}_i) \qquad (e)$$

$$r(d) = \ln(d_i) - \ln(\hat{d}_i) \qquad (f)$$

Which of these two residual distances is used for the minimisation depends on the experimental arrangement. For a dead-loaded microhardness machine, such as the Leitz Miniload, most of the error occurs in the measurement of the indentation diagonals at a 'fixed' load. Therefore the errors in 'd_i'are minimised here by using r(d).

The sum of the squares of the residual distances is S', defined in equations (g) to (i).

$$S' = \sum_1^N r^2(d_i) \qquad (g)$$

$$S' = \sum_1^N \left[\ln(d_i) - \ln(\hat{d}_i)\right]^2 \qquad (h)$$

$$S' = \sum_1^N \left[\ln(d_i) + \frac{\ln(a)}{n} - \frac{\ln(L_i)}{n}\right]^2 \qquad (i)$$

Now S' must be minimised with respect to 'a' and 'n', which is difficult with the equations in their present form, so S' will be minimised with respect to A and B where these are defined in equations (j).

$$A = \frac{-\ln(a)}{n} \qquad B = \frac{1}{n} \qquad \text{(j) (j)}$$

$$S' = \sum^{N} \left[\ln(d_i) - (A + B.\ln(L_i))\right]^2 \qquad \text{(k)}$$

The ISE index is 'n' which is easily calculated from A and B. The 'ten micron hardness' ($H_{10\mu m}$), the interpolated hardness measured from a perfect indentation of diagonal ten microns, which is also derived from 'a' and 'n' can also be derived from A and B:

$$H_{10\mu m} = 18.544 \,.\, a \,.\, 10^{n} \qquad \text{(l)}$$

Differentiation is used to minimise S' in the usual manner:

$$\frac{\partial S'}{\partial A} = 0 \qquad \frac{\partial S'}{\partial B} = 0 \qquad \text{(m) and (n)}$$

using these relations and equations (j), equations (o) and (p) are obtained:

$$A.N - \sum^{N} \ln(d_i) + B \sum^{N} \ln(L_i) = 0 \quad \text{(o)}$$

$$A \sum^{N} \ln(L_i) - \sum^{N} \ln(d_i)\ln(L_i) + B \sum^{N} \ln(L_i)^2 = 0 \quad \text{(p)}$$

These are two simultaneous equations in A and B with solutions $[A]$ and $[B]$. They can be used to calculate the best-fit values for 'a' and 'n', and hence $H_{10\mu m}$, using equations (q) and (r),(see equations j):

$$n = 1/[B] \qquad \text{(q)}$$

$$\ln(a) = -[A]/[B] \qquad \text{(r)}$$

An alternative, and completely equivalent, method for calculating 'a' and 'n' is by the use of matrices (quoted here without proof from Draper and Smith, 1966). This approach is more suited to automatic computation.

The N data points are paired sets of values of $\ln(d_i)$ and $\ln(L_i)$, these can be considered to be 2 vectors $\underline{Y}$ and $\underline{\lambda}$ respectively, of length N. Now, there is a matrix (of dimension 2*2) which contains the variences and covariences of the two estimates of the two fitted parameters [A] and [B]:

$$\text{matrix} = \begin{pmatrix} \text{cov}([A],[B]) & \text{var}([A]) \\ \text{var}([B]) & \text{cov}([A],[B]) \end{pmatrix} = D \qquad (s)$$

it can be shown that:

$$D = (X'X)^{-1}\sigma^2 \qquad (t)$$

where (i) X is an N*2 matrix, the first column of which is all 'ones' and the second column of which is the vector $\underline{\lambda}$ (the list of all the $\ln(L_i)$ values), and (ii) where σ^2 is estimated by s^2, the mean square of the residuals (equation u); this estimation is only valid if the distribution of errors is normal.

$$(N-1)s^2 = \text{sum of squares} = \sum^{N} r(L_i)^2 \qquad (u)$$

In practice the matrix D is calculated from the output of Harwell subroutine VC04.

Now, in order to calculate the best fit values [A] and [B], the vector $\underline{b}$ is defined:

$$\underline{b} = \begin{pmatrix} [A] \\ [B] \end{pmatrix} \qquad (v)$$

which is a constant, whereas vector $\underline{\beta}$ is a variable:

$$\underline{\beta} = \begin{pmatrix} A \\ B \end{pmatrix} \qquad (w)$$

Now it can be proved that:

$$\underline{b} = (X'X)^{-1}X'Y \qquad (x)$$

where Y was defined earlier to be the vector of the values $\ln(d_i)$. Hence $\underline{b}$ can be calculated .

Now if a plot is made of the A/B plane it can be seen that $\underline{b}$ is a fixed point and that $\underline{\beta}$ is a general point (see figure 3/10).

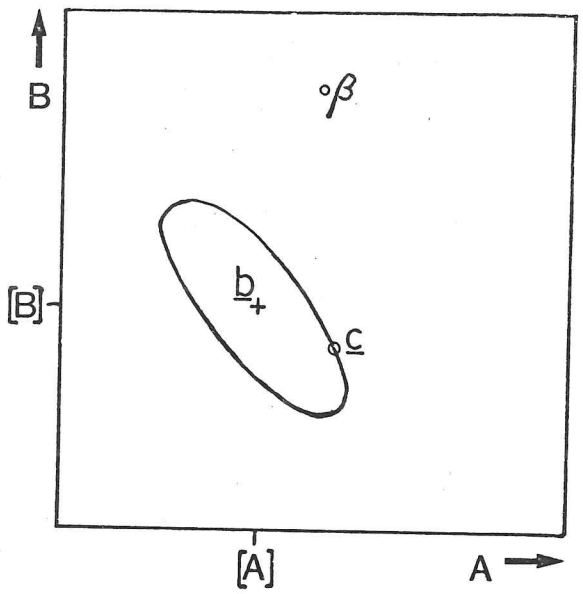

Figure 3/10

Confidence ellipsoid plotted in A/B space.

b is the best-fit point, but, because of the inherent variation in experimental quantities, there is a finite chance that the 'real' values of A and B lie instead at a point β. The probability that this is so can be calculated using equation y:

$$(\beta - \underline{b})'D^{-1}(\beta - b) = 2F \qquad (y)$$

Now a locus of all the points, c for example, which have the same probability of being the 'correct' point can be plotted and it has the form of an ellipse described by (y) when $c = \beta$. F is the F-statistic for N-2, and 2, degrees of freedom.

If the probability value is 5% then there is only a 5% chance that the 'real' values of A and B lie outside the ellipse, and a 95% that the lie within it. The ellipse is then known as the 95% confidence region.

Calculation of the Ellipse

Define the matrix D^{-1}, the inversion of the matrix D, as M. M has elements M_{11}, M_{22}, and $M_{21} = M_{12}$. Now it is easier if the origin of A/B space is shifted to the point b and the axes relabled x/y, then the equation of the ellipse becomes:

$$x^2.M_{11} + y^2M_{22} + 2xyM_{12} - 2F = 0 \qquad (z)$$

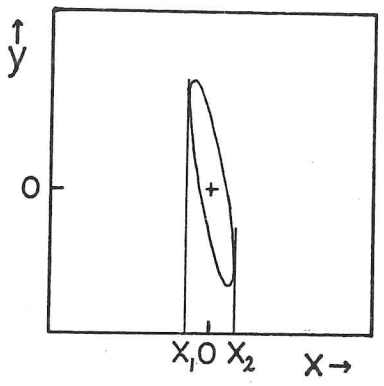

Figure 3/11

The extremes of the ellipse at x_1 and x_2 are defined by differentiating the function describing the ellipse with respect to y and setting the result equal to zero, hence:

$$x_1^2 = x_1^2 = \frac{2FM_{22}}{(M_{11}M_{22}-M_{12}^2)} \qquad (aa)$$

and hence, from z:

$$y = \frac{x}{M_{22}}\left[-M_{12} \pm \left(M_{12}^2 - M_{22}(M_{11} - \frac{2F}{x^2})\right)^{1/2}\right] \qquad (ab)$$

was used to plot the ellipse, the $\pm$ values being the two branches of the ellipse between x_1 and x_2.

Hence the ellipse was plotted in x/y space, and by shifting the origin, also in A/B space. Every point on the ellipse was then transformed using equations q and r into a point in 'n' (ISE index) and 'a' space, they were then transformed using equation 1 into points in 'n' and H_{10} space. This sequence changes the ellipse into an ellipsoid but retains the validity of the meaning of the 95% confidence region.

Weighted Least Squares Fit

When the original ln/ln transformation is made it transforms the normal (Gaussian) distribution of the errors in the data into a log--normal distribution which means that a plain least-squares fit is inappropriate and that a weighted least-squares fit should be used. Each experimental point d_i & L_i should be assigned a number, a weight w_i whose increasing magnitude indicates increased importance. The problem is that a ln/ln transformation compresses the data at higher values of d and L, and thus larger weights should be assigned to these points to compensate for the smaller residual distances from the fitted line. The relevent formulae are then:

$$S'' = \sum w_i . r(d_i)^2 \qquad (ac)$$

instead of (g), and (ad) and (ae) instead of (o) and (p):

$$0 = A \sum w_i - \sum w_i \ln(d_i) + B \sum w_i \ln(L_i) \qquad (ad)$$

$$0 = A \sum w_i \ln(L_i) - \sum w_i \ln(d_i)\ln(L_i) + B \sum w_i \ln(L_i)^2 \qquad (ae)$$

these are two simultaneous equations for A and B and hence the ellipsoid in 'n' and $H_{10_{\mu m}}$ can be calculated.

The equivalent matrix treatment uses the N*N matrix W where the elements are defined by:

$$W_{ij} = w_i \quad (i=j)$$
$$= 0 \quad (i \neq j) \qquad (af)$$

The matrix D is redefined by:

$$D = (X'WX)^{-1}\sigma^2 \qquad (ag)$$

and the solution vector $\underline{b}$ by:

$$\underline{b} = (X'WX)^{-1}X'WY \qquad (ah)$$

and hence the confidence ellipsoid can be calculated as above. One problem remains, of how to decide what the weights should be.

A good estimate of W can be obtained by considering the equations to be solved if the original function (a) were to be fitted to the data

instead of the ln/ln transformed function. Thus :

$$\hat{d}_i = (L_i/a)^{\frac{1}{2}} \qquad (ai)$$

from $$L_i = a\hat{d}_i^n \qquad (aj)$$

is used to define :

$$S = \sum \left[d_i - \hat{d}_i\right]^2 \qquad (ak)$$

and $$S = \sum \left[d_i - (L_i/a)^{\frac{1}{2}}\right]^2 \qquad (al)$$

rewriting in terms of A and B and minimising:

$$\exp(A) \sum L_i^{2B} - \sum L_i^B.d_i = 0 \qquad (am)$$

$$\exp(A) \sum L_i^{2B}.\ln(L_i) - \sum L_i.d_i.\ln(L_i) = 0 \qquad (an)$$

L_i^B can be approximated by:

$$L_i^B \simeq 1 + B.\ln(L_i) \qquad (ao)$$

which is only valid when L_i is close to 1.0 (this condition will be relaxed later). Now:

$$\hat{d}_i = \exp(A).L_i^B \qquad (ap)$$

from equations ai and r. Therefore:

$$\hat{d}_i/\exp(A) \simeq L_i^B \quad \text{which is also close to 1.} \qquad (aq)$$

Therefore it is reasonable to assume that $d_i/\exp(A)$ is also close to 1 (note that this and the previous statement differ in the terms for $\hat{d}_i$ and d_i). Now:

$$\exp(A).L_i^{2B} \simeq (1 + B.\ln(L_i)).\hat{d}_i \qquad (ar)$$

therefore:

i.e.:
$$\sum \hat{d}_i.(1 + B.\ln(L_i)) - \sum L_i^B.d_i = 0 \qquad (as)$$

$$\sum \hat{d}_i.(1 + B.\ln(L_i)) - \sum \frac{d_i.\hat{d}_i}{\exp(A)} = 0 \qquad (at)$$

Now, using (ap):

$$d_i/\exp(A) \simeq 1.0 \simeq 1 + \ln(d_i/\exp(A)) \qquad (au)$$

and (at):

$$\sum \hat{d}_i + B \sum \hat{d}_i.\ln(L_i) - \sum \hat{d}_i(1 + \ln(d_i/\exp(A)) = 0 \qquad (av)$$

i.e.

$$A \sum \hat{d}_i - \sum \hat{d}_i.\ln(d_i) + B \sum \hat{d}_i.\ln(L_i) = 0 \qquad (aw)$$

Now if (aw) is compared with equation (ad) it can be seen that the values $\hat{d}_i$ are the weights to be used. Unfortunately the values $\hat{d}_i$ are obtained from the data by making the fit and cannot be used to make the fit in the first place. Thus the solution adopted was to take the mean value of the diagonal measurements at a particular load and to use this $\bar{d}$ instead of $\hat{d}_i$ (see figure 3/12):

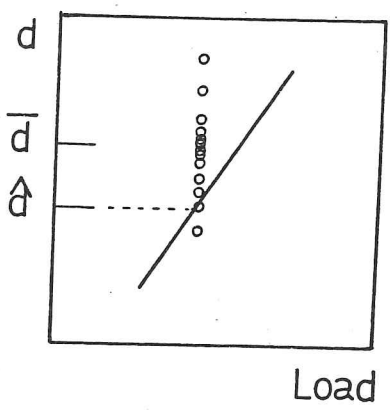

Figure 3/12

The condition that all the values of d_i and L_i lie close to 1.0 will now be relaxed. If one considers that all the data is scaled by dividing each measurement by the geometrical mean of the extremes of the data:

$$\text{new } d_i = d_i/(d_1.d_N)^{\frac{1}{2}} \qquad \text{(ax)}$$

If the range was d_1=50 microns and d_N=55 microns, then the new range would be 0.953 to 1.049. Then, since the least squares fit is not dependent on the numbers involved, the best-fit values can be rescaled afterwards. This procedure can only work when d_1 and d_N (and L_1 and L_N) are close together; realistically the range for the diagonals is between 3.5 and 15 microns, which gives a scaled range of 0.48 to 2.07, which means that in the practical situation the weights are only approximately correct. However, this standard method has been used for all the analysis in this thesis; the suite of programs which were written for this purpose are called ISEMH and are listed in appendix I.

3.2.4 Random and Systematic Differences

By remeasuring indentations under different lighting conditions, degree of eyestrain and under- or over-focus it has been established that possible variations due to measurement are of the same order as the random variation within each set of measurements. However, experimentally it has been found that results from sets of indentations made on different occasions on the same material often seem to vary between the sets by more than would be expected from random scatter (e.g. see figure 4/19). If this observation can be shown to be statistically significant, it would indicate that the variables that remain to be accurately controlled are important and not insignificant. Therefore, a technique was developed which compares one set of results with another and gives an estimate of the probability that the two sets are essentially the same and that the diffference is due only to the random scatter within each set of data.

Thus two specimens can be prepared differently, or the same specimen indented under different conditions, and then it is possible to test rigorously whether the different treatments have had a significant effect on the hardness and the ISE. When this is done for a single variable, Student's t test can be used, but when two mutually dependent random variables are involved (i.e. $(n_i-\bar{n})$ and $(H_{10_i}-\bar{H}_{10})$ have a covariance which is not equal to zero), a different technique involving the residual standard deviations from the linear regressions is required.

One simple and quick approach is to look at the confidence ellipsoids for two specimens; if they overlap to an appreciable extent then it is likely that their indentation behaviours are the same. However, a more accurate estimate of the probability of coincidence can be obtained by the method described below.

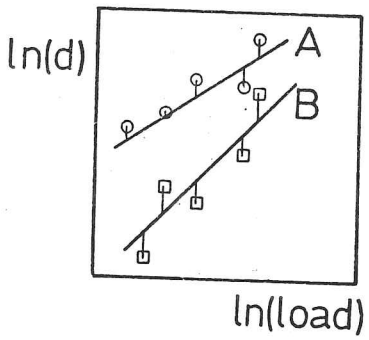

Figure 3/13

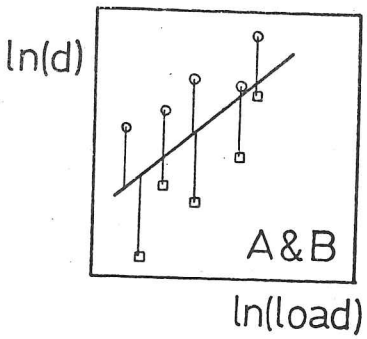

Figure 3/14

If the two sets of data are termed P and Q then the first action is to merge them into one set (using the MERGE program, see appendix I) termed P&Q. Then the ISEMH program (see appendix I) is run on all these three sets of data: P, Q, P&Q. The three fitted functions are shown as straight lines in figures 3/13 and 3/14. For each fit the program calculates the weighted sum of squares of the residual distances: S", see figure 3/9 and equations 3.2.3f, 3.2.3ac and 3.2.4a:

$$S'' = \sum^{N} \left[w_i \ln(d_i) - \ln(d_i) \right]^2 \qquad 3.2.4a$$

These residual distances are shown in figures 3/13 and 3/14 as vertical lines joining the data points with the function line. It can be seen that when the sets of data P and Q are very different, as in the figures, then S''_P and S''_Q are much smaller than $S''_{P\&Q}$.

If the number of data points in P is N_P, in Q:N_Q, and in P&Q: $N_{P\&Q} = N_P + N_Q$, and the sum of squares $S''_{P\&Q}$ is related to the variance by:

$$V = S''/(N-2) \qquad 3.2.4b$$

because (N-2) is the number of degrees of freedom of the fit, then:

$$V_P = S''_P/(N_P-2) \qquad 3.2.4c$$

and similarly for Q and P&Q.

Now, remembering the relative magnitudes of S''_P, S''_Q and $S''_{P\&Q}$ from figures 3/13 and 3/14, it can be seen that if the two sets of data are really different then the quantity F (equation 3.2.4d) will be significantly more than unity, whereas if P and Q represent the same behaviour F will be close to unity.

$$F = \frac{V_{P\&Q}}{V_P + V_Q} \qquad 3.2.4\,d$$

Quantitatively it is possible to find out to what degree of significance F is greater than unity by examining the F-statistic* tables for degrees of freedom (2):(N_P+N_Q-2). Thus if $N_{P\&Q}$ is 32 the relevent statistics are:

0.10	(90% confidence):	2.49
0.05	(95% confidence):	3.32
0.01	(99% confidence):	5.39

If F is calculated to be 3.4 then P and Q are significantly different 'to the 0.05 level' i.e. with a confidence of 95%. If F is 2.3 then any difference between P and Q could just be random scatter in P and Q (less than 90% confidence is generally considered 'not significant') but more data should be gathered as 2.3 is only just less than 2.49. If F were 1.5 then there would be little doubt that the P and Q sets of data described the same material.

---

*Footnote: A ratio of variances which describe Gaussian distributions has itself the 'F' distribution.

"There are nine and sixty ways

of constructing tribal lays,

And - every - single - one - of - them - is - right !"

Rudyard Kipling

"There are nine and sixty ways

of constructing tribal lays,

And - every - single - one - of - them - is - right !"

Rudyard Kipling

Chapter 4 - Experimental Investigations

4.1 Introduction

The numerous physical and chemical phenomena which can influence the indentation behaviour of materials have been described in chapter2, and in chapter 3 the phenomena that can affect the measurement of these indentations have been described. In this chapter several of the points raised are discussed in more detail with reference to the results of several series of experiments and measurements performed by the author.

A summary of the relationships between the physical and chemical phenomena and their effects is given in figure 4/1 (the frontispiece) and each relationship is marked with the number of the section where the effect is described, and where relevent, discussed in detail and investigated experimentally.

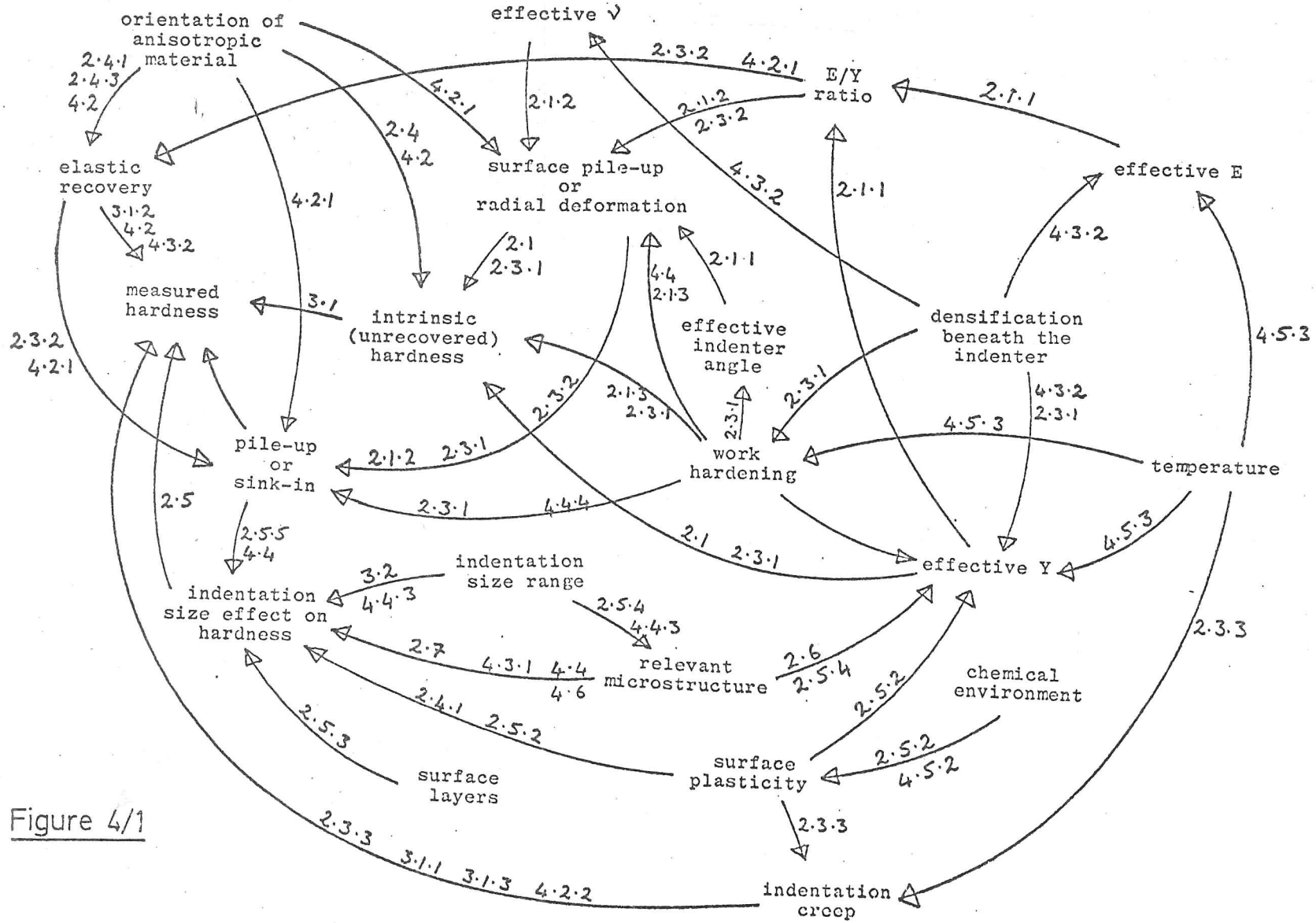
orientation of anisotropic material
effective ν
E/Y ratio
elastic recovery
surface pile-up or radial deformation
effective E
measured hardness
intrinsic (unrecovered) hardness
effective indenter angle
densification beneath the indenter
pile-up or sink-in
work hardening
temperature
effective Y
indentation size range
indentation size effect on hardness
relevant microstructure
chemical environment
surface plasticity
surface layers
indentation creep
2·4·1 2·4·3 4·2
4·2·1
2·1·2
2·3·2 4·2·1
2·1·1
2·4 4·2
4·3·2
3·1·2 4·2 4·3·2
2·1 2·3·1
3·1
4·4 2·1·3
2·1·1
2·3·2 4·2·1
2·1·3 2·3·1
2·3·1
4·3·2 2·3·1
4·5·3
2·1·2 2·3·1
2·5
2·5·5 4·4
2·3·1 4·4·4
2·1 2·3·1
3·2 4·4·3
2·5·4 4·4·3
2·7 4·3·1 4·4 4·6
2·6 2·5·4
2·5·2
2·4·1 2·5·2
2·5·3
2·5·2 4·5·2
2·3·3
2·3·3 3·1·1 3·1·3 4·2·2

Figure 4/1

4.2 Vickers and Knoop Hardness Anisotropy

A comparison of the two types of indentation on a well characterised anisotropic material can give insights into the stress and strain distributions beneath the indenters which cannot be readily obtained in any other way. In addition to setting the study of hardness anisotropy on a firmer footing, this study of the two types of indentation has implications relevant to all indentation hardness testing.

4.2.1 Definition of Hardness for Anisotropic Materials

The conventional method of measuring hardness (or microhardness) in anisotropic materials, whether they are single crystals or textured by microstructure or grain orientation, is to measure only one diagonal of the indentation.

The hardness 'in a particular direction', e.g. $\underline{f}$ in figure 4/2, is generally defined (e.g. Brookes et al. 1971, Armstrong and Raghuram 1973, or Mellor and Edmonds 1978) by taking the projected length of the diagonal of an indentation which lies along that direction ($\underline{f}$) and using the standard relationship for the relevent indenter (equation 4.2.1a) to obtain a value for 'the hardness in that direction'.

$$H = \text{geometrical factor} \cdot \frac{\text{load}}{\text{diagonal}^2} \qquad 4.2.1a$$

4.2.2 Hardness Anisotropy of Materials with Orientated Microstructures

In the current work, Vickers and Knoop indentations were made using a 50 gf. load on a directionally solidified Al-$CuAl_2$ eutectic with an average interlamella spacing of 2.8μm, and reference will also be made to the work of Mellor and Edmonds who made Vickers indentations with 300 gf. loads on unidirectionally transformed Cu-30 wt% In eutectoid (Cu/In pearlite) with interlamella spacings of 0.79μm and 2.0μm (Mellor 1974, and Mellor and Edmonds 1978).

Figures 4/3 to 4/7 are micrographs of the indentations made in the Al-$CuAl_2$ eutectic and display the microstructure of this material; the Cu/In pearlite looks very similar. Figures 4/3 and 4/4 show the effect of the orientated microstructure on the shape of the Vickers indentations; despite the foreshortening due to the axial tilt in the SEM (scanning electron microscope) in 4/3, the diagonal perpendicular to the eutectic alignment direction is obviously larger than the other diagonal. In 4/4 both diagonals are the same length but the indentation is rectangular, not square; again, similar effects were observed by Mellor and Edmonds (1978) in Cu/In pearlite. (Figure 4/4 also defines the eutectic alignment direction as the vector $\underline{e}$.)

The Knoop and Vickers hardness anisotropies for the Al-$CuAl_2$ eutectic were measured by the method described in 4.2.1 (using 4 indentations at each orientation) and they are shown in figure 4/8, the error bars are $\pm$ 2 standard deviations. This plot covers 90° from parallel to, to perpendicular to, the direction $\underline{e}$.

There are two curves for the Knoop, and one for the Vickers, hardness anisotropy in 4/8 because the two indenters have different plane symmetries (2mm and 4mm respectively). The points derived from the short diagonals of the Knoop indentations have no error bars because of the difficulty of estimating their reliability, the lengths of the short diagonals are very ill-defined, as can be seen in figures 4/5 to 4/7.

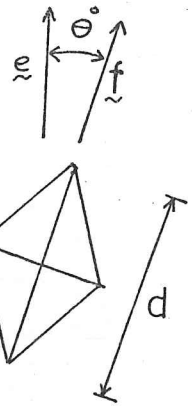

Figure 4/2

This figure defines the angle θ with respect to a fixed direction in the microstructure (in this case e, the eutectic alignment direction) and the orientation of the indenter. When measuring hardness anisotropy only one diagonal of the indentation is measured.

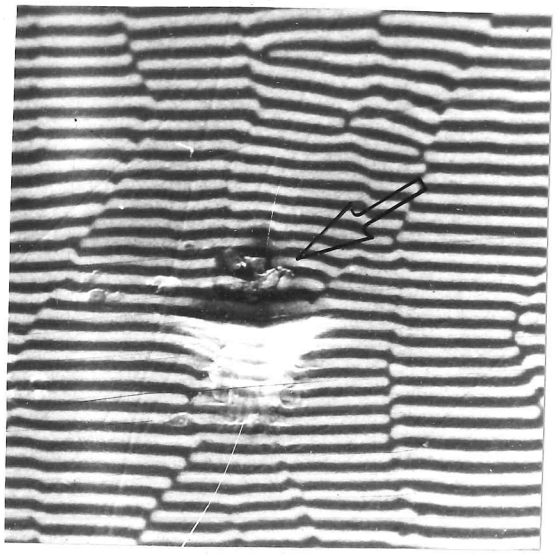

Figure 4/3 Al-$CuAl_2$ eutectic 50 gf. Vickers indentation at θ = 0° and 90° (SEM secondary image, 30° tilt). Note the cracking (marked by an arrow).
1080x

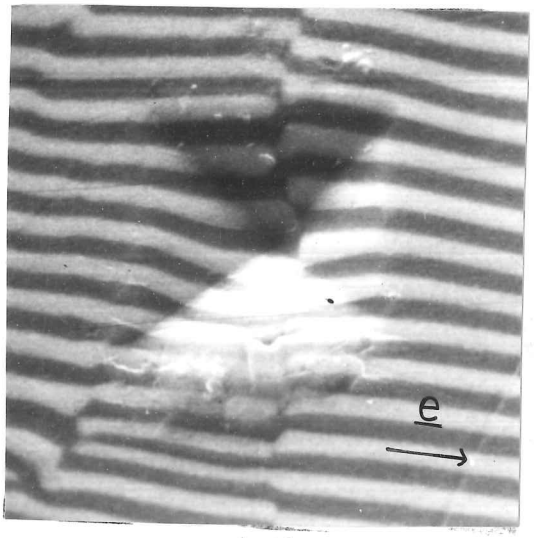

Figure 4/4 Al-$CuAl_2$ eutectic 50 gf. Vickers indentation at θ = 45° (SEM secondary electron image, 30° tilt). Note the less severe cracking which still occurs on the sides of the indentation parallel to the eutectic alignment direction e.
2232 x

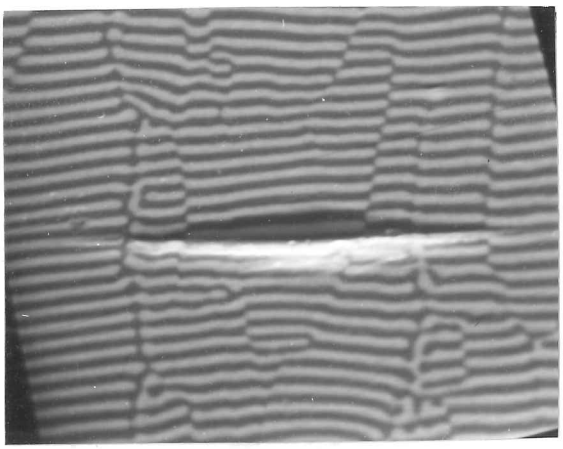

Figure 4/5

900×

SEM secondary electron image

50 gf. Knoop indentation

at θ = 0°.

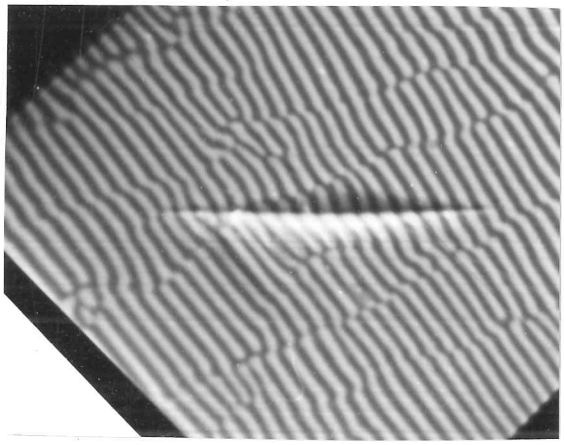

Figure 4/6

900×

SEM secondary electron image

50 gf. Knoop indentation

at θ = 45°.

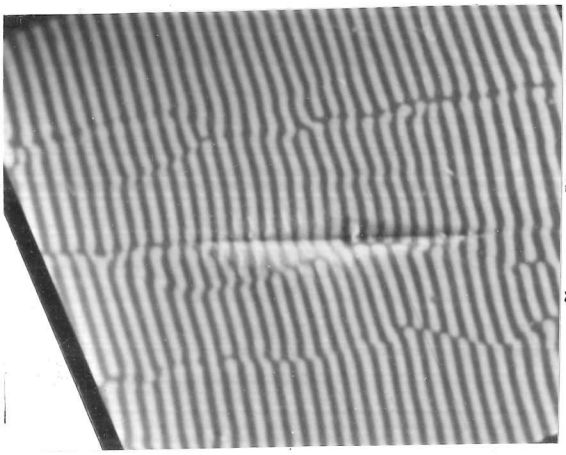

Figure 4/7

900×

SEM secondary electron image

50 gf. Knoop indentation

at θ = 90°.

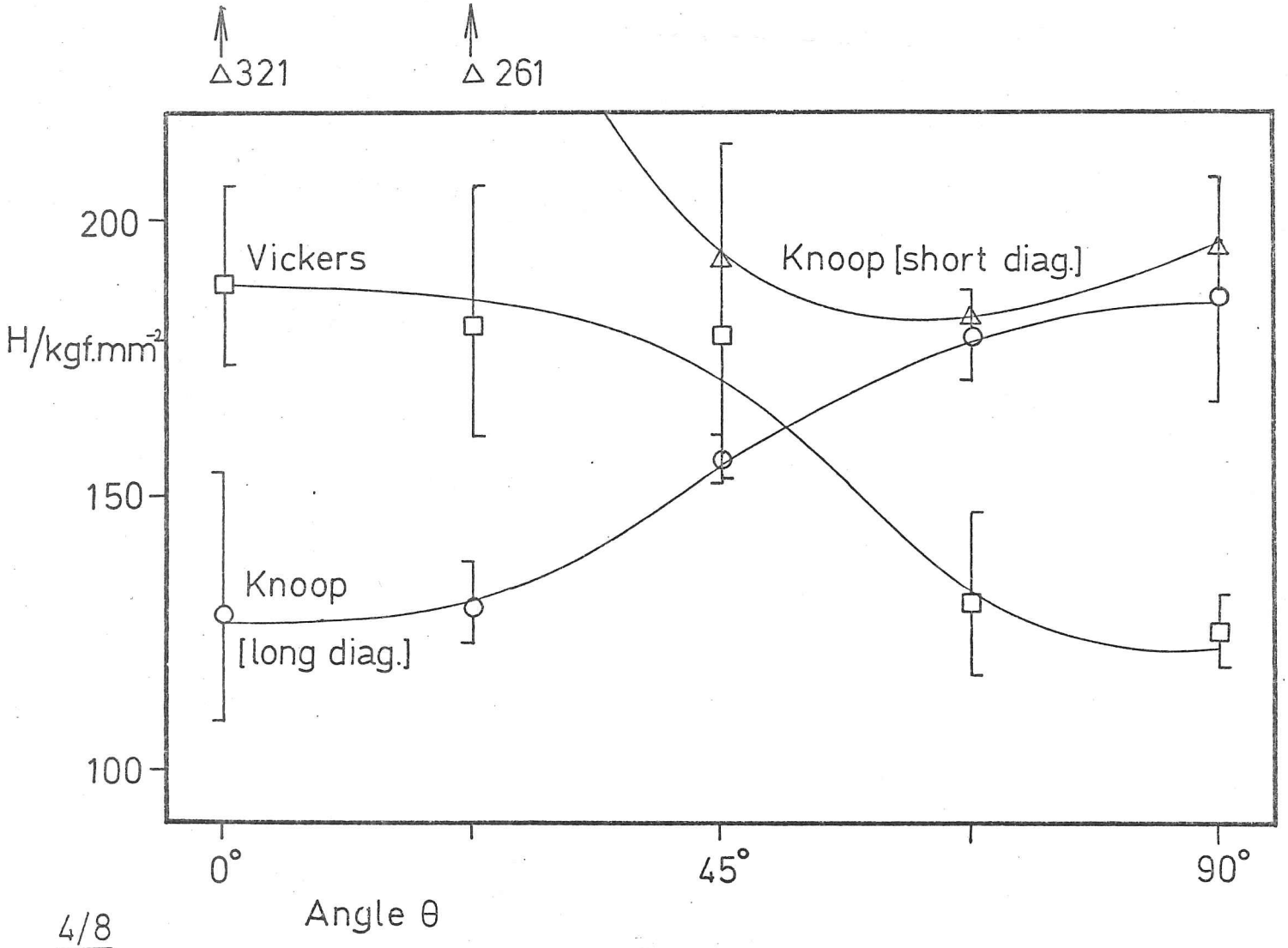
△321
△261
200
150
100
H/kgf.mm⁻²
Vickers
Knoop [short diag.]
Knoop
[long diag.]
0°
45°
90°
Angle θ

4/8

From figure 4/8 it can be seen that the KHN (long diagonal) is 90° out of phase with the VHN and KHN (short diagonal) hardness anisotropies. Clearly the simple method for measuring and describing hardness anisotropy (4.2.1) leads to ambiguous results and the explanation for this behaviour must be found.

Elastically Driven Recovery

Whilst an indentation is in the process of being made in an anisotropic material, it is presumed to be the same shape as the indenter. When the load is released the indentation relaxes into a less symmetric shape, as shown in figures 4/3 and 4/4. The shape of these Vickers indentations is different from the ideal 4mm symmetrical shape because of this anisotropic contraction. When an indentation is made in an anisotropic material there will be both elastic and plastic deformation but the proportion of the strain taken by these two mechanisms will be different in different directions in the material. When the indenter is removed, the most highly stressed directions will contract more, driven by the more highly elastically compressed material. Hence the indentation will be asymetrical. This hypothesis of the cause of the asymmetry of the indentations, obvious as it may seem, has not appeared in previous published work on the subject.

The equilibrium stress field beneath an indentation is very complex and no adequate description of it exists. However, in an anisotropic material, it is reasonable to assume that the stress in the material in contact with the indenter, when it is fully loaded, is the flow stress. Now, if the flow stress (Y_θ) and the Young's modulus (E_θ) both vary with orientation (θ), then an estimate of the extent of the contraction in any direction will be given by Y_θ/E_θ. Note that this is an estimate of the driving force for the contraction. If plastic as well as elastic deformation occurs on unloading it will not affect this estimate of the extent of the contraction that takes place.

Two Causes of Hardness Anisotropy

The elastically driven contraction (or 'recovery') affects the measured hardness anisotropy by superimposing an effect which has the same symmetry as the microstructure which affects the shape of the indentations. There is also the effect of the anisotropy on the 'intrinsic' or unrecovered hardness which has the same symmetry as that of the indenter which controls the indentation size. This intrinsic hardness anisotropy could only be measured if it were possible to measure the indentation size whilst the indenter was still under load. This could be achieved by using a displacement controlled machine (see 3.1.3 and chapter 5).which would enable the unrecovered hardness to be measured for different indenter orientations on the specimen and the degree of contraction in each direction to be established by post facto examination. At present,it is only possible to measure the results of the combination of these two effects and it is thus very difficult to separate the two factors quantitatively.

Estimates of the Contraction of Vickers Indentations

The different forms of anisotropy observed in the eutectic (figure 4/8) can now be explained in terms of the above theory. Each measured anisotropy, whether for Vickers, Knoop (long diagonal) or Knoop (short diagonal), is a combination of two effects, one with the symmetry of the microstructure (2mm in this case) and the other with the symmetry of the indenter, and the relative magnitudes of these two effects also depends upon the shape of the indenter.

Thus the hardness numbers, as shown in 4/8, have different meanings for different orientations and their usefulness,as hardness numbers, to the further understanding of the subject is limited.

Nevertheless, despite the lack of the dimensions of the unrecovered (intrinsic) indentations, from the data available it is possible to estimate the extent of the recovery in each of the two principal directions

in the two orientated materials.

Figures 4/3 and 4/4 demonstrate that a greater degree of contraction occurs parallel to, rather than perpendicular to, the direction e. If it is assumed that the recovery perpendicular to e is zero and then the dimensions of the indentation are used to calculate the contraction parallel to e, then a lower bound estimate is obtained for the extent of the contraction. This is shown in table I where the contractions are expressed as percentages of the (assumed) unrecovered indentation size.

The Anisotropy of the Youngs Modulus

Now, despite the fact that the elastic moduli of the two phases in a eutectic or eutectoid can be very different, it will be shown that the average Youngs modulus of the composite is fairly isotropic. This will be demonstrated for the Al-$CuAl_2$ eutectic; the Youngs moduli of the constituent phases are 70 GPa (Al) and 142 GPa ($CuAl_2$). Now the stress and strain fields beneath indenters are very complex but a fair estimate of the degree of elastic anisotropy can be obtained by considering the two cases of uniaxial compression parallel to, and perpendicular to, the direction e.

In a lamella material with approximately equal volumes of the two phases (the exact proportions are not critical) the effective moduli in the two principal directions are the same-strain mean (parallel to e) and the same-stress mean (perpendicular to e) and in this case they are 106 GPa and 94 GPa respectively.

Thus the degree of elastic anisotropy is of the order of one tenth which will only make a small contribution (in the opposite sense) to the anisotropic contraction i.e. the lower bound estimate for Al-$CuAl_2$ should be revised to be approximately: 18% - 18%/10 $\simeq$ 16%. Therefore, to a first approximation, elastic isotropy can be assumed to hold.

Another Estimate of the Contraction

If the contraction is proportional to Y_θ/E, where E is not dependent on direction, then an upper bound estimate for the contraction can be obtained by considering the anisotropy of the flow stress. From 4/3 and 4/4 the flow stress can be seen to be greater in the direction $\underline{e}$ because that is the direction of greatest contraction. Mellor and Edmonds (1978) measured the microhardness of the proeutectoid alpha and delta phases (102 and 430 $kgf.mm^{-2}$ respectively) as well as that of the eutectoid pearlite (332 $kgf.mm^{-2}$). These results are used here to give an upper bound for the flow stress anisotropy by setting the flow stress parallel to $\underline{e}$ to be proportional to 430 $kgf.mm^{-2}$ and that perpendicular to $\underline{e}$ to be proportional to 102 $kgf.mm^{-2}$. If the recovery of the indentation in the proeutectoid phases were taken into account these two values would be even more disparate, so this is not a true upper bound, merely an estimate.

Thus, if the unrecovered diagonal of an indentation is 'd', then (if k is a constant of proportionality):

$$d - d_1 = 430.k \qquad 4.2.2a$$

$$d - d_2 = 102.k \qquad 4.2.2b$$

Hence the estimates of the recovery in the fourth column of Table I were calculated.

Section 4.2.2 - Table I

	d_1 (// to $\underline{e}$)	d_2 ($\perp$ to $\underline{e}$)	lower bound estimate	another estimate
Al-$CuAl_2$ λ =2.8μm (50 gf.)	22.19 ± 0.96	27.20 ± 0.71	18%	-
Cu/In λ =0.79μm (300 gf.)	39.5 ± 0.3*	42.9 ± 0.5*	8%	10.1% & 2.4%
Cu/In λ =2.9μm (300 gf.)	38.4 ± 1.1*	43.4 ± 0.7*	11.5%	14.6% & 3.5%

*from Mellor and Edmonds (1978)

These estimates of recovery are not accurate as they do not take into account the strengthening effects in the composite which are not present in the proeutectoid phases, i.e. the presence of solute atoms (to saturation), dislocation networks produced by differential thermal shrinkage on quenching and the interlamella interfaces. For the same reasons the effect of the intrinsic single crystal hardness anisotropies of the two phases (which, in any eutectic or eutectoid colony, are two single crystals) will be minimal (Page 1979).

Stress Field Beneath the Vickers Indenter

Although the recoveries have been calculated for the $\theta=0^\circ$ and $\theta=90^\circ$ orientations of Vickers indenters (figure 4/4), a much larger relaxation ~~anisotropy~~ is to be expected (and is observed) for the $\theta=45^\circ$ position (figure 4/4). This is because the largest compressive stress parallel to the surface (i.e. the largest stress susceptible to anisotropic effects) is probably roughly perpendicular to the indenter's facets (see figure 4/9). This is consistent with the presumed maximum tensile stresses being parallel to

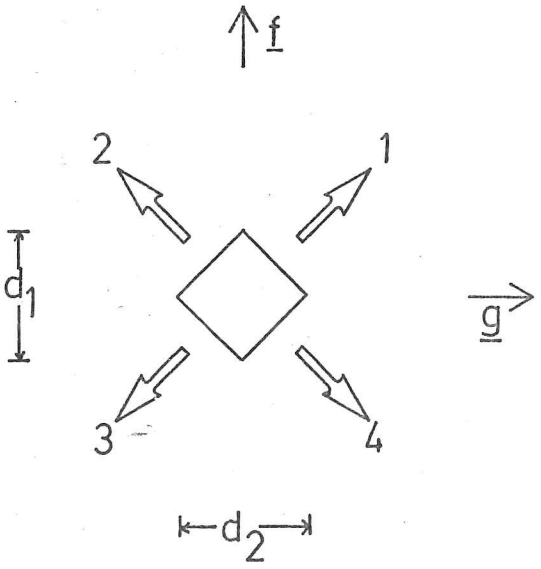

Figure 4/9

This is a plan diagram of a Vickers indentation showing the two projected diagonal lengths d_1 and d_2 and the four directions of largest compressive stress (postulated) as arrows.

the indentation diagonals, as evidenced by the position of median cracks around Vickers indentations in brittle materials (Page 1979). Therefore the largest fractional change in indentation shape is to be expected when the facets are roughly parallel with the principal directions in the test material's microstructure. In this position the indentation (after recovery) is rectangular and both indentation diagonals are the same length, therefore the shape as well as the size of the indentation must be examined in anisotropic materials.

Stress Field Beneath the Knoop Indenter

For Knoop indentations the situation is different. The greatest stresses parallel to the surface can still be considered to be perpendicular to the facets but the similarity between the shape of the indenter and that of a wedge means that the greatest horizontal compressive stress is approximately perpendicular to the longest diagonal (see figure 4/10) and the greatest elastic contraction occurs in this direction of greatest stress. Therefore the Knoop (long diagonal) intrinsic hardness anisotropy (which affects the size of the indentation) is always 90° out of phase with the recovery anisotropy (which affects the indentation shape), whereas the Knoop (short diagonal) intrinsic hardness anisotropy is exactly in phase with the recovery anisotropy.

Figure 4/10

The arrows show the direction of the greatest compressive stress in the Knoop indentation

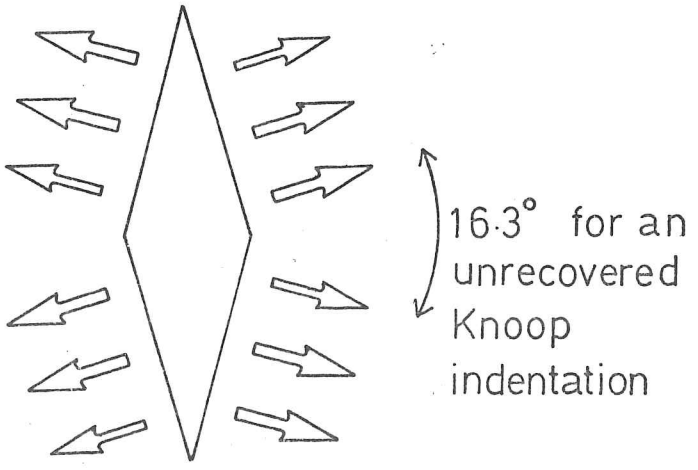

Thus it can be seen that the apparent symmetry between the Vickers and the Knoop (long diag.) curves in 4/8 is fortuitous and for this reason the curves have been drawn to fit the points and not to cross over at the 0 = 45 position.

Intrinsic Unrecovered Hardness Anisotropy

The validity of these hypotheses about (a) the maximum compressive stresses around both types of indentation, and (b) the direction and magnitude of the recovery in aligned microstructures, can only be tested against the experimental data if some measure of the intrinsic unrecovered hardness anisotropy is available.

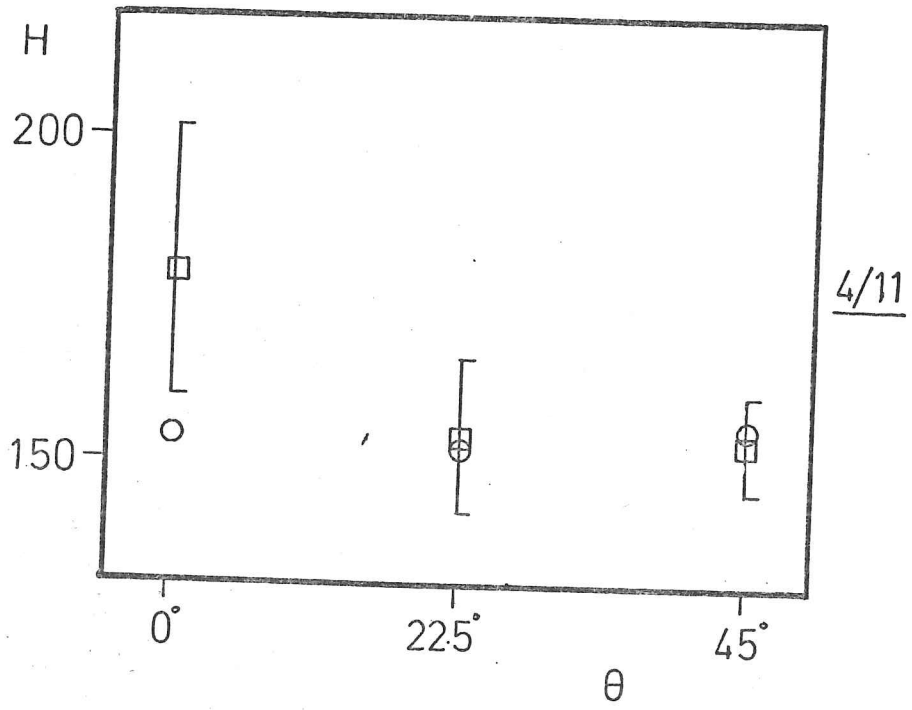

Figure 4/11

□ Moore's method - from Vickers indentations

○ R & A's method - from Knoop indentations

error bars are ± 2 standard deviations

An approximate idea of the form of the unrecovered hardness anisotropy can be obtained by using Moore's method for averaging the diagonals of asymmetrical Vickers indenters (see 3.3.1(b)) and Raghuram and Armstrong's method for averaging two Knoop measurements at right angles (error bars are not appropriate for these points and are not plotted in the figure 4/11). No definite conclusions can be drawn from this exercise as the recoveries affect the measurements which are used by both methods, but it does appear that the estimate of the intrinsic hardness anisotropy shown by both methods is not severe.

Explanation of the Observed Hardness Anisotropies

The hypotheses about the forms of the stress distributions beneath Vickers and Knoop indenters will now be shown to be consistent with the experimental results.

If the intrinsic Vickers hardness is not very sensitive to the orientation of the microstructure, as has been indicated by the above section, then the Vickers curve in figure 4/8 is explained completely in terms of the differential recovery, i.e. the contraction anisotropy effect dominates the intrinsic anisotropy effect.

The Knoop results show that the intrinsic anisotropy dominates the contraction anisotropy for the case of the long diagonal, whereas for the short diagonal both anisotropy effects combine in phase. The contraction acts principally along the direction of greatest compressive stress which is why it has opposite effects on the two diagonals (see 4/10).

Conclusion

In conclusion it appears that the eutectic and eutectoid materials both have definite 'hard' and 'soft' directions, that the Vickers

hardness anisotropy is controlled by the elastically driven recovery and the Knoop anisotropy by the orientation dependent intrinsic hardness, and that the anisotropy in elastic moduli plays a minor role.

It is interesting to note that the differential contraction will only have a dominant effect on the hardness anisotropy when the elastic deformation is a significant proportion of the total, that is, when the E/Y ratio is less than about 114 (see 2.1.2). In fully plastic materials with E/Y much greater than 114 it is to be expected that hardness anisotropy will be more obvious without the masking effects of the elastic recovery , but it is also to be expected that Vickers indentations in such materials will be perfectly square.

Bückle (1973) made Vickers indentations in pure bismuth single crystals, a material with a high E/Y ratio, but the indentations were by no means square. This may be because the restricted number of slip systems did not permit a fully plastic pile-up to form all around the indentation and thus lead to a greater degree of elastic radial displacement than would be expected from theaverage E/Y ratio. This limited plasticity effect may also occur where a very stiff, hard phase may not allow the formation of a localised pile-up even if the average E/Y ratio for the whole composite is greater than 114.

4.2.3 Room Temperature Hardness Anisotropy of MgO

Published work on the hardness anisotropy of MgO (see 4/12) shows that both the Vickers and Knoop anisotropies on the (001) face display 4mm plane symmetry and that they are 45° out of phase. This contrasts with the orientated microstructure materials where both the hardness anisotropies displayed 2mm symmetry and were 90°out of phase.

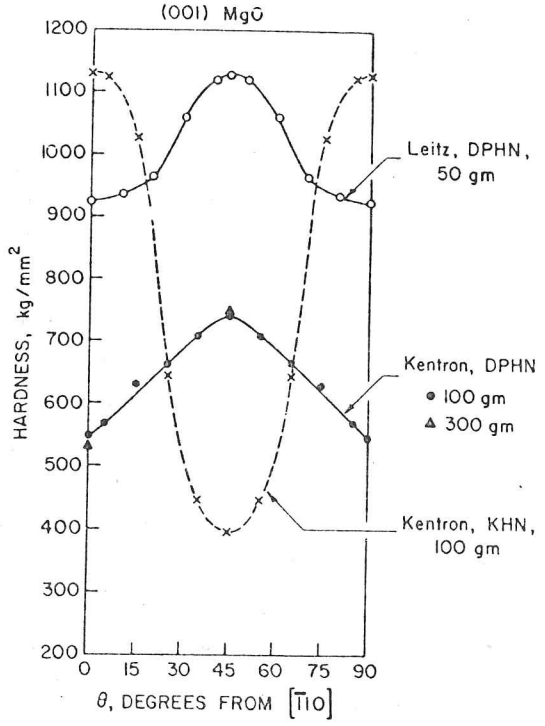

Figure 4/12

Knoop and Vickers (DPHN) hardness anisotropies on (001) MgO. From Armstrong and Raghuram (1973), 'Kentron' and Leitz' are manufacturers of microhardness machines. Note that (a) there is an indentation size effect on the Vickers hardness, and (b) that the ISE does not affect the shape of the anisotropy significantly.

The Knoop hardness anisotropy on MgO is well described by the effective resolved shear stress model (ERSS) of Brookes et al. (1971) (see 2.4.2) but Armstrong and Raghuram (1973) and Boyarskaya et al.(1979) have developed other theories to explain the Vickers hardness anisotropy. The former theory, concerning the possible effect of median cracks on the stress field, was described in 2.4.3 and Boyarskaya'a theory is qualitatively similar to the ERSS theory in that it concerns the effects of the stresses resolved onto particular slip systems by the force

exerted on each facet of the indenter.

In the current work, an extended and revised ERSS model has been developed (see 2.4.2 and appendix I) which can produce hardness anisotropy predictions for Vickers as well as for Knoop indenters and these are shown in figures 4/13 and 4/14. The shaded area in these figures shows the variation between predictions made using different forms of the constraint factor, equations 2.4.2h to k. From these figures it can be seen that the complex interactions between the indenter facets and the slip systems which are considered by the ERSS program are sufficient to explain the different hardness anisotropies for the two indenters. This has two consequences, firstly, that the theory of Armstrong and Raghuram is unnecessary, and secondly, that there are no absolute 'hard' or 'soft' directions in MgO single crystals.

Thus the mechanisms controlling the hardness anisotropy in MgO are completely different from those operating in orientated microstructure materials (4.2.2).

Wonsiewicz and Chin's (1973) model of hardness anisotropy mechanisms is only applicable to approximately wedge-shaped indenters (i.e. Knoop, but not Vickers) and implicitely assumes that every direction in a crystal, irrespective of indentation plane, has a definite hardness or softness. Therefore this model is not appropriate for MgO, or probably, for any other semi-brittle material with restricted capacity for slip (2.4.2).

The success of the ERSS type of model in predicting the forms of anisotropies of both types of indenter shows clearly that it is the active slip systems in the bulk of the solid which control the anisotropy. However, the absolute magnitude of the hardness will be affected by other deformation mechanisms. These may be secondary slip, elastic deformation, block shear, or the stress activated diffusion of crowdions (see 2.4.1).

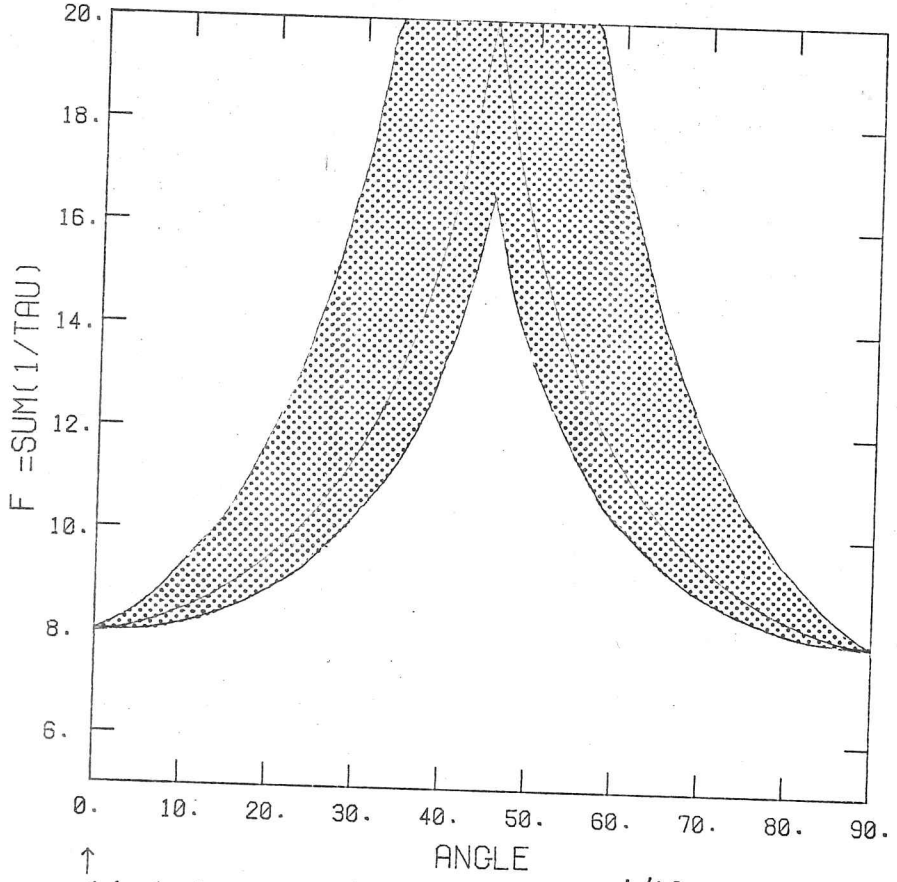

↑
< 1 1 0 >
(1 1 0) < 1 -1 0 >
ON (0 0 1)
LAUE CLASS M3M

4/13

TENSILE STRESS AXIS
VICKERS INDENTER

PHILIP SARGENT 1979

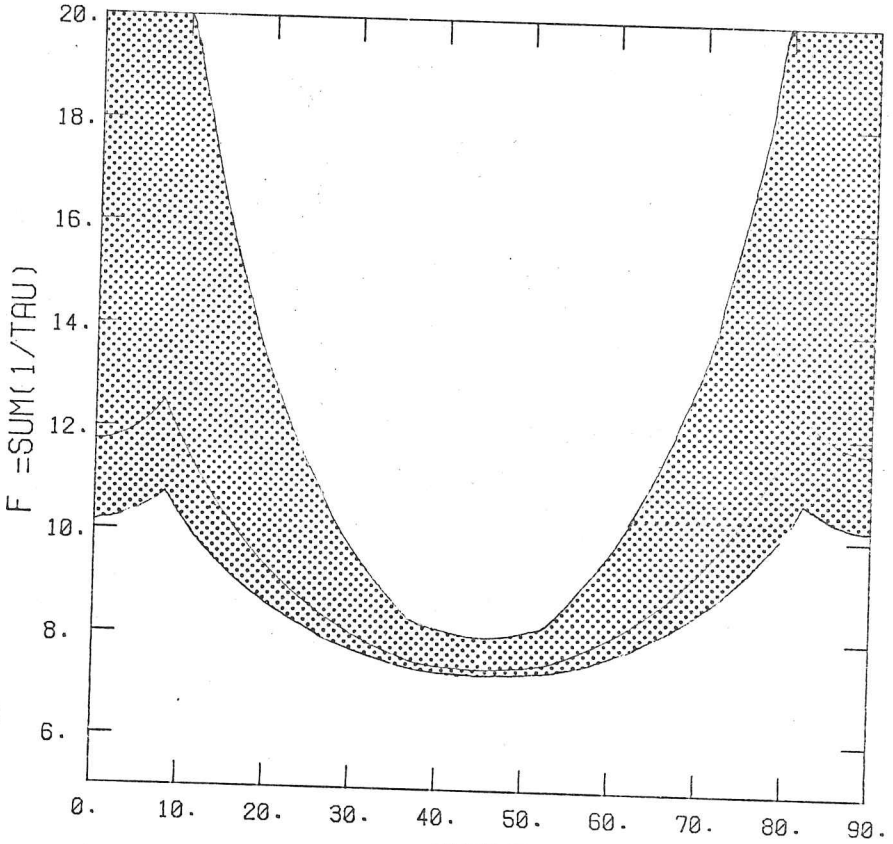

↑
< 1 1 0 >
(1 1 0) < 1 -1 0 >
ON (0 0 1)
LAUE CLASS M3M

4/14

TENSILE STRESS AXIS
KNOOP INDENTER

PHILIP SARGENT 1979

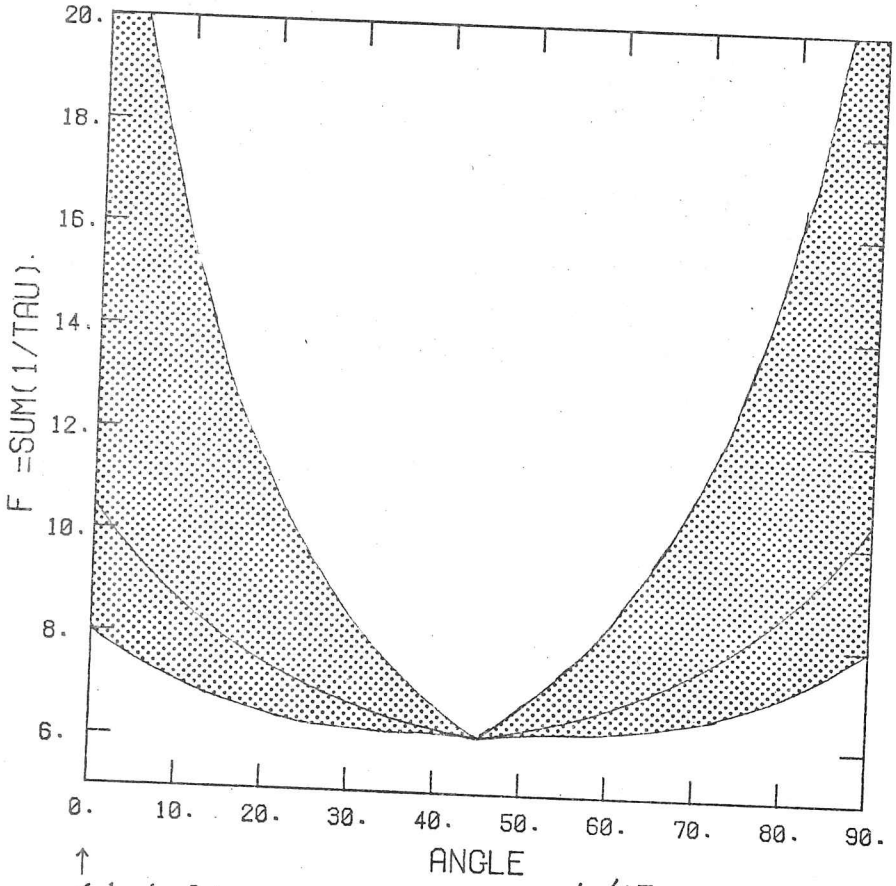

↑
< 1 1 0 >
(0 0 1)-< 1 1 0 >
ON (0 0 1)
LAUE CLASS M3M

4/15

TENSILE STRESS AXIS
VICKERS INDENTER

PHILIP SARGENT 1979

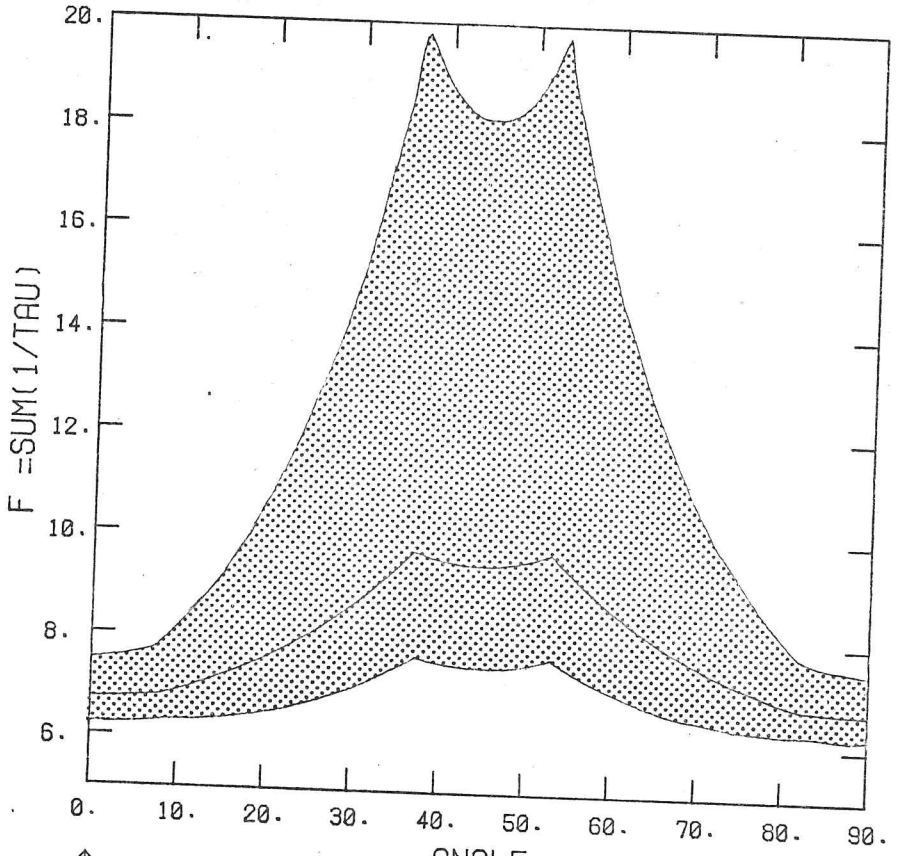

↑
< 1 1 0 >
(0 0 1) < 1 1 0 >
ON (0 0 1)
LAUE CLASS M3M

4/16

TENSILE STRESS AXIS
KNOOP INDENTER

PHILIP SARGENT 1979

4.2.4 Indentation Creep Anisotropy in Alkali Halides

At high homologous temperatures and long indentation times Brookes et al.(1975) have shown (see 2.3.3) that in MgO, LiF and NaCl the Knoop anisotropy is the opposite of that predicted by their ERSS model for the $\{1\,10\}\langle 1\bar{1}0\rangle$ slip system. This was discussed in section 2.4.1 and it is thought that the effect may be due to indentation creep on the $\{100\}\langle 1\,\bar{1}0\rangle$ slip system which would produce the required anisotropy, see figures 4/15 and 4/16 which were produced using the revised ERSS model and agree with the earlier predictions of Brookes et al.(1975). It is thought that slip on $\{100\}\langle 1\,\bar{1}0\rangle$ may even occur in MgO at room temperature for long indentation times.

4.3 Microhardness of Metallic Glasses

An investigation of the microindentation behaviour of metallic glasses was made because their unique properties make a good test of the validity of several theories of indentation plasticity. These properties are, firstly, that they are homogeneous over any distance greater than a few atomic diameters, their structures are similar to those of extremely viscous liquids, and therefore orientation and micro-structure effects on microhardness are absent. Secondly, they are metallic, i.e. good electron conductors, and thus the effects of moisture on the surface plasticity can be expected to be minimal (see 2.5.2). Thirdly, work hardening effects are not observed and they are model elastic-plastic materials (apart from slight anelastic effects). Fourthly, they deform inhomogeneously on indentation by 'shear bands', not by dislocation mechanisms, and since their densities are close to those of their crystalline forms densification is not a significant mechanism as it is in oxide and polymeric glasses.

Thus metallic glasses are perfect model materials to test the surface-directed and radial displacement models of indentation plasticity with the novel plasticity mechanism testing the general applicability of the models. A range of E/Y ratios and strengths in the experimental materials can be achieved by using a variety of alloys.

Metallic glasses were also appropriate materials to study for several reasons unconnected with their structure or properties. Samples were easily available in a well characterised form and reliable composition from Allied Chemical Corp. Inc. and a great deal of recent work is in progress with these particular alloys on their structure, yielding and crystallisation behaviour in the department of metallurgy in Cambridge. Much of this work depends on the interpretation of the results of micro-hardness tests as the glasses are only available in ribbon form (35 to 50 microns thick, 5 to 25 mm wide) and microindentation is the easiest

test to make on the mechanical properties of such ribbons.

A de facto standard load of 100 gf. is used by most researchers for microhardness tests but often little account is taken of the indentation size effect (ISE) on microhardness and sometimes such hardness values are used for calculating bulk properties, such as yield stress, for which they unsuited.

Therefore some critical study of the microhardness of metallic glasses was felt to be useful both to the study of microindentation tests and to those working on the mechanical properties of these materials.

4.3.1 Structure and Yielding of Metallic Glasses

Metallic glasses are novel materials which have only recently become available in quantity and, also only recently, has some agreement been reached on appropriate models for their structures and the unique mechanisms by which they flow. Therefore the subject will be briefly reviewed* here before describing the results of microhardness tests on these materials.

Flow beneath microindentation at temperatures below the glass transition temperature (T_g) occurs by the operation of shear bands (see 4.3.2(c)) but the operation of these is intimately connected with the structure of these alloys (see 4.3.2(a)) and to compare their behaviour with other 'low E/Y' materials it is necessary to understand the influence of the structure on the elastic properties (see 4.3.2(b)). The importance of homogeneous (viscous) flow to microindentation is generally assumed to be small because of the high strain rates involved.

---

* Footnote: For further information on the subject of metallic glasses the proceedings of the 2nd and 3rd international conferences on 'Rapidly Quenched Metals' (published 1976 (MIT Press) and 1978 by the Metals Society, London) are recommended, especially Davis (1976) and Spaepen (1978).

4.3.1(a) Structure and Structural Relaxations

Metallic glasses are formed by rapidly quenching the melt ($\sim 10^6$ Ks^{-1}) onto a cold metal surface. Eutectic compositions of transition metals (i.e. Pd, Ni, Fe, Co, Cr, Ti, Zr, Ag, Au, and Cu), other metals (i.e. Be and Al) and metalloids (i.e. P, B, Si, and C) are the most successful. There are broadly two classes of alloys, metal-metal alloys such as $Cu_{50}Zr_{50}$ and $Be_{40}Ti_{50}Zr_{10}$, and metal-metalloid alloys such as $Fe_{80}B_{20}$ and $Pd_{77.5}Cu_6Si_{16.5}$, though in the past year some lithium alloys and (perhaps) pure silicon have been successfully quecned to glass (Pavuna, 1979).

It is generally agreed that the structure of the glasses is approximately described by a dense, randomly packed structure of touching spheres with a high degree of short range order and metallic bonding (Gilman, 1975b). However, great difficulties have been encountered in attempting to formulate good structure models which reproduce the same short range order that is observed in real alloys.

Experimentally the alloys have been investigated by polarised neutron scattering, small angle x-ray scattering (SAXRS), x-ray absorption, NMR, magnetic moment measurements, MHz and kHz pulse echo techniques, low temperature heat capacity measurements, density measurements and indirectly by differential scanning calorimetry (DSC) and transmission electron microscopy (TEM) of specimens undergoing the glass transition and crystallisation. There are clearly differences between the two classes of alloys described above, the metalloid atoms are completely sheathed by metal atoms and the hardness and elastic behaviour is different in the two classes (Davis 1976b).

In metallic glasses theoretical study of point, line and planar defects has shown them to be unstable, if they existed they would spontaneously break up into small perturbations of the existing structure (Argon 1979).

over an extended region. The various atomic transport processes (diffusion, structural relaxation and plastic flow) are therefore governed by the concentration and mobility of these defects.

The very rapid quenching means that the same glass can exist in a range of metastable states, with slightly different types of short range order, and structural rearrangements occur easily when the glasses are stressed or annealed, long before they phase-separate or crystallise.

These structural relaxations are extremely important to the understanding of the variation in the mechanical properties of the glasses both below and above the glass transition point (T_g).
However the distinctions between the different types of relaxation, their modes of operation, when they occur and their implications are not well understood (Chen and Lo 1978, Greer and Leake 1979) and even the nomenclature is not well defined.

4.3.1(b) Elasticity

The moduli of metallic glasses are less than those of the crystallised alloys but the yield stresses are high. Thus the glasses have low E/Y ratios, usually in the range 45 to 60, and therefore the proportion of elastic strain in yielding material is significant.

The Youngs and shear moduli are usually 30% less, and the bulk modulus 5 to 10% less, than the crystalline material, and the Poisson's ratios being high: 0.4 to 0.45 . The Poisson's ratios are higher, and the shear moduli lower, than is to be expected just from the contribution of the disorder alone in the glassy state (Chen et al. 1975) which is attributed to the existance of highly mobile extended defects and has implications for the low temperature plasticity of these materials. Some idea of the mobility of these defects can be gathered from the fact that the elastic parameters are measured by kHz and MHz pulse-echo techniques.

At high stress levels metallic glasses display nonlinear anelastic behaviour and show a hysteresis loop on loading and unloading (Masumoto and Maddin, 1975) which may be due to mobile defects or to structural relaxation. The elastic limit is quoted by some researchers as the yield stress whereas others think that the flow-initiated fracture stress is more significant; this makes calculating H/Y and E/Y ratios difficult to do in a consistant manner.

Metallic glasses only increase in density very slightly when they crystallise (by about 1.2% for a typical alloy, Gilman 1975b) but the elastic moduli increase significantly. Thus the application of high hydrostatic pressure can be expected to have minimal effects on the density, since both glassy and crystalline forms are close packed, but large effects on the elastic moduli and Poisson's ratio of the glasses. Unfortunately these effects are largely uninvestigated, apart from the indirect and unclear evidence from microhardness tests.

4.3.1(c) Heterogeneous Shear Band Plasticity

Below T_g the deformation at high stress levels occurs heterogeneously in localised shear bands (Spaepen 1978) about 2 to 200nm thick. These form very rapidly (in less than 7 ns) and although the total plastic strain to fracture in a metallic glass is only of the order of 2% the shear strain inside the shear bands can be very large indeed as they do not strain harden.

Shear bands are regions of permanent structural change which are caused by very localised high strains. If shear bands are initiated in a ribbon and then it is polished further straining will cause the re-initiation of the same shear bands, which implies a work softening effect. Shear bands also etch differently from the bulk material (Patterson 1979, Gibbs 1979).

During yield the structural change is likely to be a local increase

in the excess free volume, a shift in the equilibrium between the stress driven creation of free volume and its annihilation due to diffusional rearrangements. However, the nature of the permanant change in the shear bands is unknown.

A relatively successful model has been put forward by Argon (1979) which describes possible structural changes in the shear bands. The model describes two related mechanisms, one occurring above, and one below $0.68T_g$ both utilising the defect structure of free volume sites; the former being diffuse and the latter being a more intense shear transformation localised in a disc shaped volume.

The high Poisson's ratio of metallic glasses is indicative of the ease of atomic regroupings and hence responsible for the ductile deformation by shear bands. This has been convincingly demonstrated by Chen et al.(1975) who showed that the reduced microhardness H/K (where K is the bulk modulus), if divided by T_g to take account of the contribution associated with the disorder of the glassy state, decreases monotonically with increasing Poissons ratio for a number of alloys. That is, the higher the Poissons ratio, the easier the material yields.

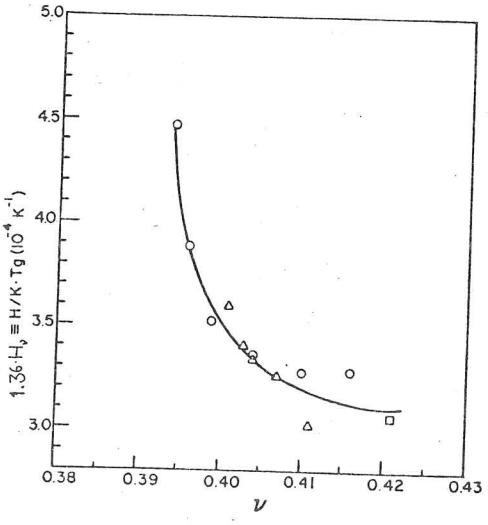

Figure 4/17

From Chen et al.(1975).
The reduced parameter H
$H = H/KT_g$ as a function of Poisson's ratio for metallic glasses: Pd-Ni-P (o), Pd-Fe-P (△), Pt-Ni-P (□), $Pd_{77\frac{1}{2}}Cu_6Si_{16\frac{1}{2}}$ (▽) where H is the Vickers hardness, K the bulk modulus and T_g the glass transition temperature.

The sensitivity of the mechanics of shear band plasticity to the structures of the metallic glasses, which is indicated by Argon's model, is confirmed by measurements of the SAXRS which show that cold rolling and low temperature annealing have roughly opposite effects on the short range order (Waseda et al. 1979).

The sensitivity of mechanical properties to annealing is demonstrated by the load-relaxation measurements of Hadnagy et al.(1978) who showed that 'as received' metallic glasses displayed varying behaviour, but that a uniform annealing treatment removed these variations.

Thus, while different structures in the same metallic glass certainly do affect the mechanics of shear, there are as yet no adequate models for the effects and a paucity of data.

4.3.2 Indentation Hardness Models and Metallic Classes

The responses of metallic glasses to indentation are very similar to those of crystalline metals, pile-ups are always observed surrounding the indentations and the H/Y ratio is generally about 3.2. The pile-ups are not smoothly rounded as they are in crystalline metals because the plasticity is due to shear bands and these can be seen forming the pile-up in figure 4/18. Nevertheless, these characteristics show without ambiguity that metallic glasses deform by surface-directed displacements.

Figure 4/18

Metglas 2826A (as received)
$Ni_{36}Fe_{32}Cr_{14}P_{12}B_6$
Vickers indentation 100 gf.
30 s dwell time. Taken in
a Stereoscan SII SEM with
30° axial tilt at 30 kV

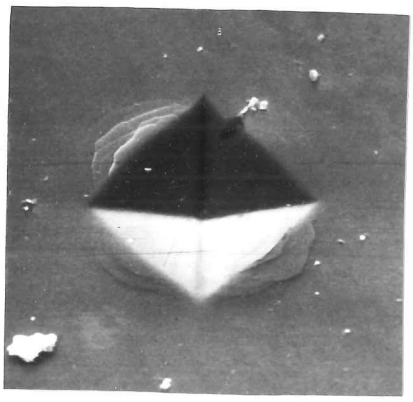

1300×

Now metallic glasses have unusually low E/Y ratios (see 4.3.1(b)) and therefore the theories of indentation plasticity (see 2.1.2 and 2.3.2) predict that they will deform by radial displacements. Thus the experimental behaviour is precisely the opposite of that expected.

The magnitude of the problem can be seen in figure 4/19 This is the same as figure 2/2 (duplicated here) but with the circles showing the behaviour of 5 metallic glasses (2 points for different values for Pd/Cu/Si - Davis 1976, Chen and Polk 1974), the lines showing the behaviour predicted by the Studman, Moore, Jones and Field model(SMJF) for three values of ν and the lines showing the range of predictions on a basis of pile-up displacements. The SMJF model was shown to be the

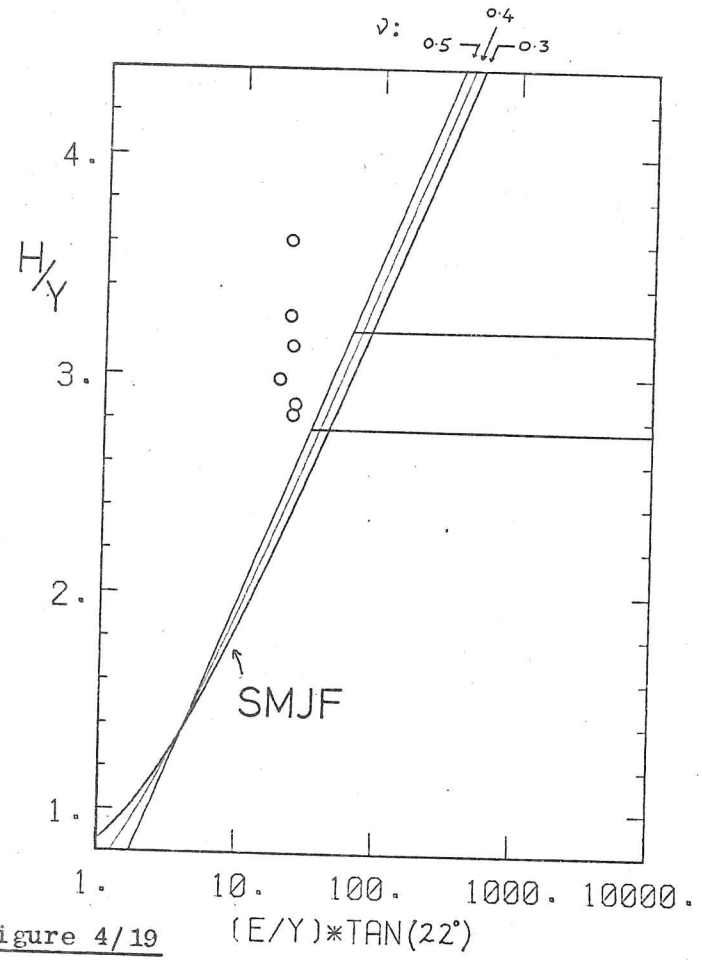

Figure 4/19

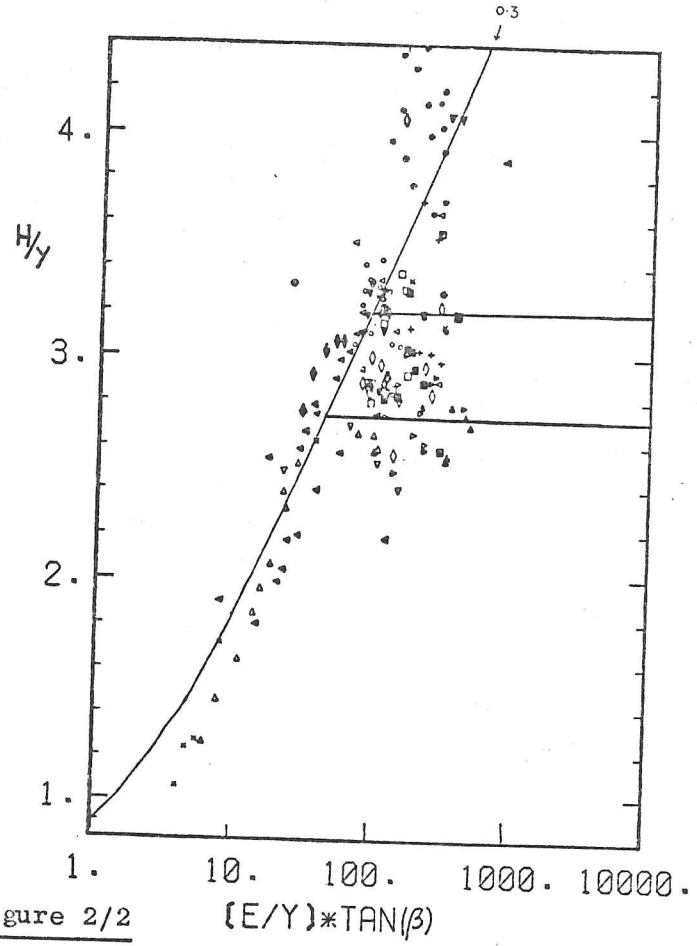

Figure 2/2

Data for metallic glasses compared with the theoretical model (SMJF) for radial displacements, see figure 2/2 opposite.

best radial displacement model in 2.1.2, the model due to Gerk yields almost exactly the same H/Y to E/Y curve (see figures 2/3 & 2/4). Many of the points shown in 2/2 have H/Y values in excess of those predicted by either model, which is to be expected for two reasons. Firstly, the effects of elastic recovery make all materials, especially those with low E/Y ratios, appear much harder than they 'really' are; the models predict the behaviour under load and not after relaxation. Secondly, work hard-ening in crystalline materials increases the flow stress relevant for indentation deformation and, whilst this can be taken into account by using Tabor's 8% representative strain method, the method is not exact.

The position of the metallic glass data is such that either new indentation theories must be formulated which can explain why metallic glasses appear to behave differently from all other materials, or the data must be examined to see if it is possible that the flow stresses and elastic moduli relevant to indentation are sufficiently different from those measured in the bulk to enable corrected data to be encompassed by the existing theories. This latter course will now be followed and will show what kind of strange effects must operate in metallic glasses if they are to be described by conventional models.

Elastic recovery has already been mentioned as leading to over-estinates being made of H/Y, especially in low E/Y materials. Pd/Cu/Si metallic glass ($Pd_{77.5}Cu_6Si_{16.5}$) has an E/Y value of about 57 and H/Y of 3.17 (Davis 1976). If it is to obey the SMJF model it should have an H/Y value of about 1.34. This means that if this difference is to be explained only in terms of elastic recovery a 100 gf. indentation would have to recover elastically from 27.9 to 19.3 microns, i.e. by about 35%, and this is typical for all the metallic glasses for which the relevent data exists. This is not a totally unreasonable degree of recovery, the Al-$CuAl_2$ eutectic recovered by at least 18% (see 4.2) and 35% could be achieved without any distortion of the indentation as the edges are not strain hardened.

However, the discrepancy between the experimental results and the predictions of the model cannot be explained only in terms of elastic recovery. The critical observation is that surface pile-ups, or 'coronets' are formed around indentations, the 'wrong' deformation mode definitely occurs and the H/Y ratio is a parameter of secondary importance. The primary cause of the discrepancy is that the E/Y ratio is observed to be too low, therefore the elastic moduli and the flow stresses will now be examined to see whether the E/Y ratio relevent to the behaviour beneath indenters is really as low as it appears from bulk measurements.

Since the plasticity mechanisms depend on the degree of free volume in the material (see 4.3.1) it is to be expected that the hydrostatic stress beneath indenters will affect (i.e. raise) the flow stress more than is the case for crystalline materials. If this occurs then the E/Y ratio will be even smaller than the value measured from bulk properties, making surface-directed displacements appear even more unlikely. However, the elastic moduli will also increase under pressure (and, presumably Poisson's ratio will decrease, though this only has a small effect on the SMJF model's predictions) and if E increases more than Y the pile-up regime value (E/Y greater than 95 for ν=0.4) may be achieved.

The above conjecture will now be put to the test: Pd/Cu/Si has a yield stress between 102 and 186 kgf.mm^{-2} (various authors use different definitions of yielding, Masumoto and Maddin 1975, Davis 1975, Chen et al. 1975, Davis 1976, Davis et al.1976b) and a Youngs modulus E between 8400 and 10006 kgf.mm^{-2}, the crystalline form has E = 13260 kgf.mm^{-2}. Even if it is assumed that under indentation E increases to the crystalline value, whilst at the same time the flow stress is only 140 kgf.mm^{-2}, can an E/Y value as high as 95 be attained. (The yield stress of 102 kgf.mm^{-2} is an elastic limit stress, not a flow stress.) Therefore it is very unlikely that the effect of hydrostatic pressure on the Young's modulus can bring the behaviour into agreement with the SMJF theory.

There is one remaining possibility that may reconcile theory and observation, that is if the work softening effect in the shear bands beneath the indenter reduces the relevant flow stress by about 40%. Such a work softening effect inside shear bands may well exist (Patterson 1979, Gibbs 1979) but no way of measuring it has been devised.

In conclusion, metallic glasses do test the applicability of the theories of indentation plasticity to the limit and these theories appear to fail. In the light of this failure it would be useful to reexamine the data on other materials which appear to diverge from these models' predictions. It may become apparant that they are not, as has been previously assumed, freak results, but valid counter examples. However, it must be admitted that previous data has, almost without exception, been collected without regard for elastic recovery; a new experimental program would have to take this into account.

It may be that the principle of two regimes of yielding distinguished by different E/Y ratios may continue to be valid and that the models to date have only been quantitatively in error. However it is also possible that the E/Y ratio (and the Poissons ratio) may be insufficient to separate the two regimes and that the mechanism of flow, by shear bands, dislocations or densification, may have to be taken into account.

Patterson et al. (1978) have observed that when metallic glasses crystallise the hardness and the flow stress increase dramatically and the pile-ups disappear. Thus in the microcrystalline form these same alloys again appear to obey the models' predictions. This indicates that it may be the shear band mechanism of plasticity which is causing the failure of the models as the partially crystalline glasses flow homogeneously in a viscous fashion and the crystalline alloys by dislocations and grain boundary sliding. Alternatively, this is also evidence for the possibility that it is the work softening effect in the shear bands which increases E/Y such that pile-up deformation occurs.

Davis (1975, 1976) noticed that the H/Y and E/Y ratios were incompatible with the observed pile-up deformation but attributed it to the metallic bonding in the metallic glasses, not appreciating that the radial displacement models , as they are stated at present, do not assume any kind of bonding or plasticity mechanism and should be valid for all materials.

When considering the theoretical and experimental H/Y and E/Y ratios the problem of the ISE on hardness must be taken into consideration. The 100 gf. standard load may be large enough for the continuum model of plasticity, as used by the indentation plasticity theories, to apply. However, the role of the ISE, which has proved to be a largely empirical subject, cannot usefully be discussed without some attempt to measure it; this is the topic of the next section.

Summary

1. Metallic glasses deform by surface directed displacements and not by the radial displacements which are predicited by the SMJF theory.
2. The surface directed displacement mode of deformation is not due to hydrostatic pressure effects on the flow stress or the Young's modulus.
3. The reason for the behaviour is definitely connected with the shear band mechanism of flow as the behaviour becomes conventional on crystallisation.
4. None of the surface directed or radial displacement theories fit the observed data, even if work softening is assumed to occur.

4.3.3 ISE in Metallic Classes

Vickers indentations were made using loads in the range 10 to 100 gf. on four different glassy alloys; one alloy was available in two different ribbon widths and both of these were tested. A number of sets of measurements were made on each ribbon, each set consisting of 4 or 5 indentations at each load (see 3.2.1). All indentations were observed by optical and scanning electron microscopy to be surrounded by surface pile-ups, or 'coronets'.

Two series of measurements were made, one on the clean, shiny surface of the as-received ribbons, and the other series on the reverse side after an erosive vibratory polishing treatment. This latter process involved gluing a 20 mm length of ribbon to a metal block with cyano--acrylate resin and vibratory polishing it in 0.25 micron alumina powder for up to 79 hours, details are given in tables I and II.

Section 4.3.3 - Table I

Metglas © code	PMS code	Ribbon width	Composition
2605A	Q	1.0 mm	$Fe_{78}Mo_2B_{20}$
2826	R	1.8 mm	$Ni_{40}Fe_{40}P_{14}B_6$
2826A	S	1.8 mm	$Ni_{36}Fe_{32}Cr_{14}P_{12}B_6$
2826	T	25.4 mm	$Ni_{40}Fe_{40}P_{14}B_6$
2605	U	1.3 mm	$Fe_{80}B_{20}$

The data was analysed by the methods described in section 3.2.2 and appendix I. A larger scatter than would be expected from the random scatter within each set was observed between sets of results collected at different times from the same piece of ribbon. This is illustrated in figure $4/19_8$ which shows the results from 11 sets of data from the eroded and uneroded 2605A (Q) glass in the form of

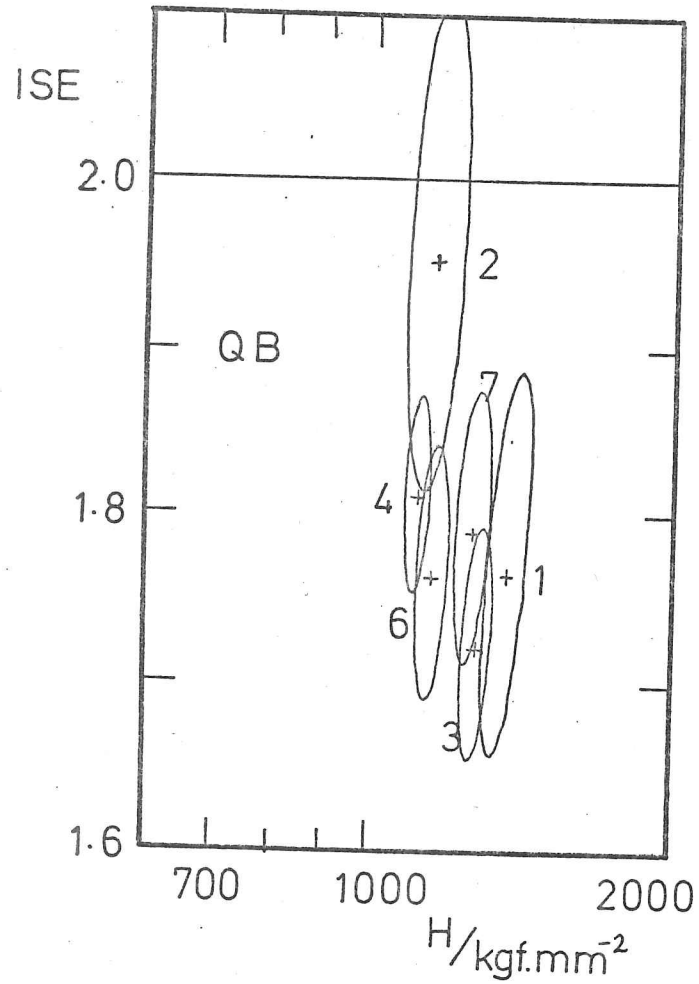
ISE
2·0
1·8
1·6
QB
2
7
4
1
6
3
700
1000
2000
H/kgf.mm⁻²

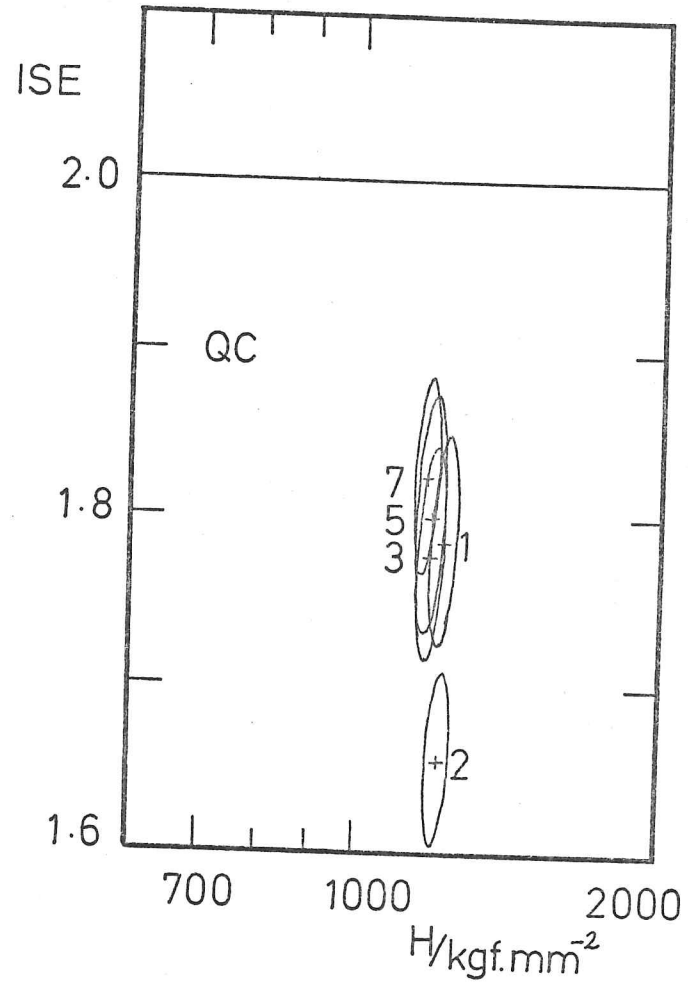
ISE
2·0
1·8
1·6
QC
7
5
3
1
2
700
1000
2000
H/kgf.mm⁻²

Section 4.3.3 - Table II

Metglas © code	PMS code	Hours in the erosion polisher	thickness of the ribbon/μm
2605A	QB	23½	30 ± 3
	QC	0	38
2826	RB	23½	55 ± 3
	RC	0	58
2826A	SA	10	35 ± 3
	SB	0	38
2826	TB	79	40 ± 3
	TA	0	51
2605	UC	79	30 ± 3
	UB	0	31

error ellipsoids* on a plot of ISE index against a log-scale of inter-polated 'ten micron hardness' values (see chapter 3). The variation between the ellipsoids is due to uncontrolled systematic differences in the testing conditions, if the scatter were due only to random effects the ellipsoids would be much more tightly clustered , as are the sets labelled 1,3,5 and 7 in the right hand figure. In this case the systematic differences are much greater in QB and are very likely to be due to variations in surface topography. The undersides of ribbons,

---

* Footnote: The number by each ellipsoid denotes the name of that set of data, thus QB4 etc., to distinguish metallic glass data from that from other materials all dataset names are prefixed by AC (Allied Chemical), thus the full name is ACQB4, for example. The 'missing' names (i.e. QB5) were used for intermediate merged sets of data, QB5 contained all the data from QB1,2,3, and 4.

i.e. those sides in contact with the quenching wheel, are rough with undulations about a micron or so deep which extend about 30 microns or so sideways, for comparison, the indentations made ranged from 3.5 to 12.8 microns in diameter, i.e. 0.5 to 1.4 microns deep. The erosion treatment removes tens of microns of material but the undulations persist since erosion, unlike grinding or polishing, affects the whole surface at once.

In the case of the uneroded material (QC) the cause of the deviation of QC2 is not clear, but it is unlikely to be due to inhomogeneities in the ribbon as such a change in properties would have to exist over an area of 1 mm^2, the area over which one set of measurements is made. The deviation is more likely to be due to loading-rate or measurement effects. Nevertheless, the QC2 results were included with the rest of QC and, when compared with the merged sets of QB data, no significant difference was found. This was the case for all the alloys, the erosion treatment did not affect either the ten micron hardness or the ISE index significantly, and the statistical method mentioned in 3.2.3, and described in appendix II, showed that the pairs of sets of results were identical to the 99% confidence level.

Therefore the indentation behaviour is qualitatively and quantitat-ively the same in the interior of the ribbon as it is on the surface, there appears to be no change in mechanical properties through the thickness of the ribbon in any of these alloys. It is true that the erosion treatment never removed as much as 50% of the ribbon, but the strain field beneath an indenter penetrates a distance into the interior which is at least ten times the indentation depth (Tabor 1951).

Tests on the 25.4 mm 2826 ribbon (TA) showed that there was no significant difference between the indentation behaviour in the centre and that along the edge of the ribbon. In the same ribbon 10gf. Knoop indentations were made parallel to, and perpendicular to, the melt-

-spinning direction, i.e. along and across the ribbon, and no difference was detected. There was no hardness anisotropy.

The data from the eroded and uneroded specimens was merged and the results are shown in figure 4/20 and table III. The ellipsoids in this latter figure are smaller than those in figure $4/19_{\beta}$ because each one represents data from at least 100 indentations and, since these measure--ments were made on a number of different occasions, it is hoped that the remaining effects of poorly controlled systematic errors have also become much smaller.

4/20

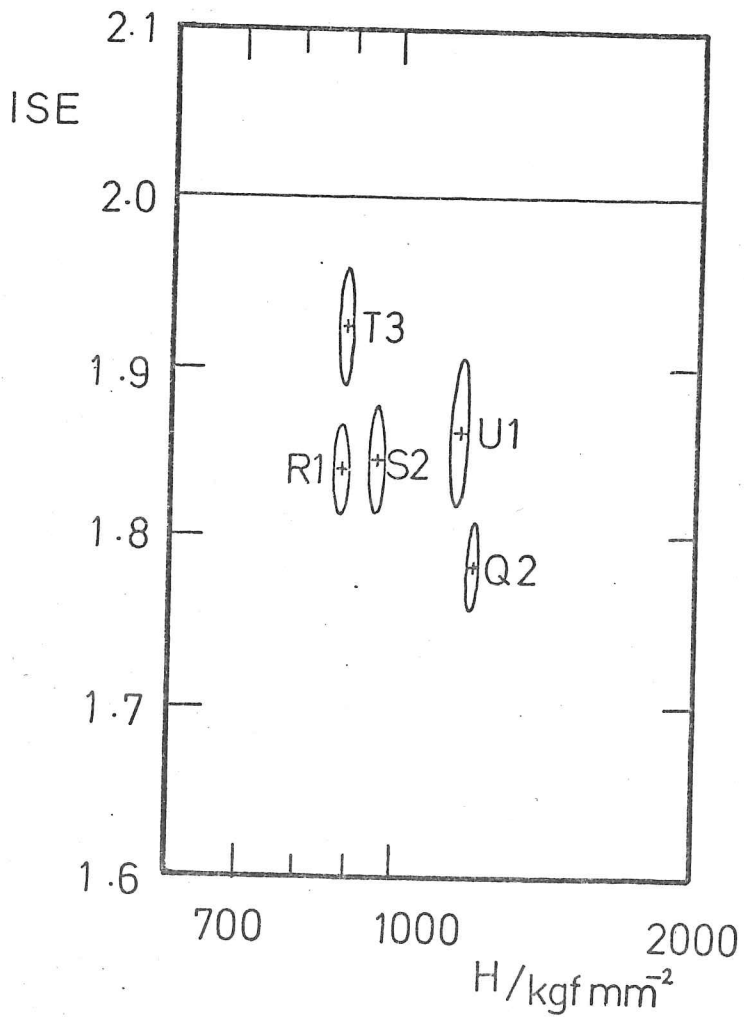

Section 4.3.3 - Table III

Code		H (ten-micron)	ISE index	H (10 gf.)	H (100 gf.)
Q2	<	1190	1.78	1487	1132
		(1109 - 1277)	(1.76 - 1.80)	(1431 - 1546)	(1117 - 1148)
R1	<	896	1.84	981	818
		(820 - 936)	(1.82 - 1.86)	(942 - 1022)	(808 - 828)
S2	<	954	1.85	1052	896
		(881 - 1032)	(1.82 - 1.87)	(1002 - 1105)	(881 - 911)
T3	<	887	1.92	962	865
		(817 - 962)	(1.90 - 1.95)	(917 - 1010)	(851 - 879)
U1	<	1153	1.86	1277	1105
		(1034 - 1286)	(1.83 - 1.90)	(1198 - 1364)	(1086 - 1124)

Ranges in brackets are to the 95% confidence level.

Hardness values (H) are all in $kgf.mm^{-2}$

4.3.3(a) The Existence of the ISE

The most important observation is that all the alloys whose behaviour is shown in figure 4/20 have ISE indicies in the range 1.8 to 1.9 (approx.), there is a strong effect of the indentation size on microhardness: smaller indentations cause higher hardness numbers to be measured.

It is very difficult to explain this observation in terms of what is known about the causes of the ISE. It was hoped that metallic glasses would have ISE indices of 2.0 so that by modifying their composition, crystallinity and by adding surface layers of different thicknesses the various causes of the ISE could be investigated individually.

There is some evidence that phosphorus segregates to the surface of the ribbons (Patterson 1979), but the erosion experiment shows that the ISE is not caused by a segregated surface layer, and any layer of oxide on the surface is likely to be only a few atoms thick. The shear bands are smaller than the indentations and do not form cells or subgrains as dislocations can in crystalline metals. There is no independent evidence of any microstructure on the scale necessary to produce the observed ISE, the inhomogeneities observed by Patterson et al. (1978) are too large at 15 microns, and too sparse (5 mm^{-3}) to have the required effect. Inhomogeneities on a scale of about 100 nm would cause the ISE if they had the effect of softening the material (see 2.5.4 and 4.4.3) but magnetic coercivity measurements show that metallic glasses in the as-quenched condition, before annealing, are completely devoid of inhomogeneities (Gibbs 1979 and Gibbs et al.1979).

Surface pile-ups occur, but they are only a symptom (2.5.5) of the ISE and not a cause. There are no line defects in metallic glasses and therefore smaller indentations cannot force a tighter curvature, as they may for dislocations, and hence increase the flow stress. The only

possible effects in terms of the mechanisms previously described in chapter 2 are (a) scaling effects due to the shear bands themselves, and (b) the effect of the free surface on the mobility of defects near the surface. However, the structure of a glass means that the stress field of a defect will drop off more rapidly with distance than it will in a crystalline solid, therefore the effect of the free surface is likely to be minimal.

Thus the only effect which can possibly cause the observed ISE is the scaling effect due to the finite size of the shear bands. They are usually about 20 nm thick but can be up to 200 nm thick* which is the size necessary to affect microhardness indentations 1 micron deep. Shear bands do not exist in the as-quenched material and therefore cannot be detected by coercivity measurements as they are not initiated until penetrated by the indenter, and they are certainly softer than the bulk of the glass. If they caused hardening of the material then an ISE would exist but the index would be greater than 2 (see 4.4.3).

Conclusion

The ISE in metallic glasses is caused by the scaling effect of the finite size of the shear bands compared with the size of the indentations. Detailed study of the ISE may therefore aid the understanding of the operation of shear bands and vice versa.

---

*Footnote: Personal communication: Donovan (1979).

4.3.3(b) 'Ribbon Width' Effect

The second observation to be made from figure 4.3.3B is that materials R and T have the same ten micron hardness but different ISE indicies. R and T are the same alloy, Metglas 2826, and it is to be expected that their behaviours should be identical as they only differ in the width of the ribbon.

Allied Chemical Inc. do not publicise their manufacturing methods but the narrow ribbon (R) is almost certainly made by melt-spinning using a single jet from a circular nozzle, whereas the wide ribbon is probably made using multiple circular nozzles (rather than using a slit). This difference is sufficient to increase the ISE index from 1.84 to 1.92, i.e. to decrease the 10gf. hardness by 2% and to increase the 100gf. hardness by 6%.

The effect must be due to different quenching rates affecting the state of structural relaxation of the alloy and hence the (postulated) inhomogeneities. If both wide and narrow ribbons were given the same annealing treatment it is to be expected that a smaller difference would be observed between their ISE ellipsoids.

This observation shows that mechanical properties, as well as magnetic properties (Greer and Leake, 1979) can be sensitive to details of the structure of metallic glasses.

4.4 Microhardness and Grain Size in Stainless Steel

These experiments with a ductile, single-phase, crystalline metallic alloy are intended to provide a reference for the work with semi-brittle (to be described in section 4.5).

There has been much research published on the effect of 'grain size' on 'the hardness number' of metallic alloys (see 2.7.1) but none of it is suitable for direct comparison with the MgO studies. In the current work standard procedures have been developed for the systematic measurement of grain size, microhardness and the indentation size effect on microhardness (see chapter 3).

4.4.1 Choice of Alloy and Thermomechanical Treatment

The alloy: 20%Cr - 25%Ni - 0.05%(C+N) - balance Fe, was chosen for experimentation because it is single phase. It is wholly austenitic (f.c.c structure) and very ductile (12 possible slip systems), it is also non-ferromagnetic. It is highly corrosion resistant which not only meant that specimens could be stored without special precautions but that oxide layers did not interfere with microhardness measurements (see below).

A very similar alloy (as above but with the addition of 0.5%Nb) has been the subject of study by other workers in the Department of Metallurgy and Materials Science in Cambridge and procedures have been developed for electropolishing, electroetching and for the preparation of thin foils for TEM (see, for example, Howell et al. 1975).

The current work, however, required a number of specimens of different grain size, each to be homogeneous with a sharply peaked size distribution of equiaxed grains. Therefore a programme of thermomechanical treatments was embarked upon aimed at developing this type of microstructure.

Thermomechanical treatments were originally attempted with the niobium stabilised alloy but it was found that the NbC precipitates pinned some of the grain boundaries, thus causing discontinuous grain growth and inhomogeneity in the specimens. This same effect has also been observed by Healey et al. (1973). Therefore the alloy actually used for the experiments reported here was the niobium free alloy(supplied by the UKAEA, Springfields).

The method chosen to increase the grain size was that of critical strain annealing whereby specimens are strained to a critical extent and, on annealing, recrystallise into very much larger grains (Cottrell, 1975). This process works very well for aluminium and alpha-brasses but the critical strain effect was found to be very small for the alloy of stain-less steel used in the current work. Later studies (Brown, 1978) have confirmed this finding. Generally, anneals at temperatures less than 800°C did not permit complete recrystallisation in less than 45 minutes and anneals at temperatures in excess of 930°C caused rapid grain growth by grain boundary migration after recrystallisation. Although large grain size specimens could be obtained by the latter method they were not used for microhardness measurements because of the possibility of greater grain boundary segregation than would be expected for the smaller grain size specimens produced by recrystallisation. These latter specimens were produced by rolling to between 13 and 49% reduction in thickness prior to recrystallisation. (For full details of the treatments used see appendix II).

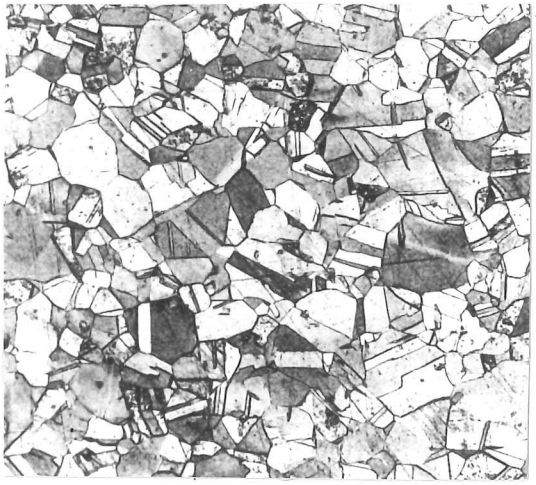

Figure 4/21

optical micrograph of specimen STU2, the largest grain size specimen. 55× magnification, the scale bar is 100 microns.

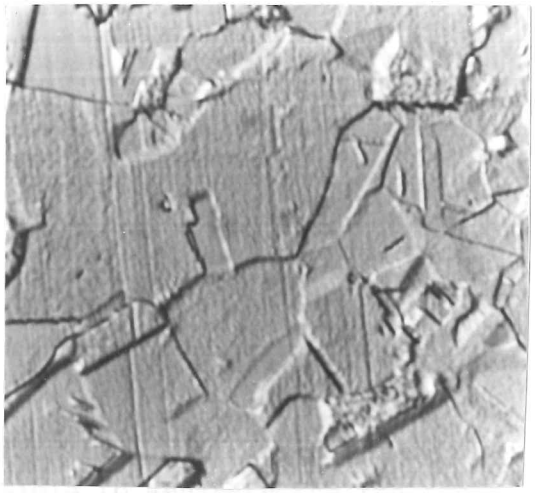

Figure 4/22

optical micrograph (Nomarski interferometry) of specimen STU4A, the smallest grain size specimen. 795× magnification, the scale bar is 5 microns

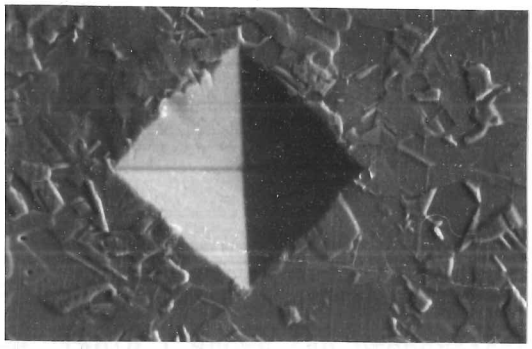

Figure 4/23

Scanning electron micrograph of a 100 gf. Vickers indentation in STU4A, 30° specimen tilt
500 ×

Figure 4/24

Scanning electron micrograph of the same 100 gf. indentation as above and a 300 gf. indentation, 83° specimen tilt
415×

4.4.2 Quantitative Microscopy

The microstructures were examined by optical microscopy of electro-etched electropolished surfaces (see appendix II). Tracings of these micrographs were scanned by a Metals Research Quantimet 720B which was programmed to calculate the grain boundary surface area per unit volume (S_v) a well behaved stereological parameter which could be measured from sections without making any assumptions about the shape of the grains. S_v is also related to the mean linear intercept value for the grain size ($\bar{\ell}$) by (Hanson 1979):

$$\bar{\ell} S_v = 2 \qquad 4.4.2a$$

Use of S_v enables separate account to be taken of the grain boundary and the twin boundary surface areas per unit volume. The separation is achieved by tracing the two types of boundary onto separate pieces of paper prior to analysis by the quantimet. Unfortunately it did not prove possible to separate the the two features in the finer grained specimens and all the S_v values used in the comparison of microhardness measurements are the sums of the twin boundary and grain boundary S_v values. This approach was used by Babyak and Rhines (1960) for their work on brass, but the method was challenged by Thomas (1960) on the grounds that their grains were not randomly shaped. The materials used in the current work have equiaxed grains (see figures 4/21 and 4/22) so this difficulty does not arise. Table I shows the proportions of the surface areas of grain and twin boundaries for the specimen (STU22) with the largest grains.

Table I

$S_v(gb)/\mu m^{-1}$	$\bar{\ell}(gb)/\mu m$	$S_v(tb)/\mu m^{-1}$	$\bar{\ell}(tb)/\mu m$
0.091 ± 0.014	22 ± 3	0.032 ± 0.010	63 ± 25

The ratio of twin boundary (tb) surface area to grain boundary (gb) surface area is 35% in this specimen. The ranges shown in table I are $\pm$ two standard deviations, i.e. a confidence level of about 95%.

The Vickers microindentations were roughly square (in projection) for all the loads used (see 3.2.1) in all the specimens. No consistent 'starring' or 'barrelling' was observed, that is, there was no piling-up or sinking-in except sporadically, when a particular grain was orientated for that kind of deformation. This can be seen in figures 4/23 and 4/24 ; the 300 gf. indentation in the latter figure has a slight pile-up along part of one edge.

This lack of pile-up in general indicates that the material deforms by radial displacements. However, the models described in 2.1.2 cannot be used to describe the behaviour because of the significant work--hardening that occurs in this alloy.

4.4.3 Expected Behaviour

Some ideas on the effects of 'varying scale of microstructure' on the microhardness behaviour have been discussed in 2.7.1 and specific predictions will now be made for the behaviour of stainless steel based on these ideas.

When considering the effects of grain size on the hardness it is sensible to use the hardness measured from an indentation of a standard size; if a standard load hardness were used, the differently sized indentations in materials of different hardness would cause difficulty in interpreting the results. Therefore the 'interpolated ten micron hardness' (see chapter 3) is used here.

If the grain boundaries (or the dislocation tangles along grain boundaries after straining) have a significant effect on the flow stress, and hence the hardness, then the hardness is expected to behave in the manner described in figure 4/25 . However, if the flow stress is affected more by other mechanisms than by the effect of grain boundaries, then the dependence of H on the grain size will be weak.

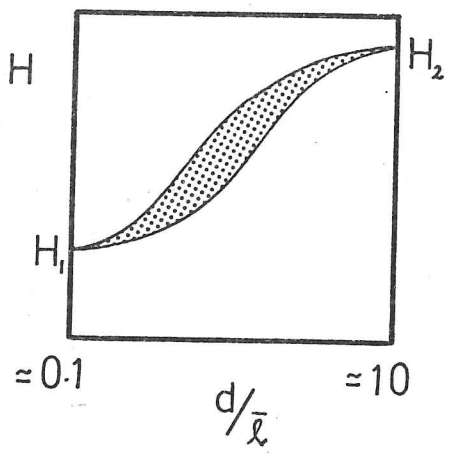

Figure 4/25

Diagram of the likely relationship between hardness and grain size in a ductile metal. d is the indentation diameter and $\bar{\ell}$ is the grain size. The shaded area indicates experimental scatter.

There are two regimes of behaviour where the hardness does not change rapidly with grain size. Firstly, the pseudo single crystal regime, where the indentations are much smaller than the grains, and secondly, the continuum regime, where all the grains are much smaller than the indentations. In the transition region the hardness can be expected to be very sensitive to the precise distribution, shape and orientation of the grains being indented and this is represented by the shaded areas on the two figures (4/25 and 4/26).

At each of the extreme regimes the ISE index will be about 2*, as a change in the size of the indentations, that is, a change in the relative sizes of the indentations and the grains, does not cause a large change in measured hardness. In the transition region larger indentations will cause higher hardnesses to be measured and the ISE index will increase to values above 2, see figure 4/26. If a particular hardness/indentation size relationship is postulated, as in figure 4/25, then the relevent ISE index/indentation size relationship can be calculated using equation 2.5.3d:

$$n = 2 + \frac{\partial H}{\partial d}\cdot\frac{d}{H} \qquad 2.5.3d$$

---

*Footnote: assuming that there are no causes of the ISE not connected with the microstructure. This assumption will be shown to be false in the light of the results, however, the ISE index will still be smaller at the extremes than in the transition regime.

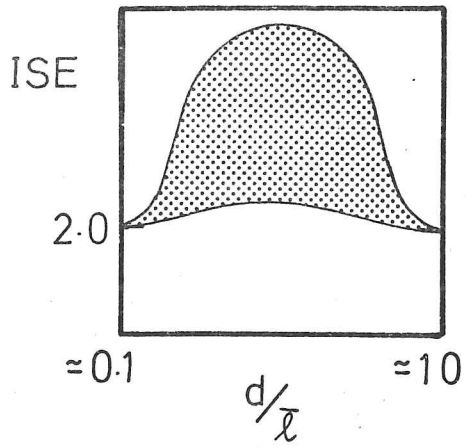

Figure 4/26

The expected variation of ISE index with grain size and indentation size, based on figure 4/25 and equation 2.5.3d.

4.4.4 Results and Discussion

The microhardness measurements were processed by the program ISEMH (described in chapter 3) and ellipsoid plots are shown in figure 4/27 . From this it can be seen that the four specimens have indentation behaviours which are sometimes distinct and not dependent monotonically on the grain size (see grain sizes in table II). This can also be seen from figures 4/28 & 4/29 and the former shows that there is certainly no Hall-Petch type relation operating here.

This very small effect of the grain size on the microhardness is very probably due to the 'cleanliness' of the alloy, and hence its grain boundaries, and its work hardening behaviour. The action of indentation strain hardens the material to such an extent (according to Tabor, to a representative strain of 8%) that the hardening effect of the grain boundaries is insignificant by comparison. The work hardening rate for the alloy has not been determined directly, but annealed austenitic materials generally have very high work hardening rates, though in this case the rate can be expected to be ~~lower~~ greater than average because of the low stacking fault energy in the alloy (Porter et al. 1979) which renders cross slip difficult.

Section 4.4.4 - Table I

Code	H(ten-micron)	ISE index	S_v/mm^{-1}	H (10 gf.)	H (100 gf.)
STU22	267 (240 - 298)	1.90 (1.86 - 1.94)	122 (98 - 147)	266 (246 - 288)	240 (233 - 247)
STU1C4	208 (182 - 238)	1.72 (1.67 - 1.77)	104 (94 - 116)	212 (194 - 232)	145 (141 - 149)
STU4A15	245 (186 - 325)	1.93 (1.81 - 2.04)	167 (149 - 183)	227 (203 - 256)	217 (199 - 239)
STU4A3	202 (175 - 234)	1.78 (1.73 - 1.84)	284 (227 - 340)	207 (191 - 224)	156 (150 - 162)

Ranges in brackets are approximately to the 95% confidence level, Hardness values (H) are all in $kgf.mm^{-2}$ and S_v is the sum of the twin and grain boundary surface areas per unit volume.

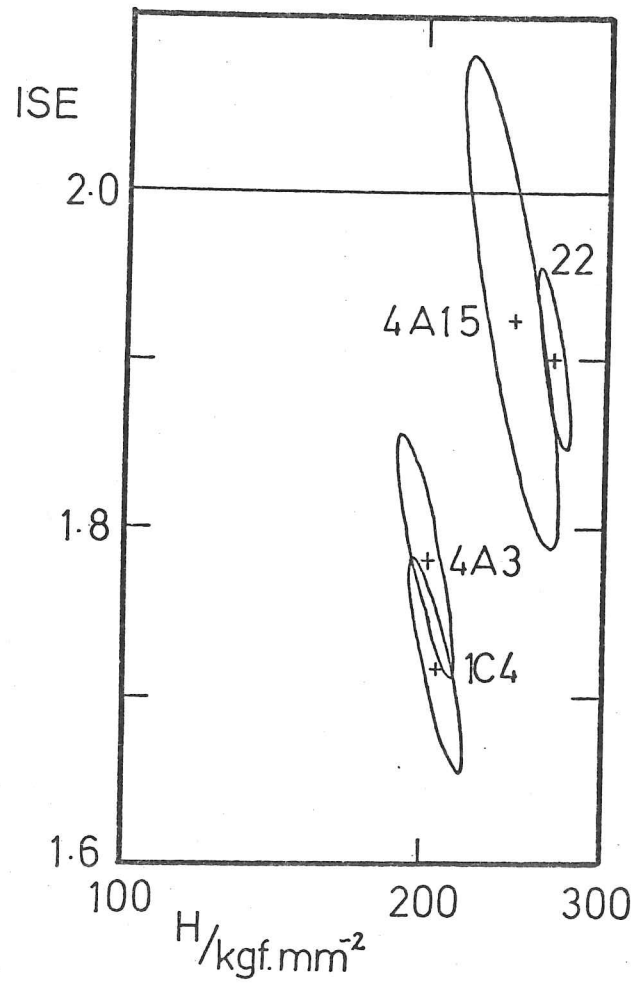

Figure 4/27

The 95% confidence ellipsoids produced by the programme ISEMH from the data for four specimens of stainless steel. ISE is the indentation size effect index and H is the interpolated 'ten micron hardness'.
The codes labelling the ellipsoids are identified in table I.

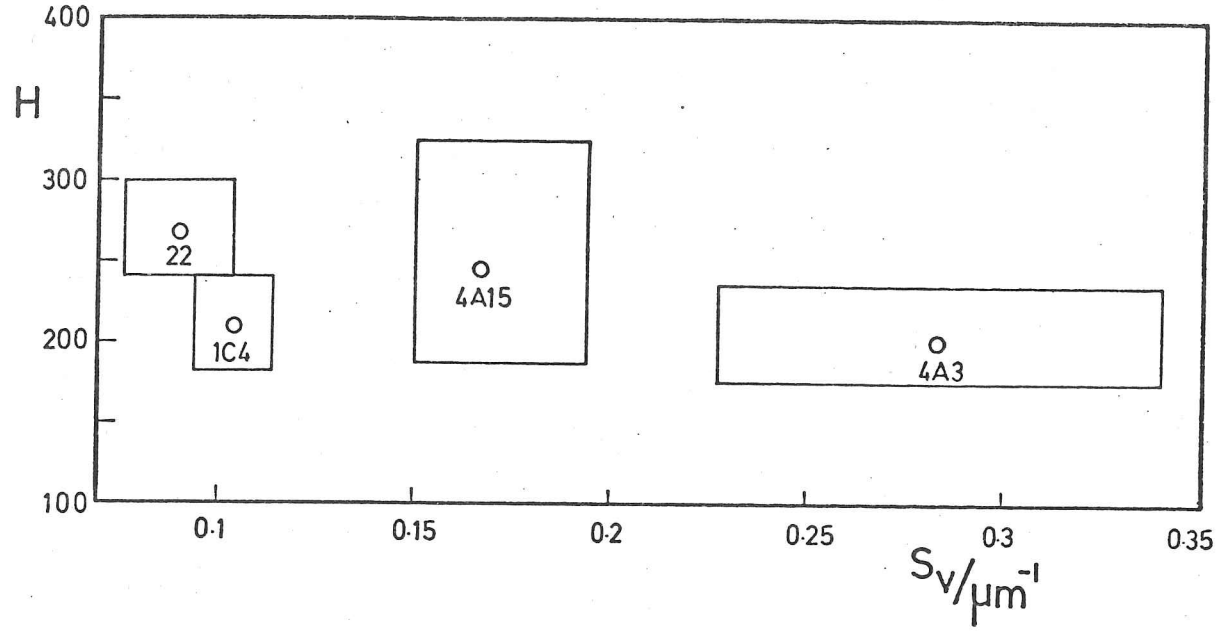

Figure 4/28 The ten micron hardness (H) plotted against the grain boundary and twin boundary surface area per unit volume (S_v).

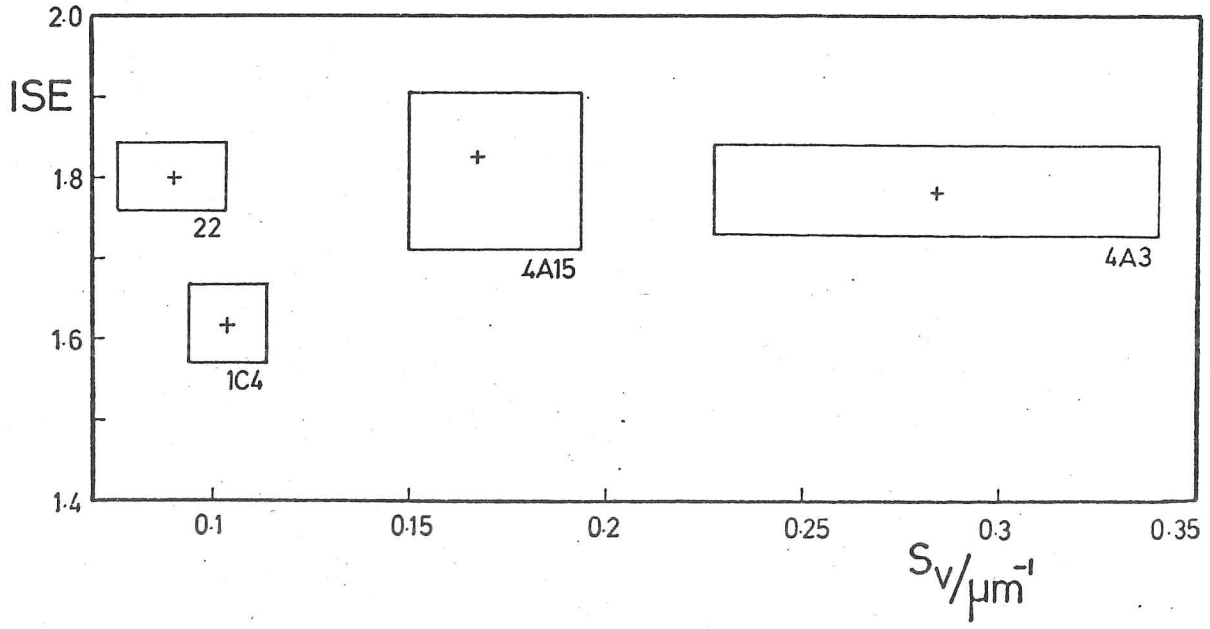

Figure 4/29 The ISE index plotted against the grain boundary and twin boundary surface area per unit volume (S_v).
The boxes in both this figure and 4/28 are 95% confidence limits on S_v and ISE (H in 4/28).

Since the grain boundaries have no significant strengthening effect* no ISE is to be expected and the index should be 2, unless an additional indentation size effect is caused by other mechanisms. Figure 4/29 shows that there is a definite indentation size effect on the hardness, the index is consistantly less than 1.9, for all four specimens. That this is not due to the presence of grain boundaries can be seen from (a) the fact that the effect is negative (n less than 2),rather than positive as predicted, and (b) the fact that the index does not vary systematically with grain size.

The indentation diameters ranged from 9 to 36 microns and the mean linear intercept grain size ($\bar{\ell}$) varied from about 7 to about 28 microns. Therefore it is to be expected that, had the grain boundaries had any effect upon indentation mechanisms, this would have become apparent in the experiments.

In this material, austenitic stainless steel, the ISE is unlikely to be caused by precipitates, or other microstructural defects on a smaller scale than the grains for two reasons. Firstly, because theory predicts that the ISE due to microstructure will be higher than the extremes (see previous section) and secondly,because the annealed and recrystallised alloy is very clean in the microstructural sense.

The surface preparation treatments were designed specifically to exclude the possibility of hard surface layers persisting from the cutting, grinding or polishing operations (see appendix II.II) and,since there is such a high proportion of chromium in the alloy, any residual oxide layer is probably only a few atoms thick.

---

*Footnote: To investigate the scaling effects of grain boundaries upon the ISE a better experimental material would be a metal with heavy segregation at grain boundaries, a low strain hardening rate and very few defects within the grains themselves, e.g. a soaked low-alloy ferritic steel.

Therefore the conclusion can be drawn that the indentation size effect in this material is caused by the detailed mechanics of dislocations i.e. the effect of the finite size of dislocation sources, the mechanisms of dislocation sources activated by an expanding stress field, the effect of dislocation curvature on the flow stress and the elastic effects of the free surface on the near-surface dislocations. These are the only mechanisms which can cause the ISE which have not been eliminated by the experimental procedure, further investigation of these effects is, however, likely to be very much more difficult.

This conclusion can be compared with the similar conclusion that was reached for the cause of the ISE in metallic glasses. Despite the very different nature of shear bands as compared with dislocations, the fine scale mechanics of deformation in both types of material appear to cause an indentation size effect on the measurement of microhardness.

4.5 Microhardness of Magnesium Oxide Single Crystals

Magnesium oxide was chosen for this study because its microhardness is known to be sensitive to several of the mechanisms and effects described in chapter two. Indeed, in the appropriate circumstances, it can probably be susceptible to all these effects (see figure 4/1), which makes it difficult to design experiments to test these factors individually. Nevertheless, the microindentation behaviour of single crystals of MgO has been more intensively studied, by researchers worldwide, than that of any other single material.

This study concentrates on the mechanics of the indentation process as MgO changes from semi-brittle to fully ductile behaviour as the temperature increases. This occurs because secondary deformation mechanisms become more important with respect to primary slip on the $\{110\}\langle 1\bar{1}0\rangle$ systems. As this change occurs the E/Y ratio of the crystal also changes and thus this material is ideal for investigating the application of the models of radial and surface directed displacement to the situation where there is only limited ductility. This problem was first raised in 4.2.1 in connection with materials with orientated microstructures. Clearly, the models describe only ideally plastic, isotropic, homogeneous materials, but since such materials do not exist, the limits to the applicability of the models must be investigated experimentally if they are to be of any real use.

The study of the room temperature indentation behaviour of MgO single crystals included here is a necessary preliminary to both the high temperature experiments and the study of the effects of grain boundaries on the hardness of MgO which is described in 4.6.

Parallel studies have also been made on LiF whose behaviour at room temperature (about 0.27 T_m for LiF) may be similar to that of MgO at elevated temperatures.

4.5.1 Environmental Effects

Environmental effects on the microhardness must be considered before undertaking any series of experiments on non-metallic materials and the effects of the dipole moment and charge density of liquid environments on LiF and MgO is well documented (Westwood and Macmillan 1973). However, the only environmental condition which is likely to be present and to have an effect on the microhardness of LiF and MgO during experiments designed to investigate other, non-environmental, effects is water vapour. Therefore, prior to experiments on the effects of temperature, anisotropy and indenter load on the microhardness of LiF and MgO, the effect of moisture on the hardness of these crystals was investigated.

Effects of Moisture - LiF

An experiment was designed to compere the hardness measured from indentations made on perfectly dry and on wetted LiF crystals. An investigation was also made to check whether the wetting process affected the measurement of indentations which were made under perfectly dry conditions. The purpose of this latter experiment was to find out whether wetting changed the surface reflectivity of LiF, and hence the measurement of indentations. This was necessary in order to be able to make a comparison between indentations which differed only by the conditions under which they were made, and not by the conditions under which they were measured.

A LiF crystal (LIF1) was cleaved under dry toluene (from a freshly opened bottle). Both halves were indented, without removing them from the toluene, using a range of loads. Both halves were removed from the toluene and rinsed in water, dried on a paper tissue, and re-indented, again using a range of loads. One of the halves was then etched (see appendix II.II) to produce an etch pit rosette and the other was sputter-coated with gold prior to measuring the indentations optically.

Section 4.5.1 - Table I

LIF1AW	Cleaved under toluene	water rinse	indented in air	kept in .air	gold sputter coat
LIF1AD	"	kept under toluene	indented under toluene	water rinse	"
LIF2	"	"	"	kept under toluene	"

The whole sequence was completed in less than 48 hours, A Vickers indenter was used.

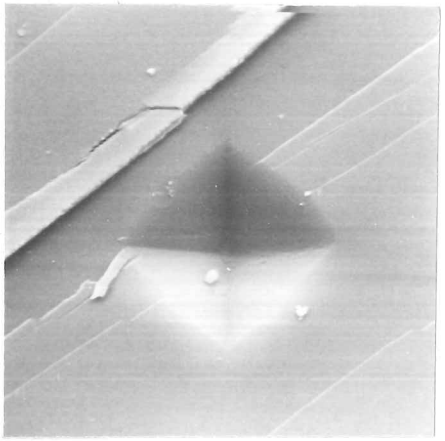

Figure 4/30

50 gf. Vickers indentation on the (001) plane of LiF cleaved and indented under dry toluene. Indentation diagonals parallel to ⟨010⟩ Secondary electron image, 1100×

Note the barrelling due to a slight pile-up at the sides of the indentation (see figure 2/16).

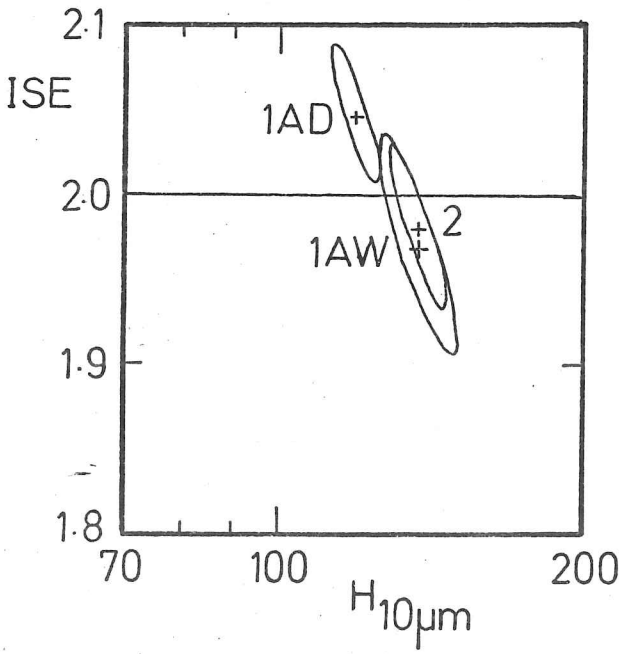

Figure 4/31

Results for LiF, see table I for key to codes.

A second crystal (LIF2), cleaved from the same block as the first, was cleaved and indented under toluene and measured without being rinsed; Table I summarises the treatments. All specimens were examined by scanning electron microscopy and figure 4/30 shows an unrinsed, unetched indentation.

It is expected that environmental effects affect the surface plasticity mechanisms and therefore that small indentations are more environmentally sensitive than large ones; Table II shows the hardness values measured from only the six 5 gf. indentations made on each of the crystals. Figure 4/31 shows the complete set of data (from 200 gf., 50 gf. and 5 gf. loads) displayed on the standard ISE index : log $H_{10\mu m}$ plot. Using the t-test on the data in Table II and the F-test method (see 3.2.4) on all the data the same results were obtained: the set of data LIF1AD is different from LIF1AW to a confidence of 90% and different from LIF2 to a confidence of better than 97%.

Section 4.5.1 - Table II

	$H/kgf.mm^{-2}$	$ste./kgf.mm^{-2}$
LIF1AW	139	11
LIF1AD	115	4
LIF2	132	5

(ste. is the standard error in the mean)

This shows that the damp air environment raises the hardness (1AW compared with 1AD) and that rinsing in water before measurement but after indentation has a significant effect (1AD compared with 2). The first conclusion disagrees with the results of Westbrook and Jorgensen (1965) who found that LiF indented under toluene was about 15% harder than that indented in damp air (using a load of about 3 gf.). This discrepancy may be due to their drying treatment (they did not cleave

specimens under toluene) but is more likely to be due to the higher load, shorter dwell time and high indenter velocity (500 $\mu m\ s^{-1}$) used in the current study.

Moist LiF is known to be susceptible to anomalous indentation creep (see section 2.3.3) whereas dry LiF is not. It appears that in the current study the anomalous surface sensitive creep mechanisms are not given sufficient time to reduce the measured hardness significantly. Instead, a hardening effect is observed which may be due to the effect of moisture on the plasticity mechanisms which operate at high strain rates.

In conclusion, the effects of the moisture on the hardness of LiF cleaved single crystals are complex and deserve further study. However, the purpose of this investigation was to determine whether special precautions should be taken when making indentations in LiF. Hardness measurements made in the damp air of the laboratory were reproducible and consistent if the crystals were freshly cleaved, hence no special drying treatments have been used in the further studies on the hardness anisotropy of LiF (see section 4.5.2).

Effects of Moisture - MgO

Burnand (1972) measured the hardness of MgO cleaved under toluene and found it to be slightly lower than the hardness of MgO cleaved in air or mechanically polished, but the effect was small. Westbrook and Jorgensen (1965) measured a 20% decrease in hardness for indentations about one micron deep when MgO crystals were first dried in argon and indented under toluene. This is a significant decrease and therefore experiments were performed to measure the effect with the apparatus used for the high temperature study. High temperatures (Westbrook and Jorgensen used 300°C) cause water to be desorbed from the surface of the crystal, thus room temperature hardness measurements could be anomalously high compared with those at higher temperatures if moisture effects are significant.

In this study, instead of cleaving the crystals under toluene (as

was done for LiF), dry surfaces of MgO were prepared by baking at high temperatures under vacuum. Mechanically polished MgO single crystals were heated in the high temperature, controlled environment microhardness apparatus (described by Naylor (1978) and Naylor and Page (1979)) to 800°C and annealed at that temperature for 30 minutes at 10^{-6} torr with the chamber vacuum connected to a liquid nitrogen cooled water vapour trap. The specimens were cooled to 50°C over a period of 4 hours and indented under a vacuum of 10^{-7}torr. Damp nitrogen was then admitted to the chamber directly from the cylinder; experiment showed that there was no difference in the measured hardness when the nitrogen was first bubbled through water and it is presumed that the nitrogen in the cylinder was damp as it is unlikely that nitrogen itself affects the hardness of MgO. The chamber was then re-evacuated to 10^{-7}torr and the specimen re-indented; it was then let up to atmospheric pressure, the specimen exposed to the laboratory atmosphere and indented again. The data from this sequence is shown in table III and similar results were obtained using Knoop indenters.

Section 4.5.1 - Table III

	H/kgf.mm^{-2}	ste./kgf.mm^{-2}
Dry - vacuum	1496	35
Damp - vacuum	1411	50
Damp - atmosphere	1581	58

ste. is the standard error in the mean. This table summarises data from 70 measurements of Vickers indentation diagonals made using 10 gf. loads for dwell times of 15 s on a specimen at 50°C.

Use of the t-test to study the data in table III shows that there is no significant difference between either of the 'damp' measurements and the 'dry' measurement.

In conclusion, there is no significant effect of moisture on the hardness of MgO measured using the high temperature, controlled environment apparatus and the dwell times and indentation rates stated above.

Action Taken

Although these investigations of the water vapour sensitivity showed no significant effects, nevertheless the polycrystalline MgO specimens were indented in air immediately after mechanical polishing and rinsing in water, for consistency.

The furnace controllers on the controlled environment machine made it easier to make a sequence of measurements whilst cooling, rather than whilst heating, the specimen. Therefore, as a matter of course, all MgO crystals tested at high temperatures were first annealed at 800°C for 30 minutes under vacuum.

4.5.2 Crystal Anisotropy and Indentation Size Effects

It is important to investigate the inter-relationships between these two effects of hardness anisotropy and indentation size effect because, whilst neither are well understood, it may be possible to discover whether the same, or different, mechanisms are responsible. For example, if it is found that indenter orientation affects the hardness but not the ISE index then this would indicate that the two effects have their origins with different mechanisms (or with the same mechanism in a different part of the deformation volume).

MgO and LiF are known to have the same form of hardness anisotropy (see 2.4.1 and 2.3.3) but of different magnitudes and it may be possible to correlate the effect of orientation on the ISE with the known similarities and differences between MgO and LiF.

The success of the effective resolved shear stress models for hardness anisotropy (see 2.4.2) indicates that it is the dislocation activity on the primary slip system immediately adjacent to the hydrostatic core which determines the form of the hardness anisotropy as this is the region whose stresses are modelled. However, the relative importance of the primary mechanisms in the modelled zone compared with the same mechanisms outside this zone and the secondary mechanisms (see 2.4.1) is not likely to be the same for LiF and MgO and may be the cause of the different magnitudes of the hardness anisotropy (about 10% and 50% respectively). Therefore a slight difference in the orientation dependence of the ISE is expected between the two materials if the secondary mechanisms, which are not thought to be strongly orientation dependent, are responsible for the indentation size effect.

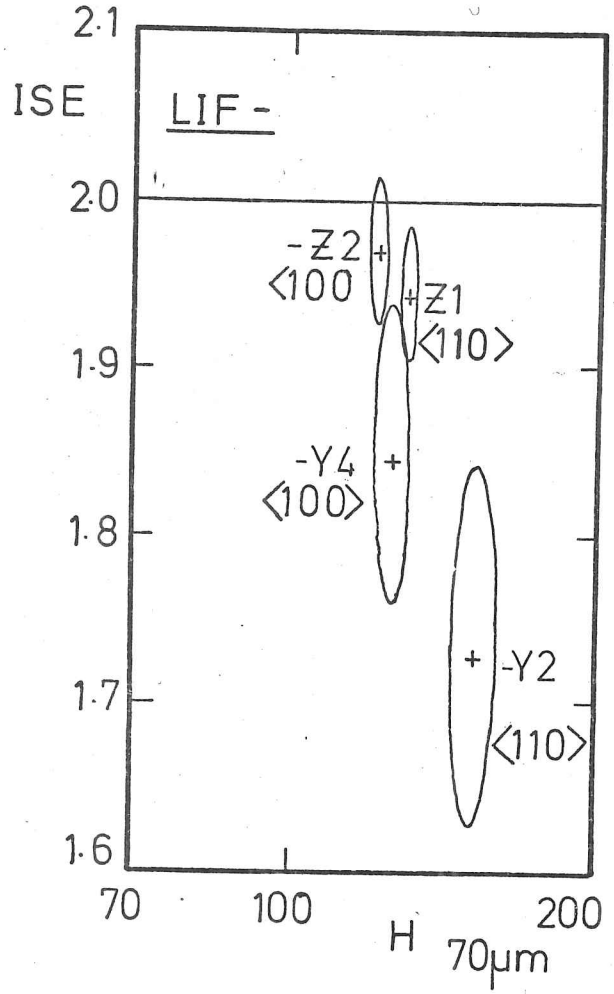

Figure 4/32 - LiF Results

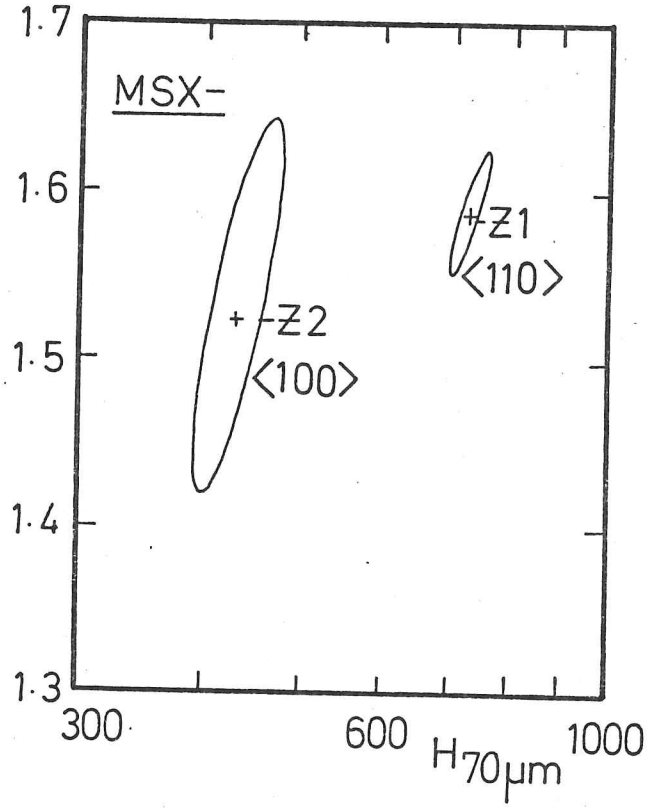

Figure 4/33 - MgO Results

Anisotropy/ISE Results for LiF - Knoop Indenter

Knoop hardness anisotropy measurements were made on two crystals, one freshly cleaved (LIFZ) and the other which had been exposed to the laboratory atmosphere for two months (LIFY). It is evident from figure 4/32 that the long exposure hardens the crystal and increases the magnitude of the orientation dependence of both the hardness and the ISE index. (Z2 and Y4 are sets of data from indentations with their long diagonals parallel to ⟨100⟩ directions and Y2 and Z1 from indentations parallel to ⟨110⟩, all on (001) cleaved planes.)

The ISE indices for Z1 and Z2 are not significantly different whereas those for Y2 and Y4 are different to a confidence level of 95% (using the t-test). Therefore it is possible to conclude that at least some of the mechanisms which control the ISE are orientation dependent and are also influenced by long term moisture effects.

The hardening effect of exposure to moisture which is evident here is in agreement with the hardening effect observed by Westbrook and Jorgensen (1965) but contradicts the measurements reported in section 4.5.1. This indicates that the length of time exposed to water is an important parameter, in addition to the length of time the indenter is under load. The time scale suggests a diffusion process or slow corrosion but the phenomenon has not been further investigated here.

Anisotropy/ISE Results for MgO - Knoop Indenter

A freshly mechanically polished crystal (MSXZ) was tested and the results are shown in figure 4/33. If this is compared with figure 4/32 it can be seen that:-

a) The MgO crystal is harder and the indentation size effect more pronounced (i.e. ISE index further from 2.0) at all orientations than in LiF.

b) The hardness anisotropy is of greater magnitude in MgO than in LiF.

c) The effect of orientation on the ISE index is different for the two materials. In LiF the ⟨100⟩ indentations ISE index is larger than that for the ⟨110⟩ indentations whereas in MgO the opposite effect is observed.

This last observation confirms the hypothesis that the indentation size effect is affected by the unmodelled mechanisms in that the anisotropy/ISE behaviour is different. However, this would have been indicated had the anisotropy/ISE relationship merely differed in magnitude, in fact it differs in sign. This shows that the unmodelled mechanisms are also orientation dependent which points towards primary slip (not in the modelled volume) or secondary slip rather than diffusive mechanisms.

Anisotropy/ISE Results for MgO - Vickers Indenter

This data is presented here to confirm that the Vickers and Knoop hardnesses are 45° out of phase (see 4.2.2) and to show that use of the Vickers indenter leads to a smaller magnitude of hardness anisotropy.

Figure 4/34 shows the results and table I summarises the procedure and the preparation and orientation of the crystals (which were all mechanically polished). If only the effect of anisotropy on the ISE index is considered, a trend can be discerned for the index to increase as the indentation diagonal orientation is changed from ⟨110⟩ to ⟨100⟩ but it is barely noticeable above the experimental errors; the ISE indices of specimens E1 and A11 are different to a confidence of only just better than 90%.

The data from MSXRCI is included here for comparison although the indentations were made with a different microhardness apparatus. The $H_{10\mu m}$ for RCI is 1314 $kgf.mm^{-2}$ whereas that for A11 is 1144 $kgf.mm^{-2}$, an increase of 15%. This is thought to be due to the different indenter velocities and indenter-arm inertias rather than the effect of moisture which has been shown to be smaller than this in section 4.5.1.

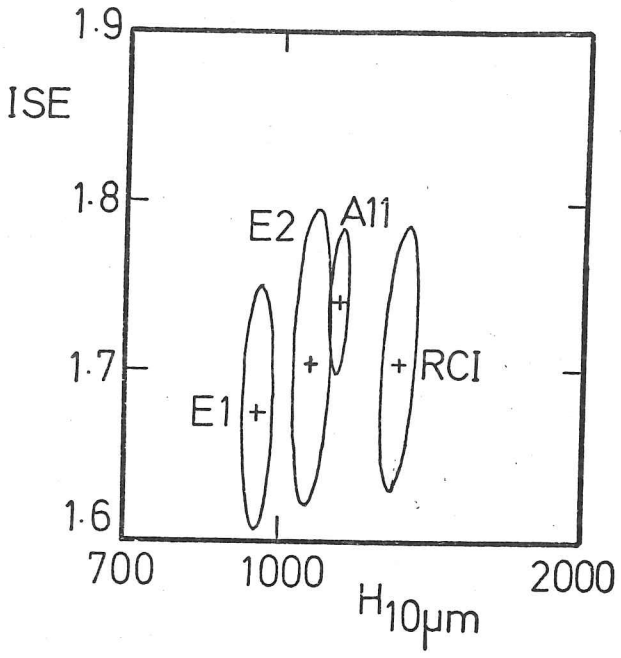

Figure 4/34

Crystal Anisotropy Effects on the Hardness and ISE index on the (001) surface of MgO at room temperature.

Section 4.5.2 - Table I

	diagonal parallel to	apparatus	conditions
MSXE1	⟨110⟩	Leitz Miniload	in air, 15s dwell time
MSXE2	⟨210⟩	"	" "
MSXA11	⟨100⟩	"	" "
MSXRCI	⟨100⟩	Wilberforce Machine*	vacuum, 10s dwell time

*described by Naylor and Page (1979) and Naylor (1978).
All indentations were measured, after sputter-coating with gold, with the optical microscope on the Leitz Miniload. The set of data MSXRCI was collected from specimens which had been heated at 800°C for 30 mins. under vacuum and kept under vacuum whilst they were cooled to room temperature.

Conclusions

It would be a mistake to read too much into these results as no account has been taken of the indentation contraction on unloading due to the elastic compressive stresses. These will depend on indenter orientation and on the proportion of elastic to plastic deformation, i.e. the E/Y ratio (see 2.1.2) where Y is the effective flow stress beneath the indenter. This ratio is likely to be different for large and small indentations when an indentation size effect on hardness exists because the higher the hardness, the higher the effective flow stress is likely to be. This effect is not small; in MgO, for Knoop indentations aligned with their long diagonals along $\langle 100 \rangle$ on (001) surfaces, the hardness measured using a 10 gf. load is 803 $kgf.mm^{-2}$ and that measured using 100 gf. is 446 $kgf.mm^{-2}$.

Elastic contraction can be seen to have occurred if the aspect ratios of the Knoop indentations are examined. If there is no contraction, or equal contraction in all directions, then the long diagonal should be seven times the short diagonal in length. The aspect ratio has been measured for the largest indentations made on MgO from the sets of data MSXZ1 and MSXZ2. It is 5.51 $\pm$ 0.08 for indentations with long diagonals along $\langle 100 \rangle$ and 10.28 $\pm$ 0.08 for indentations for indentations with long diagonals along $\langle 110 \rangle$ (errors are $\pm$ two standard errors).

The aspect ratio differences are not due to the pile-ups which occur on the surface of MgO (see 2.4.1) because these are too small to account for the differences; they must be due to elastically driven recovery. Therefore this investigation could usefully be repeated using a displacement controlled microhardness machine so that unrecovered microhardness values could be measured.

4.5.3 Experiments on MgO at Elevated Temperatures

The main aim of this thesis is to show that the quantitative investigation of the microindentation behaviour of elastic-plastic solids, particularly the indentation size effect, yields information about the mechanisms and distribution of plasticity beneath indenters.

At room temperature secondary plasticity mechanisms (see 4.2.1) are known to be active in MgO but have never been directly observed. A study of the indentation behaviour as the temperature is increased and the deformation mechanisms change in relative importance was thought to be a good test of the information that can be obtained from only the quantitative microhardness measurements.

Increasing the temperature affects the flow of magnesium oxide in a number of ways, in addition to facilitating flow by secondary mechanisms. Firstly, the Young's modulus (E) decreases with increasing temperature in addition to the flow stress decreasing with temperature; the overall effect is to increase the E/Y ratio. The change in E also affects the strain fields of individual dislocations and hence the work hardening rate because of the effects on the multiplication and interactions of dislocations. Secondly, the increase in temperature increases the strain rate dependence of slip, hence the indenter velocity becomes a more important parameter. In the current study the indenter velocity has been kept constant at all temperatures. Thirdly, the creep mechanisms (vacancy and interstitial diffusion along dislocation cores and in the bulk) increase in importance. Therefore the dwell time at full load was kept constant at 5 s to reduce these effects on the measured hardness (except for the room temperature tests when 10s was used)

It is possible that the same mechanisms which operate in the bulk at elevated temperatures may be activated by the high stress levels beneath indenters at lower temperatures. Therefore, as the temperature is

increased, it is to be expected that this core region in which the stress activated mechanisms occur will increase in size relative to the size of the indentation because they will be easier to intiate at higher temperatures. Such a scaling effect should be detectable by study of the indentation size effect on microhardness.

Experimental Procedure

The Wilberforce Instruments high temperature, controlled environment microhardness machine was used for this investigation; it is fully described by Naylor (1978), who commissioned it.

Mechanically polished MgO single crystals were stuck to silver steel blocks using a few drops of aluminophosphate cement. This was prepared afresh for each specimen; a small quantity of commercial purity alumina powder (supplied by Cawood Refractories) with a bimodal particle size distribution (i.e. a mixture of 100 and 200 mesh powders) was mixed to form the paste with dilute orthophosphoric acid. The MgO, paste and silver steel block were then baked at 200°C for an hour to set the cement. The thermocouple used to measure the temperature of the specimen was spot welded to the steel block.

The specimen and indenter were baked at 800°C for 30 minutes under a vacuum of 10^{-6} torr before each sequence of measurements to anneal the specimen and to completely outgas the furnace and cement. The liquid nitrogen trap was filled at the beginning of the anneal and kept topped up throughout the course of the experiments.

For each set of indentations at a particular temperature the specimen was aligned under the microscope and then positioned under the indenter whilst they both cooled to the correct temperature. They were left at that temperature for a few minutes to check that the temperature had stabilised and then all the indentations were made rapidly in case the temperature control drifted. On each specimen 16 indentations were

made at each temperature, a procedure which took 9 minutes. Four indentations were made at each of 10, 20 50 and 100 gf. loads without moving the specimen from beneath the indenter furnace. The specimen was positioned using the micrometer controls on the stage.

All indentations were measured at room temperature using the microscope on the Leitz Miniload. Measurement of indentations at 800°C showed that there was no significant change in dimensions on cooling.

The control knob used to move the specimen stage between the indenting and the observing positions is the same control that is used to rotate the specimen. A degree of 'play' in this control meant that the orientation of the specimen with respect to the indenter sometimes varied from the standard position (Vickers indenter diagonals along ⟨010⟩directions on the (001) surface). The orientation of such sets of indentations was measured later using the rotating stage on the Miniload and is indicated in the results. On the basis of room temperature Vickers hardness anisotropy measurements, it is not thought that these mis-orientations have had a significant effect on the measured hardness.

Hardness and ISE Measurements

The variations of the ten-micron hardness and the ISE index with temperature are shown in figures 4/35 and 4/36; figure 4/37 displays the same data on the ISE index/$\lg(H_{10\mu m})$ plot and table I identifies the different sets of data. Figure 4/35 shows that the hardness decreases monotonically with temperature. It is presumed that this merely indicates that the Peierls' stress for slip and the stresses required for the activation of secondary mechanisms decrease with temperature.

Figures 4/36 and 4/37 show that the ISE index is significantly less than 2.0 at all temperatures, and therefore the use of the ten-micron hardness in figure 4/35 is a significant advance over using, for example, the 100 gf. hardness because the complicating effect of the indentation size (see figure 4/36) is removed from the measurements.

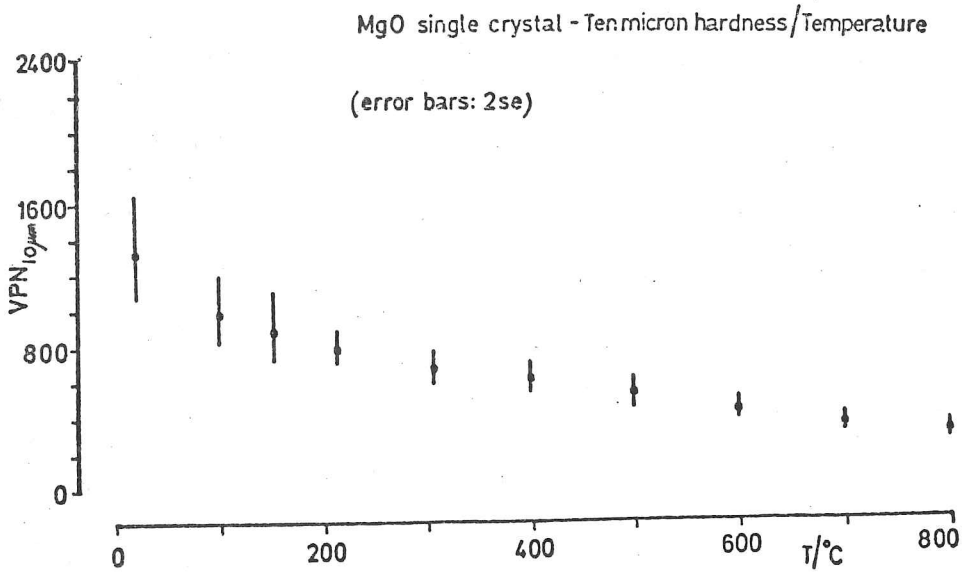

Figure 4/35

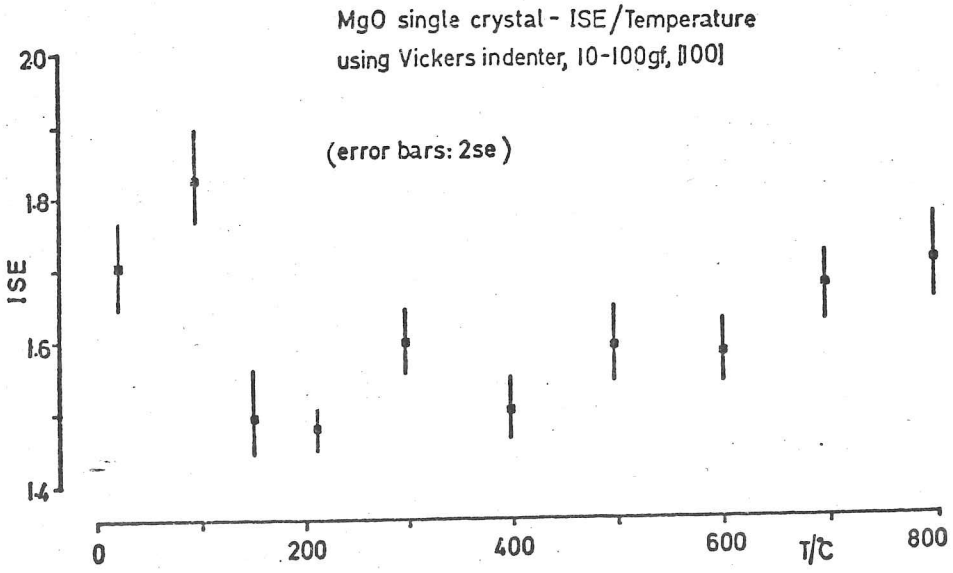

Figure 4/36

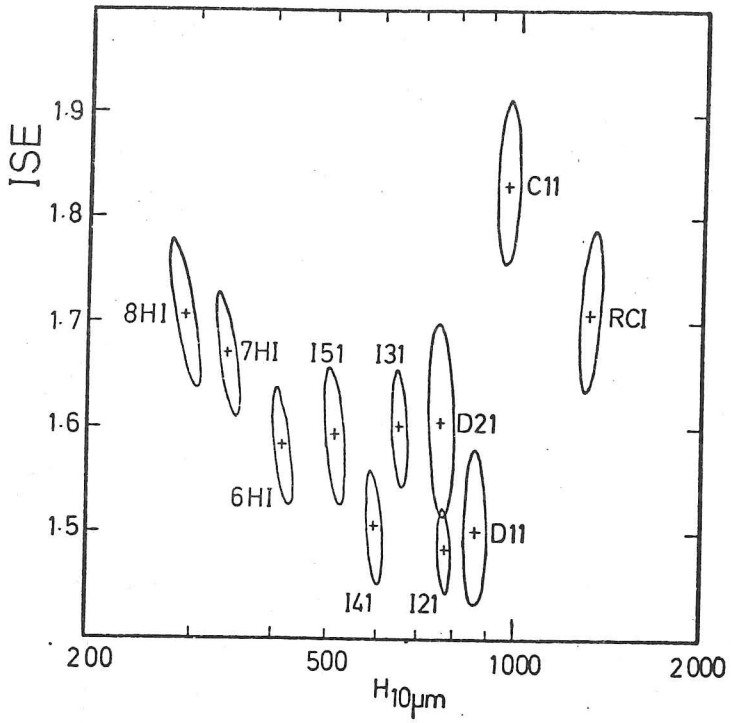

Figure 4/37

This shows the same data as figures 4/35 and 4/36 with the additional inclusion of D21.

Section 4.5.3 - Table I

Data set	temperature/°C	specimens used	degrees misorientation from standard ⟨0 1 0⟩
RCI	25	MSXC & MSXI	0
C11	100	MSXC	0
D11	150-155	MSXD	0
I21	210-215	MSXI	8
D21	205-230	MSXD	14
I31	304-310	MSXI	7
I41	400	MSXI	8
I51	500	MSXI	8
6HI	600	MSXH & MSXI	0
7HI	700	MSXH & MSXI	0
8HI	800	MSXH & MSXI	0

The indentation size effect in MgO is almost certainly not due to defect density effects (see 2.5.4) or surface layers; in dry vacuum the only surface plasticity effects will be those of image forces on dislocations near the surface and the possible effects of electronic surface states on the interactions of dislocations containing charged jogs. These effects are thought to be small. The ISE is probably due to the effects of the finite sizes of dislocations and dislocation loops which were thought to be the cause of the ISE in stainless steel (see 4.4.4).

The steady increase in ISE index with temperature above 100°C (apart from the deviation at 300°C and 400°C) which can be seen in figure 4/36 means that for the higher temperatures the indentation size effect of hardness is smaller. Now, the cause of the ISE in MgO single crystals was thought to be that the fundamental deformation mechanisms had critical lengths associated with their operation which were significant fractions of the sizes of the indentations. The decrease in the magnitude of the effect is therefore thought to be due to types of mechanism with shorter critical lengths (presumed to be the diffusion of point defects) becoming dominant at higher temperatures. This is consistent with the disappearence of dislocation rosettes at higher temperatures (Boyarskay and Grabko) and the expansion of the core which was postulated above.

There is a contributory cause to the increase in ISE index with increasing temperature in that the indentation size range at 800°C is 7 to 30 μm whereas at 100°C it is 3.5 to 16.5 μm because the same load range was used for all temperatures. Thus the index will be higher at 800°C because the indentations are, on average, larger relative to the deformation processes. To retain the same indentation size range at 800°C would mean using loads in the range 2 to 40 gf. which would require some modification of the high temperature microhardness apparatus.

The high values of the ISE index at and below 100°C are thought to be due to competition between the mechanisms which are particulaly sensitive to low stress/long times and those sensitive to high stress/ short times (where a long time seems to be more than a second). The data indicates that even though dwell times were kept to 5s, creep mechanisms dominate at higher temperatures (as shown by the increasing index) whilst below 100°C 'impact' sensitive mechanisms dominate which are less sensitive to the indentation size effect. This hypothesis could be investigated by repeating the entire set of measurements using different dwell times (1, 10, 20, 60s for example). The longer times should depress the transition temperature between the two types of behaviour.

The relatively high index value at 300°C and the low index value at 400°C are not thought to be significantly different from the general increasing trend.

Implications of the Young's Modulus and the Hardness

The radial displacement models described in section 2.1.2 do not describe indentation in anisotropic solids with limited ductility but have been applied here to investigate points of comparison.

If the material displacement vectors are assumed to be radial then a knowledge of the Young's modulus (E) and the hardness (H) makes it possible to calculate the flow stress beneath the indenter (see appendix I for the program used to calculate this). These calculations have been done using the $H_{10\mu m}$ data and published values of the modulus of MgO at the relevant temperatures (Simmons 1965). The results are presented in figures 4/38 and 4/39. Figure 4/38 shows the E/Y = 114 line above which the surface directed displacement mode of deformation is, theoretically, likely to become important (see section 2.1.2). It is interesting to note that the data shows that this may occur for MgO

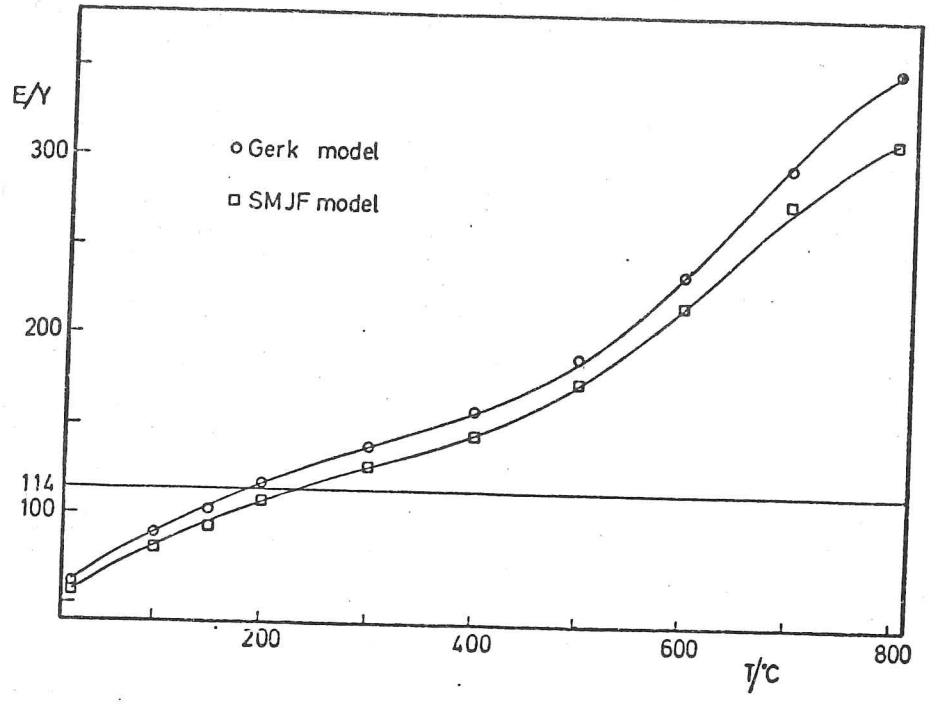

Figure 4/38

E/Y ratio for MgO calculated from H and E

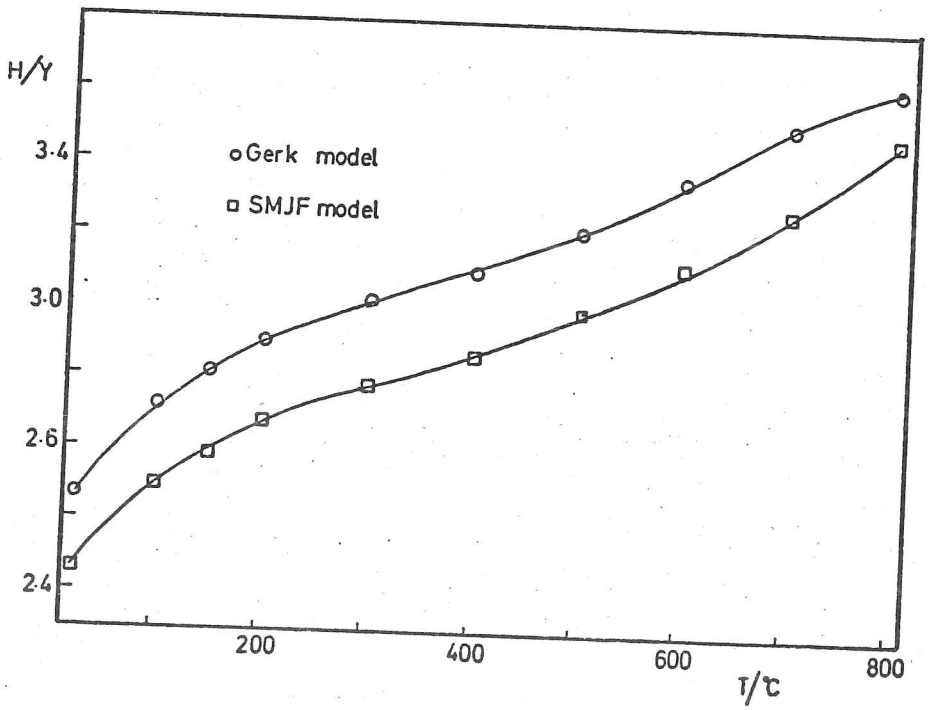

Figure 4/39

H/Y ratio for MgO calculated from H and E

above 200°C and it is observed that above this temperature 'Keh' type cracks on {110} planes are not formed. The lack of these cracks suggests that the dislocation rosette is not formed (see section 2.4.1) hence the deformation is more concentrated around the indentation, which is consistent with a greater emphasis on surface directed displacements. It should be remembered though, that pile-up occurs around indentations in MgO at room temperature (see 2.4.1), so that the effect observed is merely a slight change in the relative proportions of the active mechanisms.

The H/Y ratio (shown in figure 4/39) varies between 2.4 and 3.6 which is a much more reasonable range than the value of 35 which was obtained by Westbrook (1958, and see section 2.3.1) when he used for Y the critical resolved shear stress for yield on the primary slip system.

The accuracy of the models is difficult to assess as it is almost impossible to measure the relevant flow stress directly and although it is known that the models are inappropriate, they provide the only estimate available for these stresses in MgO (i.e. 536 $kgf.mm^{-2}$ and 81 $kgf.mm^{-2}$ for room temperature and 800°C respectively).

The change in the E/Y ratio over the temperature range means that the elastic recovery of the indentations will be different over the temperature range which will lead to overestimates of the ten-micron hardness for the measurements made at the lower temperatures. Accurate measurements of the effect of temperature on the indentation plasticity of MgO and all other stiff solids requires the use of apparatus which can measure the size of indentations under loaded indenters.

Conclusions and Suggested Further Work

The radial displacement models provide sensible interpretations of the data but do not give more insight into the operative processes than the surface directed displacement model which gives H/Y = 3 (approximately). Independent measurement of the flow stresses of MgO at very high hydrostatic pressures for a range of strain rates and imposed strain geometries is required to test the models properly.

Quantitative measurement of the microhardness of MgO has demonstrated that the deformation modes and dominant plasticity mechanisms change significantly over the range 25°C to 800°C and the information obtained is sufficient to suggest further specific lines of research.

If surface directed displacements are favoured above 200°C and if secondary plasticity mechanisms allow general ductility then pile-up should be observed parallel to the facets of the indenter for all orientations of the indenter on the crystal and not just when the diagonals lie along $\langle 010 \rangle$ directions. This will depend upon whether secondary mechanisms are dependent on crystallographic orientation. If secondary slip is dominant then a situation similar to that of single crystal aluminium will occur, where the pile-up is still crystallographically determined (see 2.4.1), but if diffusive processes are important, and the diffusion rates are not orientation dependent (as is likely in cubic materials like MgO - Page (1979)) then the pile-up will always be at the facets of the indenter as in fine grained polycrystalline metals.

The distribution of the pile-ups could be observed qualitatively by scanning electron microscopy (SEM) but quantitative measurement would require stereo microscopy or multiple beam optical interferometric microscopy (Tolansky interferometry).

Transmission electron microscopy (TEM) has been performed on MgO specimens indented at room temperature by Velednitskaya et al.(1975) (see section 2.4.1) and Hockey et al.(1978) and no slip on the $(001)\langle 1\bar{1}0 \rangle$ slip system was observed. Slip on this system has been observed by TEM

on MgO specimens deformed in compression at high temperatures (Langdon and Pask 1970) but no TEM observations have been reported for MgO specimens indented at high temperatures.

In conclusion, there is a great deal of detailed information which can be obtained from careful analysis of microhardness data which is complementary to the information obtainable from microscopy.

4.6 Microhardness of Polycrystalline Magnesia

Indentations in brittle materials are susceptible to the formation of cracks if the load on the indenter (of a particular geometry) is greater than a critical value dependent on the material (Lawn and Evans 1977). For sharp indenters on glasses and relatively tough polycrystals, these cracks are of two types: median cracks, which are perpendicular to the surface, and lateral cracks, which are roughly parallel to the surface. In polycrystalline MgO, the grain boundaries are weak and indentations larger than the grains cannot be measured because catastrophic intergranular cracking occurs, rather than either of the two types of crack described above. However, indentations of roughly the same size, and smaller than, the grains can be formed entirely by plastic flow and are easily measured.

Many ceramics are produced commercially for applications where abrasion and erosion resistance is a design consideration and it is generally realised that, besides indentation fracture characteristics, grain size and surface microplasticity are important materials parameters. However, very few studies (see, for example, section 2.7.2) have been made on the effect of grain size on the formation of plastically formed indentations in ceramics. Therefore this investigation was undertaken to fill this gap, specifically to aid the interpretation of friction and wear measurements made in the ceramics laboratory in Cambridge on silicon carbide and silicon nitride (Adewoye 1976, Sawyer 1979).

During the investigation two objectives were considered:-

1. to develop the most appropriate methods for the investigation of microindentation behaviour and for measuring representative plastic hardness values for polycrystalline ceramics, and
2. to attempt to understand the meaning of 'representative plastic hardness values' for nominally brittle materials.

Much of this thesis is directed towards fulfilling these two objectives and here only the experimental results on the hardness of

polycrystalline MgO will be presented.

The published work on the grain size/microhardness relationships in BeO and Al_2O_3 (which was reviewed in section 2.7.2) shows that in the former material the presence of grain boundaries leads to lower hardness measurements whereas, in Al_2O_3, the increased density of grain boundaries has a strengthening effect (over much of the range of grain sizes). This current study is directed towards finding out whether the behaviour of MgO resembles that of BeO or Al_2O_3 and to establish the reasons for the behaviour, by using both microhardness and indentation size effect on microhardness measurements.

4.6.1 Choice of Material

If the effects of only the crystallographic mismatch at grain boundaries on the flow in semi-brittle materials beneath indenters is to be studied, it is important that the grain boundaries in the test material are 'clean'. Ideally, a single phase, fully dense, semi-brittle ceramic with no grain boundary segregation is required for such an investigation.

Hot-pressed magnesia comes close to fulfilling these requirments. Magnesia powder can be hot pressed to form fully dense (better than 99% of theoretical density) billets without the use of additives (Vasilos and Spriggs 1963, Rice 1971). However, LiF is often added to the MgO powder to reduce the temperatures and pressures necessary for hot pressing and it is found that the LiF can be evaporated from the billet during a later, higher temperature phase of the process: Benecke et al.(1967) used a powder containing 4% LiF but their hot pressed MgO contained only 75 ppm of Li.

No significant difference was found in the current study between the mechanical properties of MgO hot pressed with 4% LiF and MgO aquired from Eastman Kodak, which (it is presumed) was hot pressed without additives.

The problem of porosity, which can weaken grain boundaries or aid plasticity by supplying dislocation sources and sinks (stress concentations and free volume), would appear to be not important in hot-pressed MgO. However, it should be remembered that only 1% porosity (by volume) is equivalent to twenty 0.1 μm diameter pores in every cubic micron of material. The location of the porosity in hot-pressed MgO may also complicate the behaviour; porosity is known to be present in grains in large grain sized specimens, and in grain boundaries in smaller grain sized specimens (Evans and Langdon 1976).

Unfortunately, the properties of ceramics are generally very sensitive to grain boundary structure and segregation so even the very low levels of impurities and porosity in MgO may have significant effects on the mechanical properties. Nevertheless, hot-pressed MgO is close enough to the ideal experimental material for experiments to be worth attempting, if its shortcomings are kept in mind.

Polycrystalline alkali halides, formed by hot-forging of single crystals, are potentially better experimental materials for the study of grain bounday density effects as extremely clean grain boundaries can be produced by this process (Evans and Langdon 1976). However, there is a strong texture in such materials and hence plastic flow across grain boundaries might be easier than in a randomly orientated polycrystal. In addition, those alkali halides which can be hot-forged are those which have low melting points, and therefore creep mechanisms may be active at room temperature.

4.6.2 Specimen Preparation

Hot pressed MgO ('IRTRAN 5 (evaporative grade)) was obtained from Eastman Kodak as 'random chunks' (identified in the current study by the prefix EKM). Cylindrical billets (identified by the prefix MGO) were also hot-pressed from selected MgO powders (with 4% LiF) using a laboratory scale apparatus constructed by Martin (1978) and used for annealing experiments by Jepps(1979). This apparatus consists of an RF inductively heated graphite die with a graphite plunger; the pressure is applied to the charge in the die by admitting compressed nitrogen to a piston which

connected with the graphite plunger via a water cooled brass plattern. The die is supported by water cooled brass fittings, surrounded by a silica glass tube and flushed with argon (to prevent the die burning). The temperature was measured using an optical pyrometer focused on the die and a correction for the emissivity of graphite was applied to the measurement.

The charge was MgO powder, with a bimodal particle size distribution, with the addition of 4% LiF powder.

Specimens were hot-pressed at a pressure of 7.46 MPa for 45 to 75 minutes at about 830°C, followed by 45 to 60 minutes at 1250°C, and some specimens were given a further anneal in air. Different grain sizes were produced by varying the hot pressing times at the two temperatures.

Only one of the 'random chunks' of the Eastman Kodak magnesia was selected for the investigation. It was cut in two, one half (EKM2) was tested after polishing and etching whilst the other (EKM6) was first annealed at between 1300°C and 1400°C in air to increase the grain size.

The specimen preparation treatments are fully described in appendix II.I and appendix II.II gives details of the polishing and etching treatments prior to indentation.

4.6.3 Microscopy

The etchant used to reveal the grain boundaries had a 'relief polishing' effect on the finer grain sized specimens and hence Nomarski interference microscopy was used to produce photographs of the microstructure. These were used to calculate S_v (the grain boundary density) using the Quantimet by the same procedure that was used for the stainless steel specimens. The grain size distribution was also measured and found in all cases to be approximately Gaussian, despite the fact that the original powder had a bimodal distribution of particle sizes. This effect has also been observed by Evans and Langdon (1976).

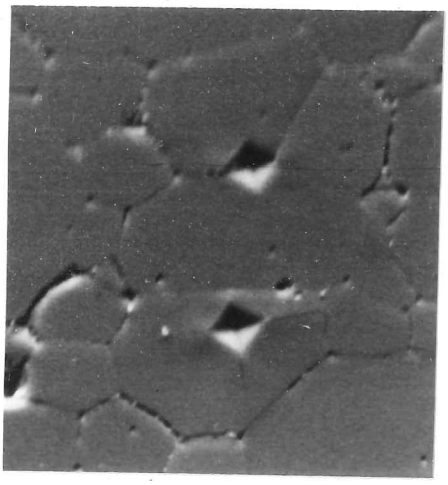

Figure 4/41

MGO9 specimen, two 100 gf. indentations.
30 tilt, 30kV SEM. 450x

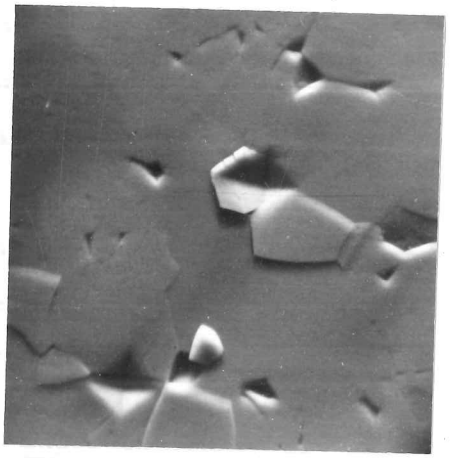

Figure 4/42

EKM2C specimen, two 100 gf. indentations.
30 tilt, 30 kv SEM. 600x
Note the intergranular fracture leading to whole-grain pullout.

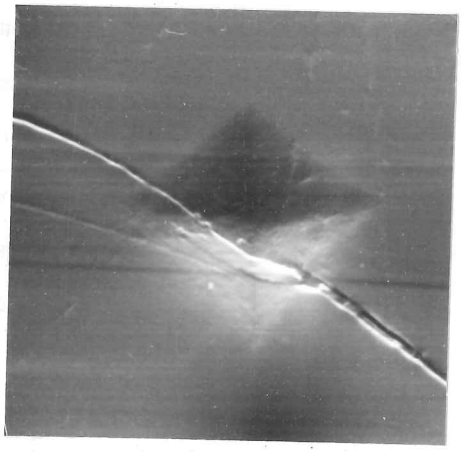

Figure 4/43

EKM6E specimen, one 50 gf. indentation on an etched grain boundary.
30 tilt, 30 kV SEM. 3000x
Note the distortion of the indentation caused by different degrees of elastic recovery in the two grains. The different elastic modulus: yield stress ratio in the two grains is caused by their different crystallographic orientation.

Figures 4/41, 4/42 and 4/43 are scanning electron micrographs of indentations on etched surfaces of the specimens MCO9, EKM2C and EKM6E (see table I in section 4.6.5). No pile-up or sink-in was observed around any of the indentations but the indentations were asymmetrical when, as in figure 4/43, they were made across a grain boundary. The smaller grain sized specimens tended to suffer from spalling of entire grains next to the indentations and this can be seen to be occurring in figure 4/42.

Because the grain boundaries were attacked by the etchant in preference to the dislocations, it proved to be impossible to reveal dislocation etch pit rosettes in the polycrystalline MgO specimens, even in specimen EKM6E which had the largest grain size. Two etchants were used for MgO (see appendix II.II) and both only required a few seconds to etch up grain boundaries whereas the formation of etch pits required more than a minute. Indentations were made on polished specimens and then heavily etched and examined at high magnification (5000×) in the SEM but no traces of etch pits were observed.

4.6.4 Expected Behaviour

A simple plot of hardness against grain boundary density should show whether MgO is 'hardened' or 'softened' by grain boundaries. If it is hardened, then the operative mechanisms are expected to be the same as those in metals, where high back stresses occur in dislocation pile-ups at grain boundaries (in order to initiate slip in the next grain) and work hardening occurs due to secondary slip along grain boundaries (which is required to prevent intergranular fracture (Sargent 1976)). If MgO is softened, then the expected mechanism is the relaxation of the necessity to flow on secondary slip systems beneath the indenter. The differently orientated grains around the indenter, between them, may be able to supply five independent shears on the primary slip system, if the requirement for continuity along the grain boundaries is relaxed. The ease of intergranular cracking in MgO, referred to above, indicates that a softening effect is expected.

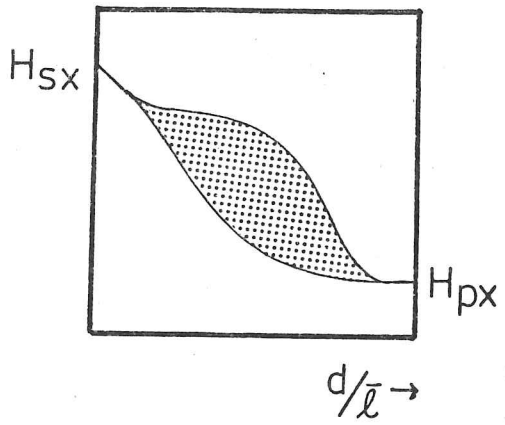

Figure 4/44

This is a diagram of the expected possible variations of hardness with the ratio of the indentation size (d) to the grain size ($\bar{\ell}$). H_{sx} is the hardness of the single crystal and is shown here as being greater than H_{px}, the hardness of the polycrystal. There are different gradients at the points $H = H_{sx}$ and $H = H_{px}$ because the ISE index at the former point is 1.7, and at the latter 2.0.

The shaded area shows the possible range of experimental variation (as in figures 4/25 and 4/26) where the measurements depend on the precise orientation and size of the grains surrounding the indenter.

In stainless steel the work hardening that occurred on indentation obscured the expected hardening effect of the grain boundaries. The effects of work hardening on the measured hardness of MgO at room temperature is unknown, though much work has been performed on the work hardening at elevated temperatures (Routbort 1979).

The behaviour of the ISE index is likely to be complex. If the polycrystalline MgO behaves like metals and alumina then the arguments presented in section 4.4.3 are directly relevant: the presence of grain boundaries is expected to raise the index above 2.0. However, if the grain boundaries are weaker than the bulk (as in BeO and as appears to be the case for MgO) then, using the same arguments, the presence of grain boundaries can be expected to lower the ISE index below 2.0.

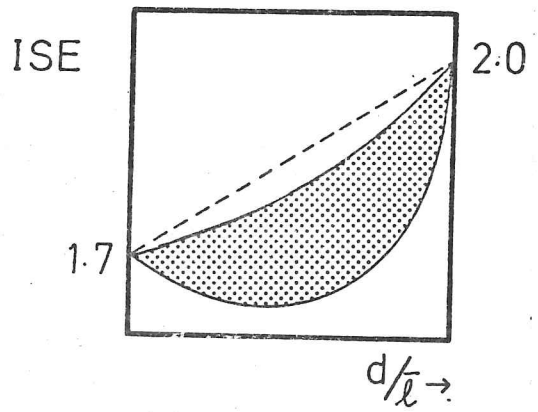

Figure 4/45

This shows a diagram of the expected variation of the ISE index if the hardness follows the behaviour shown in figure 4/44. The ISE index can be calculated from the H and d values using equation 2.5.3d.

Now, the behaviour of single crystal MgO has been studied and at room temperature the ISE index has been found to be 1.7 $\pm$ 0.1 for all orientations of the Vickers indenter on the (001) plane section. Hence the expected effects of the grain boundaries on raising and lowering the ISE index must be taken with reference to the value of 1.7 and not 2.0.

Figures 4/44 and 4/45 show the expected ideal variation of the hardness and ISE index with indentation size (d) and grain size ($\bar{\ell}$) if grain boundaries have a weakening effect (as in beryllia); these figures should be compared with figures 4/25 and 4/26 which describe the expected behaviour for ductile metals with no intrinsic indentation size effect on microhardness. Figure 4/45 is derived from figure 4/44 in the same way that figure 4/26 was derived from figure 4/25, by using equation 2.5.3d :-

$$\text{ISE index} = 2 + \frac{d}{H} \cdot \frac{\partial d}{\partial H} \qquad 2.5.3d$$

The index for high $d/\bar{\ell}$ ratios will be expected to be 2.0 and not 1.7 because if the indentations are much larger than the grains then they will certainly be larger than the critical lengths associated with the fundamental deformation mechanisms, and it is these critical lengths being a significant fraction of the indentation size which is thought to cause the identation size effect in single crystals (see section 4.5).

Figures 4/44 and 4/45 show the ideal expected behaviour, in reality indentations are not measureable for large $d/\bar{\ell}$ ratios because catastrophic cracking occurs.

When indentations are much smaller than the grains (low $d/\bar{\ell}$ ratios) then the behaviour predicted here is for a random dispersion of indentations over the specimen. However, it is possible to place indentations precisely, either close to grain boundaries or close to grain centres, and this has been done for the larger grain sized specimens. Indentations placed in grain centres on a specimen are

are expected to show similar behaviour to that of indentations which have been randomly placed on a specimen of larger grain size as the distance of the indentations from the grain boundaries will be, on average, similar in the two cases. Similarly, the behaviour of indentations placed on grain boundaries can be expected to resemble that of indentations on specimens with smaller grain sizes.(Roberts 1979).

Whether the ISE index decreases or increases with increasing density of grain boundaries will depend on whether the average indentation size is large or small compared with the average grain size in addition to whether alumina-type or beryllia-type behaviour is found. If the behaviour resembles that of beryllia then figure 4/45 shows the expected ISE index relationships. Increasing grain boundary density (S_v) means that the grain size ($\bar{\ell}$) decreases and therefore that the $d/\bar{\ell}$ ratio increases if the indentations are roughly the same size throughout. Clearly, from the figure the index may increase or decrease and no prediction of the behaviour can be made, but if the ISE index is found to be less than 1.7 for any specimen this would indicate that the behaviour would be of the beryllia type. If the behaviour resembles that of alumina then the envelope of possible measurements (the shaded area in the figures) will probably lie above the dotted line in figure 4/45 and the index will always be greater than 1.7.

4.6.5 Results

Table I gives the measured ISE indices, ten-micron hardness values and grain boundary densities of the specimens used in this investigation and the symbols which identify the positioning of the indentations on the specimens.

Figure 4/46 shows the variation of hardness with grain boundary density and it can be seen that there is no significant trend for the ten-micron hardness over the range of grain sizes used. The grain sizes

Section 4.6.5 - Table I

specimen	data set code	$H_{10\mu m}$	ISE index	S_v/mm^{-1}	symbol
MSXA	11	1144 (1018 - 1286)	1.74 (1.71 - 1.78)	0	◇
MSXE	1	952 (790 - 1150)	1.68 (1.62 - 1.73)	0	□
EKM6E	4	1189 (918 - 1540)	1.64 (1.53 - 1.75)	8	○
EKM6E	6	984 (717 - 1351)	1.56 (1.53 - 1.75)	8	▼
MGO9A	11	981 (740 - 1301)	1.57 (1.49 - 1.65)	39 ± 2	■
MGO10C	11	1024 (882 - 1188)	1.65 (1.60 - 1.69)	131 ± 10	■
EKM2C	6	1079 (843 - 1381)	1.54 (1.47 - 1.60)	134 ± 2	○
MGO10A	21	819 (625 - 1073)	1.74 (1.66 - 1.83)	310 ± 10	■
EKM3A	4	931 (663 - 1306)	1.91 (1.80 - 2.03)	709 ± 27	■

Footnotes to Table I

The ranges given here are ± two standard errors, about 95% confidence limits. The error bars on the figures in this section (4.6) are also 95 % confidence limits, the confidence limits on the grain sizes are shown in the figures by the width of the cross-piece on the error bars.

Specimens MGO9A, MGO10C and MGO10A are sometimes referred to as M9A, M10C and M10A for brevity.

◇ single crystal, indentation diagonals parallel to ⟨010⟩

□ single crystal, indentation diagonals parallel to ⟨110⟩

○ indentations placed on grain centres

▼ indentations placed on grain boundaries

■ indentations placed randomly

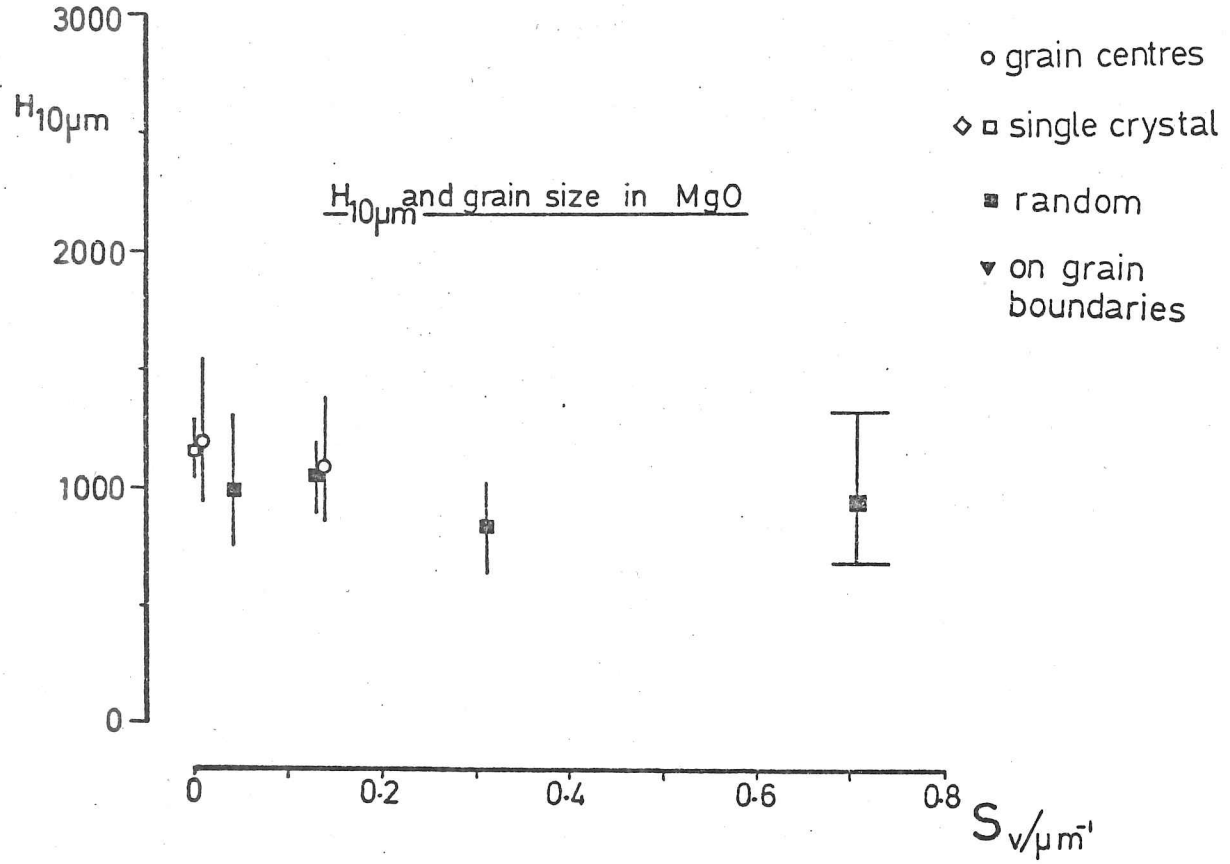

Figure 4/46

(for clarity the sets of results MSXE1 and EKM6E6 have been omitted from this plot as they are almost coincident with MSXA11 and EKM6E4, as can be seen from table I) The same Vickers indenter was used to make all the indentations.

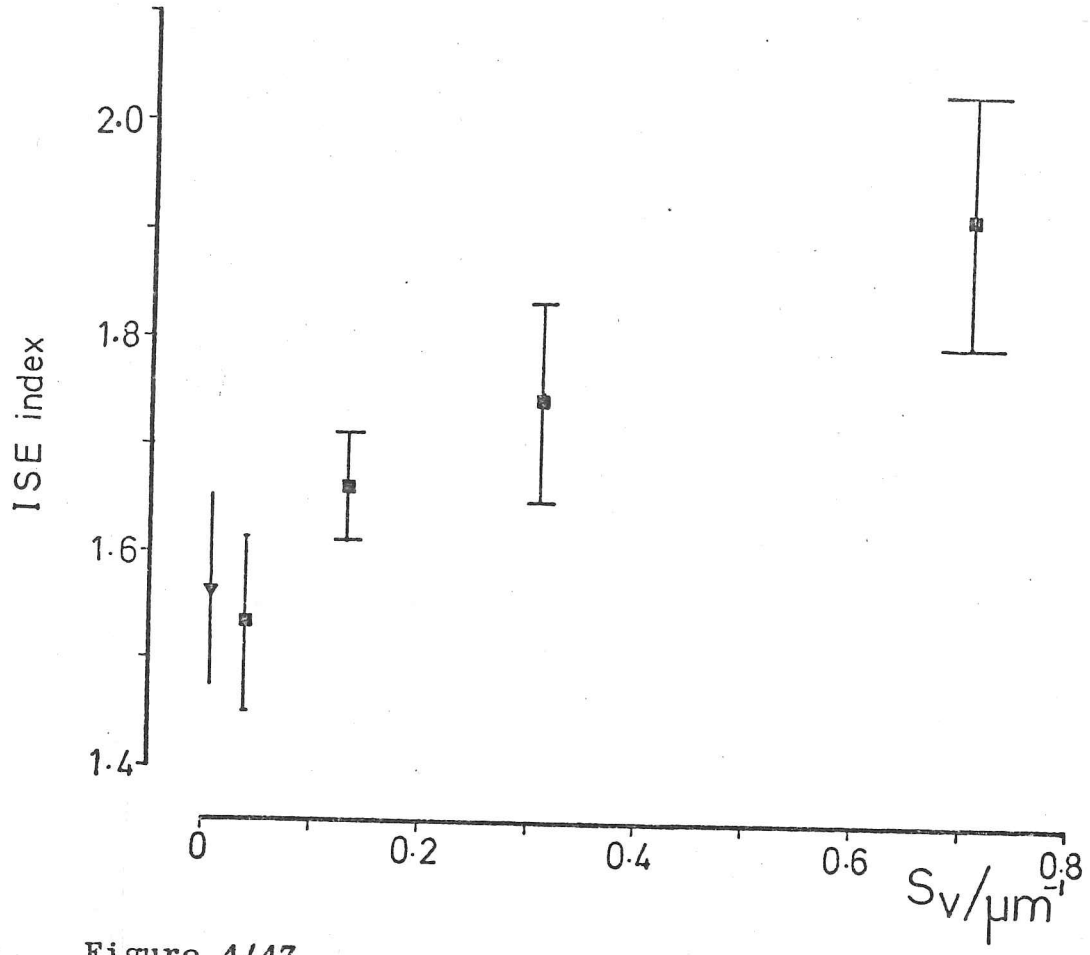

Figure 4/47

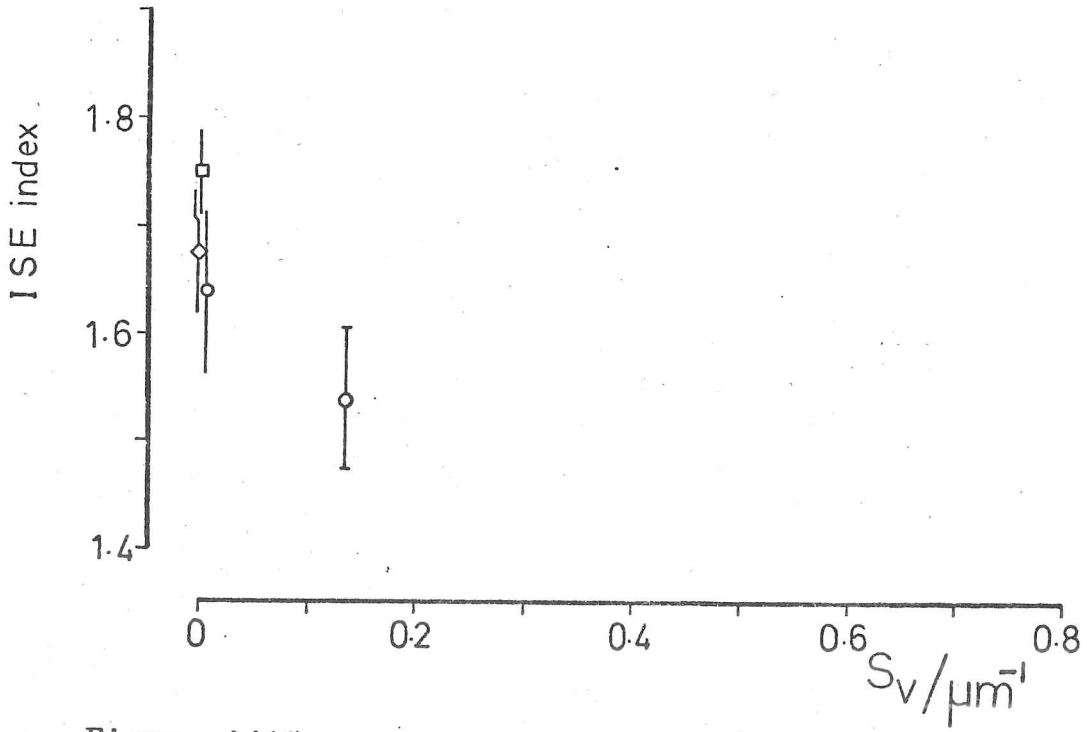

Figure 4/48

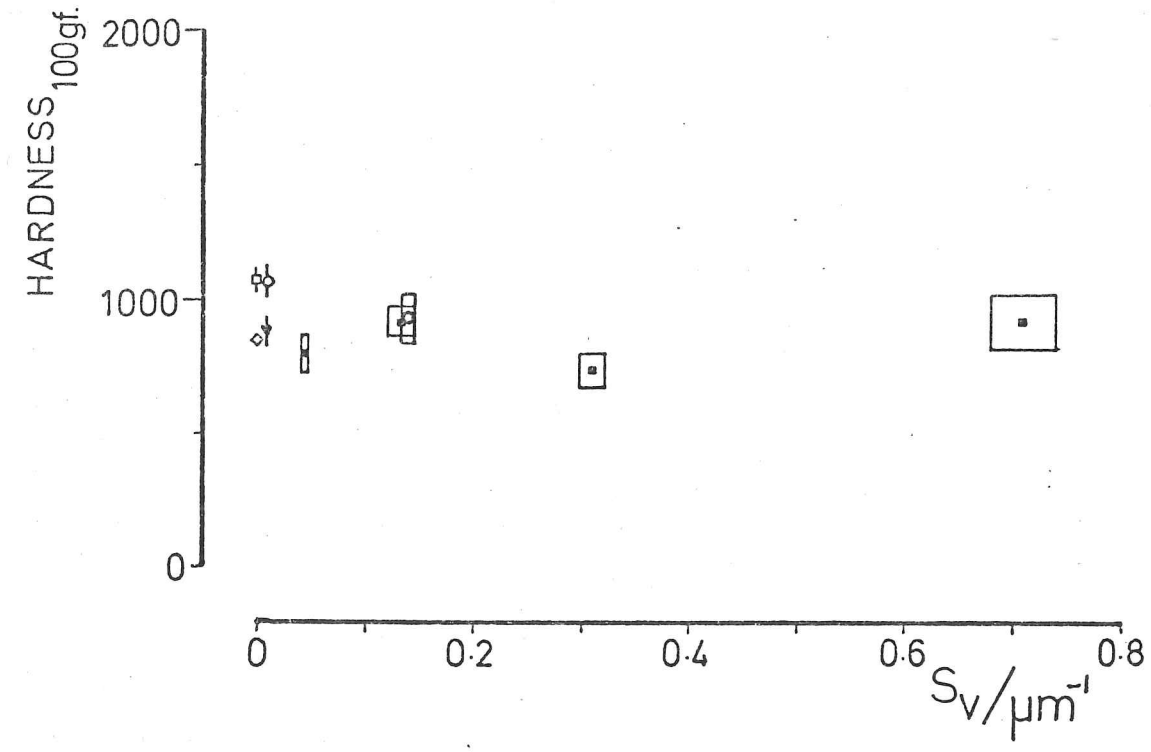

Figure 4/49 Measurements made using a 100 gf. load

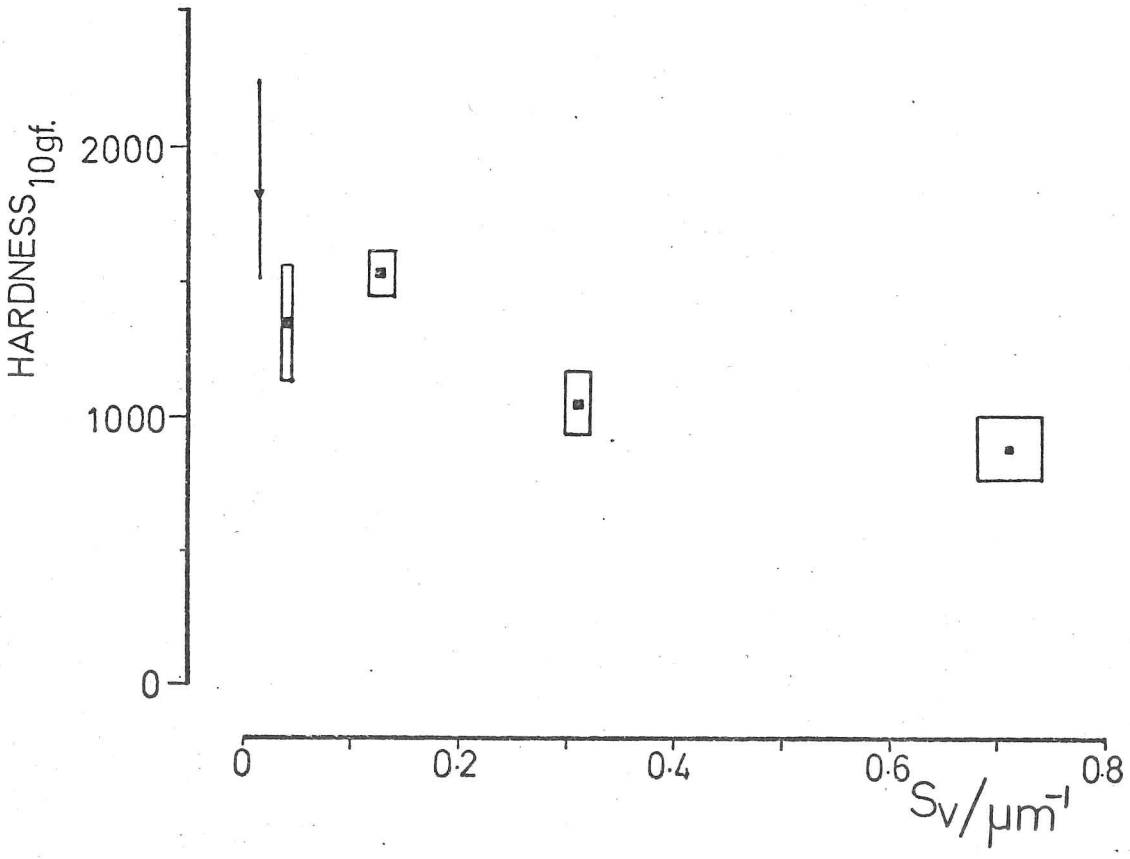

Figure 4/50 Measurements made using a 10 gf. load

($\bar{\ell}$, the mean linear intercept values) range from 0.28 um (EKM3A) to 25 um (EKM6E).

Thus, from the figure, it appears that grain boundaries in MgO neither strengthen nor weaken the solid. However, that is merely the interpretation of the data for ten micron indentations, there is more information on the behaviour contained in the ISE index results.

Figure 4/47 shows that the ISE index increases steadily from about 1.55 to 1.9 with increasing grain boundary density (S_v) for randomly placed indentations. The significant observation here is that for low grain boundary densities the index is less than 1.7. Hence the behaviour resembles that predicted in figure 4/45 where the index decreases from 1.7 and then increases towards 2.0 as $d/\bar{\ell}$ (which is proportional to S_v) increases.

Therefore the conclusion is that MgO resembles BeO in that its grain boundaries tend to be weaker than the bulk but that the effect is much smaller. Figures 4/49 and 4/50 show the hardnesses measured from the indentations made with 100 gf. and 10 gf. loads respectively, and it can be seen that it is the smaller indentations, those made with a load of 10gf., which have been most affected by the different grain sizes. Figure 4/50 shows a trend towards lower hardness measurements for higher S_v which confirms the weakening effect of the grain boundaries deduced from the ISE data.

The hypothesis that the behaviour of indentations made near grain boundaries resembles that of indentations randomly placed in smaller grain sized specimens (Roberts 1979) is supported by the evidence in figure 4/48; the ISE index decreases from 1.7 to 1.55 - the early part of the predicited relationship. Similarly, the data from indentations at grain centres (EKM6E6) would fit the rest of the data if it were displaced towards smaller grain sizes (larger S_v). However, the 10 gf. hardness

for EKM6E6 plotted in figure 4/50 would not fit the data better if it were displaced in a like manner. Nevertheless, overall the agreement with the hypothesis is good.

4.6.6 Conclusions

The data from polycrystalline magnesium oxide has been interpreted using the same model of the effect of grain boundaries on the microhardness that was used to interpret the results from stainless steel. Despite the complexity of the application of the model a self consistent and complete description has been made for all the effects observed in terms of the model alone.

The indentation size effect has been shown to be more sensitive to microstructural effects than microhardness values on their own.

Therefore it is believed by the author that a significant advance has been made in the understanding of microstructural influences on the microhardness of solids and that a mechanical testing technique has been developed which is more sensitive to certain effects than any which has been heretofore available.

4.7 Other Microhardness Results

The microhardness and indentation size effect have been measured for a number of materials, in addition to MgO, LiF and stainless steel, and these measurements and data from other workers are displayed in figure 4/51. All indentations were made using a Vickers indenter and where the load range used was not 10 to 100 gf., this is indicated in the table.

Section 4.7 - Table I

Material	Data set code	
fine grained stainless steel	STU4A3	see section 4.4
MgO ⟨100⟩	MSXA11	see section 4.5.2
MgO ⟨110⟩	MSXE1	
MgO 800°C	MSX8HI	see section 4.5.3
MgO 500°C	MSXI51	
MgO 150°C	MSXd11	
MgO fine grained	EKM3A4	see section 4.6
MgO 500°C (high loads)	MSXB51	made using loads 100 gf. to 1000 gf.
Copper (25 - 300 gf.)	CUP5A	mechanically polished polycrystal, 99.999% pure
Al/Mg/Zn (5 - 100 gf.)	D18A1 & D18A2	underaged and overaged alloy, mechanically polished, supplied by B.Livesy, Dept. Metallurgy, Cambridge.
LiF (5 - 200 gf.)	LIF###	measurements made by the final year undergraduate class (77/78) at Cambridge.
Alumina (25 - 200 gf.)	SAPPH	from Nagai et al.(1976)
Si_3N_4	NN11 & BN11	Norton and Brown Boveri hot pressed Si_3N_4
SiC hot pressed	NC12	Norton hot pressed SiC
SiC (50 - 1000 gf.)	GSC2, GSC3 & GSC17	Single crystal SiC, measurements made by Sawyer (1979).

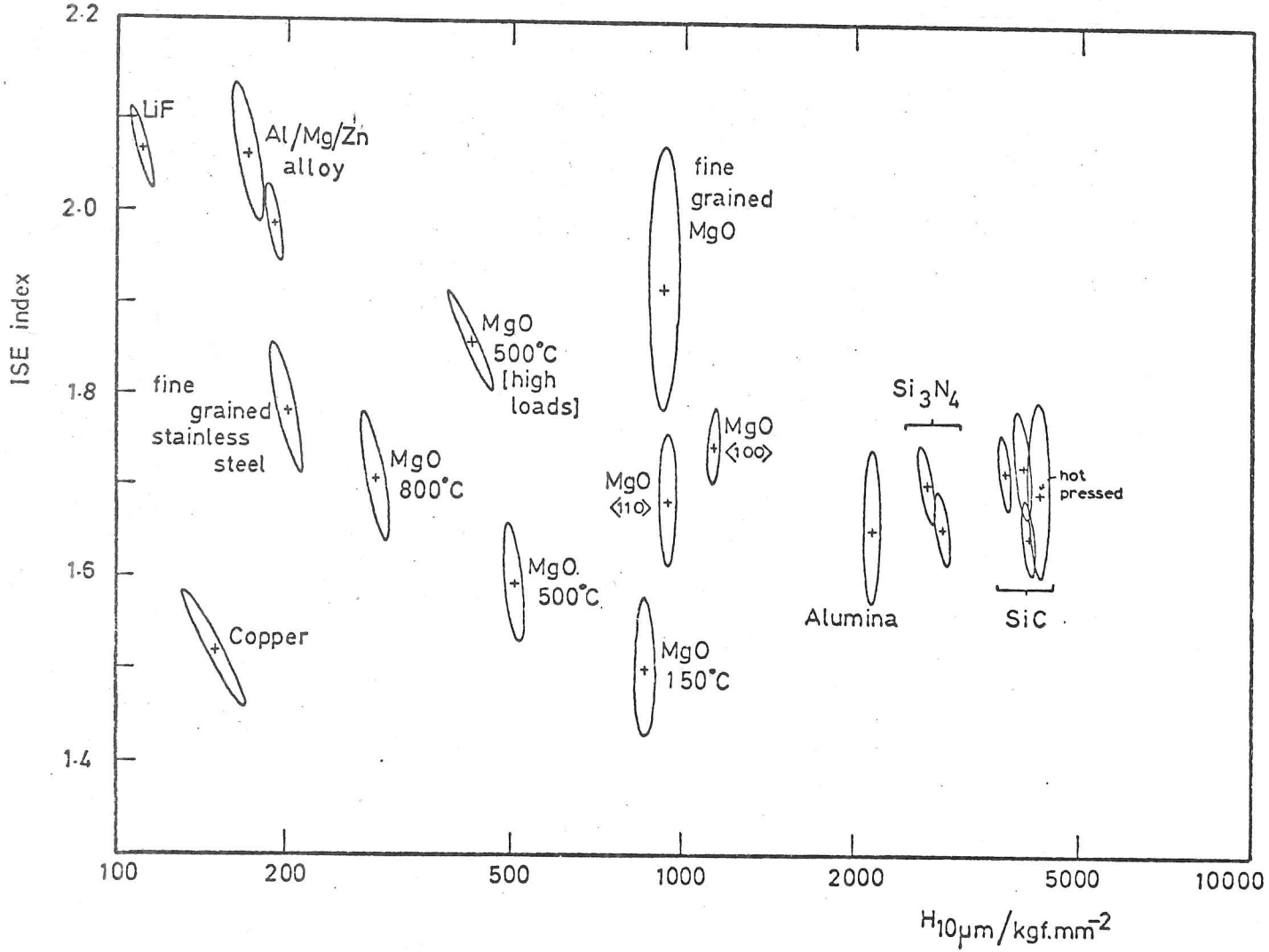
2·2
2·0
1·8
1·6
1·4
ISE index
LiF
Al/Mg/Zn alloy
fine grained stainless steel
MgO 800°C
MgO 500°C [high loads]
MgO 500°C
Copper
fine grained MgO
MgO ⟨100⟩
MgO ⟨110⟩
MgO 150°C
Si3N4
Alumina
hot pressed
SiC
100
200
500
1000
2000
5000
10000
H10μm/kgf.mm-2

Figure 4/51

Observations from the Data

The low ISE index for the copper is probably due to the hardened surface layer caused by the mechanical polishing. Therefore chemically polished surfaces would appear to be essential if the effect of grain size on the indentation behaviour were to be investigated in this material.

Testing of precipitation hardened alloys of different degrees of aging would appear to be an excellent method for further investigating the validity of the defect density model for microstructure/microhardness behaviour. The pilot results reported here for Al/Mg/Zn do not show a great deal of difference between underaged and overaged alloys. This may be due to a hard surface layer (as in copper) or to work hardening on indentation (as in stainless steel, see section 4.4).

The high load measurements from hot MgO (MSXB51) show a different ISE index from the low load measurements (MSXI51). This demonstrates that the ISE index is not constant with respect to indentation size and that the log index empirical function ($L = a.d^n$) is not a good fit for the whole indentation size range. This does not invalidate the use of the ISE index which is defined using the gradient of the hardness/indentation size relationship (see section 3.2.1).

ISE index which is defined using the gradient of the hardness/indentation relationship (see section 3.2.1) as long as the indentation size range, over which the measurements were made, is specified.

The alumina, silicon carbide and silicon nitride all have very similar ISE index values which are also similar to those for MgO single crystals. The cause of the indentation size effect is probably the same as that postulated for MgO: the critical lengths associated with the fundamental plasticity mechanisms may be large enough to be a significant fraction of the size of the indentation. This indicates that similar studies could be made on these materials as have been made on MgO.

4.8 Conclusions from the Experimental Investigations

The main conclusions from the results of the experimental work described above will now be summarised. The conclusions of the whole thesis are summarised in chapter six.

Flow in Metallic Glasses

The object of this investigation was to test the validity of the radial and surface-directed material displacement models on metallic glasses, which appeared to be ideal model materials. However, it became apparent that the shear band mechanism of flow in these materials caused significant deviations from the behaviour predicted by either model. There is an indication that work softening occurs beneath indenters and this may explain the behaviour if it does not occur uniformly throughout the deforming volume.

The existance of the indentation size effect on microhardness in metallic glasses demonstrates that the sizes of the shear bands, or critical lengths associated with shear bands' elastic strain fields, are significant fractions of the size of the deforming volume around an indentation.

"The Defect Density" Model

This model, described in section 2.5.4 and applied to grain boundaries in sections 4.4 and 4.6, describes qualitatively the effects of microstructure on the indentation size effect on microhardness. The results of experiments on stainless steel and magnesia have been explained in terms of the model. However, the results are not clear-cut as the influence of grain size on the hardness of both these materials is small.

Causes of the Indentation Size Effect

In stainless steel and magnesia, single and polycrystals, it has been hypothesised that, as in metallic glasses, the experimental results indicate that the fundamental deformation mechanisms directly

affect the indentation size effect on microhardness. This is thought to be due to critical lengths associated with the movement of dislocations being significant fractions of the sizes of microindentations in these materials. These critical lengths, analagous to the 'coherent regions' of Buckle (1960), could be slip band spacings (see Mott 1956), critical radii for the nucleation of dislocation loops (especially in alkali halide single crystals), dislocation pile-up lengths or some length typical of elastic interactions between dislocations. It should be remembered that a 3.5 micron (diagonal length) Vickers indentation is only 5000 Ångstroms deep.

Elastic Recovery

Orientation dependence of elastic recovery has been shown to dominate the hardness anisotropy measured on materials with orientated microstructures. The different degrees of elastic recovery in different directions, which cause a change in the shape of the indentations with orientation, are thought to be due to different stress levels being attained in different directions under the same indentation. The elastic moduli were shown to be insufficiently anisotropic to have the observed effect in the materials in which the measurements were made. The 'intrinsic' hardness anisotropy, which determines the change in size of the indentations with orientation, was assumed to be small on the basis of indirect evidence. Direct measurement of the intrinsic hardness anisotropy was not possible with the apparatus available.

The observations have direct relevance to isotropic materials with the same flow stress to stiffness ratios as the strong directions in the anisotropic composites. In such isotropic materials, similar degrees of elastic recovery are to be expected as were so immediately obvious in the anisotropic materials. This is not generally realised.

Hardness Anisotropy and the Indentation Size Effect

The study of hardness anisotropies measured on the same material with different indenters has been shown to be able to give information about the stress states beneath indenters which cannot be gained by other methods.

When hardness anisotropy is studied in single crystals in conjunction with measurements of the indentation size effect, it has been shown to be possible to suggest the relative importance of the possible different mechanisms of plastic flow, some of which operate on the atomic scale. These measurements appear to be directly sensitive to the lengths over which the deformation mechanisms operate.

Conclusions

The stress and strain fields beneath indentations have been investigated both directly and by testing the validity of models of the deformation geometry. There are very many problems that remain to be solved before complete solutions become available.

The results of the experiments have shown that there are reasons for believing that microindentation measurements offer a direct method for investigating mechanical properties on scales smaller than the indentations themselves. Deductions have been made here about mechanisms occurring on the scale of some tens of nanometres, these deductions lack confirmation but the fact that they can be made shows that microindentation can at least begin to be applied to such situations.

"The thing I like about Science,
is that one obtains such an enormous return in conjecture,
for such a trifling investment in fact."

Mark Twain

"Making all his nowhere plans

For nobody"

Lennon and McCartney

Chapter 5 - Suggestions for Further Work

It has been established that microhardness tests are apparently easy to perform but the results are hard to interpret. However, some of the problems of interpretation could be avoided if greater control were exercised over the making and measuring of the indentations. Therefore, the possible further lines of research will be described here in conjunction with descriptions of the most appropriate type of microhardness testing machine.

There are broadly three levels of modification that could be made to existing microhardness machines (such as the Leitz 'Miniload'):-

1. a modification for measuring the size of the indentation when the indenter is under full load.
2. a modification for continuously measuring the size of the indentation and the load on the indenter.
3. a new type of apparatus where the rate of loading and the rate of displacement of the indenter could be controlled, in addition to the size of the indentation being continuously measured.

These will now be described separately.

5.1 Measurement of Indentation under Static Load

The procedures which permit the measurement of indentation under load were described in section 2.3.2 and except for the method whereby a diamond pyramid is mounted in the optical system, they all involve time consuming application of surface films to the indenter before each indentation is made. The diamond/lens combination suffers from the difficulty of designing a system for controlling the load applied to the indenter.

It is thought that the easiest, and most widely applicable, method for measuring the size of an indentation whilst the indenter is fully loaded, would be to measure the indentation depth by measuring the displacement of the indenter. Continuous measurement of indenter displacement is almost as

easy as static measurement, and continuous measurement is the subject of the next section.

5.2 Continuous Indentation Measurement under Dynamic Loads

The indenter displacement and displacement rate could be measured by a capacitance bridge (see, for example, Cowling and Bacon (1973)) or with a laser Michaelson interferometer (as used by Barbato et al.(1978)).

If the indenter displacement can be measured continuously, the major problem then is to determine the position of the surface of the test material by an independent method so that the indentation size can be calculated. Berdikov and Babanin (1977) used an alumina sphere probe mounted on a lever arm, but the quality of their measurements (see section 2.3.2) does not inspire confidence in this method.

A number of methods for detecting the time of contact of the indenter with the specimen surface are possible. If conducting or semiconducting specimens are to be tested, then a semiconducting diamond indenter could be used and the conductance between the two measured. This apparatus could also be used for the study of phase transformations beneath indenters in semiconductors, especially where a metallic phase may be formed (Gridneva et al.1972, Trefilov et al.1977, Sawyer et al.1979 and see section 2.2.1).

A transducer for measuring acoustic emission could be mounted on either the specimen or the indenter to detect contact. An indenter mounted system would have the advantage of easy changeover between specimens, whereas a specimen mounted system would enable the acoustic emission to be studied for its intrinsic interest, especially when indentation fracture occurs.

The simplest method for detecting the contact is probably to continuously measure the load on the specimen with a load cell (see section 3.1.3) This has the great advantage that continuous measurement of load and indentation size could be made, and therefore that the change in

pressure (hardness) during indentation would be measureable. The indentation size effect could be measured from just one indentation. However, strain rate effects make it unlikely that dynamic hardness would be the same as the static measurement.

If the indenter is dead loaded and hits the specimen with a set velocity (as in the Leitz 'Miniload') it will decelerate as it penetrates. Thus strain rate effects will be inexorably linked to indentation size effects with this type of apparatus.

If static indentation hardness measurements are required, then a dead loaded machine, equipped with continuous load and indenter displacement measuring devices, would very probably give satisfactory results. Some experiments that could be performed with this type of apparatus will now be described.

Suggested Further Experiments

If indentations can be measured under load, then the 'unrecovered' hardness can be measured and the complicating effects of elastic recovery on the measured hardness can be eliminated. Alternatively, if the unloaded indentation is measured optically, the elastic recovery can be measured.

In many materials elastic recovery is not thought to have significant effects on the measured hardness, however, direct experimental evidence for this assumption is sparse. Therefore, whilst many of the experiments described below could be attempted with currently available apparatus, the interpretation of the results would not be as easy.

With an indenter displacement measuring machine, the intrinsic hardness anisotropy could be measured for the materials with orientated micro -structures described in section 4.2. The deductions that have been made about the intrinsic hardness anisotropy could be verified (or refuted) directly. The elastic recovery in different direction could be measured accurately and better estimates could be made of the stress levels attained

in different directions in the surface. Hence the stress fields of Vickers and Knoop indenters (and others) could be investigated with more confidence.

Orientated microstructures are an extreme example of two phase texture in a material. If elastic recovery could be measured then the effects of texture due to crystallographic orientation of grains in a single phase material could be measured. Quantitative results could be obtained instead of qualitative estimates (Lee 1973).

The hardness anisotropy due to plastic anisotropy has been studied, whereas the hardness anisotropy due to elastic anisotropy has not. If elastically anisotropic composites were indented, the hypothesis that the elastic recovery is proportional to the Y/E ratio could be tested.

The degree of elastic recovery that occurs in metallic glasses is unknown. It is presumed to be small because surface pile-ups are observed. However, it has been shown that yielding beneath indenters is not understood in metallic glasses, therefore elastic recovery due to the compressed hinterland may be significant. It has been argued that no shape change on elastic recovery would be expected in these materials, and the recovery may be very large. 'Unrecovered' hardness measurements would be invaluable in studying the anomalous behaviour of metallic glasses.

Measurement of the indentation size, independent of the size and shape of surface pile-ups, would facilitate the correlation of pile-up height with the stress benaeth the indenter. Buckle (1960) found an indentation size effect on the relative heights of pile-ups, which may be due to an indentation size effect on the hardness.

The measurement of surface pile-ups on MgO as a function of temperature would give information about the changing ductility and the role of secondary plasticity mechanisms as the material changed from being semi-brittle to being fully ductile. Measurement of pile-ups is probably most reliably made by Tolansky multiple beam interferometry. Stereo scanning electron microscopy could be used, but pile-ups are fairly featureless, which makes quantitative stereomicroscopy difficult.

If a technique for accurately measuring pile-ups could be developed, it would be useful to measure pile-ups around indentations in isotropic, fully work-hardened (i.e. approximately rigid-plastic) materials. The size of the pile-up could be compared with that surrounding indentation in work-hardening alloys. It is presumed that the shape of the pile-up would give information on the strain distribution beneath the indenter and that they may be similar for material which obey Tabor's relationship (H/Y=C), whether for the yield stress or the 8% strain flow stress.

If the size of the pile-up in fully plastic materials were known, the size of the pile-up could be used as an indication of the relative proportions of material displaced radially and towards the surface.

It was postulated in section 2.1 that the representative strain may be different from 8% if the strain distribution were different from that around indentations in work-hardening alloys. Study of the pile-up could be performed in conjunction with flow stress and hardness measurements on materials which do not obey Tabor's relationship.

In section 2.6 it was found that the ratios H/Y and k_h/k_e (the ratio of the 'Hall-Petch type' grain boundary hardening parameters for flow and for hardness tests) were not the same and it was postulated that $k_h/k_{e+8\%}$ might be a better ratio to measure. Such an investigation would be experimentally straightforward but would perhaps take a long time to perform for a range of materials.

The 'sink-in' phenomenon, where a work-hardened cap of material is pressed into the test surface (see section 2.1.3) may be investigated by the same microscopical techniques that could be used to study the pile-up. If the surface topography can be measured then it could be used to check the accuracy of three dimensional finite element analyses (FEA) of indentation plasticity. A program of research using FEA could also investigate 'how much' elasticity is required to permit plastic indentation in materials with restricted capacity for slip (see section 2.3.2).

The study of the effect of microstructure on the indentation size effect on microhardness could be continued in order to more rigorously test the defect density model which was used to explain the results from MgO and stainless steel. For ductile metals, an alloy is required in which the work-hardening effect on indentation is small compared with the hardening effect of the microstucture. If grain boundaries are used to harden the alloy, finding a good experimental material is difficult because the hardening effect of grain boundaries is often dependent on the work--hardening rate. A solution treated, low alloy ferritic steel, in which there is heavy segregation at the grain boundaries, might be profitably studied.

To test the "defect density" theory (see section 2.5.4) of micro--structure/ISE relationships in semi-brittle materials, the clean grain boundaries formed in hot forged single crystals of alkali halides could be used, but the effects of texture would also have to be studied in such materials.

It is clear that the study of the defect density model using grain boundaries to harden the test material is subject to many problems. The use of precipitation hardened alloys, or metals hardened by dispersed oxide particles, might produce results which are more easily interpreted.

When the sizes of indentations under load can be measured, then the quantitative measurement of the effects of the activation volumes of mechanisms of plastic flow on the indentation size effect on microhardness could be measured. This study would perhaps be simplest if a range of polymers were used as the experimental materials. Mechanisms with very different activation volumes can be activated at room temperature by the correct choice of polymer. Unfortunately, polymers are very sensitive to strain rate effects, therefore a microhardness machine in which the rate of indenter displacement was controlled would be most suited to this investigation. This is described in the next section.

5.3 Displacement Controlled Microindentation

In section 3.1.3 pilot experiments were reported on the subject of using mechanical testing machines to make indentations. The vibration and backlash problems probably exclude such machines for microhardness measurements. A loading system based on elastically expanded metal bellows, as used by Barbato et al.(1978) would be more appropriate.

For the accurate measurement of the moment of indenter: specimen contact a sensitive load cell is required which is also extremely stiff. A pietzoelectric quartz load cell may be sensitive enough. However, an alternative method is to mount the specimen on an elastically supported stage and to measure the displacement of both the indenter and the stage (see figure 5/1). Such a machine could operate with a range of indentation rates. Feedback mechanisms would enable indentations to be made using either constant displacement rate or constant loading rate.

A displacement controlled machine would enable indentations to be made in alkali halide single crystals at constant strain rates. Thus the moisture controlled softening effects for slow indentation rates (anomalous indentation creep) could be separated from the hardening effects (postulated in section 4.5.1) for fast indentation. Etch pit rosettes could be measured around indentations made using a range of strain rates and hence relationships between strain rate and dislocation velocity could be investigated. In addition, slow strain rate experiments using perfectly dry crystals would give information about secondary plasticity mechansisms (which may include creep mechanisms) occurring directly beneath indenters.

In section 2.3.3 it was deduced from the results of Boyarskaya et al.(1979) and Brookes et al.(1975) that the strain rates below Vickers and Knoop indenters were sufficiently different for Vickers indenters not to show up the inversion of hardness anisotropy with increasing homologous temperature. When the strain rate can be controlled independently, the phenomenon could be investigated systematically.

Further Refinements

The apparatus as described would be rather difficult to adapt for controlled environment, high temperature testing, but since the masses of the indenter and the stage do not affect the measurements (except at very high velocities) small heaters or cooling coils could be mounted directly on both. A temperature range of plus or minus one to two hundred degrees centigrade from room temperature could be achieved by this means.

Since the process of indentation and displacement would be under electronic control, a sophisticated digital control system could also operate stepping motors on the specimen stage and make an entire programmed series of measurements, sending the results to a computer for statistical analysis and final presentation of the data on a graph plotter.

If the displacement rate were changed continuously during indentation, the apparatus could simulate the behaviour of a dead loaded machine (if the deceleration rates of the indenter had previously been measured). Thus the characteristics of these simpler machines could be investigated in terms of the mechanical responses of specimens. Hence, measurements made on these machines would be easier to interpret in the future.

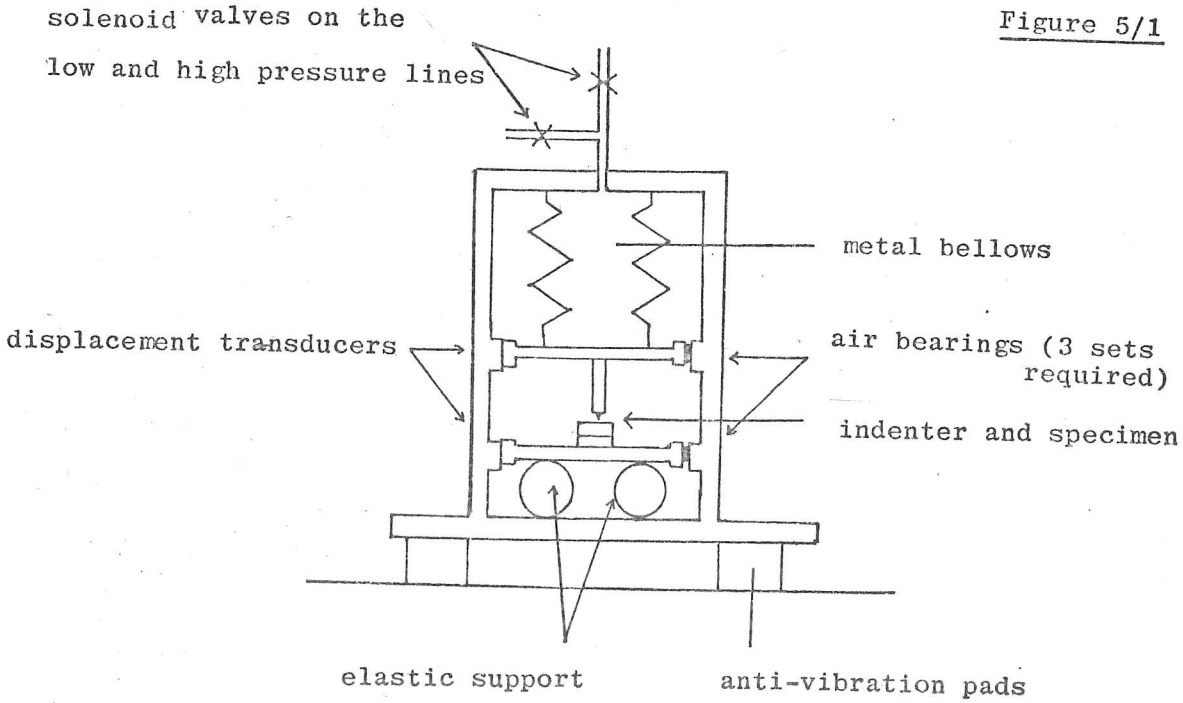

Figure 5/1

5.4 Further Microscopical Methods

Different methods of making indentations, i.e. using constant or varying displacement rates, will change the distribution of strain and the proportions of the different plasticity mechanisms beneath indenters. However, the occurrance of certain types of mechanism (e.g. $\{100\}\langle 1\bar{1}0\rangle$ slip in MgO) could be investigated, using scanning and transmission electron microscopy, in specimens indented using any microhardness machine.

Velednitskaya et al.(1975) used cathodoluminescence to look for point defects round indentations in MgO. This study could be extended to examine indentations made in alkali halides over a range of homologous temperatures and be correlated with the rosette size - indentation size relationships discussed in section 2.4.1. The distribution of dislocations close to the indentation point (i.e. not in the rays) might reveal $\{100\}\langle 1\bar{1}0\rangle$ slip beneath Knoop indenters after indentation at long dwell times in alkali halides, or alternatively, after indentation at fairly low homologous temperatures (probably 0.1 to 0.2 T_m). Transmission electron microscopy has the potential for directly examining any debris left after the operation of unusual secondary plasticity mechanisms, such as block shear, densification/phase change or crowdionic diffusion. It is very probable that the phase change on indentation occurs in silicon, and since this material has been extensively studied by TEM it would appear to be ideal for the study of indentation plasticity involving fleeting phase changes.

Conclusion

For immediate applicability, the most useful development in the use of microhardness as a research tool would be the fitting of existing microhardness machines with load cells and displacement transducers. Elastic recovery would cease to be a problem and a beginning could be made on the study of strain rate effects.

"There was a door to which I found no key
There was a veil past which I could not see"

Edward Fitzgerald

Chapter 6 - Conclusions

This chapter consists of a list of conclusions and a final summing-up.

1. The SMJF and Gerk models of radial displacements have been presented in graphical form and the SMJF model has been shown to predict a change-over from radial to surface directed displacements at the point E/Y = 114 (see section 2.1).

2. There is a great deal of experimental data, including that from metallic glasses, which does not fit any of the models of indentation plasticity. Much of this disagreement may be due to inadequate attention to the problem of elastic recovery. Detailed and careful work using improved apparatus is required to test the validity of the models of material displacement. Some experiments involving measurement of pile-ups have been described to elucidate the relative importance of the two modes of deformation. Characterisation of materials' flow under conditions of high hydrostatic pressure and high strain rates will be required for full understanding of the mechanisms involved.

3. The phase change pressure in sphalerite crystals has been shown to be almost always higher than the indentation pressure (hardness) and whilst phase changes may occur fleetingly in these crystals (especially CdS, InSb, Ge, Si and SiC), this densification does not appear to dominate the other mechanisms of plasticity.

4. If densification occurs, or plasticity mechanisms are significantly affected by hydrostatic pressure, the models of indentation plasticity become less relevant. For metallic glasses the shear band mechanism of flow means that the behaviour is not described by any of the models, whereas for single crystals of MgO the models appear to be valid approx-imations.

5. The published data on the elastic recovery of SiC and other ceramics is unreliable (see section 2.3.2).

6. The cylindrically symmetric model of hardness anisotropy has less general applicability than the ERSS model.

7. The ERSS model is capable of many extensions and revisions, but a great deal of more detailed and more accurate experimental data is required before such extensions can usefully be made.

8. Comparative hardness anisotropy measurements using different indenters has been shown to give information about the stress fields beneath the indenters.

9. The study of hardness anisotropy together with the ISE in single crystals has been shown to be able to give information about the plasticity mechanisms on very fine scales.

10. A simple model of surface hardening effects on the ISE indicates that 50% hardening in the top micron of the surface of MgO would explain the indentation size effect. However, experiments in controlled environments indicate that the hardness is not strongly environment-sensitive and therefore that the ISE is probably caused by the finite sizes of the fundamental plasticity mechanisms.

11. The ISE in stainless steel and metallic glasses is thought to be caused by the finite sizes of dislocations' and shear bands' critical interaction lengths, as in MgO.

12. Surface Layer Models may be used to model the effect of varying densities of defects on the ISE but only in the continuum range, where the defect spacing is much smaller than the indentation.

13. A semi-quantitative model has been devised for the effects of different densities of defects (for all densities) on the ISE and applied to experimental results from MgO and stainless steel.

14. Complex techniques have been shown to be necessary to obtain reliable microhardness measurements which can be interpreted in terms of plasticity mechanisms if currently available microhardness machines are to be used.

15. A short design study has been made, including pilot experiments, on the development of more appropriate microhardness testing machines. Some possible experiments using these machines to study detailed plasticity mechanisms in specific materials have been suggested.

Microhardness tests are currently most used for making semi-quantitative comparisons between materials and for such purposes the technique as it is used at present is entirely adequate.

It has been shown here that microindentation can be an extremely versatile research tool with unique capabilities for studying fundamental mechanical properties of solids. For such applications, great care must be taken to use the most appropriate experimental technique and the interpretation of the results is rarely straightforward. This thesis describes procedures which can make the technique easier to use and it highlights several areas where the application of the technique is not well understood, but where, with further research, it could be extremely useful.

REFERENCES

Adewoye O.O.
1976 Ph.D. Thesis, University of Cambridge

Adewoye O.O. Page T.F.
1976 J. Mater. Sci. 11 981

Alexander D.G. Carlson O.N.
1969 Trans. Met. Soc. AIME 245 2592

Argon A.S.
1979 Acta Met. 27 47-58

Arlt G. Schodder G.R.
1965 J. Acoust. Soc. Am. 37 384

Armstrong R.W. Jindal P.L.
1968 Trans. Met. Soc. AIME 242 2513

Armstrong R.W. Raghuram A.C.
1973 'The Science of Hardness Testing and its Research Applications', (1973) American Society for Metals, Metals Park, Ohio, USA. pp 175-185

Armstrong R.W. Raymond E.L. Vandervoort R.R.
1963 J. Am. Ceram. Soc. 53 529

Armstrong R.W. Wu C.Cu.
1978 J. Am. Ceram. Soc. 61 102-106

Arnell R.D.
1974 J. Phys. D 7 1225

Ashby M.F.
1970 Phil. Mag. 21 399

Atkins A.G. Tabor D.
1965 J. Mech. Phys. Sol. 13 149-164

Auten T.A. Radcliffe S.V.
1976 J. Am. Ceram. Soc. 59 249-258

Babyak W.J. Rhines F.N.
1960 Trans. Met. Soc. AIME 218 21

Balta-Calleja F.J. Bassett D.C.
1977 J. Polym. Sci.: Polymer Symp. 58 157-167

Barbato von G. Desogus S. Levi R.
1978 V.D.I. Berichte Nr 308

Bartenev G.M. Razumovskaya I.V. Sanditov D.S.
1969 J. Non Cryst. Sol. 1 388-398

Benecke M.W. Olson N.E. Pask J.A.
1967 J. Am. Ceram. Soc. 50 365-368

Berdikov V.F. Babanin A.V.
1977 Ind. Lab. 43 866

Blau P.J.
1977 Internal Test Report: RF 4432-A1, Dept. Metallugical Engineering, Ohio State University, USA.

Boyarskaya Yu.S. Grabko D.Z.
1973 Kristall und Technik 8 1367

Boyarskaya Yu.S. Grabko D.Z. Purich E.I.
1979 J. Mater. Sci. 14 939

Bradt R.C.
1978 Personal communication, Penn. State University, USA.

Braunovic M. Haworth C.W.
1974 J. Mater. Sci. 9 809

Brookes C.A. O'Neill J.B. Redfern B.A.W.
1971 Proc. Roy. Soc. (Lond.) A322 73

Brookes C.A. Burnand R.P. Morgan J.E.
1975 J. Mater. Sci. 10 2171

Brookes C.A. Moxley B.
1975b J. Phys. E 8 456-460

Brookes C.A.
1979 Personal communication, Dept. Engineering Science, Exeter, UK.

Brown D.J.
1978 Unpublished work, final year undergraduate project: 'The Growth of Large Grains in Stainless Steel and the Influence of Grain Boundaries on Hardness', Dept. Metallurgy and Materials Science, Cambridge, UK.

Buckle H.
1960 'L'Essai de Microdurete et ses Applications', Publications Scientifiques et Techniques du Ministere de L'Air

No. N.T.90

Buckle H.
1973 'The Science of Hardness Testing and its Research Applications', (1973) American Society for Metals, Metals Park, Ohio, USA. pp 453-485

Burke R. Auckland J.
1978 Unpublished work, Dept. Metallurgy and Materials Science, Cambridge, UK.

Burnand R.P.
1974 Ph.D. Thesis, University of Exeter.

Cahoon J.P. Broughton W.H. Kutzak A.R.
1971 Met. Trans. 2 1979-1983

Calder R.W. Armstrong R.W.
1973 J. Mater. Sci. 12 59

Carnahan R.D.
1968 J. Am. Ceram. Soc. 51 223

Chadwick G.A.
1976 Acta Met. 24 1137-1146

Chen C.C. Hendrickson A.A.
1973 'The Science of Hardness Testing and its Research Applications', (1973) American Society for Metals, Metals Park, Ohio, USA. 274-290

Chen H.S. Polk D.E.
1974 J. Non Cryst. Sol. 15 174

Chen H.S. Krause J.T. Coleman E.
1975 J. Non Cryst. Sol. 18 157-171

Chen H.S. Lo C.C.
1976 'Rapidly Quenched Metals' 2nd. Int. Conf., M.I.T. Press, Cambridge, Mass. USA. (ed. Grant & Giessen) vol. 1 413-424

Chin G.Y. Van Uitert L.G. Green M.L. Zydzik G.
1972 Scripta Met. 6 503

Chin G.Y. Green M.L. Van Uitert L.G. Hargreaves W.A.
1973 J. Mater. Sci. 8 1421

Chou C-P. Davis L.A. Narasimhan M.C.
1977 Scripta Met. 11 417-423

Copley S.M. Pask J.A.
1965 J. Am. Ceram. Soc. 48 139-146

Cottrell A.
1975 'An Introduction to Metallurgy' 2nd. edition, Edward Arnold (Publishers) Ltd., London, UK.

Crocker A.J. Wilson M.
1978 J. Mater. Sci. 13 833

Cowling M.J. Bacon D.J.
1973 J. Mater. Sci. 8 1355-1358

Crow E.L. Davis F.A. Maxfield M.W.
1960 'Statistics Manual', Dover Publications Inc., New York, USA. p84

Daniels F.W. Dunn C.G.
1949 Trans. ASM 41 419

Davidge R.W.
1967 J. Mater. Sci. 2 339

Davis L.A.
1975 Scripta Met. 9 431-436

Davis L.A.
1976 'Rapidly Quenched Metals' 2nd. Int. Conf., M.I.T. Press, Cambridge, Mass. USA. (ed. Grant & Giessen) vol. I 369-391

Davis L.A. Ray R. Chou C.-P. O'Handley R.
1976a Scripta Met. 10 541-546

Davis L.A. Chou C.-P. Tanner L.E. Ray R.
1976b Scripta Met. 10 937-940

Day R.B. Stokes R.J.
1964 J. Am. Ceram. Soc. 47 493-503

Day R.B. Stokes R.J.
1966 J. Am. Ceram. Soc. 49 345-354

Degtyarev V.I. Lagveshkin V.Yu.
1977 Ind. Lab. 43 1139

Donovan P.
1979 Personal communication, Dept. Metallurgy and Materials Science, Cambridge, UK.

Douthwaite R.M.
1970 J. Iron and Steel Institute 208 265

Dugdale D.S.
1953 J. Mech. Phys. Sol. 2 265

Dugdale D.S.
1955 J. Mech. Phys. Sol. 3 197-205, 206-211

Dugdale D.S.
1958 J. Mech. Phys. Sol. 6 85-91

Dunegan H.C.
1961 'Mechanical Properties of Engineering Ceramics' (Proc. Conf. Raleigh, North Carolina, USA; March 1960) Interscience Publishers, ed. W.W.Kriegel and H.Palmour III. pp 521-537

Edington J.W. Rowcliffe D.J. Henshall J.L.
1975 Powder Met. Int. 7 82-96

Evans A.G. Langdon T.G.
1976 Prog. Materials Science 21 : 'Structural Ceramics'

Evans A.G. Wilshaw T.R.
1977 J. Mater. Sci. 12 97

Farrell K. Loh B.T.M.
1971 J. Iron and Steel Institute 209 915

Fischmeister H.F.
1975 Powder Met. Int. 7 178

Francis H.A.
1976 Trans. Met. Soc. AIME 98 272-280

Frohlich F. Grau P. Grellman W.
1977 Phys. Stat. Sol. A42 79

Gane N.
1970 Proc. Roy. Soc. (Lond.) A317 367-391

Gane N. Cox J.M.
1970 Phil. Mag. 22 881

Garber R.I. Mikhailovskii V.M.
1972 Sov. Phys. - Solid State 14 1342

Garbato L. Rucci A.
1977 Phil. Mag. 35 1681

Garfinkle M Garlick R.G.
1968 Trans. Met. Soc. AIME 242 809

Gay P.
1972 'The Crystalline State', Oliver and Boyd, Edinburgh. p73

Gerk A.P.
1975 Phil. Mag. 32 355

Gerk A.P.
1976 J. Phys. D 9 L179-L181 and personal communication, Cavendish Laboratory, Cambridge.

Gerk A.P.
1977 J. Mater. Sci. 12 735-738

Gibbs M.R.J. Evetts J.E. Shah N.J.
1979 Proc. Joint INTERMAG-MMM Conf., New York, USA. To be published in J. Appl. Phys.

Gilman J.J.
1959 Acta Met. 7 608

Gilman J.J.
1973 'The Science of Hardness Testing and its Research Applications', (1973) American Society for Metals, Metals Park, Ohio, USA. p54

Gilman J.J.
1975a J. Appl. Phys. 46 5110

Gilman J.J.
1975b J. Appl. Phys. 46 1625-1629

Greer A.L.
1976 Unpublished work, Dept. Metallurgy and Materials Science, Cambridge, UK.

Greer A.L. Leake J.A.
1979 J. Non Cryst. Sol. (in press)

Grigoriev I.V. et al.
1977 Poroshkovaya Metallyargiya 8 72

Gridneva I.V. Milman Yu.V. Trefilov V.I.
1972 Phys. Stat. Sol. A14 177-182

Groves G.W. Kelly A.
1963 Phil. Mag. 8 877

Haason P.
1974 J. de Physique: Dissociation des Dislocations, Beaune, Colloque 7 167

Hadnagy T.D. Krenisky D.J. Ast D.G. Li C.-Y.
1978 Scripta Met. 12 45

Hagan J.T. Swain M.V. Field J.E.
1977 Phys. Chem. Glasses 18 101

Haglund B.O.
1970 Prakt. Metall. 7 173

Hannink R.H.J. Kohlstedt D.L. Murray M.J.
1972 Proc. Roy. Soc. (Lond.) A326 409

Hannink R.H.J. Murray M.J.
1972 Acta Met. 20 123

Hanson K.L.
1979 J. Am. Ceram. Soc. 27 515-521

Healey T. Brown A.F. Speight M.V.
1973 in 'Physical Metallurgy of Reactor Fuel Elements', The Metals Society, London, UK. p386

Hirst W. Howse M.G.J.W.
1969 Proc. Roy. Soc. (Lond.) A311 429

Hirth J.P.
1977 J. Mater. Sci. 12 2540-2542

Hockey B.J.
1973 'The Science of Hardness Testing and its Research Applications', (1973) American Society for Metals, Metals Park, Ohio, USA. p21

Hockey B.J. Lawn B.R.
1975 J. Mater. Sci. 10 1275-1284

Hockey B.J. Wiederhorn S.M. Johnson H.
1978 'Fracture Mechanics of Ceramics', vol. 3 (ed. R.C.Bradt, B.P.H.Hasselmann, and F.F.Lange) Plenum Publishing Corp. p379

Holm E. Holm K. Shobert E.I.
1949 J. Appl. Phys. 20 319-327

Honeycombe R.W.K.
1968 'The Plastic Deformation of Metals', Edward Arnold (Publishers) Ltd., London (1968) p238

Hopkins J.R. Miller J.A. Martin J.J.
1973 Phys. Stat. Sol. A19 591

Howell P.R. Jones A.R. Ralph B.
1975 J. Mater. Sci. 10 1351

Hu S.M.
1975 J. Appl. Phys. 46 1470

Hulse C.O. Copley S.M. Pask J.A.
1964 J. Am. Ceram. Soc. 46 317-323

Imaoka M. Yasui I.
1976 J. Non Cryst. Sol. 22 315-329

Jepps N.W.
1979 Ph.D. Thesis (in preparation) Dept. Metallurgy and Materials Science, Cambridge, UK.

Jepps N.W. Page T.F.
1979 J. Microscopy (in press)

Jindal P.C. Armstrong R.W.
1969 Trans. Met. Soc. AIME 245 623

Jindal P.C. Gurland J.
1974 Met. Trans. 5 1649

Johnson K.L.
1963 Nature 199 1282

Johnson K.L.
1968 'Engineering Plasticity', C.U.P. p341

Johnson K.L.
1970 J. Mech. Phys. Sol. 18 115

Johnson K.L. Feltner C.E.
1970 Met. Trans. 1 1161

Johnson W.C.
1976 Met. Trans. 8A 1413

Joy D.C.
1975 J. Microscopy 103 1

Keh A.S. Li J.C.M. Chou Y.T.
1959 Acta Met. 7 694-696

Keh A.S.
1960 J. Appl. Phys. 31 1538-1545

Kelly A.
1966 'Strong Solids', Clarendon Press, Oxford.

Kessler J.B. Ritter J.E. Rice R.W.
1974 'Surfaces and Interfaces of Glasses and Ceramics', Plenum, New York. pp 529-544

Kieffer A.R. Ettmeyer P. Gugel E. Schmidt A.
1969 Mat. Res. Bull. 4 153

Kumashiro Y. Itoh A. Kinoshita T. Sobajina M.
1977 J. Mater. Sci. 12 595

Langdon T.G. Pask J.A.
1970 in 'High Temperature Refractory Oxides' (ed. A.Alper), Academic Press

Latanision R.M.
1977 in 'Surface Effects in Crystal Plasticity' ed. R.M. Latanision and J.J. Fourie, NATO Advanced Study Institute Series E (Applied Science) no. 17 pp 3-48, Noordhoff publ.

Latanision R.M. Opperhauser H. Westwood A.R.C.
1978 Scripta Met. 12 475

Lawn B.R. Swain M.V.
1975 J. Mater. Sci. 10 113

Lawn B.R. Wilshire R.
1975 J. Mater. Sci. 10 1049

Lawn B.R. Jensen T. Arora A.
1976 J. Mater. Sci. 11 575

Lawn B.R. Evans A.G.
1977 J. Mater. Sci. 12 2195

Lawn B.R.
1979 Seminar - 2nd July, Dept. Metallurgy and Materials Science, Cambridge, UK.

Lee C.H. Masaki S. Kobayashi S.
1972 Int. J. of Mech. Sci. 14 417-426

Lee D.
1973 'The Science of Hardness Testing and its Research Applications', (1973) American Society for Metals, Metals Park,

Ohio, USA. p147

Leiko E.B. Luft A. Nadgornii E.M.
1977 Phys. Stat. Sol. A44 285-293

Macmillan N.H.
1977 in 'Surface Effects in Crystal Plasticity' ed. R.M. Latanision and J.J. Fourie, NATO Advanced Study Institute Series E (Applied Science) no. 17 pp 629-293, pub. Noordhoff.

Marsh D.M.
1964 Proc. Roy. Soc. (Lond.) A279 420

Marshall D.B. Lawn B.R.
1977 J. Am. Ceram. Soc. 60 36

Marshall D.B. Lawn B.R.
1978 J. Am. Ceram. Soc. 61 21

Marshall R.C. Faust J.W. Ryan C.E.
1974 (editors), 'Silicon Carbide - 1973' (Proc. Conf. Miami Beach) University of South Carolina Press, Columbia, South Carolina, USA.

Martin S.C.
1978 Ph.D. Thesis (in preparation) Dept. Metallurgy and Materials Science, Cambridge, UK.

Masumoto T. Maddin R.
1975 Mater. Sci. Engng. 19 1-24

Mathews J. Walker R.L.
1973 'Mathematical Methods of Physics', Addison Wesley, World Student Series. p404

Mellor B.G.
1973 Ph.D. Thesis, University of Cambridge.

Mellor B.G. Edmonds D.V.
1978 J. Mater. Sci. 13 571-579

Moore M.A. Richards R.C. Attwood D.G.
1972 Met. Trans. 3 2485

Moore M.A.
1974 Ph.D. Thesis, University of Newcastle.

Morgan G. Lewis M.H.
1974 J. Mater. Sci. 9 349

Mott B.W.
1956 'Microindentation Hardness testing', Butterworths.

Mulhearn T.O. Samuels L.E.
1955 J. Iron and Steel Institute 180 354-358

Mulhearn T.O. Tabor D.
1960 J. Inst. Met. 89 7

Muller K.
1973 'The Science of Hardness Testing and its Research Applications', (1973) American Society for Metals, Metals Park, Ohio, USA. pp 291-299

Nadgornii E.M. Stepanov A.V.
1963 Sov. Phys. - Solid State 5 732-742

Nagai T. Wasa K. Hayakawa S.
1976 J. Mater. Sci. 11 1509-1512

Naylor M.G.S.
1978 M.Phil Thesis, Dept. Metallurgy and Materials Science, Cambridge, UK.

Naylor M.G.S. Page T.F.
1979 Proc. Fifth Int. Conf. on Erosion by Liquid and Solid Impact (ELSI V), Cambridge 1979, (Publ. RAE Farnborough).

Neely J.E. Mackenzie J.D.
1978 J. Mater. Sci. 3 603-609

Nouet G. Deschanvres A.
1973 J. Less Comm. Met. 35 17

Nunes J. Larson F.R.
1962/3 J. Inst. Metals 91 114-117

O'Neill J.B. Redfern B.A.W. Brookes C.A.
1973 J. Mater. Sci. 8 47

Paetke S.
1979 Personal communication, Dept. Metallurgy and Materials Science, Cambridge, UK.

Page T.F.
1979 Personal communication, Dept. Metallurgy and Materials Science, Cambridge, UK.

Page T.F. Sawyer G.R. Adewoye O.O. Wert J.J.
1978 Proc. Brit. Ceram. Soc. 26 193

Page T.F. Wert J.J.
1977 Unpublished work, Dept. Metallurgy and Materials Science, Cambridge, UK.

Patel A.R. Sutaria J.N.
1971 J. Phys. D 4 1586-1588

Patterson J.P. Greer A.L. Leake J.A. Jones D.R.H.
1978 'Rapidly Quenched Metals III' 3rd.Int.Conf. Brighton, UK (July 1978) The Metals Society, London. (ed. B.Cantor) vol. 2

Patterson J.P.
1979 Personal communication, Dept. Metallurgy and Materials Science, Cambridge, UK.

Pavuna D.
1979 Seminar - 7th June, Dept. Metallurgy and Materials Science, Cambridge, UK.

Peter K.W.
1970 J. Non Cryst. Sol. 5 103

Pethica D.
1978 Ph.D. Thesis, University of Cambridge.

Pethica D.
1979 Personal communication, Cavendish Laboratory, Cambridge.

Porter A. Payne S. Mills P. Cooke B.
1979 Personal communication, 21 June, F.I.M. Laboratory, Dept. Metallurgy and Materials Science, Cambridge, UK.

Pospiech J. Grysieki J.
1970 Arch. Wum. Hutnictlia 25 267

Raghuram A.C. Armstrong R.W.
1970 J. Less Comm. Met. 22 239

Ramsdell L.S.
1947 Am. Min. 32 64

Ray R. Hasegawa R. Chou C.-P. Davis L.A.
1977 Scripta Met. 11 973-978

Reed-Hill R.E. Cribb W.R. Monteiro S.N.
1973 Met. Trans. 4 2665

Rhines F.N.
1970 Met. Trans. 1 1105

Rhines F.N.
1977 Met. Trans. 8A 127

Rice R.W.
1971 U.S. Naval Research Lab. Report 7334, Washington D.C., USA.

Richardson R.C.D.
1969 Ph.D.Thesis, University of London.

Rickerby D.G.
1979 J. Am. Ceram. Soc. 62 222

Riewald P.G. Van Vlack L.H.
1969 J. Am. Ceram. Soc. 52 370

Roberts S.G.
1979 Unpublished work, Dept. Metallurgy and Materials Science, Cambridge, UK.

Routbort J.L.
1979 Acta Met. 27 649-661

Rozhanskii V.N. Nazarova M.P. Svetlov I.L. Kalashnikova L.K.
1970 Phys. Stat. Sol. 41 579

Rowcliffe D.J. Hollox G.E.
1971 J. Mater. Sci. 6 1261, 1270

Ruff A.W. Wiederhorn S.M.
1979 in 'Materials Erosion' (ed. C.M.Preece), pub. Academic Press.

Samuels L.E. Mulhearn T.O.
1957 J. Mech. Phys. Sol. 5 125

Sargent P.M.
1976 'Work Hardening and Grain Size - A Review', unpublished work.

Sargent P.M. Page T.F.
1978 Proc. Brit. Ceram. Soc. 26 209

Savenko V.I. Shchukin E.D.
1976 Sov. Phys. - Solid State 18 2038

Sawyer G.R. Page T.F.
1978 J. Mater. Sci. 13 865

Sawyer G.R. Sargent P.M. Page T.F.
1979 Submitted to J. Mater. Sci.

Sawyer G.R.
1979 Ph.D. Thesis, University of Cambridge.

Schulson E.M., Roy J.A.
1977 Met. Trans. 8A 377

Shaffer P.T.B.
1964 J. Am. Ceram. Soc. 47 466

Shaffer P.T.B. Jin C.K.
1972 Mat. Res. Bull. 7 63

Shaskolskaya M.P. Dobrzhanskii G.F.
1962 Sov. Phys. - Crystallography 7 83

Shoshorov M.Kh. Alekhin V.P. Bulychev S.I.
1977 Phys. Met. Metall. 43 374-379

Simmons G.
1965 'Single Crystal Elastic Constants and Calculated Aggregate Properties' Journal of the Graduate Research Centre 34 1-269

Skrovanek S.D. Bradt R.C.
1965 Bull. Am. Ceram. Soc. 55 400

Skrovanek S.D. Bradt R.C.
1979 J. Am. Ceram. Soc. 62 215-216

Smith D.J. Jepps N.W. Page T.F.
1978 J. Microscopy 114 1

Spaepen F.
1978 'Rapidly Quenched Metals III' 3rd.Int.Conf. Brighton, UK (July 1978) The Metals Society, London. (ed. B.Cantor) vol. 2 253-264

Speich G.R. Warlimont H.
1968 J. Iron and Steel Institute 385-392

Spitzig W.A. Sober R.J. Richmond O.
1976 Met. Trans. 7A 1703

Srinivasan M. Stoebe T.G.
1974 J. Mater. Sci. 9 121-128

Strunk H.
1975 Phys. Stat. Sol. 28A 119

Strunk H.
1977 Mater. Sci. Engng. 27 225-238

Stubicar M.
1979 J. Mater. Sci. 14 1245-1248

Studman C.J. Field J.E.
1976 J. Phys. D 9 859

Studman C.J. Moore M.A. Jones S.E.
1977 J. Phys. D 10 949

Swain M.V. Lawn B.R.
1969 Phys. Stat. Sol. 35 909

Tabor D.
1951 'The Hardness of Metals', O.U.P.

Tabor D.
1970 Reviews in Physics in Technology 1 145-179

Tarasov L.P. Thibault N.W.
1947 Trans. ASM 38 331-353

Tarkanian M.L. Newman J.P. Raymond L.
1973 'The Science of Hardness Testing and its Research Applications', (1973) American Society for Metals, Metals Park, Ohio, USA. p187

Tate D.R.
1945 Trans. ASM 35 374-389

Thibault N.W. Nyquist H.L.
1947 Trans. ASM 38 271

Thomas D.A.
1960 Trans. Met. Soc. AIME 218 1122

Thompson A.W. Baskes M.I. Flanagan W.F.
1973 Acta Met. 21 1017

Thompson A.W.
1975 Acta Met. 23 1337

Trefilov V.I. Borisenko V.A. Gnesin G.G. Gridneva I.V. Milman Iu.V.
1977 Dokl. Akad. Nauk. SSSR 239 579 (in Russian)

Tung Y. Faust J.W.Jnr.
1974 'Silicon Carbide - 1973' (Proc. Conf. Miami Beach) University of South Carolina Press, Columbia, South Carolina, USA. p246

Upit G.P. Varchenya S.A.
1966 Phys. Stat. Sol. 17 831-825

Van Vechten J.A.
1973 Phys. Rev. B7 1479-1507

Varchenya S.A. Muktepavel F.O. Upit G.P.
1970 Sov. Phys. - Solid State 11 2300

Vasilos T. Spriggs R.M.
1963 J. Am. Ceram. Soc. 46 493-496

Vellednitskaya M.A. Rozhanskii V.N. Comolova L.F. Saparin G.V. Schreiber J. Brummer O.
1975 Phys. Stat. Sol. A32 123

Walker W.W.
1973 'The Science of Hardness Testing and its Research Applications', (1973) American Society for Metals, Metals Park, Ohio, USA. p258

Waseda Y. Aust K.T. Masumoto T.
1979 Scripta Met. 13 187-190

Westbrook J.H.
1958 quoted by J.J.Gilman in 'The Science of Hardness Testing and its Research Applications', (1973) American Society for Metals, Metals Park, Ohio, USA. p55

Westbrook J.H. Jorgenson P.J.
1965 Trans. Met. Soc. AIME 233 425

Westwood A.R.C. Macmillan N.H.
1973 'The Science of Hardness Testing and its Research Applications', (1973) American Society for Metals, Metals Park, Ohio, USA. 377-414

Wonsiewicz B.C. Chin G.Y.
1973 'The Science of Hardness Testing and its Research Applications', (1973) American Society for Metals, Metals Park, Ohio, USA. p167

Young C.T. Rhee S.K.
1978 J. of Testing and Evaluation 6 221

Zaitsev V.I. Barbashov V.I. Tkachenko Yu.B.
1977 Phys. Stat. Sol. A44 K39

Appendix I - Models and Programs

This appendix contains the detailed descriptions of two models of indentation behaviour, the data analysis used for measuring the indentation size effect (the theory of which is explained in chapter 3) and the programs used in connection with calculations made using the radial displacement models.

The first model, HSLM (Hard Surface Layer Model) predicts the indentation size effect on hardness in a composite of two layers of isotropic, ductile materials of different hardness. The results are shown in section 2.5.3.

The second model, KHAMM (Knoop Hardness Anisotropy Model for Monocrystals) takes no account of the indentation size effect and is only concerned with the effective resolved shear stresses on the slip systems of indented single crystals. This is discussed in detail and some results are shown in section 2.4.2, the name is something of a misnomer now that it has been extended to predict Vickers hardness anisotropies as well as Knoop hardness anisotropies.

All the programs have been written in fortran to run on the Cambridge University Computing Service IBM 370/165 and nearly all make extensive use of the Computing Service's graph plotting subroutines and other subroutine libraries.

Both the data analysis program (ISEMH - Indentation Size Effect on Micro-Hardness) and KHAMM are currently implemented with the Ceramics Group's facilities on the university computer and procedures and documentation have been written by this author (not included in this thesis) as part of their developement to enable other workers to use them easily and efficiently as part of their own research (Roberts 1979, Sawyer 1979, Sawyer et al. 1979, Greer 1976).

I.I - HSLM Hard Surface Layer Model

This model predicts the indentation size effect on the Vickers microhardness of a composite material which is a consequence of small indentations being dominated by the behaviour of the surface, and large indentations being dominated by the behaviour of the bulk. The model material is a layer of hard, isotropic, ductile material on top of a substrate of softer, isotropic, ductile material; it considers the problem in three dimensions and not merely on a two dimensional section. The program could easily be altered to cope with the inverse situation, which would lead to ISE indices greater than 2.0, but this extension has not been made.

Several assumptions are made about the deformation in order to produce a model which does not have so many adjustable parameters that no useful predictions can be made:-

1. That only the material in a hemisphere subtended by the diagonals of the square indentation are affected by the indenter and affect the measured hardness.
2. No account is taken of material flow or conservation of volume, the model is purely geometrical.
3. The measured hardness (H_m) depends only on the volume fractions (V_s and V_b) of the two types of material in the hemisphere and that it is given by a simple law of mixtures :

$$H_m = V_s.H_s + V_b.H_b \qquad \text{equation I.Ia}$$

where H_s is the hardness of the surface and H_b is the hardness of the bulk.

4. There is no indentation size effect on hardness in either of the two component materials in isolation, H_s and H_b are constant in any one model situation. The behaviour was predicted for situations where H_b was set to 1000 (arbitrary units) and H_s = 2000, 4000, 6000, 8000, and 10000. Plots of the results are shown in section 2.5.3.

5. The indenter does not penetrate the surface layer, neither is the layer compressed to less than its original thickness (see figure in section 2.5.3).

Given these assumptions, the mechanics of solving the problem of predicting the hardness for indentations of a range of sizes are as follows. The geometrical problem is that of finding the volumes bounded by a hemisphere and two concentric, equiangular, square-based pyramids. An analytical solution was attempted but a wholly numerical approach was found to be quicker, both for computation and for presenting the results graphically.

```
      C          Surface Hardening Model
      C
      C          This program calculates the hardness (using a
      C          simple law of mixtures) measured by indenting
      C          a layer of material on top of a substrate of
      C          different hardness. It does this over a range
      C          of indentation sizes such that the hemispherical
      C          zone beneath the indenter is at one extreme
      C          entirely contained within the layer, and at
      C          the other extreme is very much larger than the
      C          layer thickness.
      C          The program calculates the rate of change of
      C          hardness with indentation size and from this
      C          calculates the log-index for every
      C          indentation size.
      C
      REAL A(81),D(81),N(81),PD(81),PD2(81)
C
      H2=1000.
      DO 170 NH=1,11,2
      NH2=NH-1
      H1 = FLOAT(NH2)*1000.
      IF(NH2.EQ.0) H1=1100.
C
      DO 150 K=1,80
C
C          D1 is the indentation diagonal divided
C          by the layer thickness
      D1 = 200./K
      D(K)=D1
      J=K-1
      PD(K)=D1
      PD2(K)=1./D1
C
      A1=0.
      A2=0.
C
C          NUM is the number of slices used in the
C          calculation of the volumes of the sections
C          of the hemisphere. This DO-loop includes
C          a calculation of the cross-sectional areas
C          of these sections in each slice and tots
C          them up
C
      NUM=150
      DO 100 L=1,NUM
      D2=FLOAT(L)/(FLOAT(NUM)*2.)
      D3 = D2 - 1./(4*NUM)
C
C          D2 is the depth of the bottom of the slice L
C          D3 is the depth at the middle of the slice L
C
      A0=0.
      A3=0.
      A4=0.
      A5=0.
      A6=0.
C
C          A6 is the are of the cross section of the
C          hemisphere ie. a circle in each slice
C
      R1=0.
C
C          R1 is the radius of the circle in each slice
C
   30 R1=SQRT(0.25-D3**2)
      A6=3.14159*R1**2
C
C          S is the length of the side of the square which
C          is the cross-section of the pyramid which is the
C          boundary between the surface layer and the bulk
C
   50 S=2.47509*(1/D1 - D3) + 0.35355
      IF(S.GE.0) GOTO 60
      S=0
      GOTO 110
C
```

```
C          R2 is half the diagonal of the cross-sectional
CC         square
C
   60 R2=1.4142*S
      IF(S.GT.R1) GOTO 70
      IF(R2.GT.R1) GOTO 80
      A1 = A1 + 4*S**2
C
CC         A1 is the cross-sectional area of the surface
C          layer
C
      A4=4*S**2
      AO=A4
      GOTO 90
C
   70 A1 = A1 + 3.14159*R1**2
      A3=3.14159*R1**2
      AO=A3
      GOTO 90
C
   80 Z = SQRT(R1**2 - S**2)
      A5=R1**2*(3.14159 - 4*ATAN(Z/S)) + 4*S*Z
      A1 = A1 + A5
      AO=A5
   90 CONTINUE
C
  100 CONTINUE
C
  110 V1 = A1/(NUM*2) - 0.02380747
      V2 = 0.26179939 - A1/(NUM*2)
C
C        0.02380747 is the volume of the indentation itself
C        which must be subtracted as it is empty space
C         V1 is the layer volume and V2 is the bulk volume,
C         0.26179939 is the volume of the whole hemisphere
C
      V5 = V1 + V2
      A(K) = (H1*V1 + H2*V2)/V5
C
C          A is the calculated hardness for the K'th value
C          of D1
C
      P = V1/V5
C
  150 CONTINUE
C
      DO 160 K=1,79
      IF(K.NE.1) GOTO 130
      WRITE(6,145)D1,P,A(K)
      GOTO 160
C
  130 J=K-1
      L=K+1
      G=A(K)-A(J)
      G=G/(D(K)-D(J))
      G2=A(L)-A(K)
      G2=G2/(D(L)-D(K))
C
C          G is the gradient of the hardness wrt. the
C          diagonal of the indentation.
C          N is the log-index (see thesis section 2.5.3)
C
      G=0.5*(G+G2)
      N(K)=G*D(K)/A(K) + 2
C
C     WRITE(6,140)G,N(K)
  140 FORMAT(34X,F13.6,F13.6)
C     WRITE(6,145)D1,P,A(K)
  145 FORMAT(1X,F8.4,4X,F8.4,4X,F9.2)
C
  160 CONTINUE
C
      G=A(2)-A(1)
      G=G/(D(2)-D(1))
      N(1) = G*D(1)/A(1) + 2
C     WRITE(6,*)D,A,N
C.
```



```
C          Now the results are plotted
C
      CALL TRMCHR(0.,0.,0.,0.)
      CALL BRKPLT(8)
      CALL TRMCHR(3.,0.,0.,5.)
C
      CALL PLIMIT(30.,110.,30.,110.)
      CALL ULIMIT(0.,200.,H2,H1)
      CALL GRFTYP(0,'*')
      CALL ANFREQ(4,8,5,10)
      CALL PEN(3)
C
      CALL PLTGXY(PD,A,79)
      CALL BOXTYP(-1)
      CALL BOXXY(0,0)
C
      CALL ULIMIT(0.,200.,1.,2.)
      CALL PEN(2)
      CALL PLTGXY(PD,N,79)
      CALL BOXTYP(-2)
      CALL BOXXY(0,0)
C
      CALL PEN(1)
      CALL TITLE(' ',1,
     +'DIAGONAL/LAYER-THICKNESS',24,' ',1)
      CALL GULIM(XL,XR,YD,YU)
      CALL MOVETO(XL,YU)
      CALL DRAWTO(XR,YU)
C
      CALL TRMCHR(0.,0.,0.,0.)
      CALL BRKPLT(8)
      CALL TRMCHR(3.,0.,0.,5.)
C
      CALL PLIMIT(30.,110.,30.,110.)
      CALL ULIMIT(0.4,0.005,H2,H1)
C
      CALL PEN(3)
      CALL PLTGXY(PD2,A,79)
      CALL BOXTYP(-1)
      CALL BOXXY(0,0)
C
      CALL ULIMIT(0.4,0.005,1.,2.)
      CALL PEN(2)
      CALL PLTGXY(PD2,N,79)
      CALL BOXTYP(-2)
      CALL BOXXY(0,0)
C
      CALL PEN(1)
      CALL TITLE(' ',1,
     +'LAYER-THICKNESS/DIAGONAL',24,' ',1)
      CALL GULIM(XL,XR,YD,YU)
      CALL MOVETO(XL,YU)
      CALL DRAWTO(XR,YU)
C  170 CONTINUE
C
      STOP
      END
```

I.II - ISEMH The Data Analysis Procedure

The rationale behind the method of data analysis and the theory of the linear regression and the statistics are given in chapter 3, section 3.2.

The program has been adapted to produce interpolated hardness values for standard diagonal lengths other than the ten micron length used throughout the current work for Vickers indentations. A 70 micron hardness has been used to reduce the covarience in the results for Knoop indentation results, and a 35 micron hardness is currently being used in the analysis of hardness data from silicon carbide materials using a Vickers indenter (Roberts 1979).

The actual linear regression is made using the UKAEA Harwell subroutine VC04, but a replacement for this could easily be written using the theory presented in 3.2.

Essential for the use of the ISEMH program in the practical situation is the program MERGE which is used to merge two sets of data (in ISEMH readable format) into a single set with the same format. A listing of this program is appended to the listing of ISEMH.

```
      SUBROUTINE ROOT(IND)
C
C         Analysis of Load/Indent-diagonal data from
C     microhardness tests.
C
C
C         Parts of this program (ie. subroutine MUDDLE)
C     were written at AERE Harwell; July-Sept. 1975 ,
C     to fit a straight line to ln/ln data of load/
C     time in a stress relaxation test. ( This was to
C     measure crack growth in a 'Double Torsion' type
C     specimen).
C         The program was re-written for its present
C     function in Feb. 1976 (Cambridge).
C         The program was adapted and extended to draw
C     the results on the plotter in June-July 1976.
C         A weighting of the fit was introduced in Nov.
C     1976 in order to adjust for the distortion of
C     the Normal distribution of errors by the ln/ln
C     transformation.
C         The section of the program that calculates
C     the error ellipsoid for the plot of the best fit
C     Meyer-index/intercept values was written April-
C     -September 1977.
C         New weights equal to the mean diagonal measu-
C     -rements were introduced on the 28th October 77.
C         The two programs for Knoop and Vickers
C     indenters were combined in November 77.
C         The mean hardness numbers for each load were
C     inserted on 2 December 1977.
C         The ' ten micron hardness' replaced the crude
C     'one micron Meyer intercept' idea and the anno-
C     -tations on the plots were changed from linear
C     to logarithmic in April - May 78. The plot of
C     microhardness against load in subroutine WEIRD
C     was added in May 78.
C         The fitted Meyer line was added to the plot of
C     microhardness against load in June 1978.
C         The plot of microhardness against indentation
C     diagonal and the ten-micron lines on this and
C     the previous plot were added in July 1978.
C
C         Philip Sargent
C         Dept. Metallurgy and Materials Science
C         Cambridge.
C
      INTEGER STAR,ISTAR,DEE
      INTEGER NUM,COUNT,GRPS,TEST,DOL,HASH,PAGE
      LOGICAL*1 INFO(58)
      REAL     DIAG(600),LOAD(600),W(600),SIZE(50),CHECK
      REAL     SIGMA(50),MEAN(50),SL(50),HN,DISP,OSL(50)
      REAL     MAXS,MINS,ODIAG(600),OLOAD(600),A,B,C,D
      REAL*8 PROB
C
      DATA DOL,HASH,ISTAR/1H$,1H#,1H*/
C
C
      COMMON DIAG,LOAD,W
      COMMON /PIC1/ A,B,C,D,STAR
      COMMON /PIC2/ SIGMA,MEAN,SL,DISP
      COMMON /COM1/PROB,COUNT
      COMMON /COM0/ ODIAG,OLOAD
      COMMON /PIC4/ OSL
      COMMON /COM2/CONST
      COMMON /COM3/DEE
C
CC          Read the data
C
      IF(IND.EQ.1) CONST=1854.4
      IF(IND.EQ.2) CONST=14230.0
      PAGE=1
      GRPS=0
      STAR=ISTAR
      COUNT=0
      READ(5,10,END=190)INFO
   10 FORMAT(58A1)
      WRITE(6,20)INFO
   20 FORMAT('1',58A1/'+',58('_')///)
```



```
      WRITE(6,30)
   30 FORMAT(1X,' Diag.    Load ',4X,'ln(diag)  ',
     1'ln(load)',4X,'HN'/'+ ',5('_'),4X,'____',5X,
     28(' '),2X,8(' '),4X,'__'//)
   40 READ(5,*,END=200,ERR=265) LOAD(COUNT+1)
      READ(5,*,END=210,ERR=265) NUM
      GRPS=GRPS+1
C
      WRITE(6,50) LOAD(COUNT+1)
   50 FORMAT(10X,F6.1)
C
      OLOAD(COUNT+1) = LOAD(COUNT+1)
      OSL(GRPS) = LOAD(COUNT+1)
      LOAD(COUNT+1) = ALOG(LOAD(COUNT+1))
      SL(GRPS) = LOAD(COUNT+1)
      WRITE(6,60) LOAD(COUNT+1)
   60 FORMAT('+',30X,F6.3)
C
CC          Copy out the data, also write the Vickers
C           Pyramid Hardness and the ln's of the data
      SIZE(GRPS) = 0.0
      DO 70 J=1,NUM
      READ(5,*,END=220,ERR=265) DIAG(COUNT+J)
      IF(DIAG(COUNT+J).LE.0.0) STOP 1328
      SIZE(GRPS) = SIZE(GRPS) + DIAG(COUNT+J)
C
      WRITE(6,80) DIAG(COUNT+J)
      ODIAG(COUNT+J) = DIAG(COUNT+J)
      DIAG(COUNT+J) = ALOG(DIAG(COUNT+J))
      LOAD(COUNT+J) = LOAD(COUNT+1)
      OLOAD(COUNT+J) = OLOAD(COUNT+1)
      HN = CONST*OLOAD(COUNT+J)/ODIAG(COUNT+J)**2
      WRITE(6,90) DIAG(COUNT+J),HN
   70 CONTINUE
      SIZE(GRPS) = SIZE(GRPS)/NUM
C
   80 FORMAT('+',F6.2)
   90 FORMAT('+',20X,F6.3,12X,F6.1/)
C
CC          Now calculate the size of the error bars
C           for each group of data i.e. for each load
C
      CALL BARS(COUNT,NUM,GRPS,CONST)
C
CCC         Introduce the weighting factors.
CCC         These are equal, theoretically, to the
CCC         "expected" diagonal measurements for
CCC         each exptl. load. Since the expected
CCC         values are not available, of course, until
CCC         after the line is fitted; the mean
CCC         value of the diags is used instead.
C
      DO 100 J=1,NUM
      W(COUNT+J) = EXP(MEAN(GRPS))
  100 CONTINUE
C
      READ(5,110,END=230,ERR=265) TEST
  110 FORMAT(A4)
      IF(TEST.EQ.DOL) GOTO 120
      IF(TEST.NE.HASH) GOTO 240
      COUNT=COUNT+NUM
      IF(GRPS.GT.49) GOTO 250
      IF(COUNT.GT.599) GOTO 260
      GOTO 40
C
CC          The program skips to 120 when all the data
C           has been read in with no formatting errors
  120 CONTINUE
      COUNT=COUNT+NUM
C
CC          Print mean indent sizes
      WRITE(6,130)
  130 FORMAT(/)
      CALL RMXMN(SIZE,GRPS,MINS,MAXS)
      WRITE(6,140)MINS,MAXS
  140 FORMAT(' Range of indent sizes: ',
     1F6.2,' to ',F6.2)
```

```
      IF(IND.EQ.1) WRITE(6,150)
      IF(IND.EQ.2) WRITE(6,160)
  150 FORMAT(/' Vickers indenter')
  160 FORMAT(/' Knoop indenter')
C
      CALL GRFTYP(-1,STAR)
C
C         Fit a straight line to the data
      DEE=1
      CALL MUDDLE(COUNT,INFO,IND,DEE,CONST)
C
C
C
C         10 micron intercept section
C         ---------------------------
C
C         The diagonals are rescaled to be units of
C         10 microns, thus the intercept ln(a) is
C         the log of the load to make an indentation
C         of 10 microns.
C
  165 DO 170 J=1,COUNT
      DIAG(J) = DIAG(J) -2.302585
  170 CONTINUE
C
      DEE = 10
      CALL MUDDLE(COUNT,INFO,IND,DEE,CONST)
C
C         Plot the points & straight line on a ln/ln plot
C
      CALL LNPLT(GRPS,COUNT,INFO,
     +IND,DEE)
C
      DEE=10
      CALL CONF(INFO,IND,CONST)
C
      CALL SETFUN(0.75,40)
      CALL GRFTYP(-1,203)
      CALL SETFUN(.25,70)
      CALL WEIRD(GRPS,COUNT,INFO,IND)
C
      WRITE(6,180)
  180 FORMAT(//' All data manipulation completed.'//
     +' PHILIP SARGENT'/' CERAMICS GROUP'/
     +' CAMBRIDGE.  1979')
C
      RETURN
C
C         Error messages
C
  190 WRITE(6,270)
      STOP
  200 WRITE(6,280) GRPS
      STOP
  210 WRITE(6,290) GRPS
      STOP
  220 WRITE(6,300) GRPS
      STOP
  230 WRITE(6,310) GRPS
      STOP
  240 WRITE(6,320) GRPS
      STOP
  250 WRITE(6,330) GRPS
      STOP
  260 WRITE(6,340) GRPS
      STOP
  265 WRITE(6,350)
      STOP 1398
C
C         Format statements for error messages
C
  270 FORMAT(/1X,'##### ERROR #####',
     1'  No data found')
  280 FORMAT(/1X,'##### ERROR #####',
     1'  End of data found where a LOAD
     2value expected',I4)
  290 FORMAT(/1X,'##### ERROR #####',
```



```
     1'  End of data found where a NUM
     2value expected',I4)
  300 FORMAT(/1X,'##### ERROR #####',
     1'  End of data found where a DIAG
     2value expected',I4)
  310 FORMAT(/1X,'##### ERROR #####',
     1'  End of data found where # or $ expected',I4)
  320 FORMAT(/1X,'##### ERROR #####',
     1'  # expected but not found, NUM is wrong',I4)
  330 FORMAT(/1X,'##### ERROR #####',
     1'  GRPS greater than 49 and no'
     2end of data in sight',I4)
  340 FORMAT(/1X,'##### ERROR #####',
     1'  COUNT greater than 599 and no
     2end of data in sight',I4)
  350 FORMAT(/1X,'##### ERROR #####',
     1'  in input data format')
C
      END
C
C-----------------------------------------------------------
C
      SUBROUTINE MUDDLE(COUNT,INFO,IND,DEE,CONST)
C
      INTEGER COUNT,LP,NDF,STAR,LEE
      LOGICAL*1 INFO(58)
      REAL    W(600),PAR(4),DIAG(600),LOAD(600)
      REAL    LNP,LNP1,LNP2,H10,H101,H102,SIGLNP
      REAL    CORR,SIGA,SIGB,AA,BB,SIGC,PR,CONST
      REAL    A,B,ASTD,BSTD,RSTD,ABCOV,DELA,DELB
C
      COMMON DIAG,LOAD,W
      COMMON /VC04D/LP,NDF,CORR,A,B,ASTD,BSTD,ABCOV,
     1RSTD,P,Q,PSTD,QSTD,PQCOV,RMSSTD,XMEAN,YMEAN,
     2XVAR,YVAR,XYCOV
      COMMON /PIC1/ BB,SIGB,AA,SIGA,STAR
C
C   Fitting a straight line to the ln/ln plot
C
      WRITE(6,10)
   10 FORMAT('1The weighted straight line',
     1' fitted to the ',
     2'ln/ln plot',
     3/'+',51('-')//)
      IF(IND.EQ.1) WRITE(6,20)INFO
   20 FORMAT(' Vickers Indenter'/
     1' Mean diagonal weights.'/1X,58A1/)
      IF(IND.EQ.2) WRITE(6,30)INFO
   30 FORMAT(' Knoop indenter'//
     1' Mean diagonal weights.'/1X,58A1/)
      WRITE(6,40)DEE
   40 FORMAT(1X,I2,' micron intercept'//)
C
      CALL VC04B(LOAD,DIAG,W,COUNT,A,B,0)
C
      DELB=BSTD/B
      BB=1.0/B
      SIGB=3*DELB*BB
      WRITE(6,50)BB,SIGB
      Q1=BB-SIGB
      Q2=BB+SIGB
      Q11=BB-SIGB*2/3
      Q22=BB+SIGB*2/3
      WRITE(6,60) Q1,Q2,Q11,Q22
   50 FORMAT(1X,'Index      = ',F6.3,' +'/
     1'+',17X,'  _   ',F6.3,4X,'(3 sigmas)'/)
C
      DELA=ASTD/A
      AA=-BB*A
      SIGA=3*SQRT(DELA*DELA  + DELB*DELB)*AA
      WRITE(6,70)AA,SIGA
      Q1=AA-SIGA
      Q2=AA+SIGA
      Q11=AA - 2*SIGA/3
      Q22=AA + 2*SIGA/3
      WRITE(6,60) Q1,Q2,Q11,Q22
   60 FORMAT(11X,'= ',F6.3,' to ',F6.3,4X,'(3 sigmas)'//
```

```
     111X,'= ',F6.3,' to ',F6.3,4X,'(2 sigmas)'/)
  70 FORMAT(1X,'Intercept = ',F6.3,' +'/
     1'+',17X,'   _  ',F6.3,4X,'(3 sigmas)'/)
C
      PH1=CONST*EXP(AA+SIGA**2/3)/(DEE**2)
      PH2=CONST*EXP(AA-SIGA**2/3)/(DEE**2)
      PH = CONST * EXP(AA)/(DEE**2)
      WRITE(6,80)DEE,CONST,DEE,PH,PH1,PH2
  80 FORMAT(1X,I2,' micron'/' Hardness = ',F7.1,
     1' * exp(intercept)/(',I2,'**2)'//11X,'= ',
     2F7.1//11X,'= ',F7.1,
     3' to ',F7.1,2X,'(2 sigmas)'//)
C
      Q1=3*ASTD
      Q2=3*BSTD
      Q3=(COUNT-2)*RSTD*RSTD
      WRITE(6,90)RSTD,Q3,CORR,ABCOV,A,Q1,B,Q2,COUNT
  90 FORMAT(' Weighted Residual std.',6X,'= ',F8.5//
     1' Sum of Squares of Residuals = ',F8.3//
     2' "Correlation Coefficient"    = ',F8.5//
     3' "Covariance"                 = ',E12.4//
     4' "A"',25X,'= ',F6.3,' + ',F6.3/'+',37X,'_'//
     5' "B"',25X,'= ',F6.3,' + ',F6.3/'+',37X,'_'//
     6' Number of data points',7X,'= ',I4//)
C
C          Now the variables A,B,ASTD,BSTD,ABCOV IN THE
C          common block /VC04D/ still refer to the
C          quantities found by the routine VC04B and not
C          to the quantities transformed to be appropriate
C          for 'ln(a)' and 'n'.
C
      RETURN
      END
C
C-----------------------------------------------------------------
C
      SUBROUTINE BARS(COUNT,NUM,GRPS,CONST)
C
C          This subroutine calculates the size of
C          the error bars for a particular load:
C          LOAD(COUNT+1). There are NUM values
C          in DIAG(COUNT+1) to DIAG(COUNT+NUM)
C          the mean and standard deviation
C          in the mean are returned in SIGMA(GRPS)
C          and MEAN(GRPS).
C
      REAL     DIAG(600),W(600),LOAD(600),SIGMA(50)
      REAL MEAN(50),SL(50),CONST,HN,OMEAN,Q0,HARDM(50)
      REAL ODIAG(600),OLOAD(600),OSIG,HARDL(50),HARDH(50)
      REAL     HARD(600)
      INTEGER GRPS,COUNT,NUM
C
      COMMON DIAG,LOAD,W
      COMMON /PIC2/ SIGMA,MEAN,SL
      COMMON /COM0/ODIAG,OLOAD
      COMMON /NEWPIC/ HARDH,HARDL,HARDM
      COMMON /COM4/HARD
C
      SIGMA(GRPS) = 0
      MEAN(GRPS) = 0
      OSIG = 0
      OMEAN = 0
C
      IF(NUM.GE.1) GOTO 20
      WRITE(6,10) NUM,GRPS
   10 FORMAT(/1X,'##### ERROR #####',
     1'  NUM=',I4,' IN GROUP: ',I4)
      STOP
C
   20 IF(NUM.NE.1) GOTO 30
      MEAN(GRPS) = DIAG(COUNT+1)
      SIGMA(GRPS) = 0
C
      RETURN
C
   30 CONTINUE
      Q0 = CONST*OLOAD(COUNT+1)
```



```
      DO 40 J=1,NUM
      OMEAN = OMEAN + ODIAG(COUNT+J)
      MEAN(GRPS) = MEAN(GRPS) + DIAG(COUNT+J)
      HARD(COUNT+J) = Q0/ODIAG(COUNT+J)**2
   40 CONTINUE
      MEAN(GRPS) = MEAN(GRPS)/NUM
      OMEAN = OMEAN/NUM
C
      DO 50 J=1,NUM
      SIGMA(GRPS) = SIGMA(GRPS) +
     1 (DIAG(COUNT+J)-MEAN(GRPS))*
     2 (DIAG(COUNT+J)-MEAN(GRPS))
      OSIG = OSIG + (ODIAG(COUNT+J)-OMEAN)**2
   50 CONTINUE
C
      SIGMA(GRPS) = 3*SQRT(SIGMA(GRPS)
     1/((NUM-1)*NUM))
C
      OSIG = SQRT(OSIG/((NUM-1)*NUM))
C
C          Now SIGMA contains
C          3*sqrt(square residuals/((NUM-1)*NUM))
C
      HARDM(GRPS) = Q0/OMEAN**2
      HARDL(GRPS) = Q0/(OMEAN+2*OSIG)**2
      HARDH(GRPS) = Q0/(OMEAN-2*OSIG)**2
      WRITE(6,60)HARDM(GRPS),HARDL(GRPS),HARDH(GRPS)
   60 FORMAT('+',43X,F6.1/
     138X,'(',F6.1,' -> ',F6.1,')'/)
C
      RETURN
      END
C
C-----------------------------------------------------------------
C
      SUBROUTINE LNPLT(GRPS,COUNT,INFO,IND,DEE)
C
C          This subroutine finds the maximum
C          and minimum values of the measured
C          diagonals (and error bars) to adjust
C          the scaling if necessary.
C          It plots all the data points, draws an error
C          bar for each LOAD and draws an annotated
C          box around the plot. It draws the best
C          fit straight line across the data. It writes
C          labels for each axis, the title across the
C          top, and the values for the index and inter-
C          -cept of the fitted line (all characters
C          scaled by 0.7).
C          It plots two crosses as a guide for cutting up
C          the paper.
C
      INTEGER COUNT,GRPS,STAR,IND,DEE
      LOGICAL*1 INFO(58)
      REAL     X1,X2,Y1,Y2,LHE,RHE,BMAX,DEEFAC
      REAL     BMIN,SANDM(50),A,SIGA
      REAL     SL(50),MEAN(50),SIGMA(50)
      REAL     DMAX,DMIN,WMAX,WMIN
      REAL     B,SIGB,LOAD(600),DIAG(600)
      REAL     PX2,PY2,SCALX,SCALY
      REAL     MAX,MIN,W(600),LWMIN,LWMAX
C
      COMMON DIAG,LOAD,W
      COMMON /PIC1/ B,SIGB,A,SIGA,STAR
      COMMON /PIC2/ SIGMA,MEAN,SL
C
      CALL TRMCHR(0.,0.,0.,0.)
      CALL BRKPLT(8)
      CALL TRMCHR(3.5,0.,0.,5.)
C
C          This section makes sure the diagonals are in
C          microns
C
      DEEFAC = ALOG(FLOAT(DEE))
C
      DO 5 I=1,COUNT
      DIAG(I) = DIAG(I) + DEEFAC
```

```
    5 CONTINUE
C
CCC         This section finds the extremes of the data
C
      CALL RMXMN(DIAG,COUNT,DMIN,DMAX)
C
CCC         This section finds the extremes of the
CCC         error bars
C
      DO 10 J=1,GRPS
      SANDM(J) = SIGMA(J) + MEAN(J)
   10 CONTINUE
      CALL RMXMN(SANDM,GRPS,BLANK,BMAX)
      DO 20 J=1,GRPS
      SANDM(J) = MEAN(J) - SIGMA(J)
   20 CONTINUE
      CALL RMXMN(SANDM,GRPS,BMIN,BLANK)
C
C           Find the max and min
      IF(DMIN.LT.BMIN) MIN = DMIN
      IF(DMIN.GE.BMIN) MIN = BMIN
      IF(DMAX.GE.BMAX) MAX = DMAX
      IF(DMAX.LT.BMAX) MAX = BMAX
C
CCC         This next section calculates the size of
CCC         the plot-space
CCC
CCC         Calculate the window minimum : WMIN
C
      IF(MIN.LT.3.5) GOTO 30
      WMIN = 3.5
      GOTO 60
C
   30 DO 40 J=1,7
      WMIN=3.5-0.5*J
      IF(MIN.LT.WMIN) GOTO 40
      GOTO 60
   40 CONTINUE
      WRITE(6,50) MIN
   50 FORMAT(/1X,'##### ERROR #####',
     1'  Min value of data point or error'
     2,' bar below 0.0'/
     320X,'MIN = ',F7.3/)
      STOP
C
CCC         Calculate window maximum : WMAX
C
   60 IF(MAX.GT.3.5) GOTO 70
      WMAX = 3.5
      GOTO 100
C
   70 DO 80 J=1,10
      IF(MAX.GT.3.5+0.5*J) GOTO 80
      WMAX = 3.5+0.5*J
      GOTO 100
   80 CONTINUE
      WRITE(6,90) MAX
   90 FORMAT(/1X,'##### ERROR #####',
     1'  Max value of data point or error bar
     2 above 8.5'/
     320X,'MAX = ',F7.3/)
      STOP
C
CCC         Write labels to axes and title
C
  100 CALL PEN(2)
      CALL TEXT(91.,15.,130.,15.,
     1'LOADS in grams',14)
      CALL TEXT(16.,50.,16.,110.,
     1'DIAGONALS in microns',20)
      CALL TEXT(50.,110.,85.,110.,
     1INFO,7)
C
      CALL PEN(3)
      CALL TRMCHR(2.8,1.4,0.0,3.5)
      CALL LOCCHR(30.,9.0,0)
      WRITE(8,110) INFO
```



```
  110 FORMAT('+',58A1)
C
CCC         Write the index and intercept
C
      CALL PEN(2)
      CALL TRMCHR(2.8,0.,0.,4.)
      CALL LOCCHR(136.0,122.0,0)
      WRITE(8,120) B,SIGB,DEE,A,SIGA
  120 FORMAT(/1X,'Index     =',/
     1 11X,I2,' micron Intercept =',/,F6.3,' + ',F6.3//
     2F6.3//' errors :'/'     3 sigmas,'/
     3' error bars:'/'     3*error',
     4' in the mean.')
      CALL LOCCHR(136.0,122.0,0)
      WRITE(8,130)
  130 FORMAT(//9X,'_'////9X,'_'/
     1/////////'
     21X//' Mean weighted Fit'//
     3' PHILIP SARGENT 1979')
C
      CALL PEN(3)
      CALL LOCCHR(136.,50.,0)
      IF(IND.EQ.1) WRITE(8,140)
      IF(IND.EQ.2) WRITE(8,150)
  140 FORMAT(' VICKERS indenter')
  150 FORMAT(' KNOOP indenter')
C
CCC         Plot two crosses for 'tear-off' markers
C
      CALL PEN(1)
      CALL TRMCHR(3.5,0.,0.,5.)
      CALL MOVETO(213.0,3.0)
      CALL PLTCHR(78)
C
      CALL MOVETO(2.0,3.0)
      CALL PLTCHR(78)
C
CCC         Scale to fit in the 100mm range, set
CCC         up the window
C
      CALL PLIMIT(30.,130.,30.,130.)
      CALL GRFTYP(-1,STAR)
      CALL ULIMIT(1.0,8.0,WMIN,WMAX)
C
CCC         Plot the data points
C
      CALL PEN(3)
      CALL TRMCHR(3.5,0.,0.,5.)
      CALL PLTGXY(LOAD,DIAG,COUNT)
C
CCC         Plot the error bars
C
      CALL PEN(2)
      TIP = 0.07
      DO 170 I=1,GRPS
      DO 160 J=1,2
      X1=SL(I)-TIP
      X2=SL(I)+TIP
      Y1=MEAN(I)+SIGMA(I)
      Y2=MEAN(I)-SIGMA(I)
      CALL MOVETO(X1,Y1)
      CALL DRAWTO(X2,Y1)
      CALL MOVETO(SL(I),Y1)
      CALL DRAWTO(SL(I),Y2)
      CALL MOVETO(X1,Y2)
      CALL DRAWTO(X2,Y2)
  160 CONTINUE
  170 CONTINUE
C
CCC         Plot the line; go to Left Hand End
C
      LHE = (1.0-A)/B + DEEFAC
      IF(LHE.LT.WMAX) GOTO 190
      WRITE(6,180) LHE
  180 FORMAT(/1X,'###### ERROR ######',
     1'  Fitted line has DIAG off top of
     2 scale at LOAD=',
```

```
     3'1.0'/' LHE = ',F6.3/)
      STOP
C
  190 IF(LHE.LT.WMIN) GOTO 200
      CALL MOVETO(1.0,LHE)
      GOTO 250
C
  200 LHE = A + B*WMIN - B*DEEFAC
      IF(LHE.GT.1.0) GOTO 220
      WRITE(6,210) LHE
  210 FORMAT(/1X,'##### ERROR #####',
     1'  Fitted line has LOAD less than
     21.0 at DIAG=WMIN'/
     3' LHE = ',F6.3/)
      STOP
C
  220 IF(LHE.LT.8.0) GOTO 240
      WRITE(6,230)
  230 FORMAT(/1X,'##### ERROR #####',
     1'  Fitted line has LOAD greater than 8.0',
     2' at DIAG=WMAX')
      STOP
C
  240 CALL MOVETO(LHE,WMIN)
C
C         Now draw to the Right Hand End
C
  250 RHE=(8.0-A)/B + DEEFAC
      CALL PEN(2)
      IF(RHE.GT.WMIN) GOTO 270
      WRITE(6,260) RHE
  260 FORMAT(/1X,'##### ERROR #####',
     1'  Fitted line has DIAG off bottom of
     2scale at LOAD='
     3'8.0'/' RHE = ',F6.3/)
      STOP
C
  270 IF(RHE.GT.WMAX) GOTO 280
      CALL DRAWTO(8.0,RHE)
      GOTO 330
C
  280 RHE = A + B*WMAX - B*DEEFAC
      IF(RHE.GT.1.0) GOTO 290
      WRITE(6,300) RHE
      STOP
C
  290 IF(RHE.LT.8.0) GOTO 320
      WRITE(6,310) RHE
      STOP
C
  300 FORMAT(/1X,'##### ERROR #####',
     1'  Fitted line has LOAD less than 1.0 at ',
     2' DIAG=WMIN'/' RHE = ',F6.3/)
  310 FORMAT(/1X,'##### ERROR #####',
     1'  Fitted line has LOAD greater than 8.0 at',
     2' DIAG=WMIN'/' RHE = ',F6.3/)
C
  320 CALL DRAWTO(RHE,WMAX)
C
C         Draw a horizontal line at diagonal = 10
C         microns, ie. DIAG = 2.30259
C
      CALL PEN(1)
      CALL MOVETO(1.0,2.30259)
      CALL DRAWTO(8.0,2.30259)
C
C         Plot the box
C
      CALL PEN(1)
      CALL TRMCHR(3.5,0.,0.,5.)
      CALL ANFREQ(5,10,5,10)
C
      LWMIN=ALOG10(EXP(WMIN))
      LWMAX=ALOG10(EXP(WMAX))
C
      CALL ULIMIT(0.434295,3.47436,LWMIN,LWMAX)
      CALL BOXLL(0,0)
```



```
C
  330 RETURN
      END
C
C-----------------------------------------------------------
C
      SUBROUTINE MATI(M,D)
C
C         This subroutine inverts a 2*2 matrix
C
      REAL*8  M(2,2),D(2,2),DET
C
      DET = M(1,1)*M(2,2) - M(2,1)*M(1,2)
      IF(DABS(DET).GT.1.0D-12) GOTO 20
      WRITE(6,10)
   10 FORMAT(///' Matrix X is SINGULAR !')
      STOP
C
   20 D(1,1) =  M(2,2)/DET
      D(1,2) = -M(1,2)/DET
      D(2,1) = -M(2,1)/DET
      D(2,2) =  M(1,1)/DET
C
      RETURN
      END
C
C-----------------------------------------------------------
C
      SUBROUTINE CONF(INFO,IND,CONST)
C
C         This subroutine sets up the windowing
C         and scaling options for plotting the
C         contours of confidence levels. This
C         probability is highest at the centre of
C         the concentric ellipses which is the
C         calculated pair of values: Meyer
C         intercept and index. ELIPS is called to
C         draw each ellipse, then an annotated
C         box is drawn and the title written.
C
      REAL*8  Q1,Q2,Q3,Q4,PROB,VAL
      REAL*8  XMAX,XMIN,YMAX,YMIN,AMIN,AMAX,BMIN,BMAX
      REAL    PX1,PX2,PY1,PY2,A,B,PB,CONST,XORG
      INTEGER COUNT,IND,STAR,DEE
      LOGICAL*1 INFO(58)
C
      COMMON /PIC1/BB,SIGB,AA,SIGA,STAR
      COMMON /VC04D/LP,NDF,CORR,A,B,ASTD,BSTD,ABCOV,
     1RSTD,P,Q,PSTD,QSTD,PQCOV,RMSTD,XMEAN,YMEAN,
     2XVAR,YVAR,XYCOV
      COMMON /COM1/PROB,COUNT
      COMMON /COM3/DEE
C
C     The COMMON block COM1 contains PROB (real*8) and
C     COUNT(int). If PROB is smaller (e.g.50%) the
C     ellipses will be smaller, if larger(99.9%) they
C     will be larger. (not implemented - only 95%
C     available).
C
C     The COMMON block VC04D contains the intercept A,
C     gradient B, the standard deviations and the
C     covarience ASTD, BSTD, ABCOV.
C
C     The parameter space plot is bounded by the values
C     XMIN, XMAX, YMIN, YMAX in users coordinates.
C
C
C         Find the     F     statistic for the 95%
C         confidence ellipsoid from the total number of
C         observations (COUNT).
C         The number of degrees of freedom is COUNT-2
C         and 2.
C
      CALL TRMCHR(0.,0.,0.,0.)
      CALL BRKPLT(8)
      CALL TRMCHR(3.5,0.,0.,5.)
      PROB = 0.950D0
```

```
      CALL FVAL(VAL)
C
C         Set up window 30.0 to 200.0/30.0 to 200.0
C         mm in plotter space (XMIN to XMAX/YMIN to
C         YMAX in 'Meyer intercept-index space')
C         The window in user space has the same
C         scale as 'Meyer intercept-index space'
C         but its origin is at ln(a)/n in Meyer
C         space. (ln(a)=AA, n=BB).
C
C         First the range in ln(a) is determined
C         such that the ellipsoid is plotted
C         roughly in the middle of the plot.
      XMIN= AA - 1.25D0
      YMIN=1.3D0
C
      XMAX=XMIN+2.5D0
      YMAX=YMIN+1.0D0
C
      CALL PLIMIT(30.,200.,30.,291.539)
C
C         Write the cross at ln(a)/n.
C
      CALL ULIMIT(XMIN-AA,XMAX-AA,YMIN-BB,YMAX-BB)
      CALL MOVETO(0.0,0.0)
      CALL PEN(3)
      CALL PLTCHR(78)
C
C         Plot the ellipse in Meyer coordinates
C         If DEE = 1 then the diagonals are measured in
C         microns and if DEE = 10 they are measured in
C         tens of microns. The Meyer intercept for the
C         latter case is converted to an interpolated
C         hardness number for a ten micron indentation.
C
      CALL ULIMIT(XMIN,XMAX,YMIN,YMAX)
      CALL PEN(3)
      CALL ELIPS(VAL)
C
C         Plot a box in black.
C
      CALL TRMCHR(3.5,0.,0.,5.)
      CALL ANFREQ(5,10,7,14)
      QQ = CONST/(DEE**2)
      CALL PEN(1)
C
      IF(DEE.NE.10) GOTO 10
      XMIN = DLOG10(QQ*DEXP(XMIN))
      XMAX = DLOG10(QQ*DEXP(XMAX))
      CALL ULIMIT(XMIN,XMAX,YMIN,YMAX)
      CALL BOXLY(0,0)
      XORG = 3.0
      GOTO 15
C
C
   10 IF(DEE.NE.1)  GOTO 100
      CALL BOXXY(0,0)
      XORG = 0.0
C
   15 IF(XORG.LT.XMIN.OR.XORG.GT.XMAX) GOTO 20
      CALL MOVETO(XORG,YMIN)
      CALL DRAWTO(XORG,YMAX)
   20 CONTINUE
C
C         Make user coordinates the same as
C         plotter coordinates and extend the
C         window.
C
      CALL PLIMIT(1.,290.,2.,243.)
      CALL ULIMIT(1.,290.,2.,243.)
C
C         Write the title in red.
C
      CALL PEN(2)
      CALL TEXT(50.,270.,85.,270.,INFO,7)
      CALL TEXT(40.,40.,68.,40.,
     +'PHILIP SARGENT 1979',19)
```



```
C
C         Write the axes labels in red
C
      CALL TRMCHR(2.8,1.4,0.0,3.5)
      CALL LOCCHR(140.,20.0,0)
C
      IF(DEE.NE.1) WRITE(8,30)DEE
   30 FORMAT(1X,I2,' micron hardness'/
     .  18X,'kgf/(mm**2)')
      IF(DEE.EQ.1) WRITE(8,40)
   40 FORMAT(10X,'ln(a)')
C
      CALL PEN(3)
      PB=PROB*100
      CALL LOCCHR(30.0,20.0,0)
      WRITE(8,50)PB
   50 FORMAT(1X,F5.1,'%')
      WRITE(8,60)
   60 FORMAT('  Mean weighted fit.')
      CALL PEN(2)
      IF(IND.EQ.1) WRITE(8,70)
      IF(IND.EQ.2) WRITE(8,80)
   70 FORMAT(10X,'VICKERS indenter')
   80 FORMAT(10X,'KNOOP indenter')
      CALL PEN(3)
      WRITE(8,90)INFO
   90 FORMAT(10X,58A1)
      CALL PEN(2)
      CALL TEXT(16.,170.,16.,194.,
     1'index  n',8)
C
C         Plot four crosses for 'tear-off' markers
C
      CALL PEN(1)
      CALL TRMCHR(3.5,0.0,0.0,5.)
      CALL MOVETO(213.0,3.0)
      CALL PLTCHR(78)
C
      CALL MOVETO(2.0,3.0)
      CALL PLTCHR(78)
C
      RETURN
C
  100 WRITE(6,110)DEE
  110 FORMAT(' +++++ ERROR  DEE = ',I13)
      STOP
C
      END
C
C-----------------------------------------------------------
C
      SUBROUTINE ELIPS(VAL)
C
C         This subroutine plots an ellipse (in
C         green) for a particular confidence
C         limit given by VAL. It calculates
C         this ellipse using the Fisher
C         Information Matrix which is the
C         inverse of the Dispersion, or
C         Covarience, matrix. These matricies
C         and the calculation refer to to a
C         space spanned by the parameters
C         fitted by VC04B and not to the
C         derived parameters: the Meyer  index
C         and intercept. The calculations are
C         transformed to this second space by
C         subroutine  XY.
C
      REAL     ASTD,BSTD,ABCOV
      REAL*8   X1,X2,Y1,Y2,U,V,VAL
      REAL*8 M(2,2),D(2,2),E,F,G,H,EF
      INTEGER NJMP,STAR
C
      COMMON /PIC1/BB,SIGB,AA,SIGA,STAR
      COMMON /VC04D/LP,NDF,CORR,A,B,ASTD,BSTD,ABCOV,
     1RSTD,P,Q,PSTD,QSTD,PQCOV,RHOSTD,XMEAN,YMEAN,
     2XVAR,YVAR,XYCOV
```

```
C
      NJMP=100
C
C           Set up the Fisher matrix
C
      D(1,1) = ASTD*ASTD
      D(2,2) = BSTD*BSTD
      D(1,2) = ABCOV
      D(2,1) = ABCOV
C
      CALL MATI(D,M)
C
      DO 10 J=1,2
C     WRITE(6,20)M(J,1),M(J,2),D(J,1),D(J,2)
   10 CONTINUE
   20 FORMAT(///' M :  ',2(E12.4,3X),'
     1 D :  ',2(E12.4,3X))
C
C           Move to extreme edge of ellipse
C           where dF/dy = 0 where F(x,y)=0
C           is the ellipse.
C
      E = VAL*M(2,2)
      F = M(1,1)*M(2,2) - M(1,2)*M(1,2)
C     WRITE(6,30)E,F
   30 FORMAT(//' VAL*
     1M22 =',E12.4/' M11M22-M12M12 =',E12.4)
      EF=E/F
      IF(EF.LT.1.0D-5.AND.EF.GT.-1.0D-5) X1=0.0D0
      IF(EF.GT.1.0D-5) X1= -DSQRT(EF)
      IF(EF.LT.-1.0D-5) GOTO 110
C
      E = VAL*M(1,2)*M(1,2)/M(2,2)
C     WRITE(6,40)E
   40 FORMAT(' VAL*M12M12/M22 =',E12.4//)
      EF= E/F
      IF(EF.LT.1.0D-5.AND.EF.GT.-1.0D-5) Y1= 0.0D0
      IF(EF.GT.1.0D-5) Y1= DSQRT(EF)
      IF(EF.LT.-1.0D-5) GOTO 110
C
C           Adjust for rounding errors
C
C
C           Plot the ellipse in 2 halves
C
      DO 90 J=1,3,2
      K=2-J
      CALL XY(X1,Y1,U,V)
      CALL MOVETO(U,V)
C     WRITE(6,50)K,X1,Y1,U,V
   50 FORMAT(///' MOVETO: K=',I4/3X,4(E12.4,3X))
C
      PI = 3.1415926
      DO 80 I=1,NJMP
      X2 = X1*COS(I*PI/NJMP)
C     WRITE(6,60)X2
   60 FORMAT(' X2 = ',E12.4)
C
      E = M(2,2) * (M(1,1)*X2*X2 - VAL)
      H = M(2,1)*M(2,1)*X2*X2
C     WRITE(6,70)E,H
   70 FORMAT(
     1' M22 *(M11*X2*X2-VAL) =',E12.4/
     2' M21M21*X2*X2 =',E12.4)
      EF = H - E
      IF(EF.LT.1.0D-5.AND.EF.GT.-1.0D-5) F=0.0D0
      IF(EF.GT.1.0D-5) F=DSQRT(EF)
      IF(EF.LT.-1.0D-5) GOTO 110
      G = -M(2,1)*X2/M(2,2)
      Y2= G + K*F/M(2,2)
      CALL XY(X2,Y2,U,V)
C
      CALL DRAWTO(U,V)
C     WRITE(6,100)I,X2,Y2,U,V
   80 CONTINUE
   90 CONTINUE
  100 FORMAT(' ',I4,3X,4(E12.4,3X)//)
```



```
C
      RETURN
  110 WRITE(6,120)EF
  120 FORMAT(//' URK! -ve argument.',E12.4)
      STOP
C
      END
C
C-----------------------------------------------------------------
C
      SUBROUTINE XY(X,Y,U,V)
C
C           Subroutine to convert from VC04B
C           parameters to "meyer space".
C           Both measured as deviations from the
C           A,B (AA,BB) point.
C
      REAL*8  U,V,X,Y,XX,YY
      COMMON /VC04D/LP,NDF,CORR,A,B,ASTD,BSTD,ABCOV,
     1RSTD,P,Q,PSTD,QSTD,PQCOV,RHOSTD,XMEAN,YMEAN,
     2XVAR,YVAR,XYCOV
C
C           V=Meyer index
C           U = ln(a) = meyer intercept
C
      XX= X + A
      YY= Y + B
      IF(YY.LT.0.01D0) V=100.0D0
      IF(YY.GE.0.01D0) V=1.0D0/YY
      U = -XX*V
C
      RETURN
      END
C
C-----------------------------------------------------------------
C
      SUBROUTINE FVAL(V)
C           This routine supplies the value of twice the
C           F statistic for a probability of 5% (for 95%
C           confidence limits) and degrees of freedom: 2
C           and COUNT-2 .
      INTEGER COUNT
      REAL*8  PROB,V
C
      COMMON /COM1/PROB,COUNT
C
      N=COUNT-2
      V=3.0
      IF(N.LE.0) GO TO 10
      IF(N.LE.90) V=3.
      IF(N.LE.50) V=3.07
      IF(N.LE.50) V=3.15
      IF(N.LE.35) V=3.23
      IF(N.LE.30) V=3.32
      IF(N.LE.24) V=3.4
      IF(N.LE.20) V=3.49
      IF(N.LE.17) V=3.59
      IF(N.EQ.14) V=3.74
      IF(N.EQ.13) V=3.81
      IF(N.EQ.12) V=3.89
      IF(N.EQ.11) V=3.98
      IF(N.EQ.10) V=4.1
      IF(N.EQ.9) V=4.26
      IF(N.EQ.8) V=4.46
      IF(N.EQ.7) V=4.74
      IF(N.EQ.6) V=5.14
      IF(N.EQ.5) V=5.79
      IF(N.EQ.4) V=6.94
      IF(N.EQ.3) V=9.55
      IF(N.EQ.2) V=19.0
      IF(N.EQ.1) V=199.0
C
      V=2*V
      RETURN
C
   10 WRITE(6,20)N
   20 FORMAT(//' +++++ ERROR N.LE.0 N=',I5)
```

```
      STOP 7
C     END
C
C-----------------------------------------------------------
C     SUBROUTINE WEIRD(GRPS,COUNT,INFO,IND)
C
CC        This subroutine plots a hardness/load plot
C
      REAL     MINH,MAXH,MINL,MAXL,OSL(50),DUM,HTOP
      REAL     HARDH(50),HARDL(50),HARDM(50)
      REAL     MEAN(50),SL(50),SIGMA(50),HARD(600)
      REAL     ODIAG(600),OLOAD(600),CHECK,PMAXL
      INTEGER  GRPS,IND,DEE,COUNT,STAR
      LOGICAL*1 INFO(58)
C
      EXTERNAL LINE
      EXTERNAL ODD
      EXTERNAL TML
C
      COMMON /COMO/ODIAG,OLOAD
      COMMON /PIC1/N,SIGB,LNA,SIGA,STAR
      COMMON /PIC2/ SIGMA,MEAN,SL
      COMMON /NEWPIC/ HARDH,HARDL,HARDM
      COMMON /PIC4/ OSL
      COMMON /COM2/CONST
      COMMON /COM3/DEE
      COMMON /COM4/HARD
C
CCC       Set up box size limits on a scale such that
CCC       the plots are always superimposable
C
      CALL TRMCHR(0.,0.,0.,0.)
      CALL BRKPLT(8)
C
CC        Plot two crosses for 'tear-off' markers
C
      CALL TRMCHR(3.5,0.,0.,5.)
      CALL MOVETO(2.0,3.0)
      CALL PLTCHR(78)
C
      CALL MOVETO(213.0,3.0)
      CALL PLTCHR(78)
C
CC        Write a title and labels
C
      CALL PEN(2)
      CALL TEXT(50.,210.,85.,210.,INFO,7)
      CALL TEXT(40.,40.,68.,40.,
     +'PHILIP SARGENT 1979',19)'
      CALL PEN(3)
      CALL TRMCHR(2.8,1.4,0.,3.5)
      CALL LOCCHR(30.,10.,0)
      WRITE(8,30)INFO
   30 FORMAT(1X,58A1)
C
      CALL RMXMN(OSL,GRPS,MINL,MAXL)
      CALL RMXMN(HARDH,GRPS,DUM,MAXH)
      HTOP = 4000.
      IF(MAXH.LE.500.) HTOP=500.
      IF(MAXH.LE.150.) HTOP=150.
      IF(MAXL.GT.100.)MAXL=1000.
      IF(MAXL.LE.100.)MAXL=100.
C
      CALL PLIMIT(30.,200.,30.,230.)
      CALL ULIMIT(0.0,MAXL,0.,HTOP)
C
CC       Plot the points
C
      CALL PEN(3)
      CALL TRMCHR(3.5,0.,0.,5.)
      CALL PLTGXY(OLOAD,HARD,COUNT)
      CALL PLTGXY(OLOAD,HARD,COUNT)
C
```



```
C       Plot the fitted line
C
      CALL PLTFUN(5.0,MAXL,0,ODD)
C
CC          Plot the error bars
C
      CALL PEN(2)
      TIP = 12.*MAXL/1000.
      DO 20 I=1,GRPS
      DO 10 J=1,2
      X1=OSL(I)-TIP
      X2=OSL(I)+TIP
      Y1=HARDL(I)
      Y2=HARDH(I)
      CALL MOVETO(X1,Y1)
      CALL DRAWTO(X2,Y1)
      CALL MOVETO(OSL(I),Y1)
      CALL DRAWTO(OSL(I),Y2)
      CALL MOVETO(X1,Y2)
      CALL DRAWTO(X2,Y2)
   10 CONTINUE
   20 CONTINUE
C
CCC         Plot the Ten Micron Line
CCC
      CALL PEN(2)
      PARMX = CONST*MAXL/100.
      IF(PARMX.GT.HTOP) PARMX = HTOP
      CALL PLTFUN(0.,PARMX,0,TML)
CCC
CCC         Plot the box
C
      CALL PEN(1)
      CALL TRMCHR(3.5,0.,0.,5.)
      CALL ANFREQ(5,10,5,10)
      CALL BOXXY(0,0)
C
      CALL PEN(2)
      IF(IND.EQ.1) CALL TITLE('HARDNESS/LOAD PLOT',18,
     1'LOAD IN GRAM.F.',15,'VICKERS HARDNESS NUMBER',23)
C
      IF(IND.EQ.2) CALL TITLE('HARDNESS/LOAD PLOT',18,
     1'LOAD IN GRAM.F.',15,'KNOOP HARDNESS NUMBER',21)
C
      CALL ULIMIT(30.,200.,30.,230.)
C
CCC         Now plot hardness versus diagonals
C
      CALL TRMCHR(0.,0.,0.,0.)
      CALL BRKPLT(8)
      CALL PLIMIT(0.,250.,0.,250.)
      CALL ULIMIT (0.,250.,0.,250.)
C
CC          Plot four crosses for 'tear-off' markers
C
      CALL TRMCHR(3.5,0.,0.,5.)
      CALL MOVETO(2.0,3.0)
      CALL PLTCHR(78)
C
      CALL MOVETO(213.0,3.0)
      CALL PLTCHR(78)
C
      CALL MOVETO (2.0,257.)
      CALL PLTCHR(78)
C
      CALL MOVETO(213.,257.)
      CALL PLTCHR(78)
C
      CALL PEN(2)
      CALL TEXT(40.,40.,68.,40.,
     +'PHILIP SARGENT 1979',19)'
C
CCC         Write a title and labels
C
      CALL TEXT(50.,210.,85.,210.,INFO,7)
```

```
      CALL PEN(3)
      CALL TRMCHR(2.8,1.4,0.,3.5)
      CALL LOCCHR(30.,10.,0)
      WRITE(8,40)INFO
   40 FORMAT(1X,58A1)
C
      MAXD=70.
      CALL PLIMIT(30.,598.,30.,230.)
      CALL TRMCHR(3.5,0.,0.,5.)
      CALL ULIMIT(0.,MAXD,0.,HTOP)
C
C         Plot the Ten Micron Line
C
      CALL MOVETO(10.,0)
      CALL DRAWTO(10.,HTOP)
C
      CALL PEN(2)
      CALL PLTGXY(ODIAG,HARD,COUNT)
      CALL PLTGXY(ODIAG,HARD,COUNT)
      CALL PLTFUN(1.,MAXD,0,LINE)
      CALL PEN(1)
      CALL BOXXY(0,0)
C
      CALL PEN(2)
      IF(IND.EQ.1) CALL TITLE('HARDNESS/DIAGONAL PLOT',
     +22,'DIAGONALS IN MICRONS',20,
     +'VICKERS HARDNESS NUMBER',23)
C
      IF(IND.EQ.2) CALL TITLE('HARDNESS/DIAGONAL PLOT',
     +22,'DIAGONALS IN MICRONS',20,
     +'KNOOP HARDNESS NUMBER',21)
C
      RETURN
C
      END
C
C-----------------------------------------------------------
C
      SUBROUTINE ODD(PARM,LOAD,H)
C
C      Subroutine to return H and LOAD values to plot
C      the fitted Meyer line.
C
      REAL    LNA,SIGA,N,SIGB,CONST,LOAD,H
      INTEGER DEE,STAR
C
      COMMON /PIC1/N,SIGB,LNA,SIGA,STAR
      COMMON /COM2/CONST
      COMMON /COM3/DEE
C
      LOAD = PARM
      H = ALOG(CONST/(DEE*DEE)) +
     1    (1. - 2./N)*ALOG(LOAD) +
     2    (2./N)*LNA
      H = EXP(H)
C
      RETURN
      END
C
C-----------------------------------------------------------
C
      SUBROUTINE LINE(PARM,DIAG,H)
C
C         Subroutine to return H and DIAG values to plot
C         the fitted Meyer line.
C
      REAL LNA,SIGA,N,SIGB,CONST,PARM,DIAG,H
      INTEGER DEE,STAR
C
      COMMON /PIC1/N,SIGB,LNA,SIGA,STAR
      COMMON /COM2/CONST
      COMMON /COM3/DEE
C
      DIAG = PARM
      H = ALOG(CONST) - N*ALOG(FLOAT(DEE)) +
     +    LNA + (N -2.)*ALOG(DIAG)
      H = EXP(H)
```



```
C
      RETURN
      END
C
C-----------------------------------------------------------
C
      SUBROUTINE TML(PARM,LOAD,H)
C
C         To plot the Ten Micron Line on an H/Load plot
C
      REAL PARM,LOAD,H,CONST
C
      COMMON /COM2/CONST
C
      H = PARM
      LOAD = H*100./CONST
C
      RETURN
      END
```

Program MERGE

```
C
C       Program to merge two sets of data
C
C       Philip Sargent          9 June - 8 July 1977
C       Dept. Metallurgy and Materials Science
C       Cambridge.
C
      REAL    DIAG(200,3),SL(50,3)
      INTEGER INFO(58),COUNT(3),NUM(4),GRPS(3)
      INTEGER TEST,DOL,HASH,N(50,3)
C
      DATA DOL,HASH/1H$,1H#/
C
C
C       Read the data
C
      DO 60 K=1,2
      GRPS(K) = 0
      COUNT(K)=0
      READ(K,10,END=260)INFO
   10 FORMAT(58A1)
C
   20 GRPS(K) = GRPS(K) + 1
      READ(K,*,END=270) SL(GRPS(K),K)
      READ(K,*,END=280) NUM(K)
      N(GRPS(K),K) = NUM(K)
C
C
      M=NUM(K)
      DO 30 J=1,M
      M2=COUNT(K)+J
      READ(K,*,END=290) DIAG(M2,K)
   30 CONTINUE
C
C
      READ(K,40,END=300) TEST
   40 FORMAT(A4)
      IF(TEST.EQ.DOL) GOTO 50
      IF(TEST.NE.HASH) GOTO 310
      COUNT(K)=COUNT(K)+NUM(K)
      IF(GRPS(K).GT.49) GOTO 320
      IF(COUNT(K).GT.199) GOTO 330
      GOTO 20
C
C       The program skips to 50 when all
C       the data has been read in with no
C       formatting errors.
C
   50 CONTINUE
      COUNT(K)=COUNT(K)+NUM(K)
C
   60 CONTINUE
C
C       Now do the merge, first the sets at the
C       same load.
C
      NUM(3)=0
      NUM(1)=0
      M=0
      GRPS(3)=0
C
      M=GRPS(1)
      M2=GRPS(2)
      DO 110 I=1,M
C
      NUM(2)=0
C
      DO 100 J=1,M2
C
      IF(SL(J,2).NE.SL(I,1)) GOTO 90
      GRPS(3)=GRPS(3)+1
      SL(GRPS(3),3) = SL(J,2)
      SL(J,2) = -2.0
      SL(I,1) = -1.0
C
      M3=N(I,1)
      DO 70 K=1,M3
      DIAG(NUM(3)+K,3) = DIAG(NUM(1)+K,1)
      DIAG(NUM(1)+K,1) = 0.0
   70 CONTINUE
      NUM(3) = NUM(3) + N(I,1)
      M3=N(J,2)
      DO 80 K=1,M3
      DIAG(NUM(3)+K,3) = DIAG(NUM(2)+K,2)
      DIAG(NUM(2)+K,2) = 0.0
   80 CONTINUE
      NUM(3) = NUM(3) + N(J,2)
      N(GRPS(3),3)= N(I,1) + N(J,2)
C
   90 NUM(2) = NUM(2) + N(J,2)
C
  100 CONTINUE
C
      NUM(1)=NUM(1)+N(I,1)
  110 CONTINUE
C
C
C       Now empty the rest of diag(1) and diag(2)
C       directly into diag(3) one at a time
C
      DO 120 I=1,10
  120 CONTINUE
C
      DO 160 K=1,2
      NUM(K)=0
      M=GRPS(K)
      DO 150 I=1,M
      IF(SL(I,K).EQ.-1.0) GOTO 140
      IF(SL(I,K).EQ.-2.0) GOTO 140
      GRPS(3) = GRPS(3) + 1
      N(GRPS(3),3) = N(I,K)
      SL(GRPS(3),3) = SL(I,K)
C
      M2=N(I,K)
      DO 130 J=1,M2
      DIAG(NUM(3)+J,3) = DIAG(NUM(K)+J,K)
  130 CONTINUE
C
      NUM(3) = NUM(3) + N(I,K)
  140 NUM(K)=NUM(K) + N(I,K)
  150 CONTINUE
  160 CONTINUE
C
C       Now write out the new data onto unit 3
C       from diag(3), sl(3), and n(3) .
C
      NUM(4) = NUM(3)
      NUM(3) = 0
      M=GRPS(3)
C
      DO 180 I=1,M
C
      WRITE(3,200) SL(I,3)
      WRITE(3,240) N(I,3)
      M2=N(I,3)
C
      DO 170 J=1,M2
      WRITE(3,210) DIAG(NUM(3)+J,3)
  170 CONTINUE
C
      NUM(3) = NUM(3) + N(I,3)
      IF(NUM(3).GE.NUM(4)) GOTO 190
      WRITE(3,230)
```

```
143  C
144     180 CONTINUE
145  C
146     190 WRITE(3,220)
147  C
148     200 FORMAT(F6.1)
149     210 FORMAT(F6.2)
150     220 FORMAT('$')
151     230 FORMAT('#')
152     240 FORMAT(I2)
153  C
154  C
155  C
156         WRITE(6,250)
157     250 FORMAT(////' All data manipulation completed.')
158  C
159         STOP
160  C
161  C          Error messages
162  C
163     260 WRITE(6,340)
164         STOP
165     270 WRITE(6,350) GRPS(K),K
166         STOP
167     280 WRITE(6,360) GRPS(K),K
168         STOP
169     290 WRITE(6,370) GRPS(K),K
170         STOP
171     300 WRITE(6,380) GRPS(K),K
172         STOP
173     310 WRITE(6,390) GRPS(K),K
174         STOP
175     320 WRITE(6,400) GRPS(K),K
176         STOP
177     330 WRITE(6,410) GRPS(K),K
178         STOP
179  C          Format statements for error messages
180  C
181     340 FORMAT(/1X,'##### ERROR #####',
182        1' No data found')
183     350 FORMAT(/1X,'##### ERROR #####',
184        1' End of data found where a LOAD value expected',2I4)

185     360 FORMAT(/1X,'##### ERROR #####',
186        1' End of data found where a NUM value expected',2I4)

187     370 FORMAT(/1X,'##### ERROR #####',
188        1' End of data found where a DIAG value expected',2I4)

189     380 FORMAT(/1X,'##### ERROR #####',
190        1' End of data found where # or $ expected',2I4)
191     390 FORMAT(/1X,'##### ERROR #####',
192        1' # expected but not found, NUM is wrong',2I4)
193     400 FORMAT(/1X,'##### ERROR #####',
194        1' GRPS greater than 49 and no end of data in sight',
                                                        2I4)
195     410 FORMAT(/1X,'##### ERROR #####',
196        1' COUNT greater than 199 and no end of data in sight',
                                                        2I4)
197  C
198         END
```

I.III - KHAMM Hardness Anisotropy Model

This model is described in detail in section 2.4.2 and, briefly, in Sawyer et al.(1979). The original version was written in 1975 using the theory of Brookes et al.(1971) but since then the extensions and revisions discussed in 2.4.2 have been added and it has been adapted to predict Vickers, as well as Knoop, microhardness anisotropy.

```
C
C           KHAMM
C
C           Knoop  Hardness  Anisotropy  Model  -  Monocrystals
C
C
C           This program  calculates and plots  the anisotropy in
C           the effective resolved shear stress,tau,on the facets
C           of a Knoop microhardness indenter.
C           It is based, largely, on my third-year  undergraduate
C           project (Part II Materials Science 1974-1975).
C           The theory was developed by  C.A.Brookes, J.B.O'Neill
C           and B.A.W.Redfern ; B.Moxley's Ph.D. thesis  contains
C           a similar computer treatment.
C
C                                                    Philip Sargent
C                                                  May 1975 Cambridge
C
C
C           Updated 23/3/1979
      BLOCK DATA
C
      INTEGER SN(4),SD(4),IP1(4),SYS,PYRAM,SAXIS,ID(4),DIVIS,CF
      REAL    PI,ABC(3),ANGLES(3),FR1,FR2
      REAL*8  IDR(3)
      LOGICAL XDASH,ARNELL,SESS,SSUPER,FSUPER,ONEP,BLACK
C
      COMMON /COM1/SN,SD,SYS,IP1
      COMMON /COM2/ABC,ANGLES
      COMMON /COM3/PI
      COMMON /COM6/ID,IDR
      COMMON /COM10/PLT1,PLT2
      COMMON /COM11/XDASH,ARNELL
      COMMON /COM12/DIVIS
      COMMON /COM13/SESS,SSUPER,FSUPER,ONEP
      COMMON /COM14/CF,PYRAM,SAXIS
      COMMON /COM15/FR1,FR2
      COMMON /COM16/BLACK
C           ABC are the lattice parameters
C           SN and SD are the slip plane and slip direction
C           respectively (in Miller indicies)
C           IP1 is the indentation plane on the monocrystal.
C           SYS is an integer denoting the crystal system (1-7)
C           ID is the direction (Miller indicies) of the
C           indenter at the zero angle alpha position
C           PI is 3.141593
C
      DATA IP1/0,0,1,0/
      DATA SN/0,0,1,0/
      DATA SD/1,-1,0,0/
      DATA SYS/1/
      DATA ABC/1.0,1.0,1.0/
      DATA PLT1,PLT2/0.3,0.3/
      DATA XDASH/.FALSE./
      DATA ARNELL/.TRUE./
      DATA ID /0,0,1,0/
      DATA DIVIS/<DIVIS$91>/
      DATA SESS,SSUPER,FSUPER/<SESS$F>,<SSUPER$T>,<FSUPER$T>/
      DATA ONEP/<ONEP$F>/
      DATA CF/<CF$1>/
      DATA FR1,FR2/<FR1$0.>,<FR2$100.>/
      DATA PYRAM/<PYRAM$2>/
      DATA SAXIS/<SAXIS$1>/
      DATA PI/3.141593/
C
      END
C
C
C
      CALL MAIN
      STOP
      END
C
C-----------------------------------------------------------------
C
      SUBROUTINE MAIN
C
```



```
C           This subroutine  directs the  flow of command  to the
C           subroutines  designed to deal with the specific syste
C           of crystal under test.
C
      INTEGER SN(4),SD(4),IP1(4),SYS
C
      COMMON /COM1/SN,SD,SYS,IP1
C
      GOTO (10,20,30,40,50,60,70),SYS
   10 CALL CUB
      RETURN
   20 CALL HEX
      RETURN
   30 CALL TET
      RETURN
   40 CALL ORTH
      RETURN
   50 CALL TRIG
      RETURN
   60 CALL MONO
      RETURN
   70 CALL TRIC
      RETURN
      END
C
C-----------------------------------------------------------------
C
      SUBROUTINE CUB
C
C           This subroutine organises the derivation of sym-
C           -metrically identical slip systems. It calls TAU
C           to calculate the effective critical resolved shear
C           stress factor (TAU) for all 4 facets of the
C           indenter.
C
      INTEGER SN(4),SD(4),IPI(4),SYS,DIVIS
      REAL    RESULT(4,91),FR1,FR2,PI,INDESS(4,91)
      REAL    TAU(4),TEMP,QURT
      REAL*8  IPR(3),S(6),IDR(3),ALPHA,DPI
      INTEGER TOTSN(3,18),TOTSD(3,18),NSN,NSD,DT,ZERO
      INTEGER CSN(3),CSD(3),ID(4)
      LOGICAL XDASH,ARNELL,SESS,SSUPER,FSUPER,ONEP
C
      COMMON /COM1/SN,SD,SYS,IPI
      COMMON /COM3/PI
      COMMON /COM4/IPR
      COMMON /COM5/RESULT
      COMMON /COM6/ID,IDR
      COMMON /COM8/INDESS
      COMMON /COM9/TOTSN,TOTSD
      COMMON /COM11/XDASH,ARNELL
      COMMON /COM12/DIVIS
      COMMON /COM13/SESS,SSUPER,FSUPER,ONEP
      COMMON /COM15/FR1,FR2
      COMMON /COM20/DPI
C
      DPI = DACOS(0.0D0)*2
      WRITE(6,*)DPI
      SYS=1
      QURT=0.25
      DO 10 I=1,3
      CSN(I)=SN(I)
      CSD(I)=SD(I)
      IPR(I)=DFLOAT(IPI(I))
   10 CONTINUE
      CALL NORM(IPR(1),IPR(2),IPR(3))
C
C           This next bit calculates the vector ID (i.e.
C           the vector x') the crystallographic direction
C           on the surface of the crystal where the angle
C           ALPHA is zero.
C
C           If the vector x' has been set specifically
C           then that vector is used.
      IF(.NOT.XDASH) GOTO 70
      J=0
      DO 50 I=1,3
```

```
      J = J + ID(I)*IPI(I)
   50 CONTINUE
      IF(J.EQ.0) GOTO 80
C
      WRITE(6,60)ID,IPI
   60 FORMAT(//' Vector ID not in Plane IP'/
     1' ID: ',3I5,' IP: ',3I5)
      XDASH = .FALSE.
   70 ID(1)=IPI(3)
      ID(2)=0
      ID(3)=-IPI(1)
C
   80 CONTINUE
C
C           This next section mixes up the slip plane and slip
C           direction indicies, returning all possible sym-
C           -metrical slip plane normals in TOTSN and all
C           possible slip directions in TOTSD. In each array
C           there are NSN & NSD entries respectively.
C
      CALL MIXUP(CSN,TOTSN,NSN)
      CALL MIXUP(CSD,TOTSD,NSD)
      NSN=NSN-1
      NSD=NSD-1
C
C           This next section combines slip plane normals and
C           slip directions into all possible slip systems.
C
      ZERO=0
      DO 20 JJ=1,DIVIS
      RESULT(1,JJ)=0.0
      RESULT(2,JJ)=0.0
      RESULT(3,JJ)=0.0
      RESULT(4,JJ)=0.0
   20 CONTINUE
      DO 130 I=1,NSN
      DO 120 J=1,NSD
C
C           This checks that the slip system is 'legal', i.e.
C           that SN & SD are orthogonal.
C
      DT=ZERO
      DT=TOTSN(1,I)*TOTSD(1,J)
      DT=TOTSN(2,I)*TOTSD(2,J)+DT
      DT=TOTSN(3,I)*TOTSD(3,J)+DT
      IF(DT.NE.ZERO) GOTO 120
C
C           This puts the slip system into the right format
      DO 30 K=1,3
      S(K)  =DFLOAT(TOTSN(K,I))
      S(K+3)=DFLOAT(TOTSD(K,J))
   30 CONTINUE
      CALL NORM(S(1),S(2),S(3))
      CALL NORM(S(4),S(5),S(6))
C
      WRITE(6,40) (TOTSN(K,I),K=1,3),(TOTSD(K,J),K=1,3)
   40 FORMAT(/1X,'(',3(I3,1X),')',3X,'[',3(I3,1X),']')
C
      DO 90 K=1,3
      IDR(K) = DFLOAT(ID(K))
   90 CONTINUE
C
      CALL NORM(IDR(1),IDR(2),IDR(3))
C
C           This DO-loop cycles through all DIVIS angles
C
      DO 110 L=1,DIVIS
C
      ALPHA=0.5D0*PI*(L-1)/(DIVIS-1)
C
      CALL CALC(ALPHA,S,TAU)
C
C           This next bit stores the maximum value of TAU for
C           all slip systems (for every facet and angle) in
C           RESULT.
C
      DO 100 M=1,4
```



```
      INDESS(M,L)=TAU(M)
      IF(TAU(M).LT.RESULT(M,L)) GOTO 100
      RESULT(M,L)=TAU(M)
  100 CONTINUE
C
  110 CONTINUE
      IF(SESS) CALL GRAFT(4,1,I,J,.FALSE.,SSUPER)
C
  120 CONTINUE
  130 CONTINUE
C
C
C           This next bit sends  RESULT (containing the four
C           TAUmaxs  for every one  of the DIVIS angles)  to be
C           plotted; firstly the four separately,then a mean
C           value. The second number in the  parameter list
C           for GRAFT is the ink colour:- 1 (black), 2 (red),
C           and 3 for green.
      IF(ARNELL) GOTO 180
      IF(.NOT.ONEP) CALL GRAFT(4,2,1,1,.TRUE.,FSUPER)
      DO 170 L=1,DIVIS
      TEMP=0.0
      DO 160 M=1,4
      TEMP=QURT*RESULT(M,L)+TEMP
  160 CONTINUE
      RESULT(1,L)=TEMP
  170 CONTINUE
      CALL GRAFT(1,3,1,1,.TRUE.,.TRUE.)
C
      RETURN
C
  180 CONTINUE
      DO 185 L=1,DIVIS
C
      DO 184 M=1,4
      IF(RESULT(M,L).GT.0.000001) RESULT(M,L)=1.0/RESULT(M,L)
      IF(RESULT(M,L).LT.0.000001) RESULT(M,L)=FR2
  184 CONTINUE
  185 CONTINUE
C
      IF(.NOT.ONEP)CALL GRAFT(4,2,1,1,.TRUE.,FSUPER)
C
      DO 190 L=1,DIVIS
      TEMP = RESULT(1,L)+RESULT(2,L)+RESULT(3,L)+RESULT(4,L)
      RESULT(1,L) = TEMP
      IF(TEMP.GE.FR2) RESULT(1,L)=FR2
  190 CONTINUE
      CALL GRAFT(1,3,1,1,.TRUE.,.TRUE.)
C
      RETURN
      END
C
C
C
C
C-----------------------------------------------------------------------
C
      SUBROUTINE MIXUP(HKL,TOTAL,F2)
C
C           This subroutine mixes up the three integers in HKL
C           with themselves and their negatives.It returns all
C           permutations in TOTAL,which then contains (F2-1)
C           values.
C
      INTEGER HKL(3),TOTAL(3,18),F1,F2
C
C           Initialisation
C
      F1=0
      F2=2
C
      DO  10 I=1,3
      TOTAL(I,1)=HKL(I)
   10 CONTINUE
C
C           F1 is the flag used for checking a new HKL set
C           F2 is the number of HKLs in total so far
```

```
C
C
      DO 80 I1=1,2
            This DO-loop swaps HKL(1) with HKL(2)
C
C
   20 DO 70 I3=1,2
            This DO-loop does the negation twice
C
C
   30 DO  60 N=1,3
            This DO-loop negates the indices from the left
C
C
      HKL(N)=-HKL(N)
C
   40 DO 50 I2=1,3
                  This DO-loop rotates the indicies
C
C
      CALL CHECK(HKL,F2,TOTAL)
C
C
      II1=HKL(1)
      II2=HKL(2)
      II3=HKL(3)
      HKL(2)=II1
      HKL(3)=II2
      HKL(1)=II3
   50 CONTINUE
   60 CONTINUE
   70 CONTINUE
C
C           Now do the interchanging of the first 2 indices
C
      II1=HKL(1)
      II2=HKL(2)
      HKL(1)=II2
      HKL(2)=II1
C
   80 CONTINUE
      RETURN
      END
C
C-----------------------------------------------------------------
C
      SUBROUTINE HEX
C
C          This subroutine  organises the derivation  of sym-
C          -metrically identical  slip systems. It calls CALC
C          to calculate the effective critical resolved shear
C          stress factor (TAU) for all 4 facets of the
C          indenter.
C
      INTEGER SN(4),SD(4),IPI(4),SYS,S1(4),DIVIS
      REAL    ABC(3),ANGLES(3),PI,INDESS(4,181),FR1,FR2
      INTEGER TOTSN(3,18),TOTSD(3,18),NSN,NSD,DT,TEST
      INTEGER CSN(3),CSD(3),ID(4)
      REAL    TAU(4),RESULT(4,181),TEMP,QURT
      REAL*8 IPR(3),S(6),S2(3),IDR(3),ALPHA,DPI
      LOGICAL XDASH,ARNELL,SESS,SSUPER,FSUPER,ONEP
C
      COMMON /COM1/SN,SD,SYS,IPI
      COMMON /COM2/ABC,ANGLES
      COMMON /COM3/PI
      COMMON /COM4/IPR
      COMMON /COM5/RESULT
      COMMON /COM6/ID,IDR
      COMMON /COM8/INDESS
      COMMON /COM9/TOTSN,TOTSD
      COMMON /COM11/XDASH,ARNELL
      COMMON /COM12/DIVIS
      COMMON /COM13/SESS,SSUPER,FSUPER,ONEP
      COMMON /COM15/FR1,FR2
      COMMON /COM20/DPI
C
      SYS=2
      DPI = DARCOS(0.0D0)*2
      WRITE(6,*)DPI
C
      DT= SN(1)+SN(2)+SN(3)
```



```
      IF(DT.NE.0) WRITE(6,10)SN
      DT= SD(1)+SD(2)+SD(3)
      IF(DT.NE.0) WRITE(6,10)SD
   10 FORMAT(1X,'#####ERROR#####',10X,'Malformed ',
     1'Hexagonal indicies; first three :- ',3I5)
C
      DO 20 I=1,3
      CSN(I)=SN(I)
      CSD(I)=SD(I)
   20 CONTINUE
C
      CALL PERM(CSN,TOTSN,NSN,SN(4))
      CALL PERM(CSD,TOTSD,NSD,SD(4))
C
      TEST=-(SN(4)*SD(4))
      QURT=0.25
      DO 30 JJ=1,DIVIS
      RESULT(1,JJ)=0.0
      RESULT(2,JJ)=0.0
      RESULT(3,JJ)=0.0
      RESULT(4,JJ)=0.0
   30 CONTINUE
C
C          This next line transforms the indentation
C          plane into cartesian axes which are used
C          by TWIST
      CALL CHANGE(IPI,IPR)
C
C          This next section calculates the vector ID (i.e.
C          the vector x') the crystallographic direction
C          on the surface of the crystal where the angle
C          ALPHA is zero.
C          The following is all done in integers using
C          Miller indicies :-
C          x' always lies in the plane of x and z',where z' is
C          vector IP (IPI in indicies and IPR in cartesian
C          coordinates).
C
C          x',z'=0
C          x'(1)+x'(2)+x'(3)=0
C          z'(1)+z'(2)+z'(3)=0
C
C          However, if the vector x' has been set, that
C          is used instead.
      IF(.NOT.XDASH) GOTO 60
      J=0
      DO 40 I=1,4
      J = J + ID(I)*IPI(I)
   40 CONTINUE
      IF(J.EQ.0) GOTO 70
C
      WRITE(6,50)ID,IPI
   50 FORMAT(//' Vector ID not in Plane IP'/
     1' ID: ',3I5,' IP: ',3I5)
C
      XDASH = .FALSE.
   60 ID(1)= IPI(4)*2
      ID(2)=-IPI(4)
      ID(3)=-IPI(4)
      ID(4)=-IPI(1)*2
C
   70 CONTINUE
      CALL CHANGE(ID,IDR)
C
      DO 150 I=1,NSN
      DO 140 J=1,NSD
C
C          This checks that the slip-system formed is
C          legal; i.e. that  SD lies in the slip-plane
C
C
      DT=TOTSN(1,I)*TOTSD(1,J)
      DT=TOTSN(2,I)*TOTSD(2,J)+DT
      DT=TOTSN(3,I)*TOTSD(3,J)+DT
      IF(DT.NE.TEST) GOTO 140
      WRITE(6,80)(TOTSN(K,I),K=1,3),SN(4),(TOTSD(K,J),K=1,3),SD(
                                                              4)
```

```
   80 FORMAT(/1X,'(',4(I3,1X),')',3X,'[',4(I3,1X),']')
C
CC          This next section transforms the 4-index
CC          Miller's indicies into cartesian axes which
CC          are used by CALC.
C
      DO 90 K=1,3
      S1(K)=TOTSN(K,I)
   90 CONTINUE
C
      S1(4)=SN(4)
C
C
      CALL CHANGE(S1,S2)
      DO 100 L=1,3
      S(L)=S2(L)
  100 CONTINUE
C
      DO 110 K=1,3
      S1(K)=TOTSD(K,J)
  110 CONTINUE
      S1(4)=SD(4)
C
      CALL CHANGE(S1,S2)
      S(4)=S2(1)
      S(5)=S2(2)
      S(6)=S2(3)
C
      CALL NORM(S(4),S(5),S(6))
C
CC          This DO-loop cycles through all DIVIS angles (0 to 90
C        degrees)
C
      DO 130 L=1,DIVIS
C
      ALPHA=0.5D0*PI*(L-1)/(DIVIS-1)
C
      CALL CALC(ALPHA,S,TAU)
C
CC          This next bit stores the maximum value of TAU for
CC          all slip systems (for every facet and angle) in
CC          RESULT.
C
      DO 120 M=1,4
      INDESS(M,L)=TAU(M)
      IF(TAU(M).LT.RESULT(M,L)) GOTO 120
      RESULT(M,L)=TAU(M)
  120 CONTINUE
C
  130 CONTINUE
      IF(SESS) CALL GRAFT(4,1,I,J,.FALSE.,SSUPER)
C
  140 CONTINUE
  150 CONTINUE
C
CCC         This next bit sends  RESULT (containing the four
CCC         TAUmaxs  for every one  of the DIVIS angles)  to be
CCC         plotted; firstly the four separately,then a mean
CC          value. The second  number in the  parameter list
CC          for GRAFT is the ink colour;1 for black,2 for red,
C           and 3 for green.
      IF(ARNELL) GOTO 180
      IF(.NOT.ONEP) CALL GRAFT(4,2,1,1,.TRUE.,FSUPER)
      DO 170 L=1,DIVIS
      TEMP=0.0
      DO 160 M=1,4
      TEMP=QURT*RESULT(M,L)+TEMP
  160 CONTINUE
      RESULT(1,L)=TEMP
  170 CONTINUE
      CALL GRAFT(1,3,1,1,.TRUE.,.TRUE.)
C
      RETURN
C
  180 CONTINUE
      DO 185 L=1,DIVIS
C
```



```
      DO 184 M=1,4
      IF(RESULT(M,L).GT.0.000001) RESULT(M,L)=1.0/RESULT(M,L)
      IF(RESULT(M,L).LT.0.000001) RESULT(M,L)=FR2
  184 CONTINUE
  185 CONTINUE
C
      IF(.NOT.ONEP)CALL GRAFT(4,2,1,1,.TRUE.,FSUPER)
C
      DO 190 L=1,DIVIS
      TEMP = RESULT(1,L)+RESULT(2,L)+RESULT(3,L)+RESULT(4,L)
      RESULT(1,L) = TEMP
      IF(TEMP.GE.FR2) RESULT(1,L)=FR2
  190 CONTINUE
      CALL GRAFT(1,3,1,1,.TRUE.,.TRUE.)
C
      RETURN
      END
C
C
C
C
C-----------------------------------------------------------------
C
      SUBROUTINE CHANGE(S1,S2)
C
CC          This subroutine changes the Miller indicies
CC          supplied into the correct crystallographic
CC          vector components (for plane indicies only).
C
      INTEGER SN(4),SD(4),IPI(4),SYS,S1(4)
      REAL    PI,ANGLES(3),ABC(3)
      REAL*8  S2(3),S3(3),A22,A12,A13,A21
C
      COMMON /COM1/SN,SD,SYS,IPI
      COMMON /COM2/ABC,ANGLES
      COMMON /COM3/PI
C
      S2(1)=S1(1)/ABC(1)
      S2(2)=(2*S1(2)+S1(1))/(1.732051*ABC(1))
      S2(3)=S1(4)/ABC(3)
      CALL NORM(S2(1),S2(2),S2(3))
C
      A21= 0.70710678D0
      A22=-0.40824829D0
      A12= 0.81649658D0
      A13= 0.57735026D0
C
      S3(1) =                S2(2)*A12 + S2(3)*A13
      S3(2) = -S2(1)*A21 + S2(2)*A22 + S2(3)*A13
      S3(3) =  S2(1)*A21 + S2(2)*A22 + S2(3)*A13
C
      S2(1)=S3(1)
      S2(2)=S3(2)
      S2(3)=S3(3)
      CALL NORM(S2(1),S2(2),S2(3))
C
      RETURN
      END
C
C
C
C
C-----------------------------------------------------------------
C
      SUBROUTINE PERM(HKL,TOTAL,F2,ZAX)
C
CC          This subroutine permutes the three integers in
CC          HKL with themselves. It returns all permutations
CC          in TOTAL,which then contains (F2-1) values.
C
      INTEGER HKL(3),TOTAL(3,18),F2,ZAX
C
CC          Initialisation
C
      F2=2
C
      DO  10 I=1,3
```

```
      TOTAL(I,1)=HKL(I)
   10 CONTINUE
C
CC          F2 is the number of HKLs in total so far
CC
C
      DO 30 I1=1,2
            This DO-loop swaps HKL(1) with HKL(2)
C
      DO 20 I2=1,3
                  This DO-loop rotates the indicies
C
      CALL CHECK(HKL,F2,TOTAL)
C
      II1=HKL(1)
      II2=HKL(2)
      II3=HKL(3)
      HKL(2)=II1
      HKL(3)=II2
      HKL(1)=II3
   20 CONTINUE
C
CC          Now do the interchanging of the first 2 indices
C
      II1=HKL(1)
      II2=HKL(2)
      HKL(1)=II2
      HKL(2)=II1
C
   30 CONTINUE
C
CC          This section copies a negated set of indicies except
CC          when all three zero.
C
      IF(ZAX.NE.0) GOTO 40
      F2=F2-1
      RETURN
   40 K=F2-1
      J=2*K
C
      DO 50 I3=F2,J
C
      TOTAL(1,I3)=-TOTAL(1,I3-K)
      TOTAL(2,I3)=-TOTAL(2,I3-K)
      TOTAL(3,I3)=-TOTAL(3,I3-K)
   50 CONTINUE
C
      F2=J
C
      RETURN
      END
C
CC-----------------------------------------------------------------
C
      SUBROUTINE CALC(ALPHA,S,TAU)
C
CC          S is the slip system
CC          CPHI is COS(angle) between FVEC & SN
CC          CLAMDA is the COS(angle) between FVEC & SD
CC          CPSI is the COS(angle) between ARVEC & HVEC
CC          CGAMMA is the COS(angle) between SD & HVEC
CC          BOR is the Brookes,O'Neill and Redfern factor.
C
      INTEGER FACET,CF,PYRAM,SAXIS
      REAL*8 CG2,HVEC(3),FVEC(3),ARVEC(3),S(6),SN(3),SD(3)
      REAL*8 CPHI,CLAMDA,CPSI,CGAMMA,BOR,SGAMMA,ALPHA,DOT
      REAL*8 GAMMA,PSI,PI
      REAL TAU(4)
C
      COMMON /COM14/CF,PYRAM,SAXIS
      COMMON /COM20/PI
C
      DO 60 FACET=1,4
C
      CALL HALPHA(ALPHA,HVEC,FACET,PYRAM)
```



```
      CALL FALPHA(ALPHA,FVEC,FACET,PYRAM,SAXIS)
C
CC          AR is at right angles to  SD and SN
CC          AR is the axis about which the slip plane rotates
CC          ARVEC is the vector product of SD & SN and
CC          is therefore the same for all FACETS.
C
      ARVEC(1)=S(5)*S(3)-S(6)*S(2)
      ARVEC(2)=S(6)*S(1)-S(4)*S(3)
      ARVEC(3)=S(4)*S(2)-S(5)*S(1)
      CALL NORM(ARVEC(1),ARVEC(2),ARVEC(3))
C
      DO 10 JL=1,3
      SN(JL)=S(JL)
      SD(JL)=S(JL+3)
   10 CONTINUE
C
      CPHI=DOT(FVEC,SN)
      CLAMDA=DOT(FVEC,SD)
      CPSI = DOT(HVEC,ARVEC)
   20 CGAMMA=DOT(SD,HVEC)
C
      X89 = 89*PI/180
      IF(ALPHA.EQ.0.0.OR.ALPHA.GT.X89) WRITE(6,*)ALPHA,SN,SD,
     +ARVEC,HVEC,FVEC,CPHI,CLAMDA,CPSI,CGAMMA
C
CC          Test to see whether SIN(gamma) = 1.0
C
      CG2=DABS(1.0D0-CGAMMA*CGAMMA)
      IF(CG2.LE.0.000000001D0)GOTO 30
      CG2=DSQRT(CG2)
   30 SGAMMA=CG2
      IF(CF.EQ.1) BOR = 0.5D0*(SGAMMA + CPSI)
C
      IF(CF.NE.2) GOTO 40
      SGAMMA = DSQRT(SGAMMA)
      SGAMMA = DSQRT(SGAMMA)
      CPSI = DSQRT(CPSI)
      CPSI = DSQRT(CPSI)
      BOR = 0.5D0*(SGAMMA + CPSI)
   40 CONTINUE
C
      IF(CF.EQ.3) BOR = 0.5D0*(SGAMMA**4 + CPSI**4)
C
      IF(CF.NE.4) GOTO 50
      SGAMMA = DSQRT(SGAMMA)
      SGAMMA = DSQRT(SGAMMA)
      CPSI = CPSI**4
      BOR = 0.5D0*(SGAMMA + CPSI)
   50 CONTINUE
C
CC          Calculate tau.
C
      TAU(FACET)=SNGL(DABS(CPHI*CLAMDA)*BOR)
C
   60 CONTINUE
      RETURN
      END
C
CC
C
      DOUBLE PRECISION FUNCTION DOT(R,S)
C
      REAL*8 VV,R(3),S(3)
      REAL*8 DOT
C
      VV = DABS(R(1)*S(1) + R(2)*S(2) + R(3)*S(3))
      IF(VV.GT.1.0D-9)GOTO 10
      DOT=0.0D0
      RETURN
   10 DOT=DSQRT(VV)
      RETURN
      END
C
CC
C
```

```
C-----------------------------------------------------------------
C
      SUBROUTINE HALPHA(ALPHA,HVEC,FACET,PYRAM)
C
C           This subroutine will return HVEC values in
C           crystallographic axes, when HVEC is  given in
C           indenter axes for ALPHA=0
C
C
      REAL*8 HL,HM,HN,HVEC(3),ALPHA,CHM,CHN,CHL
      INTEGER FACET,PYRAM
C
      GO TO (10,20),PYRAM
C
   10 CHL = -0.707106781D0
      CHM = -0.707106781D0
      CHN =  0.0D0
      GO TO 30
C
   20 CHM= -0.1391902D0
      CHL= -0.9902657D0
      CHN= 0.0D0
C
C           From the geometry of the Indenter face(1).
C
   30 CALL FACETS(CHL,CHM,CHN,FACET)
C
      HL= CHL*DCOS(ALPHA) + CHM*DSIN(ALPHA)
      HM=-CHL*DSIN(ALPHA) + CHM*DCOS(ALPHA)
      HN= CHN
      CALL NORM(HL,HM,HN)
C
      CALL TWIST(HL,HM,HN)
C           Now we have lmn values for H ajusted for both
C           ALPHA and indentation plane
      HVEC(1)=HL
      HVEC(2)=HM
      HVEC(3)=HN
C
C
      RETURN
      END
C
C
C
C-----------------------------------------------------------------
C
      SUBROUTINE FALPHA(ALPHA,FVEC,FACET,PYRAM,SAXIS)
C
C           This subroutine will return FVEC values in
C           crystallographic axes, when FVEC is  given in
C           indenter axes for ALPHA=0
C
C          SAXIS = 1 for tensile axis, F // to the line
C          of steepest slope in the facet.
C          SAXIS = 2 for compressive axis, F perpendicular
C          to the facet.
C          PYRAM = 1 for Vickers, = 2 for Knoop.
C
      REAL*8 FL,FM,FN,FVEC(3),ALPHA,CFM,CFN,CFL
      INTEGER FACET,PYRAM,SAXIS
C
      GO TO (5,30),SAXIS
C
C          Tensile axis section.
C
    5 GO TO (10,20),PYRAM
C
   10 CFL = 0.613953625D0
      CFM = -0.613953625D0
      CFN = 0.496106733D0
      WRITE(6,1)
      GO TO 60
C
   20 CFM= -0.8959063D0
      CFL= +0.1259268D0
```



```
      CFN= +0.4260216D0
      WRITE(6,2)
      GO TO 60
C
C
C          Compressive axis section.
C
   30 GO TO (40,50),PYRAM
C
   40 CFL =  0.350800435D0
      CFM = -0.350800435D0
      CFN = -0.868261544D0
      WRITE(6,3)
      GO TO 60
C
   50 CFL =  0.0592980D0
      CFM = -0.4218746D0
      CFN = -0.9047130D0
      WRITE(6,4)
      GO TO 60
C
    1 FORMAT(' TENSILE, VICKERS')
    2 FORMAT(' TENSILE, KNOOP')
    3 FORMAT(' COMPRESSIVE, VICKERS')
    4 FORMAT(' COMPRESSIVE, KNOOP')
C
C          From the geometry of the Indenter face(1)
C
   60 CALL FACETS(CFL,CFM,CFN,FACET)
C
      FL= CFL*DCOS(ALPHA) + CFM*DSIN(ALPHA)
      FM=-CFL*DSIN(ALPHA) + CFM*DCOS(ALPHA)
      FN= CFN
      CALL NORM(FL,FM,FN)
C
      CALL TWIST(FL,FM,FN)
C           Now we have lmn values for F ajusted for both
C           ALPHA and indentation plane
      FVEC(1)=FL
      FVEC(2)=FM
      FVEC(3)=FN
C
C
      RETURN
      END
C
C
C
C-----------------------------------------------------------------
C
      SUBROUTINE FACETS(L,M,N,JJ)
C
      INTEGER JJ
      REAL*8 L,M,N
C
C          This routine rotates the vector given to it,such
C          that it returns the vector of facet JJ
C
      IF(JJ.EQ.1) RETURN
      IF(JJ.EQ.2) L=-L
      IF(JJ.EQ.4) M=-M
      IF(JJ.EQ.3) GOTO 30
      IF(JJ.LT.1) GOTO 10
      IF(JJ.GT.4) GOTO 10
C          N is unaffected as this is still working in
C          indenter coordinates
C
      RETURN
   10 WRITE(6,20)JJ
   20    FORMAT(' ###ERROR###          FACET NOT IN',
     1' RANGE 1 TO 4   JJ=',I4)
      RETURN
   30 L=-L
      M=-M
      RETURN
      END
C
```

```
      COMMON /COM1/SN,SD,SYS,IPI
      COMMON /COM2/ABC,ANGLES
      COMMON /COM6/ID,IDR
      COMMON /COM9/TOTSN,TOTSD
      COMMON /COM10/PLT1,PLT2
      COMMON /COM11/XDASH,ARNELL
      COMMON /COM14/CF,PYRAM,SAXIS
      COMMON /COM15/FR1,FR2
      COMMON /COM16/BLACK
C
      CALL BRKPLT(8)
      CALL ANFREQ(9,9,8,8)
      CALL PLIMIT(0.,230.,0.,310.)
      CALL ULIMIT(0.,230.,0.,310.)
      CALL TRMCHR(5.,0.0,0.0,10.)
      CALL LOCCHR(28.5,115.,0)
      CALL PRTCHR(101)
      CALL LOCCHR(30.,115.,0)
      CALL TRMCHR(2.1,0.,0.,3.5)
C
C         This section writes out the slip-system
C         and indentation plane
C
   10 CALL PEN(1)
      IF(SYS.EQ.2.OR.SYS.EQ.5) GOTO 40
C
      WRITE(8,20)(ID(J),J=1,3)
   20 FORMAT(' <',I2,2I3,' >')
C
      WRITE(8,30)(TOTSN(I,IQ),I=1,3),
     1(TOTSD(I,JQ),I=1,3),
     2(IPI(I),I=1,3),CF
   30 FORMAT(/1X,'(',I2,2I3,' ) <',I2,2I3,' >'//
     1' on (',I2,2I3,' )'//' Laue Class m3m'//
     2' Constraint factor ',I2)
      GO TO 70
C
   40 CONTINUE
C
      WRITE(8,50)ID
   50 FORMAT(' <',I2,3I3,' >')
      WRITE(8,60)(TOTSN(I,IQ),I=1,3),SN(4),(
     1TOTSD(I,JQ),I=1,3),SD(4),(
     2IPI(I),I=1,4),ABC,CF
   60 FORMAT(/1X,'(',I2,3I3,' ) <',I2,3I3,' >'//
     1' on (',I2,3I3,' )'//' Laue Class 6/mmm'//
     2' a,b,c : ',F7.4,',',F7.4,',',F7.4//
     3' Constraint factor ',I2)
      GO TO 70
C
   70 CONTINUE
      CALL LOCCHR(99.,108.,0)
      IF(SAXIS.EQ.1)WRITE(8,80)
      IF(SAXIS.EQ.2)WRITE(8,90)
      IF(PYRAM.EQ.1)WRITE(8,100)
      IF(PYRAM.EQ.2)WRITE(8,110)
   80 FORMAT(/' TENSILE STRESS AXIS')
   90 FORMAT(/' COMPRESSIVE STRESS AXIS')
  100 FORMAT(/' VICKERS INDENTER')
  110 FORMAT(/' KNOOP INDENTER')
      CALL PEN(2)
      IF(BLACK) CALL PEN(1)
      WRITE(8,120)
  120 FORMAT(///' PHILIP SARGENT 1979')
      CALL PEN(1)
C
C     CALL PLIMIT(30.,210.,30.,190.)
      CALL PLIMIT(30.,150.,130.,250.)
      CALL ULIMIT(0.,90.,FR1,FR2)
      CALL BOXXY(0,0)
      CALL PEN(2)
      IF(BLACK) CALL PEN(1)
      CALL TRMCHR(3.,0.,0.,5.)
      CALL TITLE(' ',1,'ANGLE',5,
     1'F =SUM(1/TAU)',13)
```



```
C
      RETURN
C
      END
C
C
C
C
C-----------------------------------------------------------------
C
      SUBROUTINE DRAW(M,INK,OPTA)
C
C          This subroutine plots the results.
C
      INTEGER INK,M,DIVIS
      REAL YPTS(181)
      REAL    RESULT(4,181),INDESS(4,181),XPTS(181)
      LOGICAL OPTA,BLACK
C
      COMMON /COM5/RESULT
      COMMON /COM7/XPTS
      COMMON /COM8/INDESS
      COMMON /COM12/DIVIS
      COMMON /COM16/BLACK
C
      CALL PEN(INK)
      IF(BLACK)CALL PEN(1)
      CALL TRMCHR(3.,0.,0.,5.)
      IF(OPTA)GOTO 20
C
      DO 10 J=1,DIVIS
      YPTS(J)=INDESS(M,J)
   10 CONTINUE
C
      CALL PLTGXY(XPTS,YPTS,DIVIS)
C
      RETURN
C
   20 DO 30 J=1,DIVIS
      YPTS(J)=RESULT(M,J)
   30 CONTINUE
C
      CALL PLTGXY(XPTS,YPTS,DIVIS)
C
      RETURN
      END
C
C-----------------------------------------------------------------
C
      SUBROUTINE NORM(X,Y,Z)
      REAL*8 X,Y,Z,L
      L=DSQRT(X*X+Y*Y+Z*Z)
C
      IF(DABS(L).GT.1.0E-40) GOTO 20
      X=0.0
      Y=0.0
      Z=0.0
C
      RETURN
C
   20 CONTINUE
C
      X=X/L
      Y=Y/L
      Z=Z/L
      RETURN
      END
```

I.IV - Calculations Using the Radial Displacement Theories

For the work with metallic glasses (section 4.3) and MgO (section 4.5.2) it was necessary to be able to quickly calculate whether the experimental data could be fitted to either of the two models of radial displacement (see 2.1.2): the Studman, Moore, Jones and Field model (SMJF) and the Gerk model. If the data does not fit, then, given three out of four of the Young's modulus (E), the yield stress (Y), the Poisson's ratio (NU), and the hardness (H), the program RADISH calculates a value for the remaining quantity which would cause the model to fit the data. It does this for both the SMJF and Gerk models together.

The program RADISH uses the subroutine C05AAF from the library of the National Algorithms Group (NAGLIB).

The program PLTRD plots H/Y as a function of E/Y for the radial displacement models of Hill, Marsh, Gerk and Studman et al.(SMJF) for Poisson's ratios of 0.3, 0.4, and 0.5. The results are shown in figures in section 2.1.2.

```
      C          Program PLTRD - Plots Radial Displacement Models
      C
            REAL EY(100),HY(100),EYB(100)
      C
            COMMON EYBMIN,EYBMAX,EY,HY,EYB
            COMMON /C2/BETA
      C
            BETA = 0.3839724435
            HYMIN = 0.8
            HYMAX = 4.4
            EYBMIN = 1.
            EYBMAX = 10000.
            EYMIN = EYBMIN/0.404026
            EYMAX = EYBMAX/0.404026
      C
            CALL GRFTYP(0,'+')
            CALL ANFREQ(1,3,4,20)
            CALL BOXTYP(+1)
      C
            DO 10 I=1,5
      C
            CALL BRKPLT(8)
            CALL PLIMIT(30.,114.5,30.,152.7)
            CALL ULIMIT(ALOG10(EYBMIN),
           +ALOG10(EYBMAX),HYMIN,HYMAX)
      C
            CALL FILL(0.3,I)
            CALL PEN(3)
            CALL PLTGLY(EYB,HY,100)
      C
            CALL FILL(0.4,I)
            CALL PEN(2)
            CALL PLTGLY(EYB,HY,100)
      C
            CALL FILL(0.5,I)
            CALL PEN(1)
            CALL PLTGLY(EYB,HY,100)
      C
            CALL PEN(1)
            CALL BOXLY(0,0)
            IF(I.EQ.1) CALL TITLE(' SMJ',4,' ',1,' ',1)
            IF(I.EQ.2) CALL TITLE(' GRK',4,' ',1,' ',1)
            IF(I.EQ.3) CALL TITLE(' HIL',4,' ',1,' ',1)
            IF(I.EQ.4) CALL TITLE(' MSH',4,' ',1,' ',1)
            IF(I.EQ.5) CALL TITLE(' JON',4,' ',1,' ',1)
      C
            CALL TITLE(' ',1,'(E/Y)*TAN(BETA)',15,' ',1)
      C
         10 CONTINUE
      C
            HY(1)=3.125
            EY(1)=56.06
            HY(2)=2.81
            EY(2)=56.06
            HY(3)=3.6
            EY(3)=52.
            HY(4)=3.26
            EY(4)=54.
            HY(5)=2.97
            EY(5)=45.
            HY(6)=2.86
            EY(6)=59.
      C
            N=6
      C
            DO 20 I=1,N
            EYB(I) = EY(I)*0.404026
         20 CONTINUE
      C
            CALL GRFTYP(-1,'+')
            CALL PLTGLY(EYB,HY,N)
      C
      C
            STOP
            END
      C
      C-------------------------------------------------------------
```



```
      C
            FUNCTION FSMJ(EY,NU)
      C
            REAL*8 X,A,P,Q,R,S,T
            REAL FSMJ,Y,E,NU,BETA
      C
            COMMON /C2/BETA
      C
            Y = 1.0
            E = EY*Y
      C
            P = 4*(1.D0 - 2*NU)
            Q = 6*(1.D0 - NU)
            R = (E/Y)*TAN(BETA)
            S = 1.D0 + DLOG( (R+P)/Q )
            T = 0.5D0 + (2.D0/3.D0)*S
            FSMJ= Y*T
      C
            RETURN
            END
      C
      C-------------------------------------------------------------
      C
            FUNCTION FGRK(EY,NU)
      C
            REAL*8 X,A,P,Q,R,S,T
            REAL FGRK,Y,E,NU,BETA
      C
            COMMON /C2/ BETA
      C
             Y = 1.0D0
             E = EY*Y
      C
            P=2*Y*(1.D0-NU)/(3*E)
            Q=(1.D0-P)**3
            R = 1.D0 - EXP(-2.*TAN(BETA)/3.)
            S = DLOG( R/(1-Q) )
            T = 1.D0 + (2.D0/3.D0)*S
            FGRK = Y*T
      C
            RETURN
            END
      C
      C-------------------------------------------------------------
      C
            FUNCTION FHIL(EY,NU)
      C
            REAL*8 P,Q,MU,LAM
            REAL FHIL,Y,E,NU,BETA
      C
            COMMON /C2/BETA
      C
            Y=1.0D0
            E=EY*Y
      C
            MU  = (1.D0 + NU)*Y/E
            LAM = (1.D0 - 2*NU)*Y/E
            P   = DLOG(3.D0/(LAM + 3*MU - LAM*MU))
            Q   = 3.D0/(3.D0-LAM)
            FHIL= (Y*2.D0/3.D0)*(1.D0 + Q*P)
      C
            RETURN
            END
      C
      C-------------------------------------------------------------
      C
            FUNCTION FMSH(EY,NU)
      C
            REAL*8 Z,B,MU,LAM
            REAL FMSH,Y,E,NU,BETA
      C
            COMMON /C2/BETA
      C
            Y=1.D0
            E=EY*Y
      C
            MU  = (1.D0 + NU)*Y/E
```

```
      LAM = (1.D0 - 2*NU)*Y/E
      Z = 3.D0/(LAM + 3*MU - LAM*MU)
      B = 3./(3.D0 - LAM)
      FMSH = Y*(0.28D0 + 0.6D0*B*DLOG(Z))
C
      RETURN
      END
C
C-------------------------------------------------------------
C
      FUNCTION FJON(EY,NU)
C
      REAL*8 Z
      REAL JFON,Y,E,NU,BETA
C
      COMMON /C2/BETA
C
      Y=1.D0
      E=EY*Y
C
      Z=ALOG(EY*0.404026/3.)
      FJON = (2.*Y/3.)*(1.D0 + Z)
C
      RETURN
      END
C
C-------------------------------------------------------------
C
      SUBROUTINE FILL(NU,I)
C
      REAL EY(100),HY(100),NU,EYMIN,EYMAX,EYB(100)
C
      COMMON EYBMIN,EYBMAX,EY,HY,EYB
C
      DO 10 J=1,100
C
      EYB(J) = EXP(ALOG(EYBMIN) + (J-1)*ALOG(EYBMAX/EYBMIN)
                                                        /99.
      EY(J)  = EYB(J)/0.404026
      IF(I.EQ.1)HY(J) = FSMJ(EY(J),NU)
      IF(I.EQ.2)HY(J) = FGRK(EY(J),NU)
      IF(I.EQ.3) HY(J) = FHIL(EY(J),NU)
      IF(I.EQ.4) HY(J) = FMSH(EY(J),NU)
      IF(I.EQ.5) HY(J) = FJON(EY(J),NU)
C
      WRITE(6,*)EYB(J),EY(J),HY(J),J,NU,I
   10 CONTINUE
C
      RETURN
      END
```



```
C          Program RADISH (Radial Displacements)
C
      REAL*8 Y,E,H,NU,BETA,EPS,ETA
      LOGICAL*1 INFO(60)
C
      COMMON Y,E,H,NU,BETA,EPS,ETA,INFO
C
      READ(5,10)INFO
   10 FORMAT(60A1)
C
      WRITE(6,15)INFO
      WRITE(7,15)INFO
   15 FORMAT('1',21X,60A1)
C
      READ(5,*)Y,E,H,NU,BETA
      WRITE(6,20)Y,E,H,NU,BETA
      WRITE(7,20)Y,E,H,NU,BETA
C
      BETA = 3.141592654D0*BETA/180.D0
      EPS = 1.D-5
      ETA = 1.D-5
C
      CALL YCALC
      CALL ECALC
      CALL HCALC
      CALL NUCALC
      WRITE(6,30)
      WRITE(7,30)
C
      STOP
C
   20 FORMAT(//21X,'Y    = ',F9.3/
     +21X,'E    = ',F9.1/21X,'H    = ',F9.3/
     +21X,'nu   = ',F9.3/21X,'beta = ',F9.3////
     +32X,'SMJ',7X,'GRK',7X,'Real'/
     +1X,31X,'___',7X,'___',7X,'____'//)
   30 FORMAT('1')
C
      END
C
C-------------------------------------------------------------
C
      SUBROUTINE SMJ(X,A,I)
C
      REAL*8 X,A,P,Q,R,S,T
      REAL*8 Y,E,H,NU,BETA,EPS,ETA
      REAL*8 Y2,E2,H2,NU2
      LOGICAL*1 INFO(60)
C
      COMMON Y,E,H,NU,BETA,EPS,ETA,INFO
C
      Y2=Y
      E2=E
      H2=H
      NU2=NU
C
      IF(I.EQ.1)Y=X
      IF(I.EQ.2)E=X
      IF(I.EQ.3)H=X
      IF(I.EQ.4)NU=X
C
      P = 4*(1.D0 - 2*NU)
      Q = 6*(1.D0 - NU)
      R = (E/Y)*DTAN(BETA)
      S = 1.D0 + DLOG( (R+P)/Q )
      T = 0.5D0 + (2.D0/3.D0)*S
      A = H - Y*T
C
      Y=Y2
      E=E2
      H=H2
      NU=NU2
C
      RETURN
      END
C
C-------------------------------------------------------------
C
      SUBROUTINE GRK(X,A,I)
```

```
C
      REAL*8 X,A,P,Q,R,S,T
      REAL*8 Y,E,H,NU,BETA,EPS,ETA
      REAL*8 Y2,E2,H2,NU2
      LOGICAL*1 INFO(60)
C
      COMMON Y,E,H,NU,BETA,EPS,ETA,INFO
C
      Y2=Y
      E2=E
      H2=H
      NU2=NU
C
      IF(I.EQ.1)Y=X
      IF(I.EQ.2)E=X
      IF(I.EQ.3)H=X
      IF(I.EQ.4)NU=X
C
      P=2*Y*(1.D0-NU)/(3*E)
      Q=(1.D0-P)**3
      R = 1.D0 - DEXP(-2*DTAN(BETA)/3)
      S = DLOG( R/(1-Q) )
      T = 1.D0 + (2.D0/3.D0)*S
      A = H - Y*T
C
      Y=Y2
      E=E2
      H=H2
      NU=NU2
C
      RETURN
      END
C
C-------------------------------------------------------

C
      SUBROUTINE YCALC
C
      REAL*8 A,B,EPS,ETA,YSMJ,YGRK,HY,HYSMJ,HYGRK
C
      REAL*8 Y,E,H,NU,BETA,EPS,ETA
      LOGICAL*1 INFO(60)
C
      COMMON Y,E,H,NU,BETA,EPS,ETA,INFO
C
      EXTERNAL FYSMJ,FYGRK
C
      YSMJ=0.D0
      YGRK=0.D0
      HYSMJ=0.D0
      HYGRK=0.D0
      HY=0.D0
C
      IF(E.EQ.0.D0) GOTO 10
      IF(H.EQ.0.D0) GOTO 10
      IF(NU.EQ.0.D0) GOTO 10
C
      A=1.D0
      B=2*H
      IFAIL=1
      CALL C05AAF(A,B,EPS,ETA,FYSMJ,YSMJ,IFAIL)
      IF(IFAIL.NE.0) RETURN
C
      IFAIL=1
      CALL C05AAF(A,B,EPS,ETA,FYGRK,YGRK,IFAIL)
      IF(IFAIL.NE.0) RETURN
C
      WRITE(6,100)YSMJ,YGRK
      WRITE(7,100)YSMJ,YGRK
C
      HYSMJ=H/YSMJ
      HYGRK=H/YGRK
      EYSMJ=E/YSMJ
      EYGRK=E/YGRK
C
      WRITE(6,200)HYSMJ,HYGRK
      WRITE(7,200)HYSMJ,HYGRK
      WRITE(6,300)EYSMJ,EYGRK
      WRITE(7,300)EYSMJ,EYGRK
C
```



```
      RETURN
C
   10 CONTINUE
C
      EY=E/Y
      HY=H/Y
      WRITE(6,400)Y
      WRITE(7,400)Y
      IF(E.EQ.0.D0) GOTO 20
      WRITE(6,500)EY
      WRITE(7,500)EY
   20 IF(H.EQ.0.D0) RETURN
      WRITE(6,600)HY
      WRITE(7,600)HY
C
      RETURN
C
  100 FORMAT(21X,'Y''     = ',2(F9.3,2X)//)
  200 FORMAT(21X,'H/Y'' = ',2(F9.3,2X)//)
  300 FORMAT(21X,'E/Y'' = ',2(F9.3,2X)///)
  400 FORMAT(21X,'Y     = ',22X,F9.3//)
  500 FORMAT(21X,'E/Y   = ',22X,F9.3//)
  600 FORMAT(21X,'H/Y   = ',22X,F9.3///)
C
      END
C
C
C-------------------------------------------------------

C
      SUBROUTINE ECALC
C
      REAL*8 A,B,ESMJ,EGRK,HY,EY,EYSMJ,EYGRK
      REAL*8 Y,E,H,NU,BETA,EPS,ETA
      LOGICAL*1 INFO(60)
C
      COMMON Y,E,H,NU,BETA,EPS,ETA,INFO
C
      EXTERNAL FESMJ,FEGRK
C
      ESMJ=0.D0
      EGRK=0.D0
      EY=0.D0
      EYSMJ=0.D0
      EYGRK=0.D0
C
      IF(Y.EQ.0.D0) GOTO 10
      IF(H.EQ.0.D0) GOTO 10
      IF(NU.EQ.0.D0) GOTO 10
C
      A=H
      B=1.D4*H
      IFAIL=1
      CALL C05AAF(A,B,EPS,ETA,FESMJ,ESMJ,IFAIL)
      IF(IFAIL.NE.0) RETURN
C
      IFAIL=1
      CALL C05AAF(A,B,EPS,ETA,FEGRK,EGRK,IFAIL)
      IF(IFAIL.NE.0) RETURN
C
      WRITE(6,100)ESMJ,EGRK
      WRITE(7,100)ESMJ,EGRK
C
      EYSMJ = ESMJ/Y
      EYGRK = EGRK/Y
C
      WRITE(6,200)EYSMJ,EYGRK
      WRITE(7,200)EYSMJ,EYGRK
C
      HY = H/Y
      WRITE(6,400)HY
      WRITE(7,400)HY
C
      RETURN
C
   10 CONTINUE
C
      WRITE(6,250)E
      WRITE(7,250)E
      IF(Y.EQ.0.D0) RETURN
      EY = E/Y
```

```
      WRITE(6,300)EY
      WRITE(7,300)EY
C
      IF(H.EQ.0.D0) RETURN
      HY=H/Y
      WRITE(6,400)HY
      WRITE(7,400)HY
C
      RETURN
C
  100 FORMAT(21X,'E''    = ',2(F9.1,2X)//)
  200 FORMAT(21X,'E''/Y = ',2(F9.3,2X)//)
  250 FORMAT(21X,'E     = ',22X,F9.1//)
  300 FORMAT(21X,'E/Y   = ',22X,F9.3//)
  400 FORMAT(21X,'H/Y   = ',22X,F9.3///)
C
      END
C
C-----------------------------------------------------------

C
      SUBROUTINE HCALC
C
      REAL*8 A,B,HSMJ,HGRK,EY,HYSMJ,HYGRK,HY
      REAL*8 Y,E,H,NU,BETA,EPS,ETA
      LOGICAL*1 INFO(60)
C
      COMMON Y,E,H,NU,BETA,EPS,ETA,INFO
C
      EXTERNAL FHSMJ,FHGRK
C
      HSMJ=0.D0
      HGRK=0.D0
      HYSMJ=0.D0
      HYGRK=0.D0
      HY=0.D0
C
      IF(Y.EQ.0.D0) GOTO 10
      IF(E.EQ.0.D0) GOTO 10
      IF(NU.EQ.0.D0) GOTO 10
C
      A=0.5D0*Y
      B=1000.D0*Y
      IFAIL=1
      CALL C05AAF(A,B,EPS,ETA,FHSMJ,HSMJ,IFAIL)
      IF(IFAIL.NE.0) RETURN
C
      IFAIL=1
      CALL C05AAF(A,B,EPS,ETA,FHGRK,HGRK,IFAIL)
      IF(IFAIL.NE.0)  RETURN
C
      WRITE(6,100)HSMJ,HGRK
      WRITE(7,100)HSMJ,HGRK
C
      HYSMJ=HSMJ/Y
      HYGRK=HGRK/Y
C
      WRITE(6,200)HYSMJ,HYGRK
      WRITE(7,200)HYSMJ,HYGRK
C
      EY=E/Y
      WRITE(6,400)EY
      WRITE(7,400)EY
C
      RETURN
C
   10 CONTINUE
C
      WRITE(6,250)H
      WRITE(7,250)H
      IF(Y.EQ.0.D0) RETURN
      HY = H/Y
      WRITE(6,300)HY
      WRITE(7,300)HY
C
      IF(E.EQ.0.D0) RETURN
      EY=E/Y
      WRITE(6,400)EY
      WRITE(7,400)EY
C
```



```
      RETURN
C
  100 FORMAT(21X,'H''    = ',2(F9.3,2X)//)
  200 FORMAT(21X,'H''/Y = ',2(F9.3,2X)//)
  250 FORMAT(21X,'H     = ',22X,F9.3//)
  300 FORMAT(21X,'H/Y   = ',22X,F9.3//)
  400 FORMAT(21X,'E/Y   = ',22X,F9.3///)
C
      END
C
C-----------------------------------------------------------

C
      SUBROUTINE NUCALC
C
      REAL*8 A,B,NUSMJ,NUGRK
      REAL*8 Y,E,H,NU,BETA,EPS,ETA
      LOGICAL*1 INFO(60)
C
      COMMON Y,E,H,NU,BETA,EPS,ETA,INFO
C
      EXTERNAL FNUSMJ,FNUGRK
C
      NUSMJ=0.D0
      NUGRK=0.D0
C
      IF(Y.EQ.0.D0) GOTO 10
      IF(E.EQ.0.D0) GOTO 10
      IF(H.EQ.0.D0) GOTO 10
C
      A=1.D-6
      B=1.D0 - 1.D-5
      IFAIL=1
      CALL C05AAF(A,B,EPS,ETA,FNUSMJ,NUSMJ,IFAIL)
      IF(IFAIL.NE.0) RETURN
C
      IFAIL=1
      CALL C05AAF(A,B,EPS,ETA,FNUGRK,NUGRK,IFAIL)
      IF(IFAIL.NE.0) RETURN
C
      WRITE(6,100)NUSMJ,NUGRK
      WRITE(7,100)NUSMJ,NUGRK
C
      RETURN
C
   10 CONTINUE
C
      WRITE(6,200)NU
      WRITE(7,200)NU
C
      RETURN
C
  100 FORMAT(21X,'nu''   = ',2(F9.3,2X)///)
  200 FORMAT(21X,'nu     = ',22X,F9.3///)
C
      END
C
C-----------------------------------------------------------

C
      DOUBLE PRECISION FUNCTION FYSMJ(X)
C
      REAL*8 X,A,FYSMJ
      CALL SMJ(X,A,1)
      FYSMJ=A
      RETURN
      END
C
C-----------------------------------------------------------

C
      DOUBLE PRECISION FUNCTION FYGRK(X)
C
      REAL*8 X,A,FYGRK
      CALL GRK(X,A,1)
      FYGRK=A
      RETURN
      END
C
C-----------------------------------------------------------

C
      DOUBLE PRECISION FUNCTION FESMJ(X)
```

```
C
      REAL*8 X,A,FESMJ
      CALL SMJ(X,A,2)
      FESMJ=A
      RETURN
      END
C
C-----------------------------------------------------
C
      DOUBLE PRECISION FUNCTION FEGRK(X)
C
      REAL*8 X,A,FEGRK
      CALL GRK(X,A,2)
      FEGRK=A
      RETURN
      END
C
C-----------------------------------------------------
C
      DOUBLE PRECISION FUNCTION FHSMJ(X)
C
      REAL*8 X,A,FHSMJ
      CALL SMJ(X,A,3)
      FHSMJ=A
      RETURN
      END
C
C-----------------------------------------------------
C
      DOUBLE PRECISION FUNCTION FHGRK(X)
C
      REAL*8 X,A,FHGRK
      CALL GRK(X,A,3)
      FHGRK=A
      RETURN
      END
C
C-----------------------------------------------------
C
      DOUBLE PRECISION FUNCTION FNUSMJ(X)
C
      REAL*8 X,A,FNUSMJ
      CALL SMJ(X,A,4)
      FNUSMJ=A
      RETURN
      END
C
C-----------------------------------------------------
C
      DOUBLE PRECISION FUNCTION FNUGRK(X)
C
      REAL*8 X,A,FNUGRK
      CALL GRK(X,A,4)
      FNUGRK=A
      RETURN
      END
```

Appendix II - Experimental Methods

II.I Materials

A systematic coding system was used to identify all the materials used in the study and it is simplest to explain the various materials preparation treatments using these codes.

The first two or three characters are letters which identify the composition of the material (see table I).

Appendix II.I - Table I

MSX	MgO single crystals, supplied by Dr.Sambell (AERE Harwell) as part of a batch bought from Semi-Elements Inc.
LIF	LiF single crystals
MGO	Hot pressed MgO, from powder containing 4% LiF
EKM	Eastman Kodak magnesia: 'IRTRAN 5 (evaporative grade)'
STU	20% Cr - 25% Ni - balance Fe, stainless steel
STS, STT	stainless steel (as above, but + 0.5% Nb)
CUP	Polycrystalline copper, 99.999% pure
ACQ	2605A Allied Chemical Metglas (metallic glass)
ACR	2826 "
ACS	2826A "
ACT	2826 (1" wide) "
ACU	2605 "
NN	Hot-pressed silicon nitride (Norton 132)
BN	Hot-pressed silicon nitride (Brown Boveri)
NC	Hot-pressed silicon carbide (Norton)

After the material composition code, a single digit may appear. This identifies a small piece of material which has been thermomechanically treated. This applies on the the polycrystalline MgO and the stainless steel specimens.

After the heat-treatment code there is a single letter which differentiates between the small pieces cut from the heat-treated specimen. Such small pieces of stainless steel were subjected to further annealing treatments and for other materials the letter serves to distinguish between different surface preparation treatments.

The last character, or pair of characters, applies only to a set of data from a specimen. Several sets of measurements were made on most specimens, sometimes under different circumstances, e.g. wet or dry, hot or cold. Thus a complete code for a set of indentation data would be: STU4A15, STU - niobium free stainless steel, 4 - rolled to 51% of its former thickness, A - annealed 10 minutes at 805°C, 1 - indentations made in the centre of the specimen where the grains are larger, 5 - amalgamation of sets of data 1, 2 and 4.

Appendix II.I - Table II - Stainless Steel

STU1	Rolled 24% reduction in thickness
STU2	As recieved (annealed)
STU4	Rolled 49% reduction in thickness
STU1C	As STU1 plus annealed 8 minutes between 895°C and 913°C
STU4A	STU4 plus 10 min anneal at 805°C

Appendix II.I - Table III - MgO Polycrystals

MGO9	Hot-pressed MgO (+4% LiF): 60 mins at 830°C and 60 mins at 1250°C followed by an air anneal at 1350 C for 24 hours
MGO10	Hot-pressed MgO (+4% LiF): 45 mins at 850°C and 45 mins at 1250°C
MGO10A	MGO10 piece vibratory polished and 'thumb' polished
MGO10C	MGO10 piece annealed 1 week at 1300°C, polished as MGO10A
EKM2	As recieved random chunk
EKM2C	Polished very slowly for several days on a cotton lap wheel with ¼ µm diamond paste

(Table III continued.)

EKM6	EKM2 annealed 150 hours at 1270°C and 408 hours at 1390°C
EKM6E	Piece of EKM6, standard metallographic polishing treatment

MgO and LiF crystals were cleaved to the required size; LiF was cleaved with a razor blade by hand at room temperature whereas MgO crystals were cleaved, after first cooling them in liquid nitrogen, with a steel blade and light hammer.

LiF crystals were always indented on the as-cleaved surface whereas MgO crystals (except where specifically indicated in the text) were first mechanically polished.

The polycrystalline ceramic specimens were cut to size with a diamond/stainless steel annular bladed saw (Capco Q35 Mk.2). The stainless steel was cut with a hack-saw and the copper by spark machining..

II.II Surface Preparation Treatments

Grinding and Polishing

Water lubricated SiC paper wheels were used to grind the surfaces of all specimens (except the metallic glasses) flat. Small specimens were waxed down (with Lakeside 70, supplied by Whitwear Lapidery Co.) to dural blocks for the polishing treatment. The steel and single crystal MgO specimens were polished with Hyprez (Engis Ltd.) diamond paste with grit sizes 6, 1 and 0.25 microns on silk lapping wheels on a Kent 2A machine (Engis Ltd.). Polishing polycrystalline MgO by this method caused whole grain pull-out in all by the larger grain sized specimens (MGO9 and EKM6). MgO single crystals were surrounded by pieces of glass microscope slide on the dural block to present a flat surface and to prevent scoring of the lapping cloths with the corners of the crystals.

Vibratory (Erosion) Polishing

Grinding produces a highly fractured surface in MgO. However, several days in a type M14 Metallurgical Vibratory Polisher (Mclean Research Engineering Ltd.), charged with 0.05 micron gamma alumina powder made into a slurry with 50/50 glycerol/water, produced smooth surfaces with no grain pull-out. These surfaces were unacceptable on the polycrystalline specimens because they were highly contoured due to the crystallographic anisotropy in the erosion rate. (This was confirmed in separate tests on single crystals cut into circular slices with an ultrasonic drill.) Erosion polishing with a slurry of diamond powder produced grain pull-out.

Flat surfaces on polycrystalline MgO specimens were produced by alternate vibratory polishing and very slow polishing on silk lapping wheels with 0.25 micron diamond paste. Some specimens were polished for an hour by hand using a clean thumb and 0.1 micron diamond paste (e.g. MGO10A).

Chemical polishing (orthosphosphoric acid, see below) and chemo--mechanical polishing (NH_4Cl etch in the alumina slurry on a polishing wheel) were not successful in polishing polycrystalline MgO.

Stainless Steel

No stainless steel specimens for which results are reported in this thesis were electropolished, but they were all electroetched. Comparative tests on the niobium stabilised alloy showed no significant difference between the hardness behaviour of electropolished and electroetched specimens. It has been assumed that the same effect holds for the niobium free alloy.

Appendix II.II - Table I

etchant/polish	use
Oxalic acid (saturated solution at room temp.) 5 volts for 1 minute.	used to electroetch grain boundaries in stainless steel
3: 1: 1 (by volume) mixture of NH_4Cl (sat. soln.): H_2O : H_2SO_4 (conc.), 1 to 2 mins.	both were used to produce etch pits in single crystal MgO and to reveal grain boundaries in polycrystals
0.5 M $AlCl_3$ solution at 55°C, 1 to 2 mins.	
0.1 g FeF_3 per litre H_2O at 55°C for one minute	used to produce etch pits in LiF
500 ml conc. orthophosphoric acid + 300 ml glycerol + 90 ml H_2O, at 8 amps dm^{-2} for a few minutes	used to electropolish flat surfaces of stainless steel
Conc. orthophosphoric acid at 100°C to 150°C for a few seconds	chemical polish for MgO

Appendix III - The Indenters

Two types of diamond pyramid indenter were used in this study, the Vickers and Knoop indenters. Diagrams of the shapes of these indenters are shown in the figure. The unrecovered depths (h) of the indentations made with the indenters are given by:-

$d/h = 30.5$ for the Knoop indenter

$d/h = 7.0$ for the Vickers indenter

where 'd' is defined in the figure.

The two diagonals of a perfect Knoop indentation are related by:-

$d/w = 7.11$.

Knoop indenter

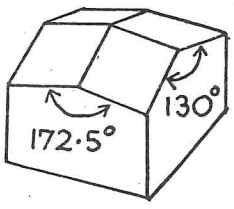

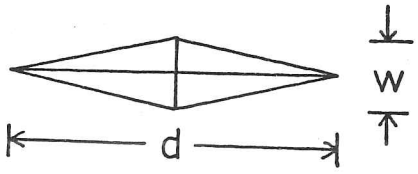

Vickers indenter

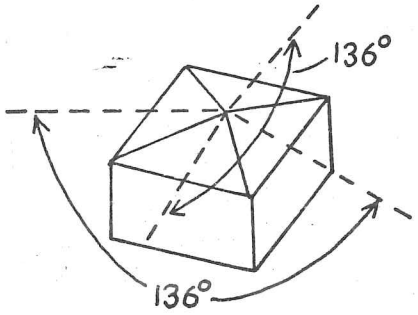

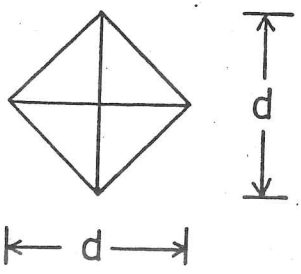

"Doesn't have a point of view
Knows not where he's going to
Isn't he a bit like you
And me"

Lennon and McCartney